A multi-tracer hydrochemical investigation of groundwater dynamics in the Lower Rhine Embayment, Germany.

Lee Paul Gumm

January 2011

A thesis submitted to the School of Environmental Sciences
University of East Anglia
in partial fulfilment of the requirements for the degree of
Doctor of Philosophy

Abstract

Geochemical tracers have been exploited to achieve an improved understanding of hydrogeological processes in the Lower Rhine Embayment, Germany. Dissolved noble gas measurements have been supported by stable isotope and hydrochemical data to form a multi-tracer approach. Helium measurements have been used to provide insight into groundwater residence times and the role of fault zones on local and regional groundwater flow dynamics.

The hydrogeology of the Lower Rhine Embayment is complex and dynamic. The geology consists of unconsolidated siliciclastic sedimentary deposits with a number of laterally continuous lignite seams. Large scale open cast lignite mining in the region has a significant impact on the groundwater system primarily due to water abstraction at a rate of 500 million m^3 $year^{-1}$ and subsequent lowering of the water table. Local groundwater monitoring suggests that groundwater levels are recovering in areas close to abandoned mines but the long-term implications of mine de-watering on this scale remain uncertain. The layered aquifer system is intersected by numerous NW-SE striking fault zones that have been shown to have the potential to act as both barriers to groundwater flow and as preferential flow paths that connect deep and shallow aquifers.

Groundwater samples taken from observation boreholes in close proximity to fault zones have provided results that indicate depleted δ^2H and $\delta^{18}O$ values relative to modern groundwater recharge, and ^4He concentrations in the shallow aquifers of up to $1.7x10^{-4}$ cm^3 STP g^{-1} H_2O which is approximately 3-4 orders of magnitude higher than expected due to solubility equilibrium with the atmosphere. Groundwater exchange between the deep basal aquifers and the upper aquifer layers is impeded by confining clay layers and very low permeability lignite. This suggests that palaeo groundwater from depth is mixing with modern groundwater of meteoric origin in the shallow aquifers as a result of conduit flow from depth towards the upper aquifer layers within the fault zone, and so confirming the fault zone control model of Bense and Person (2006).

Table of Contents

3. Dissolved Noble Gases and Stable Isotopes in Groundwater

List of Figures

List of Tables

Acknowledgments

First and foremost, I would like to thank Paul Dennis, Victor Bense and Kevin Hiscock as members of my supervisory team for giving me the opportunity to undertake this research and for providing guidance, advice and an abundance of scientific knowledge from the outset.

I am especially grateful to Alina Marca-Bell for help with $\delta^{2}H$, $\delta^{18}O$ and $\delta^{13}C_{DIC}$ analyses, and to Paul Disdle for general laboratory support.

Thanks also go to Jurian Hoogewerff and Henriette Ueckermann for conducting strontium isotope ratio analyses using the Isoprobe MC-ICP-MS, and to Graham Chilvers for assisting with total strontium measurements using the ICP-MS.

I am indebted to Nils Cremer and Stefan Simon from the Erftverband for the truly vast amount of support provided throughout this research. Thanks also go to Thomas and Harald from the Erftverband groundwater team for their help with observation borehole sampling and to the Erftverband laboratory technicians for the hydrochemical analyses.

Finally, but most importantly, very special thanks go to my family – Claudia, Samuel and Isabelle.

This research was funded by a Natural Environment Research Council studentship and CASE award from Chell Instruments Limited (NER/S/A/2006/14113).

1. Introduction

1.1. Overview

The research presented within this thesis primarily describes a multi-tracer analysis of groundwater dynamics in the Lower Rhine Embayment, Germany.

The dissolved noble gases of helium (He), neon (Ne), argon (Ar), krypton (Kr) and xenon (Xe) were utilised to gain an improved understanding of groundwater flow paths associated with fault zones and to estimate the subsurface residence time of deep circulating groundwater in the Lower Rhine Embayment. Dissolved noble gas concentrations were also used to calculate noble gas recharge temperatures and to determine excess air concentrations. The stable isotopes of hydrogen, oxygen and carbon were used in conjunction with routine hydrochemical data such as major and minor ion concentrations to provide additional evidence for determining groundwater origin, recharge conditions and hydrochemical evolution.

The study area is morphologically expressed as the Lower Rhine Embayment (LRE) and forms part of the Roer Valley Rift System (RVRS) which is the southward extension of the North Sea Basin (see Figure 2.1) and part of a Cenozoic mega-rift system that crosses western and central Europe (Ziegler, 1994). The German region of the Lower Rhine Embayment contains approximately 1300 m of Oligocene to Pleistocene unconsolidated siliciclastic sediments that form a complex layered aquifer system. The layered aquifer system is intersected by numerous NW-SE striking fault zones that have been shown to have the potential to act as both barriers to groundwater flow and as preferential flow paths (Bense and Person, 2006). Fault zones play a fundamental role in understanding groundwater flow dynamics in the Lower Rhine Embayment and fault bounded tectonic blocks form key structural features that have a large influence on local and regional groundwater flow patterns.

The sedimentary basin also contains several commercially important lignite seams. The main lignite seam has a total thickness of up to 100 m (Hager, 1993) and is currently being exploited by RWE Power AG in three large open cast mines.

The Erftverband is a public organisation that was established in the 1950s to provide comprehensive surface water and groundwater management for the German region of the Lower Rhine Embayment. The Erftverband core region is essentially the catchment of the river Erft and covers an area of 1,920 km^2 but the wider Erftverband territory extends to cover an area of 4,220 km^2 within the State of North Rhine Westphalia. The human population of the region is approximately 750,000 and land use varies from wetland habitats and agriculture to open cast lignite mining, lignite refining plants and other heavy industries such as chemical processing plants. This diversity often leads to a conflict of interests and as a result, management and conservation projects are often complex and difficult to implement efficiently and cost effectively. The Lower Rhine Embayment lignite mining industry was the focus of intense Greenpeace demonstrations in 2004.

Groundwater monitoring programmes in the region have been given high priority status and the Erftverband in collaboration with RWE Power AG have established an extensive network of 15,000 observation boreholes and piezometer nests to monitor the effects of regional lignite mining activities, and in particular the impact of large scale groundwater abstraction and lignite mine de-watering (500 million m^3 of groundwater $year^{-1}$) on local and regional groundwater flow dynamics. Groundwater monitoring has already provided strong evidence that lignite mine de-watering is responsible for lowering the water table in some areas and for a noticeable decline in the baseflow of local rivers as well as endangering susceptible wetland habitats (Erftverband, 2006). To date, approximately 30,000 people have been re-

settled as a result of open cast lignite mining. The current working depths of the mines are up to 350 m but it is anticipated that the entire lignite seam will be exploited in the future, so depths will increase to 500 m at some locations.

1.1.1. Aims and objectives

The aim of the research presented in this thesis is to develop an integrated assessment of groundwater flow dynamics in the Lower Rhine Embayment aquifer system using hydrochemical tracers (major and minor ions), stable isotopes ($\delta^{2}H$, $\delta^{18}O$, $\delta^{13}C_{DIC}$) and dissolved noble gases (He, Ne, Ar, Kr and Xe) interpreted in the context of examining geochemical evidence for the conduit-barrier fault zone model of Bense and Person (2006).

Under this aim, a number of objectives have been fulfilled as follows:

1. To investigate the relationship between noble gas determined excess air concentrations and temporal variations in water table fluctuations caused by lignite mine de-watering.

2. To determine the influence of fault zones on groundwater flow paths, and identify fluid flow conditions and transport mechanisms associated with advective flow from depth.

3. To calculate noble gas recharge temperatures to identify modern and palaeo groundwaters within the complex multi-layered aquifer systems of the Lower Rhine Embayment.

1.1.2. Thesis structure

Chapter 1 provides a general overview of the research and states the fundamental aim and objectives of the investigation. Chapter 1 also includes a brief description of the study area and outlines the multi-tracer approach that has been applied.

Chapter 2 provides a comprehensive account of the regional hydrogeology of the Lower Rhine Embayment and describes the open cast lignite mines and their impact on groundwater flow patterns. Chapter 2 defines the aquifer units and their distribution and illustrates the hydraulic head distribution and the influence of fault zones. Chapter 2 also provides general climatic information that relates to the study area and an overview of fault zone processes in sedimentary basins.

Chapter 3 provides a critical review of the literature relevant to the application of dissolved noble gases in determining noble gas temperatures, and the numerical models that are available for calculating noble gas temperatures and noble gas determined excess air concentrations. Chapter 3 also provides a general overview of stable isotopes in groundwater and Rayleigh fractionation processes. The reader is referred to relevant review papers or texts where appropriate.

Chapter 4 outlines all the methods used for sample collection and preparation as well as the analytical procedures used and the associated instruments and analysers. Chapter 4 describes the isotope dilution technique and the quadrupole mass spectrometer used for dissolved noble gas analysis as well as the isotope ratio mass spectrometry (IRMS) methodology.

Chapter 5 presents the results of the stable isotope and dissolved noble gas analyses as well as the routine hydrochemical analyses that were conducted by the

Erftverband in Bergheim, Germany. Where possible the results have been presented using spatial distribution plots to illustrate how the parameter varies with aquifer properties and recharge provenance.

Chapter 6 consists of three key sections in which hydrochemical, stable isotope and dissolved noble gases are discussed and evaluated respectively. Chapter 6 concludes by presenting a conceptual hydrochemical model for groundwater flow dynamics in the Brühl region of the Lower Rhine Embayment.

Chapter 7 provides a concise concluding statement that summarises the most important findings and finishes with a number of suggestions for further work that would significantly enhance our understanding of groundwater dynamics in the Lower Rhine Embayment, Germany.

2. Hydrogeology of the Lower Rhine Embayment

2.1. Geological Setting

2.1.1. Geological formation – Oligocene to Pleistocene (33.7 to 0.01 Myr BP)

The Lower Rhine Embayment (LRE), Germany, is part of the Roer Valley Rift System (RVRS), also referred to as the Lower Rhine Basin which is the southward extension of the North Sea Basin (Figure 2.1) and part of a Cenozoic mega-rift system that crosses western and central Europe (Ziegler, 1994). The SE region of the Lower Rhine Basin is morphologically expressed by the Lower Rhine Embayment.

The formation of the Lower Rhine Embayment began during the Oligocene with the subsidence of the Lower Rhine Basin along NW-SE striking faults on the edge of the Rheinisches Schiefergebirge (Rhenish Slate Range) allowing the North Sea to create a marine rift basin that cut into the headlands of the Rhenish Massif to form the Lower Rhine Embayment. The German region of the Lower Rhine Basin contains approximately 1300 m of Oligocene to Pleistocene sediments with a main lignite seam that has a total thickness of up to 100 m and an upper seam that has a thickness of up to 40 m (Hager, 1993). The main seam occupies the central part of the basin and the upper seam is found towards the margins of the Basin (Hager, 1993).

Sedimentation of the Lower Rhine Basin began during the late Oligocene as the North Sea breached the basin due to prior subsidence and resulting in the formation of shallow marine sediments (Schäfer *et al*., 1996). The Miocene marked the end of a cyclic sedimentation pattern caused by a number of North Sea transgressions and the marine habitat was succeeded by a coastal plain habitat dominated by swamp and forest ecosystems (Schäfer *et al*., 1996). The layers of peat that formed during this epoch created the lignite seams that are exploited today in the large scale open cast mining activities of RWE Power AG (see Figure 2.3).

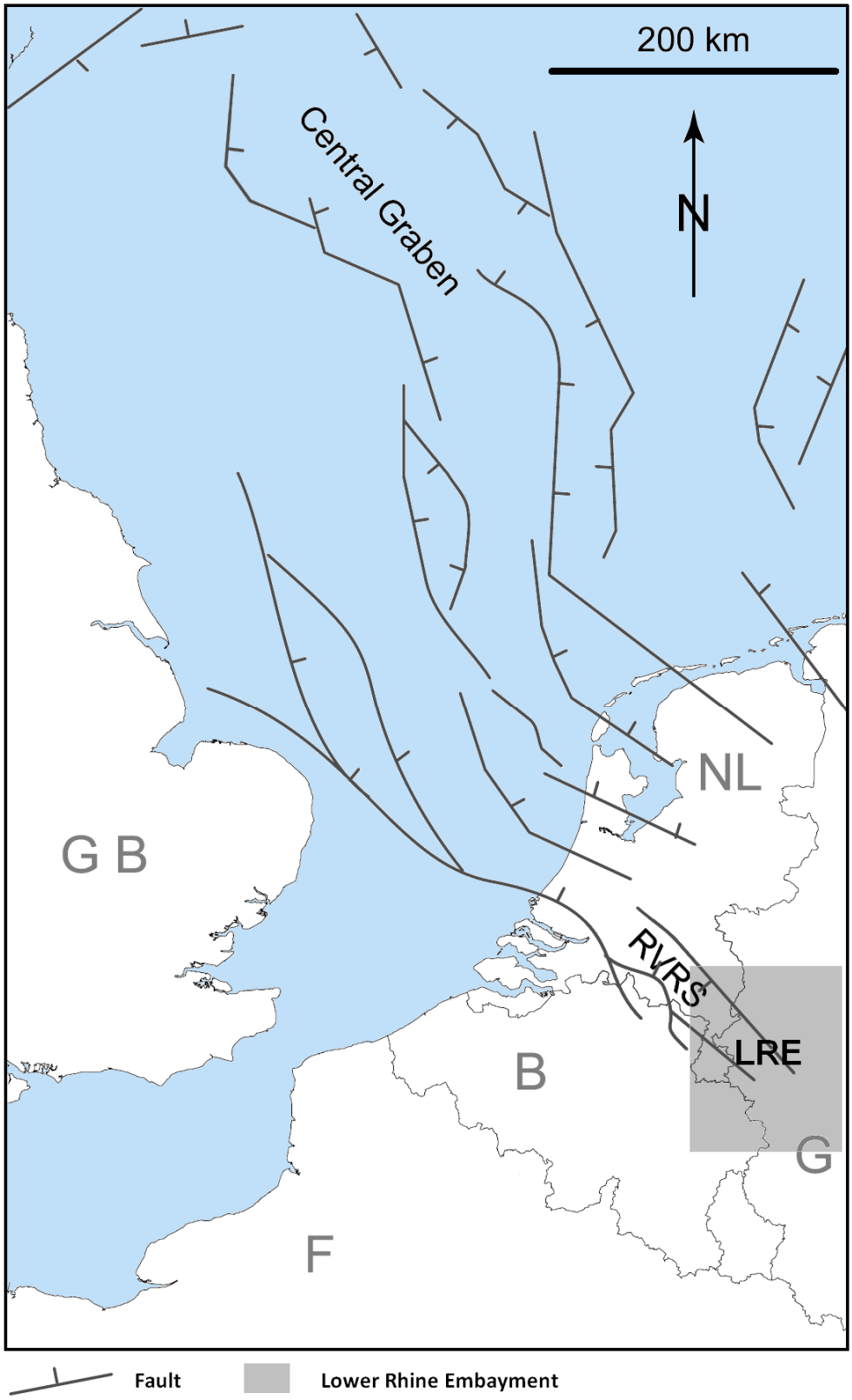

Figure 2.1. The Roer Valley Rift System (RVRS) and Lower Rhine Embayment (LRE) in Germany and The Netherlands with spatial reference to the North Sea Basin and including the major faults (after Bense *et al*., 2003).

During the Pliocene the North Sea retreated further providing an opportunity for a number of fluvial systems to develop and as the Lower Rhine Basin stabilised, terrace gravels of the river Rhine spread to cover the lowland areas. Schäfer *et al*. (2005) state that the sediments of the Lower Rhine Basin primarily consists of Oligocene, Miocene and Pliocene marine sediments and that the more recent Pleistocene sediments are mainly fluvial deposits derived from the Rhenish Massif in the south. The sediments derived purely from the Rhenish Massif are comprised of gravels that are characterised by having >90% quartz material in the coarse gravel fraction and the remaining sediment is made up of quartzites (Boenigk, 2002). Highly porous loess soils have formed due to the accumulation of wind blown silts, sands and clays, and these overlay the Pleistocene deposits. The reader is referred to Boenigk (2002) for a detailed mineralogical analysis of the shallow fluvial deposits of Pleistocene age, and to Kemna (2008) for the Pliocene and Lower Pleistocene deposits.

2.1.2. Deep sedimentary sequences and the crystalline basement

The geological structures that underlie the sediment deposits that form the deepest sand aquifers of Oligocene age are less well known. The oldest sequences identified from borehole records are Palaeozoic. It is known that carboniferous strata with a total thickness of up to 2.5 km is underlain by approximately 2 km of clastic sedimentary rocks, limestone and evaporites, and a Devonian sequence of unknown thickness and composition; which is believed to represent the beginning of the basement (Geluk *et al.,* 1994). The depth of the lower crust is given by the Mohorovičić Discontinuity which ranges from 27 km below the centre of the Roer Valley Graben to 30 km beneath the Peel Block (Figure 2.2) in the NW part of the Lower Rhine Embayment (Rijkers *et al.,* 1993). Lower Jurassic sandstone and

claystone sequences with a total thickness of up to 1.5 km are found beneath the Cenozoic sand deposits, and they overlie Permian-Triassic sandstone and conglomerate material (Geluk *et al.* 1994). A Cretaceous sequence is limited to the Peel Block and in this region separates the Cenozoic and Lower Jurassic strata (Geluk *et al*., 1994).

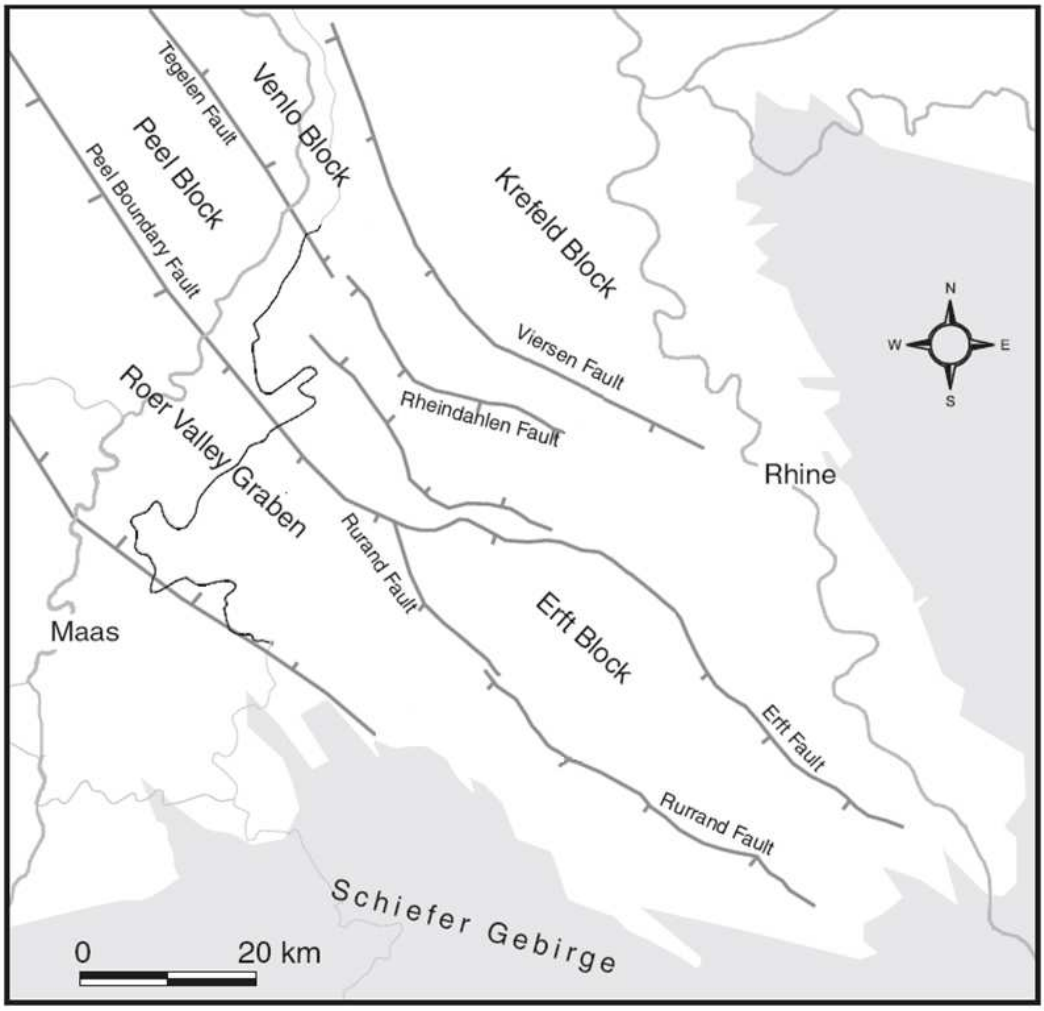

Figure 2.2. Overview map illustrating the tectonic structure of the Lower Rhine Embayment (shaded region in Figure 2.1) including the location of tectonic blocks and regionally significant faults. The shaded grey area represents the extent of the Schiefergebirge (Bense and van Balen, 2004).

2.1.3. Geological structures adjacent to the Lower Rhine Embayment

The Lower Rhine Embayment cuts into the headlands of the Rhenish Massif (Schiefergebirge) to the south, southwest and east (see Figure 2.2). This geological Massif is an uplifted region where Palaeozoic (mainly Devonian) strata outcrop. The Rhenish Massif is made up of the Ardennes and Eifel mountain belts to the west of the river Rhine and the Saulerland and Siegerland regions to the east of the river Rhine. The Aachen hot springs emanate from the Devonian limestone at the Variscan thrust front of the Rhenish Massif in close proximity to the western flank of the Lower Rhine Embayment. The hot springs of the Aachen region contain Na-Cl type groundwater that is believed to originate from the leaching of evaporites (Herch, 2000). Geochemical data suggests that the hot spring water has a meteoric origin but the exact recharge area is unknown (Herch, 2000). The occurrence of trace elements led Herch (2000) to conclude that the groundwater must have a long residence time and by using SiO_2-geothermometry Herch (2000) was able to estimate a circulation depth of >3.5 km. The deep circulating groundwater that emanates from hot springs in the Aachen region could help to elucidate the origin of deep basinal fluids that are found at shallow depth within the Lower Rhine Embayment (see Chapter 6).

To the west of the Ardennes lies the Paris Basin. The Paris Basin is a broad shallow bowl-like structure that consists of successive marine deposits of Triassic to Pliocene age and overlies a faulted basement. The Paris Basin has a diameter of 350 km and a maximum total thickness of 3 km. The Dogger aquifer is a middle Jurassic formation of oolites, marls and limestone. It is 500 m deep, has a total thickness of up to 230 m and overlies a Trias sandstone formation which forms the base of the aquifer system (Lavastre *et al.*, 2005). Overlying the Dogger aquifer is the Lusitanian limestone formation which contains marls that seal large parts of the system. Neocomian shales overlie the Lusitanian limestones, and the Albian formation which

consists of sandstones overlies the Neocomian shales (Marty *et al*., 1993). The entire system is confined by 500 m of clays, chalk, limestone and marls (Marty *et al*., 1993). The hydrogeology and geochemistry of the Paris Basin have been the focus of numerous studies and as a result is very well constrained (eg. Fontes and Matray, 1993; Matray *et al*., 1994; Pinti and Marty, 1995; Pinti *et al*., 1997; Castro *et al*., 1998; Marty *et al*., 2003; Lavastre *et al*., 2005; Lavastre *et al*., 2010).

2.1.4. Lignite deposits

Lignite is often referred to as brown coal. It is a brownish organic sedimentary material with characteristics that place it between peat and sub-bituminous coal:

Peat → Lignite → Sub-Bituminous Coal → Bituminous Coal → Anthracite

Lignite has a soft woody texture and is formed in swamp-like ecosystems. It is considered as the lowest grade of coal because of its low energy density and has a carbon content of 25-35%. The progression of peat through to anthracite represents organic metamorphism caused by exposure to heat, burial pressure and compaction over time. The burial and compaction of peat creates lignite – considered to be a low grade immature coal. As lignite matures and undergoes further organic metamorphism, the oxygen and hydrogen content decreases and the carbon content increases leading to a harder and darker material that is classified as sub-bituminous coal. Further organic metamorphism creates bituminous coal, whilst anthracite represents the highest rank of coal and ultimate maturation with a carbon content of over 87% (Tucker, 2003).

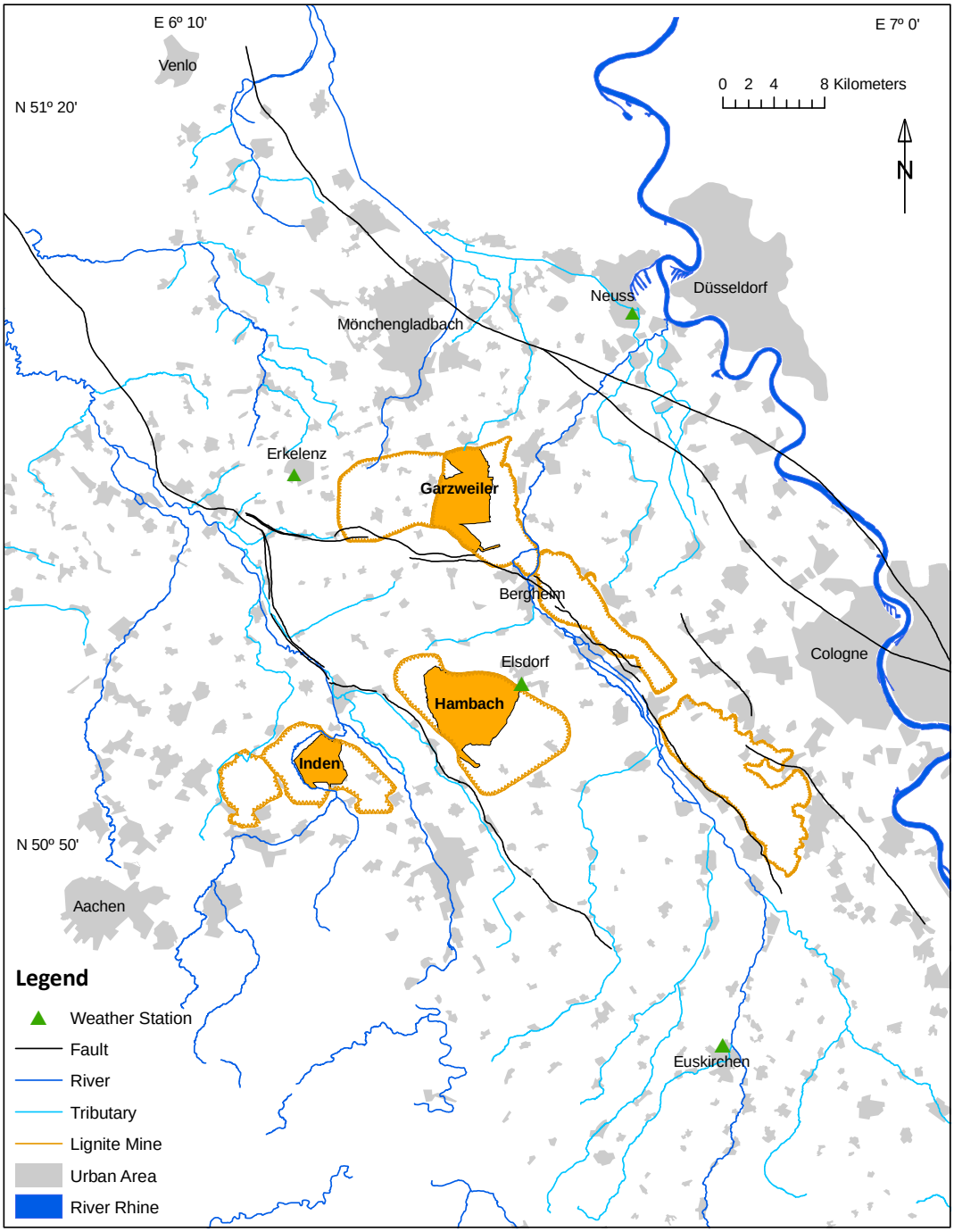

Figure 2.3. An overview map illustrating the location of the Garzweiler, Hambach and Inden lignite mines in the Lower Rhine Embayment. These are currently the only active mines but the orange outlines show the boundary of previous mines (Fortuna, Bergheim and Frechen) E and SE of Bergheim that have since been restored for recreational use and useable farmland.

The lignite deposits of the Lower Rhine region form one of the largest reserves in Europe. The region has an estimated reserve base of 55,000 Mt (Hager, 1993) and operations are scheduled to continue until 2045. Lignite deposit boundaries are established by the observed thinning of the seam and significant downward displacement by tectonic activity – lignite seams have been displaced by up to 500 m along fault planes in some areas (Hager, 1993). The Miocene lignite deposits of the Rhine Basin are characterised by a moisture content of 50-60%, an ash content of 1.5-8.0%, a sulphur content of 0.15-0.50% and a heat value of 7.8-10.5 MJ kg^{-1} (RWE Power AG). The lignite reaches a depth of 500 m and is overlain by more recent clay, sand and gravel deposits (Figure 2.4). The overburden thickness can be up to 300 m (RWE Power AG). A large proportion of the lignite mined in the Lower Rhine Embayment is used as fuel at five large power stations in close proximity to the open cast mines. For a comprehensive analysis of the Lower Rhine Basin lignite deposits and their formation the reader is referred to Mosbrugger *et al*. (1994).

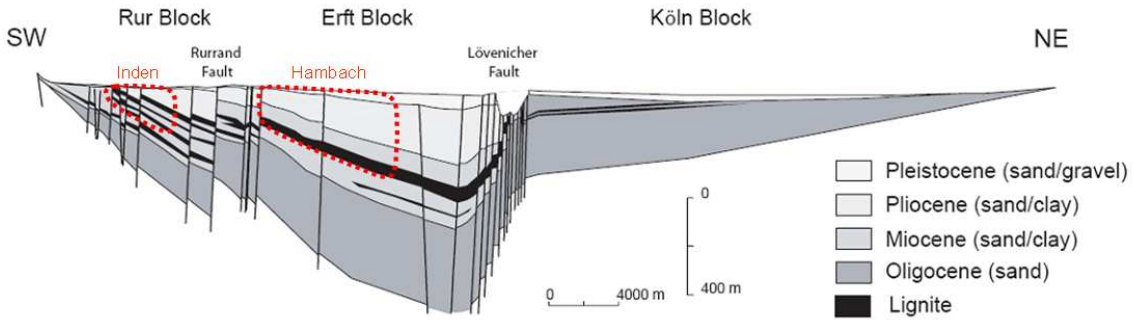

Figure 2.4. Geological cross-section illustrating the position of the main lignite seams and the location of the open cast lignite mines; Hambach and Inden (after Bense *et al*., 2008).

The Hambach, Garzweiler and Inden mines (Figure 2.3) are currently the only active mines in the region. The Hambach mine exploits the main lignite seam within the Erft block (see Figure 2.4). The Garzweiler I and II mines (Figure 2.5) are located at the southern edge of the Venlo block whilst the Inden mine exploits a number of smaller seams that occur in the Rur block. Earlier mining activities were focused along the Lövenicher and Erft faults where the lignite seam was typically at shallow depth. The Fortuna, Bergheim, Frechen and Ville mines that were situated along the Erft fault from NW-SE respectively (Figure 2.3) are now redundant and have been filled with spoil from the currently active mines. It is stated by the Erftverband (2006) that the land has subsequently been restored to useable farmland and land used for recreational purposes.

Figure 2.5. A view of the Garzweiler II open cast mine in 2009 and the lignite fuelled power stations in the distance. Note the large spoil deposit to the left of the power stations.

2.2. Hydrogeology

2.2.1. The multi-layered aquifer system

The German region of the Lower Rhine Embayment consists of five tectonic blocks. The central Erft block is adjacent to the Köln block to the east and the Rur block to the west whilst the Krefeld and Venlo blocks are situated northeast and northwest respectively (see Figure 2.2). Each of these tectonic blocks contains unconsolidated siliciclastic sedimentary deposits of up to 1300 m thick that produce a complex multi-layered aquifer system consisting mainly of sands and gravels and intercalated with low permeability clays and two main lignite seams (Figure 2.6). RWE Power AG has produced a hydrogeological schematisation (RWE-Reviermodell) of the multi-layered aquifer system for each tectonic block (Figure 2.6). This schematisation forms the basis for deriving model layers that have subsequently been used to generate hydraulic head contour maps for each of the main aquifer sequences using observation borehole data from the 1970s to the present day. Examples of these model outputs are given in Figure 2.9 and include four aquifer sequences ranging from shallow to deep using borehole data from 2005. Borehole logs provided by the Erftverband illustrate that the stratigraphy is more complex than the hydrogeological schematisation first suggests (Figure 2.8). Aquifer media and thickness vary on a local scale to some extent in many areas and this can have an impact on local groundwater flow patterns, especially where low permeability clay layers are present. Figure 2.7 and Figure 2.8 represent observation boreholes that are just 2 km apart with no geological boundaries or features partitioning them. The lithology and stratigraphy both display a degree of disparity. However, the large regional discontinuous nature of the aquifers, primarily due to the juxtaposition of fault bounded tectonic blocks that create a horst-graben system, has a much larger impact on groundwater flow dynamics than small local variations.

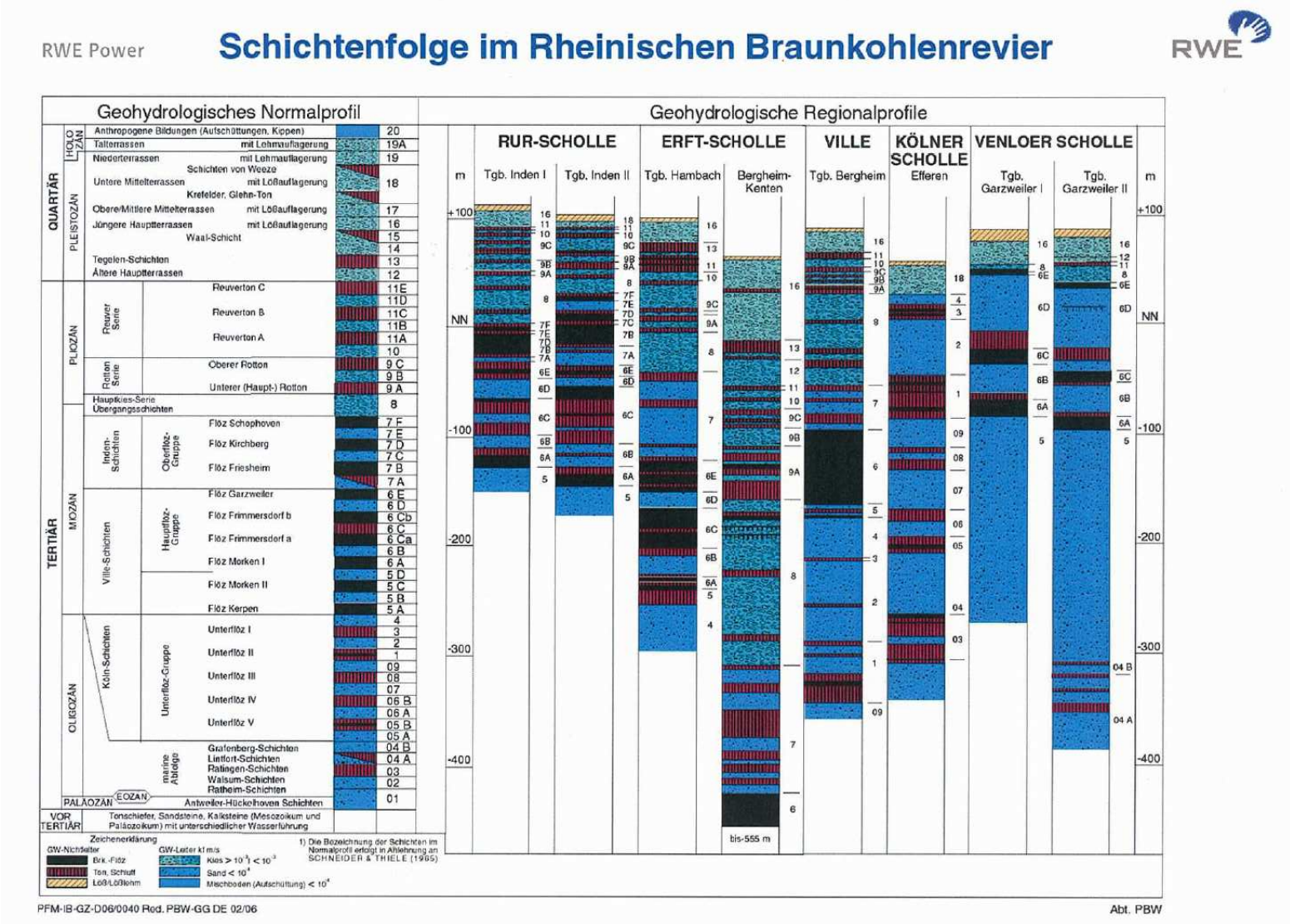

German
Brk-Flöz
Ton, Schluff
Löß
Kies
Sand
English
Lignite Seam
Clay, Silt
Loess
Gravel
Sand

Figure 2.6. The complexity of the multi-layered aquifer system is illustrated by the hydrogeological schematisation of each tectonic block in the Lower Rhine Embayment (RWE Power AG).

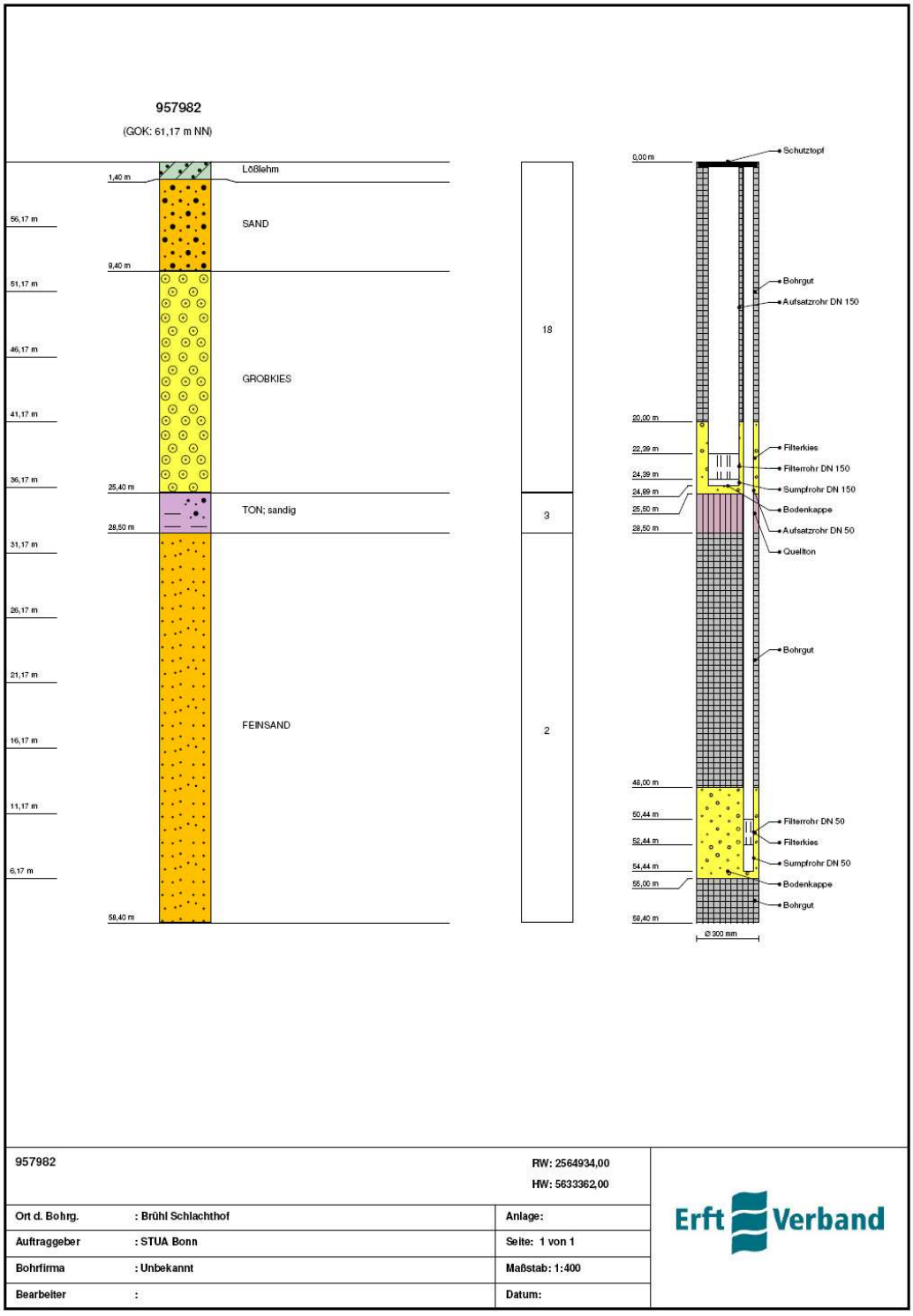

German
Brk-Flöz
Ton, Schluff
Löß
Kies
Sand
English
Lignite Seam
Clay, Silt
Loess
Gravel
Sand

Figure 2.7. Borehole log for the Brühl 1 piezometer nest. Borehole identification numbers are 27/957981 and 27/957982 for the shallow and deep piezometers respectively. Note the 3 m thick confining clay layer between 25 m and 28 m and a shallow sand sequence below the loess.

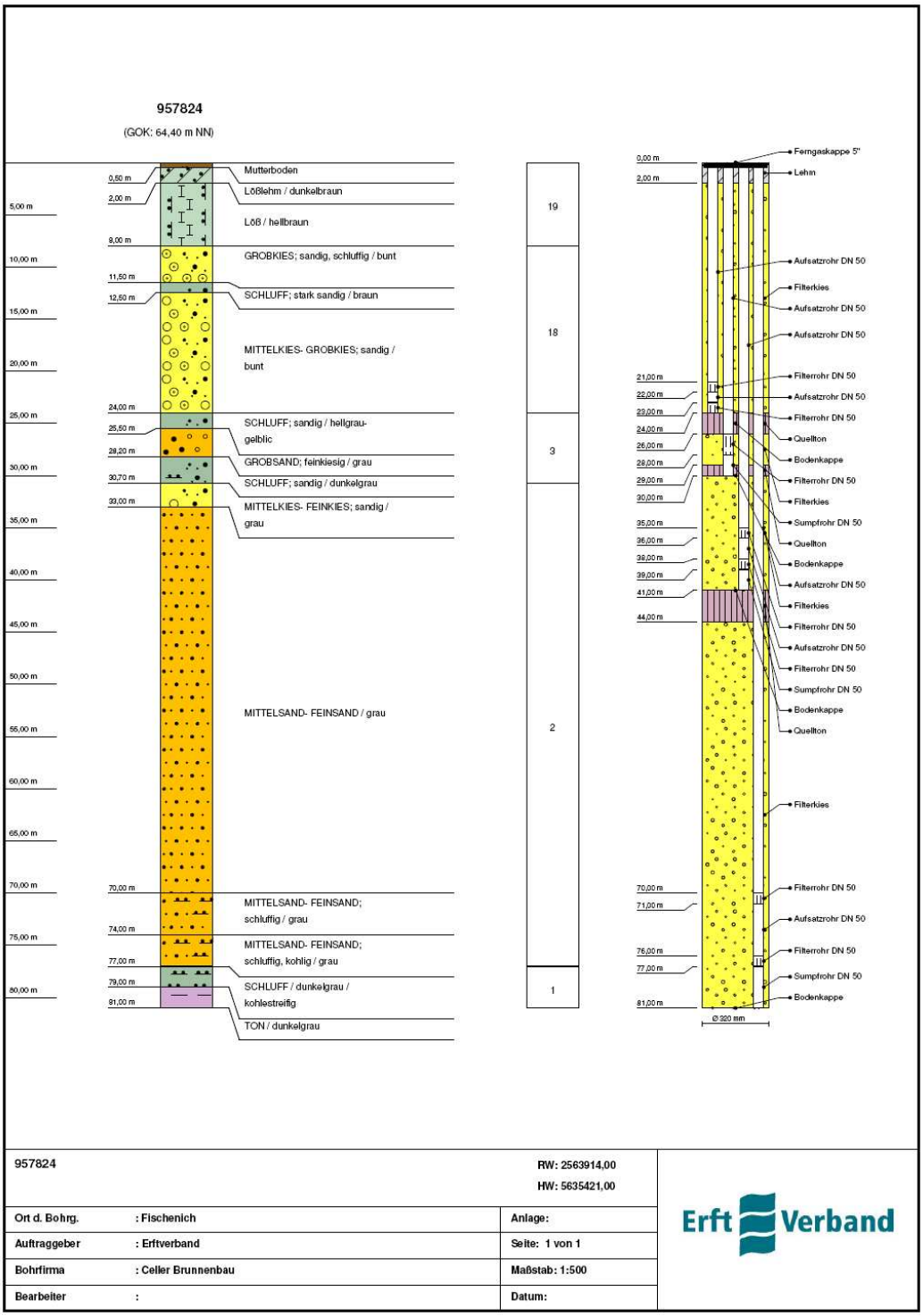

Figure 2.8. Borehole log for the Fischenich piezometer nest. Borehole identification numbers are 27/957822, 27/957823 and 27/957824 for the shallow, intermediate and deep piezometers respectively. Note the absences of the 3 m thick clay layer and the shallow sand sequence, along with the additional silt and loess deposits.

2.2.2. Regional flow patterns

Regional groundwater flow patterns have been determined by examining the hydraulic head distribution within each tectonic block. This was first completed on a regional scale in the 1960s by the Erftverband, whilst Wallbraun (1992) looked at the impact of faults on hydraulic head distribution in the Lower Rhine Embayment as part of a PhD Thesis and the findings were also later reported by Bense (2004). This approach is made quite complicated by the large number of aquifer units that have been identified in the layered system (Figure 2.6). Each aquifer responds differently to the groundwater abstraction that occurs at each of the large open cast lignite mines (see Figure 2.9). Regional lowering of the water table can be observed to a greater extent in some of the deeper aquifer layers and is essentially dependent upon the depth at which groundwater is abstracted ie. the specific aquifer sequence and the connectivity of the aquifer layers. It can be seen from Figure 2.9 that hydraulic head distribution varies significantly between each fault bounded tectonic block. The largest influence on hydraulic head is clearly mine de-watering and the cone of depression that exists beneath each of the major lignite mines provides good evidence to support this (see Figure 2.11). However, it can also be seen that in some areas the major graben fault structures act as sealing mechanisms and support large hydraulic head gradients (eg. the Rurrand Fault) but in other areas fault zones appear to have little influence on horizontal groundwater flow and hydraulic head distribution. Therefore, spatial variability in fault zone permeability must exist as a result of the physical properties of a given fault and due to various deformation processes that commonly occur in sedimentary faulted basins such as cataclasis, diagenesis and clay smearing (see Section 2.4.2). In many cases the juxtaposition of an aquifer unit against sealing lithology as a result of faulting, and the relative thickness of each unit

is the most likely cause of the observed hydraulic head gradients across some of the fault zones in the Lower Rhine Embayment (Wallbraun, 1992).

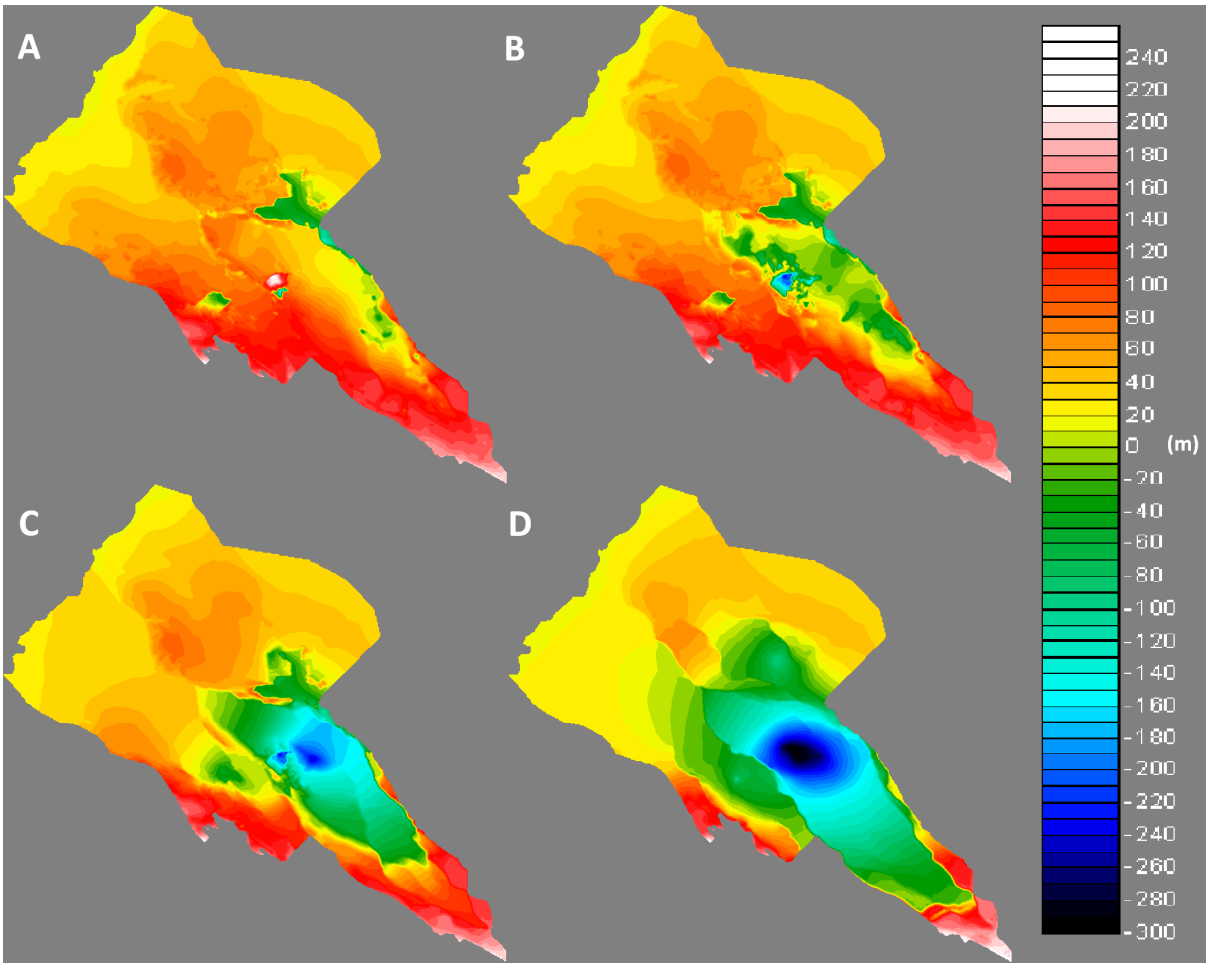

Figure 2.9(A-D). Model generated hydraulic head distribution of the Lower Rhine Embayment using RWE's hydrogeological schematisation (Figure 2.6) of the aquifer layers and based on observation borehole data from 2005. The model outputs A to D represent increasing aquifer depth, with the deeper aquifers being impacted to a greater extent by lignite mine de-watering than the shallow aquifers (RWE-Reviermodell, Erftverband).

The observation boreholes situated in the Lower Rhine Embayment are generally not used for pumping test purposes but the hydraulic properties of the aquifer system have been modelled extensively in terms of hydraulic conductivity by RWE Power AB using their groundwater model (Figure 2.10). According to the model results, the sand and gravel aquifers have a typical hydraulic conductivity in the range of 10^{-6} m s^{-1} indicated by the blue shaded regions in Figure 2.10, but also increase to 10^{-3} m s^{-1} in some areas. Investigations made by the Ruhr-University Bochum found the total porosity to be 39% and the effective porosity to be between 20 and 26% using model simulations (pers. comm. Nils Cremer, 2010). The typical range for total porosity and effective porosity values for unconsolidated sedimentary deposits are given in Table 2.1 and are in agreement with the modelled results.

Table 2.1. Typical values of porosity for unconsolidated sedimentary deposits.

Deposit	**Total porosity**	**Effective porosity**
	(%)	
Gravel	25-40	13-44
Sand	25-50	16-46
Silt	35-50	1-39
Clay	40-70	1-18

(Freeze and Cherry, 1979)

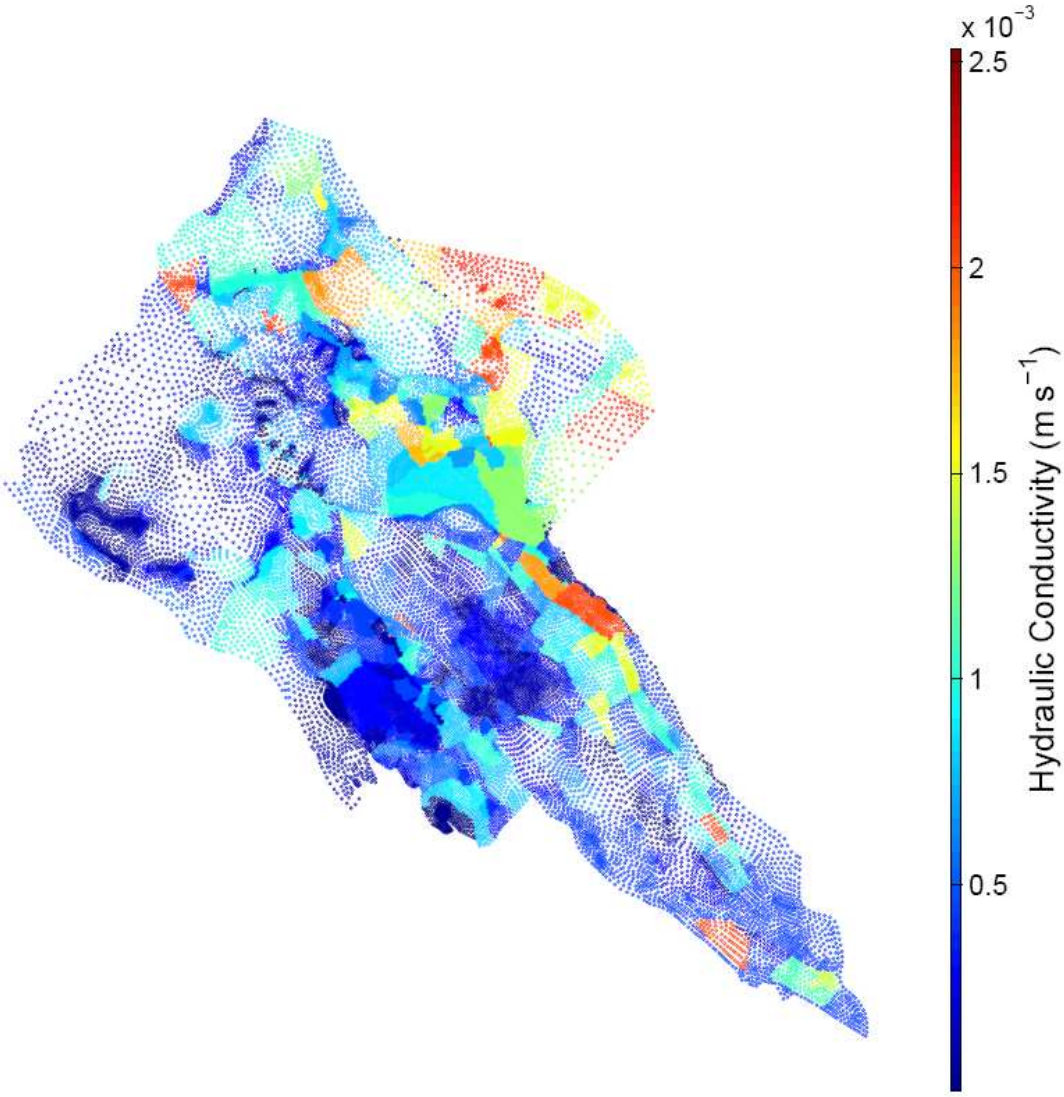

Figure 2.10. Hydraulic conductivity of the Lower Rhine Embayment based on RWE's groundwater model for the entire lignite mining region (RWE-Reviermodell, Erftverband).

2.2.3. Groundwater conditions and recharge zones

The aquifer units of the Lower Rhine Embayment are intercalated with clay layers and several lignite seams of low permeability. Figure 2.9A provides evidence that large scale lignite mine de-watering has less impact on the shallow aquifer layers because the level of groundwater drawdown is lower than that observed in the deeper aquifers from which the groundwater abstraction occurs (Figure 2.9C and Figure

2.9D), suggesting that there is limited connectivity between aquifers in these areas and allowing perched water table conditions to develop in the upper part of the aquifer system.

The direction of groundwater flow on a regional scale is generally from south to north. On a local scale, groundwater flow is influenced by topographic features and natural discharge areas include the Rhine and Maas rivers (Bense, 2004). However, large scale lignite mine de-watering has created enhanced groundwater flow conditions and combined with the sealing properties of the major graben faults, has significantly altered natural groundwater flow conditions as well as creating additional discharge areas. The large lignite mines of Hambach, Inden and Garzweiler are now essentially acting as artificial discharge zones.

Recharge zones are typically indicated as topographically elevated areas where the water table reaches a maximum height (Freeze and Cherry, 1979). By analysing the hydraulic head distribution in the shallow unconfined aquifers (Figure 2.9A) one can deduce that the most important groundwater recharge zones are located in the south and along the south western flank of the Lower Rhine Embayment, in areas where the topographic elevation and potentiometric surface reach a maximum. The Erftverband has recently implemented an artificial recharge programme in an area northwest of the Garzweiler lignite mine in an attempt to resolve some of the problems associated with the regional lowering of the water table (pers. comm. Nils Cremer, 2008). Herrmann *et al*. (2009) conducted a groundwater recharge rate modelling study of the Lower Rhine Embayment which focussed specifically on direct recharge to the shallow Pleistocene deposits of the Rur Block. Herrmann *et al*. (2009) calculated a mean recharge rate of 170 mm $year^{-1}$ for the Rur Block region which equates to approximately 25% of the precipitation received.

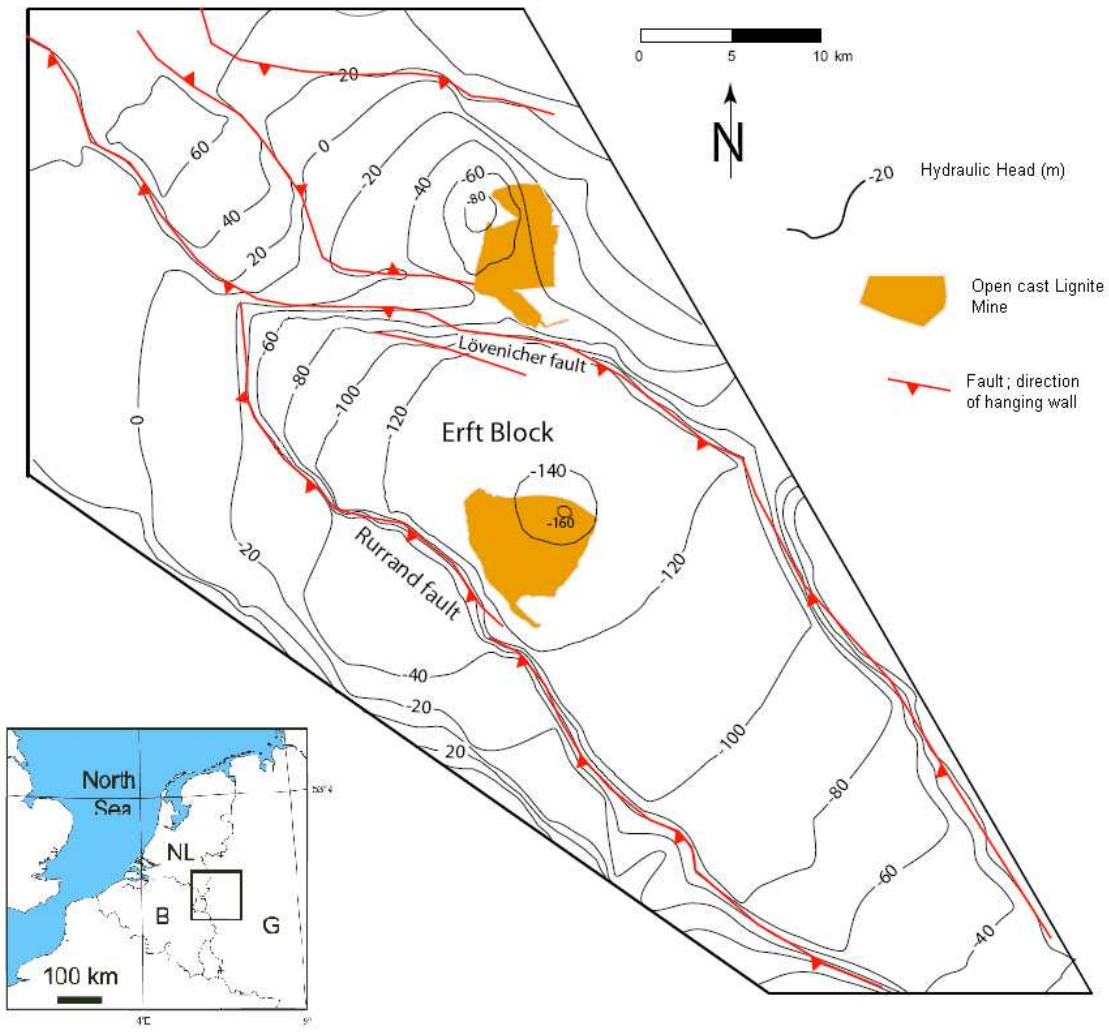

Figure 2.11. Hydraulic head distribution within the deeper aquifer system of the Lower Rhine Embayment (Figure 2.9D) with spatial reference to the Hambach and Garzweiler lignite mines. Note the cone of depression below each mine created by de-watering (after Bense *et al*., 2008).

2.2.4. Local groundwater usage and management

The required water supply from the Erftverband territory is 642 million m^3 per year for a human population of 2.7 million as well as for industrial purposes (Erftverband, 2006). Another 500 million m^3 per year is pumped from lignite mines for de-watering purposes (Erftverband, 2006). Water abstraction on this scale causes a regional lowering of the water table with many wells drying out in recent years. The

baseflow of nearby rivers and streams has also decreased and this has led to a quantifiable change in habitat and a loss of biodiversity (Erftverband, 2006). In an attempt to reduce the impact of groundwater abstraction, about 10 million m^3 of the 'mine' groundwater is cleaned each year and pumped back into endangered wetland habitats and rivers and as part of an experimental artificial recharge programme (pers. comm. Nils Cremer, 2008).

2.3. Hydrology and Meteorology

2.3.1. Surface waters of the Erft catchment

The river Erft is the primary river system in the central region of the study area and is a tributary of the river Rhine that flows from south to north in the eastern part of the Lower Rhine Embayment. The river Erft was naturally a small tributary of the Rhine but it is currently being used as a conduit for channelling large quantities of groundwater from nearby open cast lignite mines (Erftverband, 2006). The Erftverband state that in order to accommodate this volume of water the course of the river Erft has been altered and the discharge has increased significantly. In many areas the course of the river has been artificially straightened to form long sections of featureless habitat and fish stocks have failed to adapt to increased flow rates and temperatures and the general loss of biodiversity (Erftverband, 2006). The Erftverband continually monitor water quality parameters and has established numerous river gauging stations that provide essential flow data for the river Erft and its tributaries. The Erftverband intends to restore the natural meandering course of the river Erft at the end of mining operations in 2045.

2.3.2. Climate and precipitation

The prevailing climatic conditions are of great significance to hydrogeological studies, catchment management programmes and the assessment and monitoring of regional climate change. Both long-term and seasonal variations in temperature and precipitation affect the recharge regime of the regional aquifer system and influence the stable isotope composition of groundwater at the time of recharge as well as influencing the hydrochemistry of ground- and surface waters. Climate monitoring stations were established in the Lower Rhine Embayment at a number of locations during the 1950s to improve the resolution of existing data. The Erftverband undertake regular and routine data collection and monitoring of the regional climate system and have provided detailed temperature and precipitation data from four weather stations within the Lower Rhine Embayment for the purposes of this research. The precise locations of these weather stations can be seen in Figure 2.3.

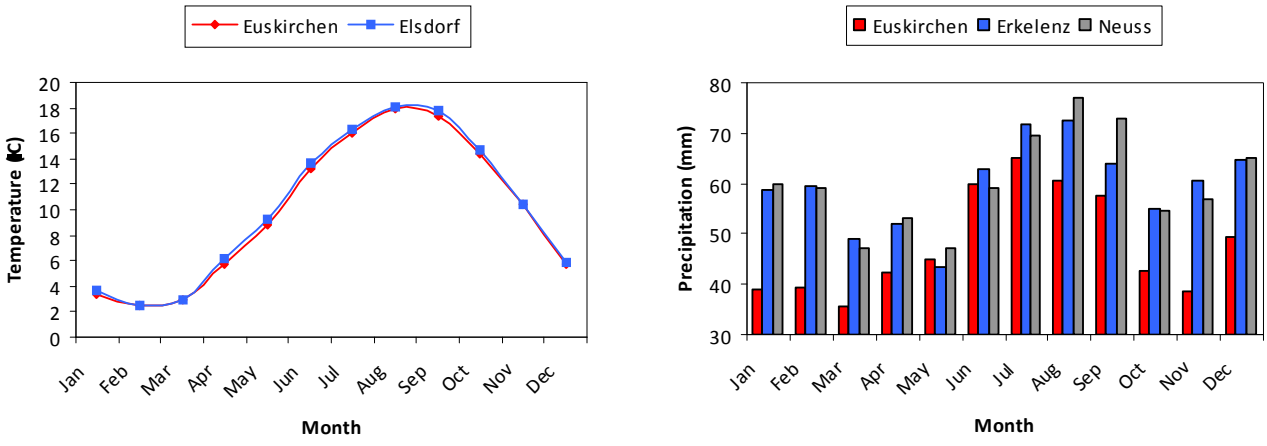

Figure 2.12. A. The weather stations at Euskirchen and Elsdorf exhibit an identical trend in average monthly temperatures over the period from 1951-2009. B. Median monthly precipitation values for the period 1951-2009 from Euskirchen, Erkelenz and Neuss.

Average monthly temperatures have been calculated from temperature records obtained from the Euskirchen and Elsdorf weather stations for the period 1951-2009 and displayed in Figure 2.12A. The average monthly temperature recorded at the Euskirchen and Elsdorf monitoring stations both reach a peak during August at approximately 18 ºC and the lowest average monthly temperature occurs in February at 2.4 ºC. Precipitation gauging occurs at 73 locations within the Erftverband territory. For the purpose of this study data from three gauging stations (Erkelenz, Neuss and Euskirchen) have been used as they all provide detailed precipitation records dating from 1951-2009. Some small differences are evident between each of the gauging stations but the general trend is represented in Figure 2.13. The highest level of precipitation occurs during the summer months of July and August with approximately 65-75 mm of rainfall.

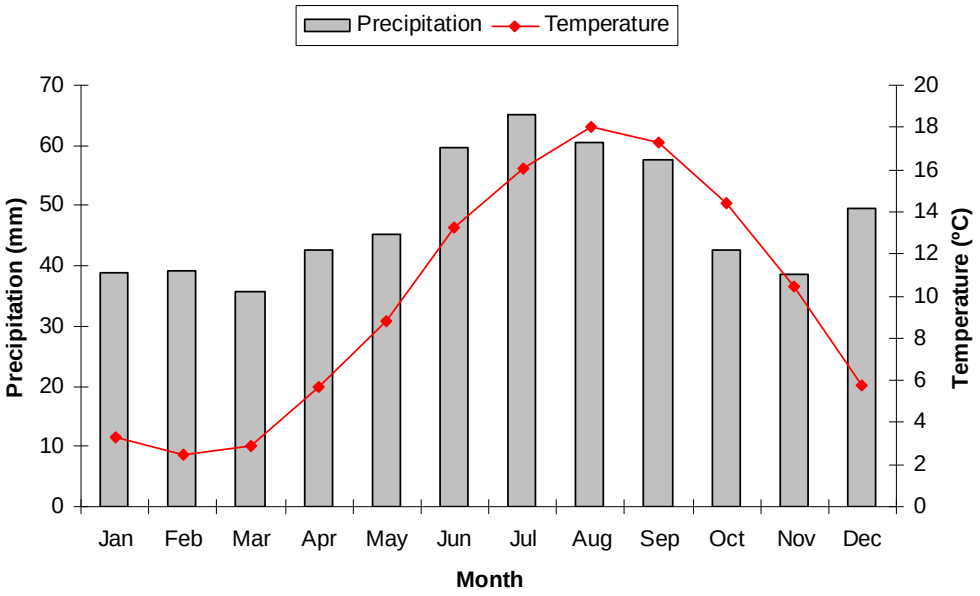

Figure 2.13. Climograph of data collected from the Euskirchen weather station located south of the lignite mining region of the Lower Rhine Embayment. The data represents median monthly values from 1951-2009.

The isotopic composition of precipitation is also of great interest, especially when utilising environmental isotope tracers in groundwater studies (Gat, 1996). The IAEA Global Network for Isotopes in Precipitation (GNIP) programme was established to determine the temporal and spatial variations of environmental isotopes in precipitation. Knowledge of the current regional isotopic composition of meteoric water such as the average annual $\delta^{18}O$ value can be particularly useful in providing evidence for recharge provenance and groundwater residence times.

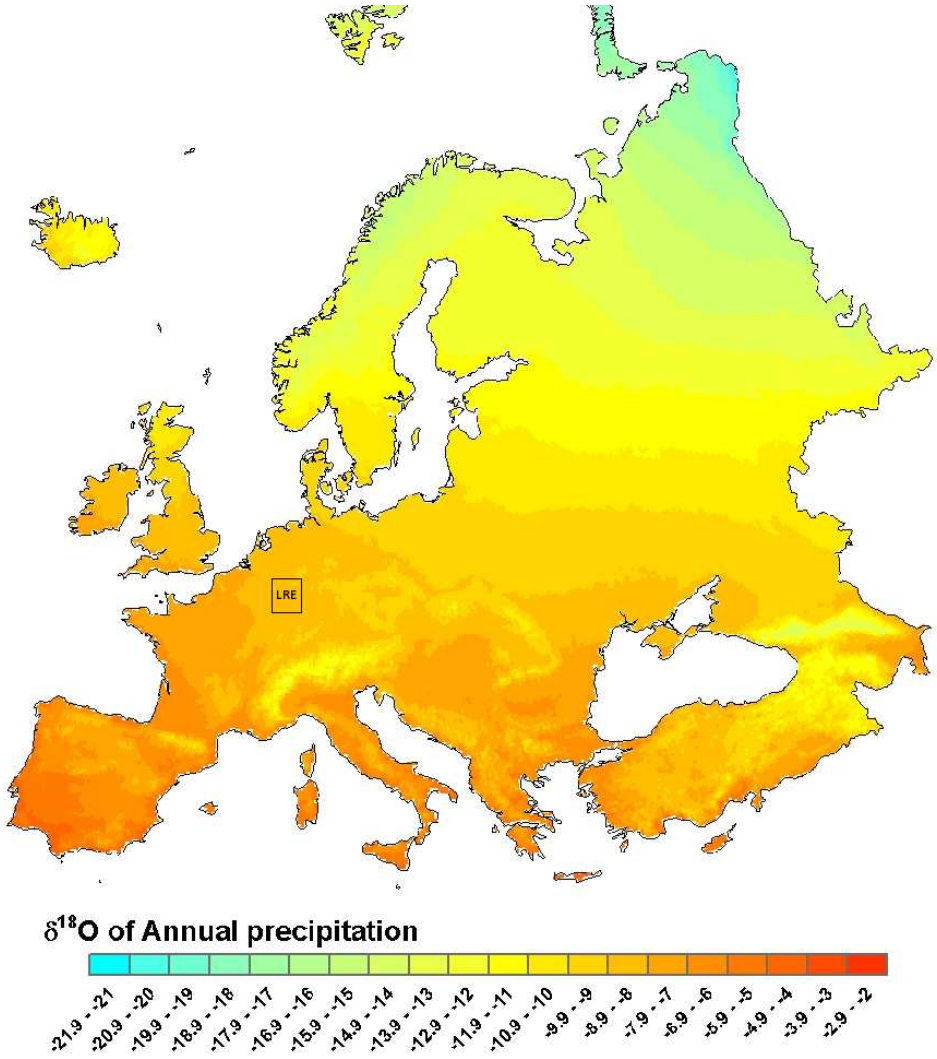

Figure 2.14. Long-term annual average $\delta^{18}O$ values for precipitation. Precipitation has a value of -8 – -7‰ under current climatic conditions in the region of the Lower Rhine Embayment (Bowen and Revenaugh, 2003).

The isotopic composition of precipitation is strongly correlated to mean annual surface temperature (Dansgaard, 1964; Fricke and O'Neil, 1999), and has formed the basis of numerous palaeoclimate studies (eg. Vaikmäe *et al*., 2001; Rozanski, 1985).

2.4. Fault Zones

The faults that developed in the Lower Rhine Embayment are described as normal faults. Normal faults are characterised by having a fault plane that is vertical or dipping towards the downthrown side of the fault (Figure 2.15). Normal faults are a consequence of lithosphere stretching and form key structural features in many sedimentary rift basins such as the Lower Rhine Basin. The normal faults that develop in extensional basins are often segmented and consist of numerous overstepping segments (Bense and van Balen, 2004). As a consequence of overstepping segmented normal faults, fault relay structures often develop and typically form areas of hydraulic contact between otherwise isolated groundwater reservoirs (Bense and van Balen, 2004). The reader is referred to Bense and van Balen (2004) for an analysis of relay structures in the Lower Rhine Embayment.

The fault zones of the Lower Rhine Embayment can also be described as synsedimentary (or growth faults) in that during sedimentation, the active fault significantly influences sediment deposition resulting in thicker and generally more sand dominated layers of strata forming on the downthrown side in comparison to the time-equivalent formation of strata on the upthrown side (Childs *et al*., 2003). The reader is referred to Childs *et al*. (2003) for a detailed account of synsedimentary faults.

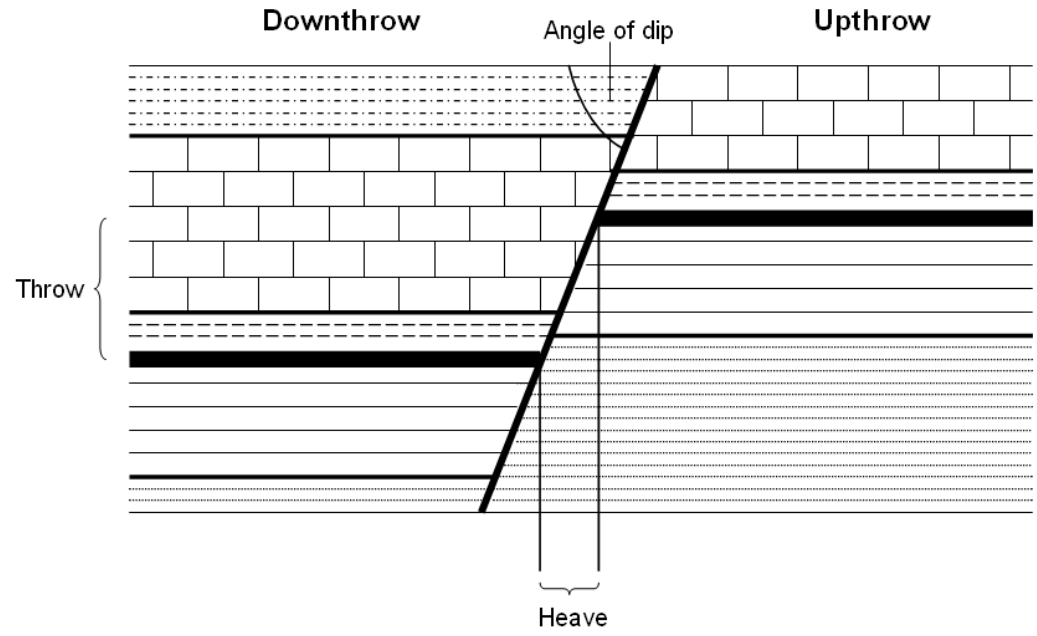

Figure 2.15. An example of a cross section through strata displaced by a normal fault.

Synsedimentary normal faults have been exposed in the open cast lignite mines of the Lower Rhine Embayment. The synsedimentary normal faults were observed in an exposed deltaic sequence within the open cast mine known as Frechen and field measurements indicated that the average angle of dip for these faults in this region was 70º and fault throws were measured up to 100 m (Lehner and Pilaar, 1997).

2.4.1. Spatial distribution of faults

The Lower Rhine Embayment is a highly faulted region with a large number of NW-SE striking fault zones (Figure 2.16). Major block sealing graben faults such as the Erft, Rurrand and Peel Boundary faults have a fundamental impact on groundwater flow within the Lower Rhine Embayment. In combination with enhanced flow conditions caused by current large scale lignite mine de-watering, faults influence groundwater flow patterns in many areas. The most notable features are the large hydraulic head gradients that exist across faults that separate adjacent tectonic blocks (Figure 2.11). Figure 2.16 illustrates the spatial distribution and high density of fault zones in the Lower Rhine Embayment as well as showing the proximity of the lignite mines in relation to the major faults that bound each of the tectonic blocks. For an overview map of the tectonic blocks the reader is referred back to Figure 2.2. However, although regionally significant fault zones clearly have a large influence on groundwater flow dynamics, smaller faults have also been shown to influence groundwater flow patterns on a local scale (eg. Ernst and De Ridder, 1960).

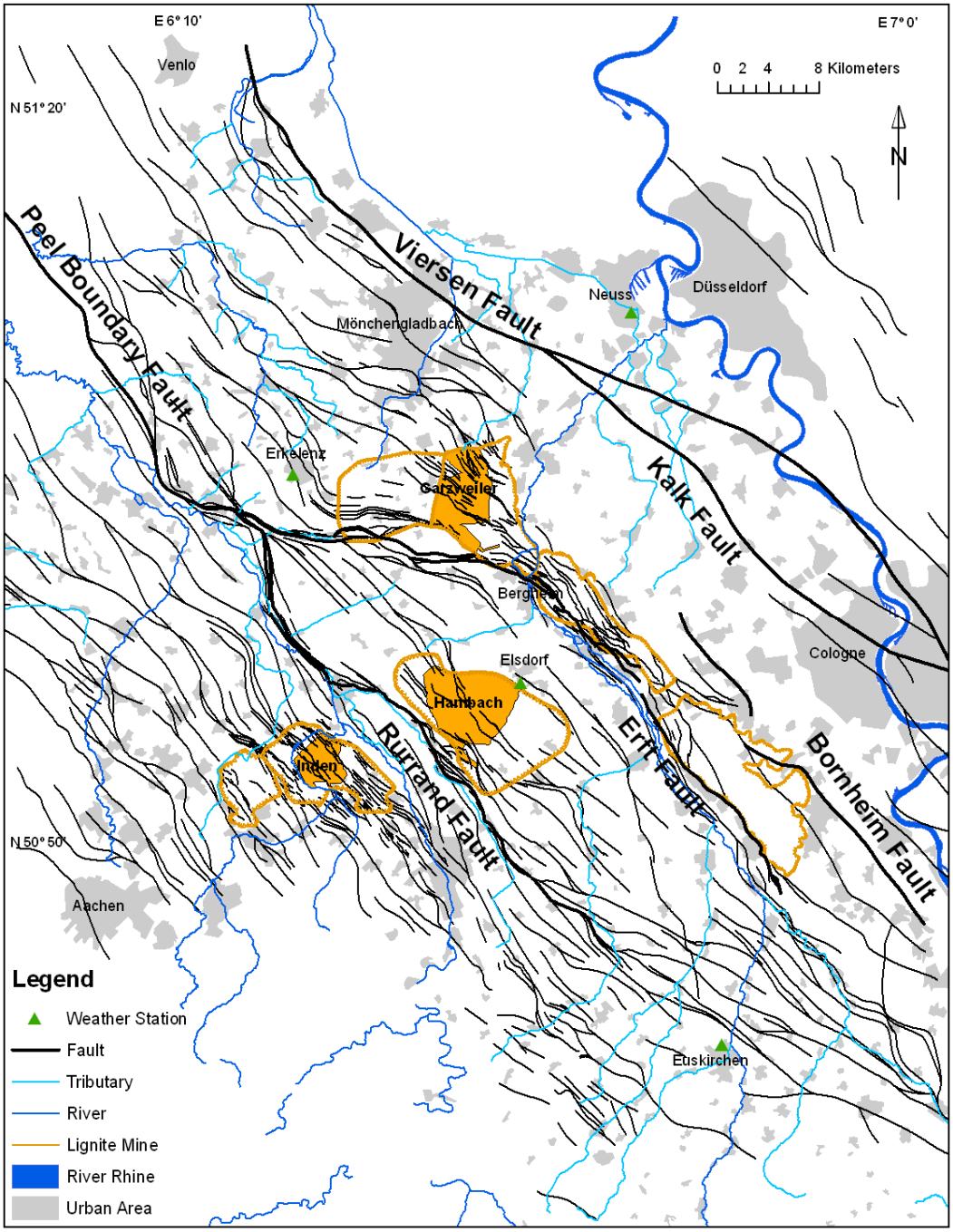

Figure 2.16. Spatial distribution of faults in the Lower Rhine Embayment, Germany.

2.4.2. Deformation processes within fault zones

The physical and chemical properties of a fault zone determine the distribution of porosity and permeability within the fault zone. Deformation processes play a key role in creating impermeable barriers, reducing porosity and permeability and/or creating preferential pathways. The main deformation processes that are important in understanding faults and their impact on groundwater flow in the Lower Rhine Embayment are cataclasis, diagenesis/cementation and clay smearing (Bense e*t al.*, 2003).

2.4.2.1. Sand

The deformation processes that involve sand require consideration based on the relative clay content of the sand material as this will have a strong influence on the significance of a given deformation mechanism and the resultant change in fault zone permeability and porosity.

For sand media that contains less than 10% clay, the active deformation mechanism varies as a function of depth and porosity (Fulljames *et al*., 1997). At shallow depths (<1.5 km) there are essentially only two important mechanisms – cataclasis and particulate flow. Cataclasis describes the process of grain crushing and grinding along discrete shear faults and results in sand grains that are relatively fine in comparison to the initial grain size (Fulljames *et al*., 1997). Subsequent compaction and potential cementation can reduce fault porosity and permeability quite significantly (Fulljames *et al*., 1997). Cataclasis is the most dominant deformation process at a depth of greater than approximately 1 km according to Fulljames *et al*. (1997) and often leads to a reduction in fault permeability. At shallower depths (<1 km), particulate flow becomes more common than cataclasis but during the transition from one process to the other it is possible that both processes occur simultaneously.

Particulate flow describes the displacement and sorting of sand grains with a corresponding increase in pore size which would lead to an increase in the hydraulic conductivity of the fault zone (Sperrevik *et al*., 2002) although data supporting this hypothesis is limited.

For sands with a clay content of greater than 10%, the compaction and mixing of sand will typically result in reduced bulk porosity and a more homogenous distribution of low permeability clay particles reducing the hydraulic conductivity of the fault zone.

2.4.2.2. Clay smearing

Clay smearing is a process where dragging or ductile flow of clay layers along the plane of a fault between blocks of strata on either side of the fault plane ie. the footwall and hanging wall; results in a clay smear along the fault plane (Caine *et al*., 1996; Rawling *et al*., 2001). The smear forms a continuous band of low permeability clay and is an important fault sealing mechanism that affects groundwater systems (see Figure 2.17). In recent years there has been increasing interest in fault sealing mechanisms such as clay smearing. This has been due to a need for an improved understanding of the formation mechanics and the sealing potential of faults with regard to proposed Carbon Capture and Storage (CCS) programmes, as faults could provide leakage pathways for sequestrated CO_2 in deep subsurface reservoirs (Bickle *et al*., 2007). However, the precise physical development of clay smears is still poorly understood. A number of authors have studied clay smearing at outcrop locations (Lehner and Pilaar, 1997; Van Der Zee and Urai, 2005; Bense *et al*., 2003) as well as creating laboratory experiments (eg. Schmatz *et al*., 2010; Cuisiat and Skurtveit, 2010; Sperrevik *et al*., 2000).

Clay smears that occur in some major faults of the Lower Rhine Embayment have a thickness of up to 1m (Lehner and Pilaar, 1997). The emplacement of this quantity of clay within a fault zone is possible due to a slight fault offset in the direction of the downthrown block (Lehner and Pilaar, 1997). Clay smearing can significantly reduce the permeability of fault zones, typically forming a seal to lateral groundwater flow (Egholm *et al*., 2008). However, drag or injection of sand along the plane of the fault adjacent to the clay smear has also been observed in laboratory experiments using ring shear apparatus (Cuisiat and Skurtveit, 2010) and a number of field studies (eg. Bense and van Balen, 2004; Houtgast *et al*., 2002). If the fault core; which consists of gouge, cataclasite and mylonite components (Caine *et al*., 1996), contains both clay and sand material, fault permeability is likely to be strongly anisotropic in that fault permeability will increase along the fault plane whereas fault permeability perpendicular to the plane of the fault will be significantly reduced forming an effective barrier against lateral groundwater flow (Bense and Person, 2006). Clay smears were observed in fault zone exposures during lignite extraction in the Frechen open cast mine by Lehner and Pilaar (1997). Clay smears in the Frechen mine ranged from a few centimetres in minor shear faults to 70 m in major graben faults and reached a thickness of 1 m in some places, although 10-20 cm was more typical (Lehner and Pilaar, 1997). The thickness and length of a clay smear is determined by the thickness and number of clay source beds within the throw window and the clay smear usually decreases in thickness with increasing distance from the source bed (Fulljames *et al*., 1997; Egholm *et al*., 2008).

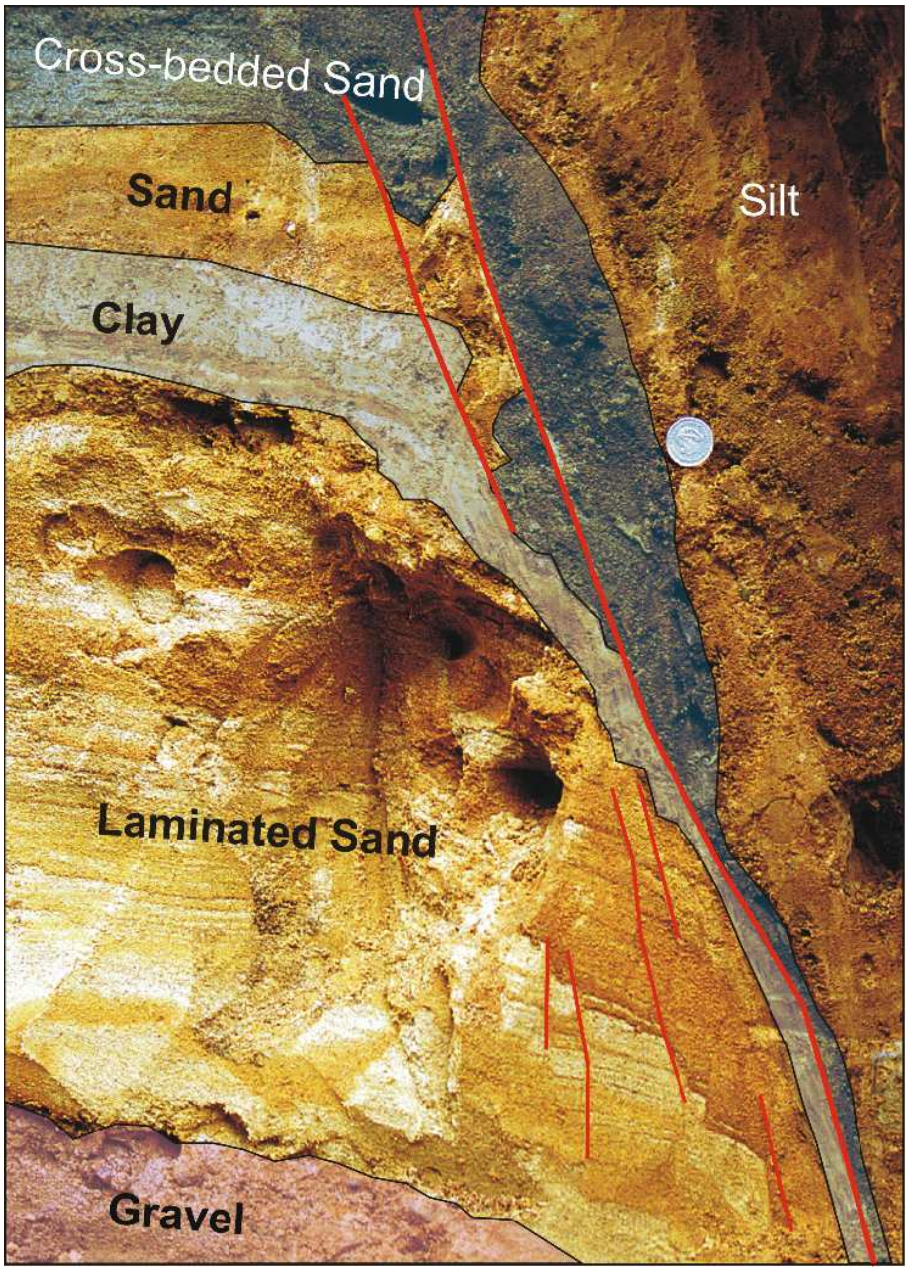

Figure 2.17. Clay smearing and sand drag/injection in the Lower Rhine Embayment (reproduced from Bense and van Balen, 2004).

2.4.2.3. Diagenesis

Diagenesis describes any physical or chemical change that occurs to sediments subsequent to their deposition, either during or after lithification. Such changes occur at relatively low temperature and pressure. Porosity usually decreases during

diagenesis and processes such as the mineral precipitation of iron and manganese oxides can cement porous fault zones to the extent that fault porosity is significantly reduced or completely eliminated (Chan *et al*., 2000).

2.4.3. Flow dynamics across and within fault zones

Large hydraulic head gradients observed across fault zones in the Lower Rhine Embayment suggest that faults often form effective barriers to lateral groundwater flow. The most straight forward explanation involves the juxtaposition of permeable aquifer media such as sand or gravel against impermeable confining layers of clay as a result of fault throw. However, deformation mechanisms such as clay smearing and diagenesis suggest that faults have the physical properties to form effective barriers to the lateral component of groundwater flow. This supports the conceptual model developed by Rawling *et al*. (2001) that fault zones in unconsolidated sediments frequently form barriers to lateral groundwater flow as a result of reduced fault permeability. However, fault zones that act as barriers to groundwater flow are not necessarily permanent features, and the formation of structural permeability networks can lead to a discontinuous fault seal resulting in a degree of leakage across the fault over time (Dewhurst and Jones, 2003). On the other hand, a fault may act as a conduit during deformation and then as a barrier when the pore spaces become cemented by mineral precipitation (Caine *et al*., 1996). Bense and Person (2006) describe faults in unconsolidated sediments as conduit-barrier systems where fault zone permeability is strongly anisotropic and vertical permeability is often much greater than horizontal permeability. In this situation, a fault zone will form an effective barrier to lateral groundwater flow as described by Rawling *et al.* (2001) and supported by the presence of large hydraulic head gradients across the fault, but the fault can

simultaneously act as a conduit for vertical groundwater flow connecting shallow and deep aquifer units that are typically isolated by an aquitard or aquiclude. Bense *et al*. (2008) present evidence for vertical conduit flow along faults in the form of thermal anomalies. Bense *et al*. (2008) conclude that numerical analysis of empirical geothermal data collected from observation boreholes in close proximity to the Rurrand fault in the Lower Rhine Embayment suggests that strong positive and negative thermal anomalies are transient features that result from upward and downward groundwater flow respectively within the fault zone. These features are believed to be the result of lignite mine de-watering and subsequent lateral flow into aquifer layers adjacent to the Rurrand fault and support the conduit-barrier model proposed by Bense and Person (2006). Stoessell and Prochaska (2005) studied the vertical movement of deep formation fluids along the Baton Rouge Fault in South Louisiana, USA. Hydrochemical and isotopic data such as Br/Cl, K/Cl and Na/Cl ratios, Mg^{2+} and SO_4^{2-} concentrations as well as $^{87}Sr/^{86}Sr$ isotope ratios provided strong evidence that suggested vertical conduit flow of deep saline formation fluids from depth to shallow aquifers along sections of the Baton Rouge fault and that these formation fluids were responsible for the observed brackish water in the upper aquifer. Another example of groundwater flow along faults was published by Chan *et al*. (2000). Chan *et al*. (2000) used isotopic evidence ($\delta^{18}O$, $\delta^{13}C$ and $\delta^{87}Sr$) and physical observations to suggest that deep reducing fluids flow upward along the Moab fault in Utah, USA mobilising iron and precipitating iron oxide (hematite) and manganese oxide as the deep groundwater mixes with modern oxygenated recharge near the surface. Fluid flow along the Moab fault is believed to occur as a multi-episode series of events due to the accumulation pattern of iron oxide mineralisation and the geometries of hematite concretions.

3. Dissolved Noble Gases and Stable Isotopes in Groundwater

Numerous environmental tracers have been utilised during this research in order to achieve the aims and objectives defined in Chapter 1. The geochemical tracers used include the dissolved noble gases of helium, neon, argon, krypton and xenon, and the stable isotopes of hydrogen, oxygen, carbon and strontium, as well as more routine hydrochemical tracers such as the major ions. Chapter 3 provides a critical review of noble gas and stable isotope geochemistry relevant to this study and outlines the necessary background information required for interpreting dissolved noble gas concentrations and stable isotope data for groundwater samples collected during 2007/08 from the Lower Rhine Embayment, Germany.

3.1. Dissolved noble gases in groundwater

The noble gases are a chemically inert group of elements that occupy group 18 of the periodic table. The noble gases that are typically applied in hydrogeological research include; helium (He), neon (Ne), argon (Ar), krypton (Kr) and xenon (Xe). The noble gas radon (Rn) has no stable isotopes and is rarely used in groundwater studies. However, radioactive ^{222}Rn (half-life of 3.8 days) has been used as a groundwater tracer in laboratory studies (eg. Hoehn *et al*., 1992). Noble gases are incorporated into the meteoric phase of the hydrological cycle by gas partitioning during air/water exchange reactions with the atmosphere. Noble gases are generally considered as conservative tracers in groundwater due to their low chemical reactivity. It is possible for the atmospherically derived noble gas component to remain constant in confined aquifers for long periods of time (10^5+ years) subsequent to a recharge event (Heaton *et al*., 1986). However, gas phase CO_2 present in the subsurface (such as a magmatic injection) in contact with the groundwater system can

'strip' dissolved atmosphere-derived and crustal/radiogenic noble gases by CO_2/water phase partitioning in the saturated zone (Gilfillan *et al.*, 2008).

The concentration of atmospherically derived noble gases dissolved in groundwater can be used to determine the temperature at the water table during recharge. This recharge temperature is often referred to in the literature as a Noble Gas Temperature (NGT), and if combined with groundwater age-dating techniques applicable to groundwater with a long residence time (eg. ^{14}C, ^{36}Cl and ^{81}Kr dating) it can be used as a tool for palaeoclimate reconstruction (eg. Andrews and Lee, 1979; Stute *et al.*, 1995a; Stute *et al.*, 1995b; Aeschbach-Hertig *et al.*, 2002; Lehmann *et al.*, 2003). Noble gases have also been shown to have useful applications in lake sediment pore waters as palaeolimnological (Strassmann *et al.*, 2005) and environmental change (Brennwald *et al.*, 2004) proxies.

3.1.1. Noble gases in meteoric and connate water

Noble gases in meteoric water are generally considered to be in solubility equilibrium with the atmosphere following Henry's Law for a dilute solution which is given by:

$$p_i = k_i(T,S) \cdot x_i \qquad (3.1)$$

Where, for a dissolved noble gas *i*, p_i is the partial pressure of the noble gas in the gas phase (fugacity), x_i is the equilibrium concentration of the dissolved noble gas as a mole fraction and k_i is a proportionality coefficient (Henry's Law constant) which is dependent on temperature (T) and salinity (S).

In many aquifer systems the groundwater consists entirely of meteoric water. However, in some deep circulating systems and in deep basement formations the

origin of groundwater is not always meteoric. Connate fluids describe water and dissolved minerals that were trapped within pore spaces during the formation of sedimentary aquifer systems. This groundwater is often referred to as juvenile water and its noble gas signature is largely unknown (Ozima and Podosek, 2002).

3.2. Noble gas components in groundwater

The origin of dissolved noble gas isotopes in groundwater typically has several components and these are illustrated in Figure 3.1. In addition to the atmospherically derived component, there are two other important non-atmospheric sources of noble gases in groundwater. These include the *in situ* radiogenic production of noble gases and terrigenic helium which describes an external flux from either the Earth's crust or mantle. The anthropogenic isotopes of ^{3}H and ^{85}Kr are particularly important for age-dating modern groundwater in the range of 0-60 years and are discussed in Section 3.4.2. However, both anthropogenic and cosmogenic isotopes have a negligible effect on total noble gas concentrations in groundwater. In general, groundwater of meteoric origin can be considered as a mixture of atmospherically derived noble gases and varying quantities of radiogenic noble gases and/or terrigenic helium (Kipfer *et al.*, 2002).

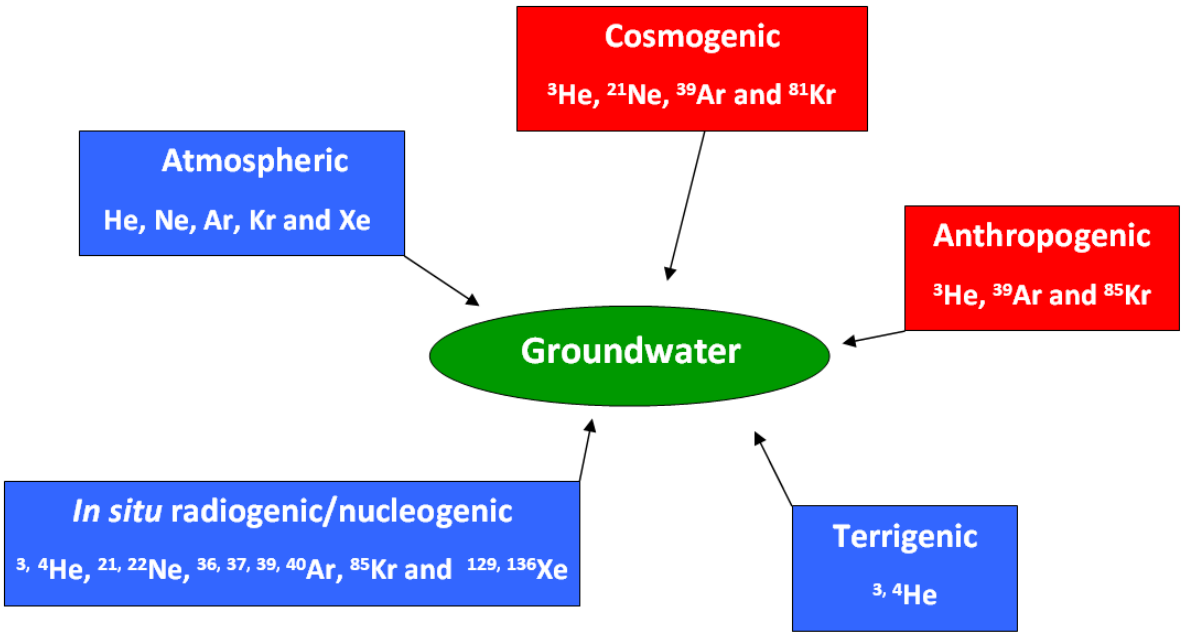

Figure 3.1. The sources of stable and radioactive noble gas isotopes in groundwater (modified from Andrews, 1992). Atmosphere-derived and *in situ* radiogenic and/or nucleogenic production of noble gases along with terrigenic crustal and/or mantle fluxes of helium can contribute significantly to total noble gas concentrations in groundwater systems. Cosmogenic and anthropogenic sources have a negligible effect on total noble gas concentrations but specific isotopes have important significance for groundwater age-dating; for example ^{3}H, ^{85}Kr and ^{81}Kr.

3.2.1. Noble gases in the atmosphere

Atmosphere-derived noble gases make up the largest and most important contribution to total noble gas concentrations in groundwater of meteoric origin. The atmospheric composition and isotopic abundance of the noble gases and their stable isotopes are given in Table 3.1. The atmospheric contribution to total noble gas concentrations in groundwater typically has two components; atmospheric solubility equilibrium and excess air.

Table 3.1. Noble gas composition of dry air and isotopic abundance.

Noble Gas	**Volume Fraction**	**Isotope**	**Abundance (%)**
Helium	5.24×10^{-6}	^{3}He	0.00014
		^{4}He	~100
Neon	1.818×10^{-5}	^{20}Ne	90.5
		^{21}Ne	0.268
		^{22}Ne	9.23
Argon	9.34×10^{-3}	^{36}Ar	0.3364
		^{38}Ar	0.0632
		^{40}Ar	99.6
Krypton	1.14×10^{-6}	^{78}Kr	0.347
		^{80}Kr	2.257
		^{82}Kr	11.52
		^{83}Kr	11.48
		^{84}Kr	57.00
		^{86}Kr	17.40
Xenon	8.7×10^{-8}	^{124}Xe	0.0951
		^{126}Xe	0.0887
		^{128}Xe	1.919
		^{129}Xe	26.44
		^{130}Xe	4.070
		^{131}Xe	21.22
		^{132}Xe	26.89
		^{134}Xe	10.430
		^{136}Xe	8.857

(Ozima and Podosek, 2002)

3.2.1.1. Atmospheric solubility equilibrium

The most important component of dissolved noble gases in groundwater is atmospheric solubility equilibrium as this provides a reference point for observed concentrations and enables the calculation of noble gas temperatures (NGTs). Noble gases exhibit a wide range of solubilities that demonstrate increasing solubility and temperature dependence with increasing atomic mass (see Figure 3.2). Noble gas solubility in groundwater is defined by Henry's Law for dilute solution (Equation

3.1). Noble gas solubility is determined empirically from the relationship between measured Bunsen coefficients β in distilled water (defined as the quantity of gas (in cm^3 STP) dissolved in a unit volume (1 cm^3) under a partial pressure of 1 atm) and the antecedent temperature conditions. Due to the 'salting out' effect, (noble) gases are about 25 % less soluble in sea water than they are in fresh water (Ozima and Podosek, 2002). The effect of salinity on solubility equilibrium can be described by the Setchenow equation:

$$\ln\left(\frac{\beta_i(T,0)}{\beta_i(T,S)}\right) = k_i \cdot c_{NaCl} \qquad (3.2)$$

Where k_i is the Setchenow coefficient (or salting coefficient) of noble gas i and c_{NaCl} is the NaCl molarity. Empirical salting coefficients for all of the noble gases in NaCl solutions are given by Smith and Kennedy (1983).

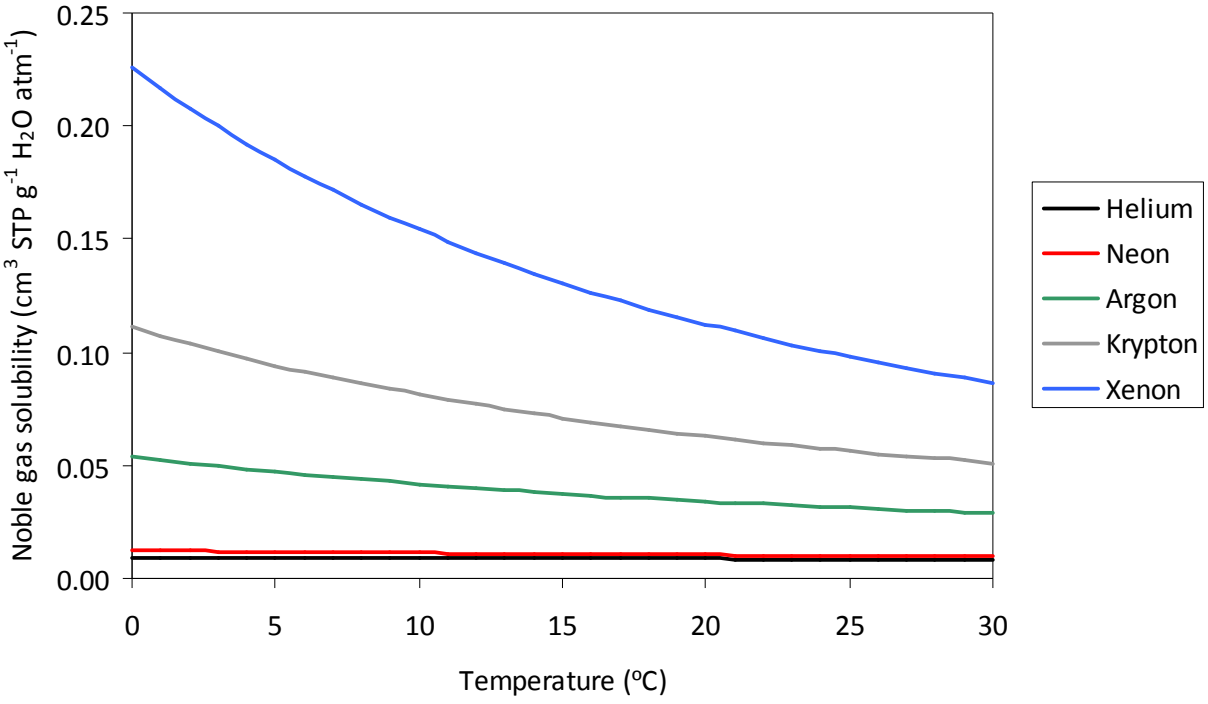

Figure 3.2. Noble gas solubility equilibrium temperature dependence. Solubility and temperature dependence increase with atomic mass.

Noble gas concentrations in groundwater are typically reported in the units of cm^3 STP g^{-1} H_2O. The solubility of noble gases in pure water are given by; Weiss (1970) for Ar, Weiss (1971) for He and Ne, Benson and Krause (1976) for He, Ne, Ar, Kr and Xe, Weiss and Kyser (1978) for Kr, Clever (1979a) for He and Ne, Clever (1979b) for Kr and Xe, and Clever (1980) for Ar. Three sets of noble gas solubility data have been calculated (Table 3.2) by Aeschbach-Hertig et al. (1999).

Table 3.2. Noble gas solubility expressed as Bunsen coefficients β, at 10 ºC, 1 atm, ΔNe of 27% and zero salinity.

Solubility	**Helium (He)**	**Neon (Ne)**	**Argon (Ar)**	**Krypton (Kr)**	**Xenon (Xe)**
	cm³ STP g⁻¹				
Weiss	6.217×10^{-08}	2.563×10^{-07}	4.141×10^{-04}	9.445×10^{-08}	1.344×10^{-08}
Clever	6.237×10^{-08}	2.576×10^{-07}	4.134×10^{-04}	9.440×10^{-08}	1.344×10^{-08}
Benson	6.271×10^{-08}	2.586×10^{-07}	4.123×10^{-04}	9.465×10^{-08}	1.343×10^{-08}

These solubility data were calculated by Aeschbach-Hertig *et al*. (1999) for the interpretation of dissolved atmospheric noble gases using an inverse fitting technique almost identical to the method developed by Ballentine and Hall (1999). The solubility data was incorporated into the MATLAB® routine NOBLE90 (Aeschbach-Hertig *et al*., 2000; Peeters *et al*., 2002) which is discussed in *Section 3.3*. The three groups of solubility data in Table 3.2 agree very well for Kr and Xe but the Benson solubility is 0.44% less than the Weiss solubility for Ar, and the Benson solubilities are 0.86% and 0.89% more than the Weiss solubilities for He and Ne respectively. Clever solubilities have intermediate values between Benson and Weiss solubilities for He, Ne and Ar. According to Aeschbach-Hertig *et al*. (1999) the choice of solubility data does not significantly affect the calculated parameters of temperature and excess air because the largest difference between the three groups of solubility data (Benson-Weiss) is of the same order of magnitude as typical experimental errors (~1%), although inconsistency with solubility data selection would introduced small systematic errors.

3.2.1.2. Excess air

Dissolved noble gases have been observed at concentrations that exceed their atmospheric solubility equilibrium concentration in many site investigations and groundwater research studies (Mazor, 1972; Andrews and Lee 1979; Heaton and Vogel, 1981; Wilson and McNeill, 1997; Ingram *et al*., 2007). It was suggested that the most likely cause of dissolved gas supersaturation occurs as a result of air bubble entrapment in quasi-saturated soils (Heaton and Vogel, 1981). It was initially propounded that air entrainment at the water table of porous media and subsequent dissolution occurs with increased hydrostatic pressure at depth, leading to noble gas supersaturation of groundwater relative to its solubility equilibrium concentration. This phenomenon is now routinely referred to in the literature as 'excess air'.

The excess air component of dissolved noble gas analyses in groundwater was typically seen as just a necessary correction and often limited the accuracy of calculated recharge temperatures (NGTs) due to a limited understanding of air entrapment and excess air formation in most aquifer systems. Heaton and Vogel (1981) first identified the potential for using excess air measurements to identify and distinguish between different areas of recharge, although few subsequent studies fully utilised the excess air parameter. However, interest in the noble gas excess air parameter has gained momentum in recent years (eg. Ingram *et al*., 2007; Klump *et al*., 2007; Aeschbach-Hertig *et al*., 2008; Sun *et al*., 2008; Osenbrück *et al*., 2009).

A number of laboratory studies have been used to gain an improved understanding of air entrapment (Faybishenko, 1995) and the subsequent formation of excess air (Holocher *et al*., 2002; Klump *et al*., 2007). Holocher *et al*. (2002) investigated the formation of excess air using two series of column experiments. Quartz sand was packed into 1 m length columns and air saturated water (ASW) was

allowed to flow through the systems. A constant water level was maintained in one column whereas a fluctuating water level was induced in the other. The results showed that both columns produced enriched noble gas concentrations relative to ASW and that the amount of supersaturation ranged from 1.4% to 16.2% ΔNe. Holocher *et al.* (2002) suggest that there are six parameters that control the formation of excess air in quasi-saturated porous media. These parameters are; hydrostatic and capillary pressure, flow regime, volume of initially entrapped air, entrapped air bubble size, initial composition of dissolved gases and the initial composition of entrapped air. Holocher *et al.* (2002) conclude that from their column experiments, the total volume of initially entrapped air and the sum of the hydrostatic and capillary pressure that acts upon the entrapped air bubbles are the most significant factors in the formation of excess air.

A number of additional factors that can influence the accumulation of excess air in groundwater have been suggested. These include the physical structure of the unsaturated zone (particularly at the capillary fringe) and seasonal patterns of precipitation that affect water table fluctuations and recharge rates (Stute and Schlosser, 1993). The relative amplitude of these water table fluctuations will also have a significant influence on excess air values (Ingram *et al.*, 2007). Human activities such as groundwater abstraction and water resource management schemes such as artificial recharge (Cey *et al.*, 2008) or large scale industrial mining operations and mine de-watering can also have a significant impact on water table elevation and fluctuations and therefore excess air concentrations. Cey *et al.* (2008) observed excess air concentrations up to ~400% ΔNe in areas of artificial recharge.

3.2.2. Terrestrial sources of noble gases

3.2.2.1. *In situ* production in the sub-surface

Noble gases are produced by radioactive decay or by subsequent nuclear reactions that are initiated by radioactive decay in the subsurface. The most significant radiogenic noble gases are ^{3}He, ^{4}He and ^{40}Ar and they are produced from ^{3}H, U-Th decay series elements and ^{40}K respectively. Helium and argon isotopes are the only noble gases routinely used in groundwater studies that have the potential for significant radiogenic production in the subsurface, although $^{21}Ne_{rad}$ is also potentially important in studies of deep circulating aquifer systems and palaeogroundwater.

Uranium and thorium are elements that occur in three natural decay series that begin with ^{238}U, ^{232}Th and ^{235}U respectively. The radionuclides of these elements generally exist in a state of secular equilibrium in which the abundance of the radioactive isotope remains constant because the production rate is equal to the decay rate. Alpha particle emissions consist of two protons and two neutrons and forms a particle that is identical to a helium nucleus and has a charge of +2 often expressed as $^{4}_{2}He^{2+}$ or $^{4}_{2}\alpha$. Alpha particles interact with the surrounding environment, stripping electrons from other atoms and creating positive ions and free electrons. Shortly after being emitted, alpha particles gain the two electrons that are required to create stable ^{4}He atoms. Radiogenic ^{4}He can accumulate to concentrations several orders of magnitude higher than atmospheric solubility equilibrium in deep circulating groundwater that has a long residence time (Torgersen and Clark, 1985).

3.2.2.2. Terrigenic flux

The terrigenic flux refers to noble gases (primarily helium isotopes) that emanate from geochemical reservoirs in the Earth's mantle or crust. Helium will accumulate in deep circulating groundwater as it ascends from the mantle and crust, and this can be used to provide a qualitative indication of groundwater residence time (Zhou and Ballentine, 2006). Uranium and Thorium are often present at high concentrations within the Earth's crust and nuclear reactions involving U-Th series elements produce significant quantities of nucleogenic noble gases. These reactions have far greater impact on the noble gas composition of deep groundwater than reactions that occur in the mantle. Crustal He and Ne contain large nucleogenic components and due to the very high diffusivity of these light noble gases they commonly migrate into aquifer systems (Ozima and Podosek, 2002). Crustal nucleogenic helium-3 is produced from the reaction described by *Equation 3.8* which essentially involves a neutron capture reaction of Li:

$$^{6}_{3}Li(n,\alpha)^{3}_{1}H \rightarrow {}^{3}_{2}He \qquad (3.3)$$

(Morrison and Pine, 1955)

The spontaneous fission of ^{238}U as well as reactions with light elements such as Na, Mg, Al and Si generates the necessary neutrons, and α-particles are emitted from the decay of U and Th (Ozima and Podosek, 2002). ^{21}Ne and ^{22}Ne have significant crustal sources from materials such as granite and also involve reactions involving α-particles and neutrons derived from the U-Th decay series.

The mantle component of the terrigenic flux will consist purely of primordial helium because there are no radiogenic sources in the mantle. If the terrigenic flux

rate can be estimated accurately and radiogenic production within the Earth's crust can be calculated from known uranium and thorium concentrations, then interpretation of groundwater He concentrations can be used in a semi-quantitative way for assessing groundwater residence times.

3.2.3. Helium isotopes in groundwater

Helium-4 has significant radiogenic and terrigenic sources in deep circulating groundwater (eg. Griesshaber *et al.*, 1992; Stute *et al*., 1992; Castro *et al*., 1998; Bethke *et al.,* 1999) as well as potential radiogenic inputs to shallow aquifers (Solomon *et al.,* 1996). Helium-3 has additional nucleogenic and tritiogenic sources in shallow aquifers (Schlosser *et al.,* 1988; 1989).

The total ^3He balance is given by:

$$^3He_{Total} = {}^3He_{Tritiogenic} + {}^3He_{Sol.\ Equilibrium} + {}^3He_{Excess\ Air} + {}^3He_{Nucleogenic} + {}^3He_{Terrigenic} \quad (3.4)$$

The corresponding ^4He balance is given by:

$$^4He_{Total} = {}^4He_{Sol.\ Equilibrium} + {}^4He_{Excess\ Air} + {}^4He_{Radiogenic} + {}^4He_{Terrigenic} \quad (3.5)$$

The helium isotope ratio $^3He/^4He$ is often used to identify gases of crustal or mantle origin, and ^4He enrichment from the *in situ* α-decay of U-Th series elements and/or crustal and mantle fluxes (terrigenic He) is frequently reported in the literature at up to 5 or 6 orders of magnitude higher than its atmospheric solubility equilibrium concentration (eg. Andrews and Lee, 1979; Castro *et* al., 1998; Bethke *et al*., 1999).

Table 3.3. Typical $^{3}He/^{4}He$ ratios in natural systems

Geosphere Component	$^{3}He/^{4}He$	Source
Atmosphere	$1.384x10^{-6}$	All
Crust	$10^{-7} – 10^{-8}$	Radiogenic
Enriched U, Th sediments	$> 10^{-10}$	Radiogenic
Mantle	10^{-5}	Primordial
Active tectonic zones	$10^{-5} – 10^{-7}$	Radiogenic and Primordial

(Clarke *et al*., 1976; Beyerle, 1999)

As a result of subsurface *in situ* production of ^{4}He, mass transfer occurs between the aquifer media and groundwater leading to a quantifiable relationship between groundwater residence time and ^{4}He concentration (Stute *et al*., 1992; Castro *et al*., 2000). However, ^{4}He groundwater age-dating is often only used as a tool for estimating groundwater age due to the complexity of groundwater containing helium from several sources and pathways such as crustal and mantle signatures in addition to the release of helium from previously trapped reservoirs of radiogenic origin (Solomon *et al*., 1996; Zhou and Ballentine, 2006). However, Torgersen (2010) suggests that it is now possible to determine uncertainty limits associated with crustal fluxes using the increased number of published data sets and thus improving ^{4}He age estimates. Helium-4 is typically used to date groundwater in the range of $10^{3}–10^{6}$ years and is often supported by additional age-dating techniques such as ^{14}C with a half-life of 5730 years, ^{81}Kr with a half-life of 229,000 years and/or ^{36}Cl with a half-life of 301,000 years (Lehmann *et al.* 2003).

3.2.4. Argon isotopes in groundwater

Argon isotopes in groundwater have significant atmospheric and terrestrial origins and combined with ^{4}He their use as geochemical tracers was recognised as early as 1935 (Savchenko, 1935). The radioactive nuclide ^{39}Ar is produced in the

atmosphere by neutrons of secondary cosmic radiation as well as in terrestrial environments by *in situ* reactions eg. $^{39}K \rightarrow (n, p)^{39}Ar$. Argon-39 has a half-life of 269 years which gives it potential as a groundwater age-dating tool, however, it application is limited due to problems arising from determining source contributions.

Groundwater with an age in the range of >1000 years will have an argon isotope ratio ($^{40}Ar/^{36}Ar$) that will usually show a variation from that of the atmospheric ratio due to the *in situ* production and accumulation of radiogenic ^{40}Ar. The quantity of ^{40}Ar that is derived from the *in-situ* decay of long lived ^{40}K can be significant, and is proportional to the potassium content of the solid aquifer material and the diffusive flux from the crust. At the same time, ^{36}Ar produced from the decay of ^{36}Cl is usually very low and generally considered negligible. This implies that ^{40}Ar is essentially the isotope that is solely responsible for altering the $^{40}Ar/^{36}Ar$ ratio in groundwater. The $^{40}Ar/^{36}Ar$ ratio of atmospheric argon is 295.5, but due to the production of ^{40}Ar in the subsurface and the uniform concentration of ^{36}Ar as previously discussed, the $^{40}Ar/^{36}Ar$ ratio in groundwater is always greater than or equal to 295.5. The $^{40}Ar/^{36}Ar$ ratio can therefore be used as a qualitative tool for the identification of very old groundwater.

3.3. Mathematical modelling of recharge temperatures and excess air

In order to resolve the atmospheric solubility equilibrium and excess air component contributions to total noble gas concentrations in groundwater a range of techniques and models have been developed. The early studies such as Heaton and Vogel (1981) calculated recharge temperatures using solubility equations and graphical techniques. These methods typically achieved a precision of ± 1-2 ºC.

Graphical methods are based upon plotting a temperature sensitive heavy gas such as xenon against a temperature insensitive light noble gas such as neon to determine the excess air concentration (helium is not typically used due to numerous non-atmospheric sources in the subsurface). These techniques are not as accurate as more recently developed mathematical solutions but they remain useful for initial assessments of the data and have been used in this study for that purpose (see Chapter 5).

Iterative techniques were developed that allowed, for the first time, simultaneous determinations of unknown parameters if the model equations were not underdetermined from the measured data. The levels of precision achieved using iterative methods improved over graphical techniques and were reported at ± 0.8 ºC (Stute *et al*., 1995).

More recently, inverse modelling has been developed by Ballentine and Hall (1999) and Aeschbach-Hertig *et al*. (1999). The two papers reported an almost identical method which is based on a least-squares minimisation process. The technique back calculates noble gas concentrations from specific conditions and compares the results to measured concentrations using chi-squared statistical analysis for testing the goodness-of-fit between the modelled data and the measured data. The chi-squared (χ^2) test weights the analysis so that the heavier temperature sensitive noble gases are used for determining the noble gas temperature (NGT) and the lighter noble gases are used to determine excess air concentrations. The level of precision for the inverse fitting method has been reported as ± 0.5 ºC (Aeschbach-Hertig *et al*., 2002).

Noble gas excess air is regularly reported as having a different isotopic composition to that of atmospheric air (Stute *et al*., 1995). Usually, this occurs as an

enrichment of the heavier noble gases and a corresponding depletion of the lighter noble gases. A number of studies have shown the potential for excess air fractionation to occur relative to an air equilibrated composition (eg. Stute *et al*., 1995; Aeschbach-Hertig *et al*., 2000). Several models have been developed to describe the formation and fractionation of excess air in groundwater and they have been incorporated into the MATLAB® routine NOBLE90 which is a freely downloadable noble gas interpretation programme available from www.eawag.ch that utilises the inverse fitting method (Peeters *et al*., 2002).

3.3.1. Total dissolution model (or Unfractionated excess air – UA Model)

Andrews and Lee (1979) first suggested a model that described the total dissolution of entrapped air in porous media; the model was subsequently modified by Stute and Schlosser (1993). The total dissolution model (TD) was the first model to represent the formation of excess air. The TD model is characterized by excess air having quantities of dissolved noble gases in ratios equal to that of atmospheric air. The concentration of dissolved gases originating from the atmosphere in the TD model is given by:

$$C_i\left(T,S,P,A_d\right) = C_i^*\left(T,S,P\right) + A_d z_i \qquad (3.6)$$

where $C_i^*(T,S,P)$ is the moist-air solubility equilibrium concentration as a function of temperature (T), salinity (S) and atmospheric pressure (P), A_d is the concentration of totally dissolved dry air and z_i is the volume fractions of the individual gases in dry air.

This model implies that the excess air has the same composition as the entrapped gas (described by the volume fraction term z_i) and is assumed to be atmospheric air. The excess air component is described by the parameter A_d. This equation represents the most basic mathematical explanation of noble gas excess air.

3.3.2. Partial re-equilibrium model

The total dissolution followed by partial re-equilibration with the atmosphere model (PR), was proposed by Stute *et al.* (1995). The PR model suggests that diffusivity-controlled fractionation of excess air occurs and leads to dissolved gases being present at ratios different to that of atmospheric air. The PR model is given by:

$$C_i\left(T,S,P,A_d,R\right) = C_i^*\left(T,S,P\right) + A_d z_i e^{-R\frac{D_i}{D_{Ne}}} \qquad (3.7)$$

Where R is the degree of re-equilibration and D_i is the molecular diffusion coefficient. Entrapped air bubbles are initially completely dissolved as described by the TD model but is then followed by diffusive loss across the water table. Due to noble gases having a range of molecular diffusivities the result is a fractionated excess air component with respect to atmospheric air. The degree of re-equilibration is given by the remaining proportion of the initial neon excess. The model assumes that the gas exchange rate is proportional to molecular diffusivity. Molecular diffusivity decreases with increasing mass number therefore indicating that the PR model would suggest that the largest depletion of the initial excess air would exist for the lighter noble gases and especially helium because of its very high diffusivity coefficient; and that the heavier gases would appear enriched relative to atmospheric air in the remaining portion of excess air.

3.3.3. Multi-step partial re-equilibration model

The multi-step partial re-equilibration model (MR) was put forward by Kipfer *et al.* (2002) in an attempt to resolve the problem of unrealistically high initial excess air concentrations that are commonly predicted using the PR model of Stute *et al.* (1995). The fundamental concept of the MR model that differs from the PR model is that periodic water table fluctuations create a cycle of air bubble entrapment, dissolution and diffusive loss across the water table. The MR model is given by:

$$C_i\left(T,S,P,A_d,R,n\right)=C_i^*\left(T,S,P\right)+A_d z_i e^{-R_i}\frac{1-e^{-nR_i}}{1-e^{-R_i}} \qquad (3.8)$$

Where A_d and R are the same as in the PR model and n is the number of steps.

3.3.4. Closed-system equilibrium model

The final model was put forward by Aeschbach-Hertig *et al.* (2000) and describes the closed-system equilibration of groundwater with only partially dissolved entrapped air (CE) leading to solubility-controlled fractionation. The CE model is given by:

$$C_i\left(T,S,P,A_e,F\right)=C_i^*\left(T,S,P\right)+\frac{\left(1-F\right)A_e z_i}{1+FA_e z_i/C_i^*} \qquad (3.9)$$

where $C_i^*(T,S,P)$ is the moist air solubility equilibrium concentration of gas i as a function of temperature (T), salinity (S) and atmospheric pressure (P), A_e is the initial concentration of entrapped air per unit mass of water, z_i is the atmospheric abundance

ratio of gas *i*, and *F* is the fractionation parameter (0 is equal to the total dissolution of A_e, and 1 represents no excess air).

The hydrostatic pressure is generally not sufficient to completely dissolve all entrapped atmospheric air within a closed system, and therefore the CE model describes the solubility-controlled fractionation that occurs.

3.3.5. Alternative numerical models

Holocher *et al.* (2003) developed a kinetic model of gas bubble dissolution (KBD) which describes the dissolution of entrapped bubbles in quasi-saturated porous media using a physical approach. The model assumes that the composition of entrapped air bubbles is equal to that of the atmosphere – ie. the bubbles consist of N_2, O_2 and the noble gases.

Mercury *et al.* (2004) introduced a negative pressure model (NP) which aimed to correct the TD Model for negative pressures within the capillary zone that have the potential to create changes in noble gas solubility values.

The oxygen depletion model (OD) suggested by Hall *et al.* (2005) questioned the fundamental assumption that solubility equilibrium with the atmosphere occurs as a result of groundwater equilibration with air of atmospheric composition. Hall *et al.* (2005) state that low calculated noble gas temperatures (NGTs) could be the result of oxygen depletion in the unsaturated zone without equal accumulation of carbon dioxide. Further research based on the OD model but with an allowance for partial re-equilibration of noble gases between groundwater and soil air via diffusion in the gas phase by Sun *et al.* (2008) and termed the gas diffusive relaxation model (GR) has also been successful in calculating NGTs.

3.4. Applications of dissolved noble gases in groundwater

3.4.1. The noble gas palaeothermometer

One of the most promising uses of atmosphere-derived noble gases in groundwater is determining the noble gas temperature (NGT) and palaeoclimate reconstruction (Stute and Schlosser, 1993). This technique was first applied my Mazor (1972) and it enables the temperature to be calculated at which water was equilibrated with the atmosphere at the point of groundwater recharge. The noble gas palaeothermometer is based on the principle that the solubility of noble gases in water is temperature dependent according to Henry's Law. Only a small number of assumptions are required to calculate NGTs and they include: noble gas partial pressures (determined from the altitude of recharge), 100% relative humidity at the capillary fringe, and temperature dependent noble gas solubility - determined from estimated surface temperature at the time of recharge (Sun *et al*., 2008). Since the early work of Mazor (1972) a large number of studies have applied the principles of noble gas solubility equilibrium in order to derive palaeoclimatic information such as Pleistocene recharge temperatures, to estimate groundwater residence times and identify recharge that occurred during the LGM (eg. Andrews and Lee, 1979; Andrews, 1992; Stute *et al*., 1992; Blavoux *et al*., 1993; Stute *et al*. 1995; Dennis *et al*., 1997; Aeschbach-Hertig *et al*., 2002; Beyerle *et al*., 2003; Zuber *et al*., 2004).

Andrews and Lee (1979) indentified palaeo groundwater in a UK aquifer system that was estimated to have a subsurface residence time in the region of 10^4 years and a recharge temperature calculated from dissolved noble gases that was 5–7 ^{o}C cooler than today, and consistent with palaeo recharge from the late Pleistocene. Dissolved noble gases were also used by Blavoux *et al*. (1993) to investigate groundwater from a deep Eocene aquifer in Aquitania, France. The palaeo

groundwater present in the deep Eocene aquifer displayed a shift of -2–-3‰ for $\delta^{18}O$ values and noble gases analyses enabled Blavoux *et al*. (1993) to conclude that a temperature shift of 5–7 ºC had occurred since the Pleistocene. Osenbrück *et al*. (1993) made a similar observation in Poland where NGTs were 2–3.5 ºC lower for palaeo groundwater than for modern recharge. Osenbrück *et al*. (1993) also noted a shift in $\delta^{18}O$ values with palaeo groundwater being more depleted than modern groundwater – the same trend was also noted by Bertleff *et al*., (1993) in southern Germany.

Stute *et al*. (1995) applied the noble gas palaeothermometer to groundwater samples collected from a tropical region of Brazil. ^{14}C dating was used to identify palaeo recharge with an age in the range of 10,000 – 30,000 years. Stute *et al*. (1995) used a graphical interpretation of dissolved noble gas data based on solubility equations to determine that a temperature shift of 5.4 ºC had occurred from the Pleistocene to the Holocene.

3.4.2. Groundwater age-dating

Groundwater age-dating describes the process of determining mean residence times. Numerous tracers exist for determining the age of groundwater, and each tracer has a specific applicable timescale. Tritium is the only tracer that forms part of the water molecule so all other techniques rely on dissolved constituents (Clark and Fritz, 1997). Groundwater age-dating of both modern and old groundwater requires consideration for this research. No direct dating methods were used to determine residence times for young groundwater within the Lower Rhine Embayment due to financial constraints. However, it was clear from stable isotope data that a large proportion of groundwater in the shallow aquifers had a modern meteoric signature. A

key element to any further work would involve constraining the modern component of groundwater by applying a suitable age-dating technique such as the ^{3}H-^{3}He method.

Determining the precise age of the 'old' groundwater component is also of great interest. Helium-4 measurements have provided preliminary data to suggest that deep groundwater with a very long residence time is present in the shallow aquifers near some fault zones. However, ^{4}He only provides a qualitative tool and more accurate techniques such as ^{36}Cl or ^{81}Kr would provide a insight into the source and origin of the 'old' groundwater. For these reasons groundwater age-dating techniques for both modern and old groundwater are discussed below.

3.4.2.1. Dating modern groundwater

The use of dissolved noble gases as groundwater age-dating tools for modern recharge generally involves utilising anthropogenic inputs of ^{3}H and ^{85}Kr.

Tritium (^{3}H or T) is a radioactive isotope of hydrogen with a half-life of 12.33 years (Unterweger and Lucas, 2000) and decays to its daughter product; the noble gas ^{3}He, through β^- emission. Tritium is continuously produced naturally by cosmic ray spallation and fast neutron interactions with nitrogen in the upper atmosphere. The removal of tritium from the atmosphere is an efficient process in which the tritium atoms are incorporated into water molecules, either by direct oxidation or exchange with protium (^{1}H) and deuterium (^{2}H or D) to form tritiated water molecules (HTO).

The testing of high yield thermonuclear fusion and fission devices, mainly between 1953 and 1963 released large quantities of anthropogenic tritium into the atmosphere causing a spike-like input. Tolstikhin and Kamensky (1969) first suggested that combining measurements of both parent tritium and daughter helium-3 could be used as a tool for dating young groundwater, and that such measurements

could provide an apparent age which would represent the length of time that had elapsed since the water had become isolated from the atmosphere. The $^3H/^3He$ age is defined by the equation:

$$\tau = \frac{T_{1/2}}{\ln 2} \times \ln\left(1 + \frac{^3He^*}{^3H}\right) \qquad (3.10)$$

where τ is the $^3H/^3He$ age in years, $T_{½}$ is the half-life of tritium (12.33 years), $^3He^*$ is the tritiogenic helium-3 concentration and ^3H is the tritium concentration.

The first array of groundwater studies that used the tritium/helium-3 age-dating technique included Takaoka and Mizutani (1987), Poreda *et al*. (1988), Schlosser *et al*. (1988; 1989), Solomon and Sudicky (1991) and Solomon *et al*. (1992; 1993).

Krypton-85 has a half-life of 10.76 years and was first released into the atmosphere from plutonium reprocessing plants in the early 1950s. Unlike tritium, ^{85}Kr does not have an 'atmospheric injection spike' because as the nuclear fuel reprocessing industry has continued to expand the concentration of ^{85}Kr in the atmosphere has also been steadily increasing. Krypton-85 has proved useful as a groundwater age-dating tool for young groundwater in the range of <60 years. Krypton-85 measurements have typically required large sample volumes for analysis using Low Level Counting (LLC) techniques (Loosli, 1992) but more recently, Atom Trap Trace Analysis (ATTA) (Chen *et al*., 1999) and second generation ATTA (Du *et al*., 2003) have reduced the sample size required, partially due to improved purification techniques (Yokochi *et al*., 2008).

Radiogenic ^{4}He from the α-decay of U-Th series elements in rocks and sediments is typically used to date groundwater in the range of 1,000 – 100,000 years and has some potential to extend to $1x10^{6}$ years and beyond. However, Solomon *et al.* (1996) used radiogenic helium-4 to date modern groundwater as young as 10 years old at the well documented Sturgeon Falls study site in Ontario, Canada due to a high release flux from a previously trapped reservoir of helium.

3.4.2.2. Dating old groundwater

The naturally occurring radionuclide krypton-81 has a half-life of 229,000 years. Krypton-81 is produced in the upper atmosphere by cosmic ray spallation involving stable krypton isotopes. Krypton-81 provides the most robust age interpretation for very old groundwater because there are fewer uncertainties relating to the initial input value at recharge and subsequent subsurface processes and sources. The atmospheric $^{81}Kr/Kr$ ratio is assumed to be constant and well constrained over the past 1,000,000 years and subsurface production is negligible. However, field sampling and laboratory analysis of ^{81}Kr is complex and challenging; primarily due to the low concentration of krypton-81 in groundwater – typically less than 1,000 atoms L^{-1} H_2O. Krypton-81 measurements have been made using Resonance Ionization Mass Spectrometry RIMS (Thonnard *et al.*, 1987) and Accelerator Mass Spectrometry AMS (Collon *et al*., 2000). Although these techniques proved successful there were a number of issues preventing routine analysis. More recently, a second generation Atom Trap Trace Analysis ATTA technique (Du *et al.*, 2003) has significantly reduced the volume of groundwater required for on-site de-gassing and by using 'table-top' laboratory equipment, has provided a much more promising tool for potential routine analysis.

Krypton-81 measurements using the ATTA technology requires the de-gassing of approximately 2 m^3 of groundwater in the field using a vacuum stripping method such as that described by Collon *et al.* (2000). The krypton is then separated and purified from the collected gases in the laboratory (Yokochi *et al.*, 2008) and then analysed using ATTA (Du *et al.*, 2003).

The radiogenic component of helium-4 in groundwater has been used as a direct estimate of groundwater age (Andrews *et al.*, 1982). The principle of using helium-4 as a groundwater age-dating tool is rather simple and assumes that helium-4 accumulation is groundwater is the result of *in situ* α-decay of U-Th series elements within the aquifer media, and therefore the higher the helium-4 concentration, the longer the groundwater residence time. To estimate the age of the groundwater, the method requires knowledge of U-Th content of aquifer material and transfer fluxes. However, many studies have shown that groundwater ages calculated in this way provide erroneously long residence times (Andrews *et al*., 1982; Torgersen 1985) and that the excess concentration of helium-4 could not simply be explained by *in situ* production from the aquifer media. A number of authors have attributed the additional helium to a deep upward flux from the crust or the release of a previously trapped 'inherited' reservoir of helium-4 (eg. Solomon *et al*. 1996; Castro *et al.*, 1998; Bethke *et al.*, 1999; Mahara and Igarashi, 2003). The external fluxes of helium-4 that are reported in these studies imply that the principle of helium-4 dating is invalid in most hydrogeological settings unless crustal fluxes can be estimated with a high degree of accuracy. Zhou and Ballentine (2006) state that estimates of crustal fluxes are typically the most unconstrained value when calculating ^{4}He groundwater ages but Torgersen (2010) suggests that with an increasing number of external flux estimates reported in the literature, the accuracy of ^{4}He groundwater age-dating is improving.

3.4.3. Indicators of recharge rates and conditions

Ingram *et al*. (2007) investigated the relationship between seasonal water table fluctuation and excess air determined using neon measurements by comparing borehole water level records over a 10 year period for a layered sandstone aquifer system in west Norfolk, UK, obtained from the UK Environment Agency. Water table fluctuation data was selected from boreholes to reflect modern groundwater recharge which was not affected by groundwater abstraction for municipal water supply purposes and therefore the artificial influence was minimal. Ingram *et al*. (2007) also explored the possibility that excess air could be used as a direct indicator of long-term average net annual groundwater recharge (R_{av}) given that:

$$R_{av} = D_w S_y \qquad (3.11)$$

Where, D_w is the depth of water above entrapped air and S_y is the specific yield. Ingram *et al*. (2007) successfully used dissolved noble gases to distinguish between groundwater bodies with different recharge histories, and demonstrated that noble gas determined excess air correlated well with annual water table fluctuations and could therefore be used as a direct indicator of long-term average net annual groundwater recharge.

3.4.4. Carbon capture and storage (CCS) and nuclear waste disposal.

Geochemical tracers are powerful tools for assessing the potential for carbon sequestration and nuclear waste storage in deep sedimentary basins over geological time scales. Specifically, dissolved gas such as CO_2 and/or noble gases can be applied to determine aquifer isolation (Marty *et al*., 2003) or to identify possibly leakage

pathways such as fault zones (Shipton *et al*., 2004; Vrolijk *et al*., 2005; Gilfillan *et al*., 2008). This is particularly relevant to this study because it is hypothesised that faults act as preferential flow paths between deep and shallow aquifers within the Lower Rhine Embayment, Germany.

Carbon Capture and Storage (CCS) is a strategy that has the potential to significantly reduce anthropogenic CO_2 emissions and stabilise the concentration of atmospheric CO_2. The CCS approach involves the capture, transport and long term storage of CO_2 from the combustion of fossil fuels and other carbon emitting industrial processes. The CO_2 is captured from flue gas emissions using a number of collection and separation techniques. Comprehensive and detailed information on all aspects of CCS theory and technology can be found in the IPCC Special Report on Carbon Dioxide Capture and Storage by Metz *et al*. (2005).

The oil and gas fields of the North Sea have potential as large capacity carbon storage sites for CO_2 emissions generated in the UK and northern Europe and have attracted much attention in recent years. However, it is estimated that deep saline aquifers in the same region could hold up to 135 times more carbon than the North Sea oil and gas fields (Metz *et al*., 2005). CCS technology using deep saline aquifer systems is generally more uncertain as little is often known about the hydrogeology and how groundwater dynamics could affect the rate of dispersion and overall residence times of the injected CO_2. The IPCC Special Report (2005) clearly states that there is "a need for better understanding of long-term storage, migration and leakage pathways" and Gilfillan *et al.* (2009) conclude that geological mineral fixation of sequestrated CO_2 is likely to form only a minor carbon sink in deep aquifer systems and that most of the injected CO_2 will be dissolved in groundwater and therefore potential fluid flow pathways would require detailed investigation.

3.5. Stable Isotopes

3.5.1. Overview

Stable isotopes are now frequently used in many hydrogeological investigations and they often form the foundation of a multi-tracer approach when it is necessary to determine the origin of groundwater, recharge processes, flow paths and to identify palaeogroundwater (eg. Edmunds, 2001; Vaikmäe *et al*., 2001; Zuber *et al*., 2004; Yuce, 2007; Von Rohden *et al*., 2010). Typically, isotopes of hydrogen, oxygen and carbon will be used together with hydrochemical and field parameter data and if necessary more exotic tracers such as noble gases or various radionuclides. These stable isotopes have the advantage of low atomic mass and therefore the relative mass difference between their isotopes is large, thus having the additional benefit of enabling small fractionations to be measured relatively easily and very precisely in the laboratory.

Isotopic fractionation processes are fundamental to stable isotope geochemistry. Isotopes of any given element will have slightly different physical and chemical properties because of differences in their mass and the strength of chemical bonds. Typically this results in mass-dependent isotopic fractionations. The two key processes that control mass-dependent fractionation are kinetic effects and isotope exchange reactions. This is because physical and chemical reaction processes are considered as either unidirectional kinetic reactions or reversible equilibrium reactions, ie. isotope exchange reactions; and the rate at which bonds are broken in chemical reactions describes these kinetic effects.

3.5.2. Notation and standards

The delta notation expresses the abundance of a given isotope of a particular element in a sample relative to the same isotope in a reference material of known isotopic composition. The delta value is expressed as:

$$\delta(‰) = \left(\frac{R_{sample}}{R_{standard}} - 1 \right) \times 1000 \qquad (3.12)$$

Where R is the heavy to light isotope abundance ratio of the sample and standard. Delta values are reported in per mil (‰) or parts per thousand with positive δ-values indicating that the heavy to light isotope ratio is higher in the sample than in the reference material and negative δ-values indicating that the heavy to light isotope ratio is higher in the standard than in the sample. The current reference standard for oxygen and hydrogen isotope measurements is Vienna Standard Mean Ocean Water (VSMOW) and the current standard for carbon isotope analyses is Vienna PeeDee Belemnite (VPDB).

3.5.3. Stable isotopes of the water molecule

The principal stable isotopes of hydrogen and oxygen have been used extensively in hydrogeological studies (eg. Rozanski, 1985; Gat, 1996; Zuber *et al*., 2004; Von Rohden *et al*., 2010). These isotopes of the water molecule provide evidence for determining the origin of groundwater due to a variation in isotopic composition that occurs as a result of isotopic fractionation processes. For example, meteoric waters tend to be enriched in the lighter isotopes whereas waters subject to

high rates of evaporation are often enriched in the heavier isotopes of hydrogen and oxygen (Gat, 1996). This can be explained by open system (Rayleigh) isotopic fractionation. The vapour pressures of lighter molecules are higher than those of heavier molecules of the same compound so the lighter isotopes of water preferentially escape into the vapour phase during evaporation with the opposite occurring during condensation leading to a vapour phase enriched in isotopically light water (Sharp, 2007). Under Rayleigh conditions condensate is continuously removed from the system so the δ value of the remaining vapour becomes increasingly more negative. This results in very large depletions of the heavy isotopes in precipitation. The reader is referred to Criss (1999) and Gat (2010) for a comprehensive account of the Rayleigh fractionation model.

Meteoric waters display a near-linear relationship between deuterium (^{2}H) and oxygen-18. Craig (1961) conducted accurate analyses on both $^2H/^1H$ and $^{18}O/^{16}O$ isotope ratios and as a result defined a global meteoric water line (GMWL) that can be represented by the following equation:

$$\delta^2H = 8\delta^{18}O + 10 \qquad (3.13)$$

Dansgaard (1964) suggested that the GMWL could be represented in a more general way using the following equation:

$$\delta^2H = 8\delta^{18}O + d \qquad (3.14)$$

This equation shows that the gradient of the GMWL remains constant at a value of 8 but the intercept, given by '*d*' is now variable. The term '*d*' was defined by Dansgaard (1964) as the deuterium excess parameter, and a value of 10 as stated by Craig (1961)

represents modern waters very well. Deuterium excess is governed primarily by the kinetic effects of the evaporation process.

3.5.4. Fractionation in the hydrological cycle

Changes in the isotopic composition of water (δ^2H and $\delta^{18}O$) during the hydrological cycle are caused by mass-dependent fractionation processes. Evaporation from the oceans and subsequent movement of vapour over land masses forms the continental phase of the hydrological cycle where precipitated water is recycled many times through evapo-transpiration and can become stored in glaciers and deep groundwater systems for long periods of time. The continental phase of the hydrological cycle only accounts for about 10%. Ninety percent is simply returned directly to the oceans by return flux precipitation (Gat, 1996).

The continentality effect describes precipitation as becoming isotopically lighter as a given air mass containing water vapour travels farther inland or from its source because of the increasing number of precipitation events that have occurred as described by the Rayleigh fractionation model. Latitude, altitude and seasonal effects are all strongly linked to temperature because temperature controls the amount of water a given air mass can hold (Sharp, 2007). Temperature decreases with increasing latitude and altitude, leading to a decrease in $\delta^{18}O$ and δ^2H values. Seasonal changes in ocean temperature also change the isotopic composition of precipitation and air-sea interaction conditions primarily affect the deuterium excess value (Gat, 1996). The isotopic composition of meteoric water is therefore strongly correlated to temperature (Dansgaard, 1964; Fricke and O'Neil, 1999) and due to this correlation it has been possible to use $\delta^{18}O$ values to identify palaeo groundwater and groundwater recharged

during the last glacial maximum (LGM) (eg. Fontes *et al*., 1991; Deák and Coplen, 1996; Vaikmäe *et al*., 2001). Vaikmäe *et al*. (2001) identified periglacial or possibly subglacial recharge of meltwater from the Fennoscandian ice sheet during the late Devensian ice age in the Cambrian-Vendian system, Estonia using $\delta^{18}O$ measurements and ^{14}C dating. The $\delta^{18}O$ values of the glacial recharge were in the range of -20 – -22‰ and significantly lower than that of modern recharge which has a $\delta^{18}O$ value of -11‰.

3.5.5. Carbon isotopes

Carbon isotopes have many applications in hydrogeology. The radioactive isotope; carbon-14 (half-life of 5730 years) is well known as an archaeological dating tool, and is also often used in hydrogeology to date older groundwater in the range of 1,000 to 25,000 years (Plummer *et al*., 1993). Stable isotopes of carbon include ^{12}C and ^{13}C, with abundances of 98.89% and 1.11% respectively (Wang *et al*., 1998). Even though natural variations in the $^{13}C/^{12}C$ ratio are small, they are sufficient to detect various physical, chemical and biological processes. Typical analytical precision for bulk $\delta^{13}C$ measurements is usually better than ±0.15‰ (Clark and Fritz, 1997), and measurements are generally based on the production of carbon dioxide gas – numerous preparation methods for producing carbon dioxide exist. For the successful application of carbon isotopes as tracers of groundwater flow, rock-water interactions along a given flow path must create a distinctive isotopic signature and produce distinguishable changes in the hydrochemistry and/or residence time. If these interactions are favourable then carbon isotopes can be used to provide information on the origin of carbonate alkalinity as well as giving an indication of the relative

importance of processes such as the oxidation of organic matter, silicate hydrolysis, carbonate mineral dissolution and methanogenesis. Carbon solutes are not conservative environmental tracers and therefore it must be noted that they do not always accurately represent the movement of groundwater.

Deines *et al*. (1974) described carbonate evolution in groundwater in terms of open and closed system models. According to Deines *et al*. (1974) open system evolution involves the reaction of carbonate minerals with water that is in contact with a gas phase of fixed P_{CO2} and continuous isotopic exchange exists between the CO_2 reservoir and the solution, whereas in closed system evolution water is isolated from the CO_2 reservoir before carbonate dissolution occurs. However, in reality most carbonate system evolution falls somewhere in between these two models. It is also possible that during the course of groundwater evolution along a flow path from recharge to discharge, carbonate dissolution will occur under both sets of conditions typically moving from open system to closed system evolution with increasing aquifer confinement.

3.5.5.1 Atmospheric and soil CO_2

The atmospheric concentration of carbon dioxide is currently 389.7 ppmv (Tans and Keeling, 2010). The $\delta^{13}C$ of atmospheric carbon dioxide was -6.4‰ (Friedli *et al*., 1986) but has been steadily decreasing as a result of the increasing global consumption and combustion of fossil fuels and is now -7‰ (Appelo and Postma, 2005).

During infiltration of the soil zone, water equilibrates with soil CO_2. Soil CO_2 concentrations are generally in the range of 10^3 to 10^6 ppmv (P_{CO2} ~10^{-3} to 10^{-1}) due

to bacterial oxidation of organic matter and CO_2 respiration in the root zone (Clark and Fritz, 1997). The dissolution of CO_2 in water produces carbonic acid with subsequent dissociation reactions that produce bicarbonate and carbonate and ultimately lower the pH value. The dissolution of CO_2 is controlled by several factors including temperature, initial pH value and soil P_{CO2}.

The dissolution of soil CO_2 and the subsequent 1st and 2nd dissociations of carbonic acid are given by the following net reaction equation:

$$CO_2 + H_2O \rightleftharpoons H_2CO_3 \rightleftharpoons H^+ + HCO_3^- \rightleftharpoons 2H^+ + CO_3^{2-} \qquad (3.15)$$

It can generally be assumed that carbonate alkalinity is given by the concentration of HCO_3^- and CO_3^{2-}, as other species do not contribute significantly to alkalinity.

The reader is referred to Clark and Fritz (1997) and Wang *et al.* (1998) for a comprehensive overview of the principles and applications of carbon isotopes in groundwater.

4. Methods

4.1. Field sampling

The Lower Rhine Embayment has an exceptionally high density of observation boreholes and piezometer nests (see Figure 4.1).

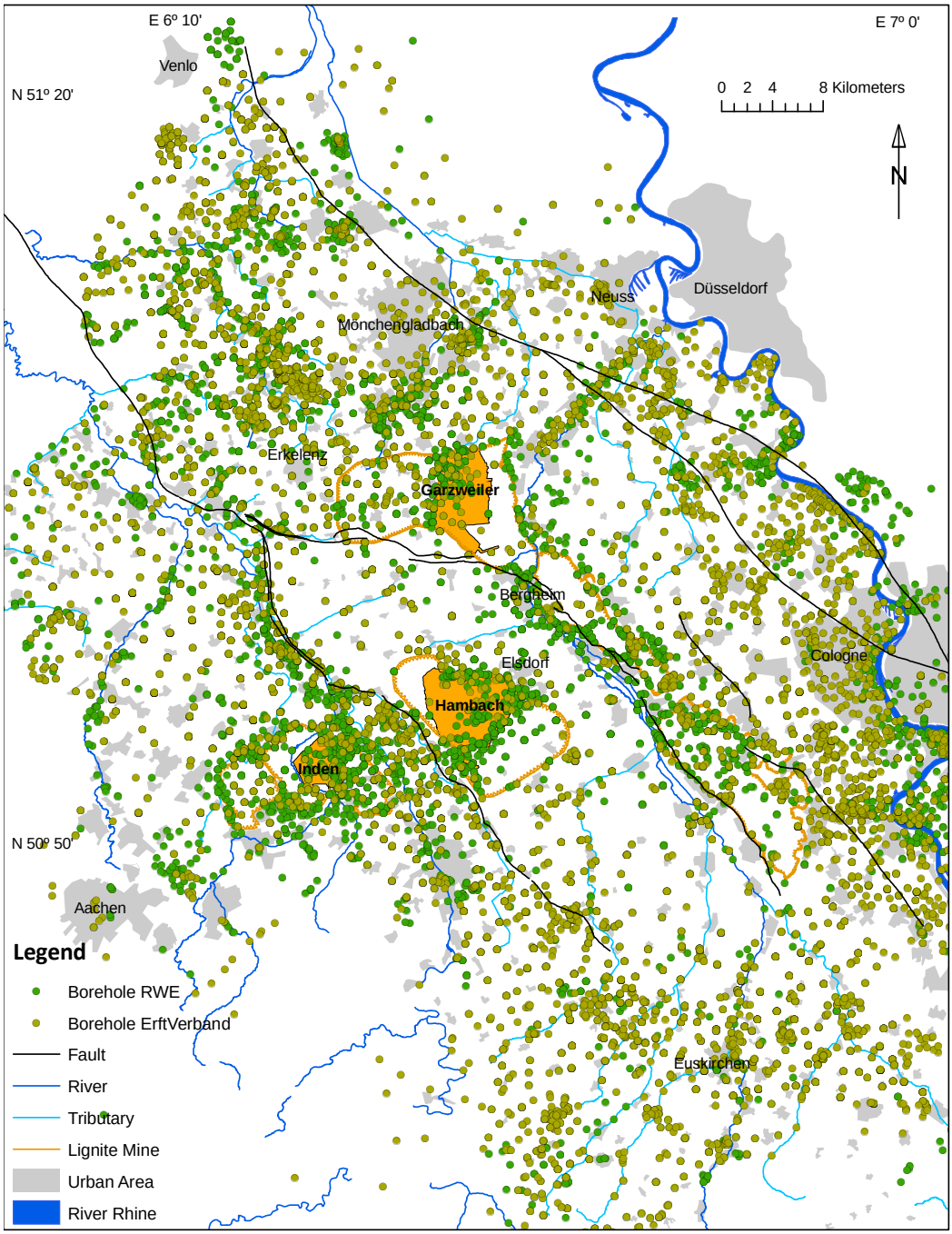

Figure 4.1. High density distribution of observation boreholes and piezometer nests in the Lower Rhine Embayment, Germany.

4.1.1. Borehole selection

The Lower Rhine Embayment is an excellent and unique region for studying groundwater flow dynamics due to an exceptionally high density of observation boreholes and piezometer nests and enhanced groundwater flow rates induced by regional-scale groundwater abstraction from three large open cast lignite mines. With such a vast number of observation boreholes available for groundwater monitoring purposes and sample collection it was essential that boreholes were selected based on a number of important criteria. Observation boreholes were selected at locations in close proximity to faults, and where good historical monitoring records detailing well head parameters and hydrochemistry were available; and in locations that demonstrated certain trends in temporal hydraulic head variations such as long-term drawdown, rebound subsequent to drawdown and natural seasonal/annual fluctuations. Physical limitations of the pumping equipment used also restricted borehole selection and generally only shallow aquifers were sampled (< 100 m).

Figure 4.2. Erftverband custom built groundwater sampling vehicle; including submersible pumps, petrol generator and wet laboratory.

Grundfos MP1 submersible pumps were provided by the Erftverband and used for sampling. The maximum depth that the submersible MP1 pumps could operate at was approximately 80 m below the ground surface.

Groundwater sampling was conducted during three field visits to the Lower Rhine Embayment, Germany that occurred during October 2007, April 2008 and October 2008. The field sampling campaigns were fully supported by the Erftverband and facilitated using their purpose built sampling vehicles (Figure 4.2), complete with mobile wet laboratory, dippers, submersible pumps and petrol generators. The vast majority of observation boreholes and piezometers (Figure 4.3) were pumped using a Grundfos MP1 submersible pump. Water level dippers fitted with an audible electronic alarm were used to determine potentiometric surface before pumping, and combined with filter depth records to determine the volume of water in the borehole.

Figure 4.3. A typical piezometer nest installed by the Erftverband and RWE Power AG.

Each borehole/piezometer was pumped for a time that represented three volumes of groundwater standing in the borehole. pH and Eh were continually monitored using a flow through cell until a steady state had been reached before any measurements were taken and/or groundwater samples collected.

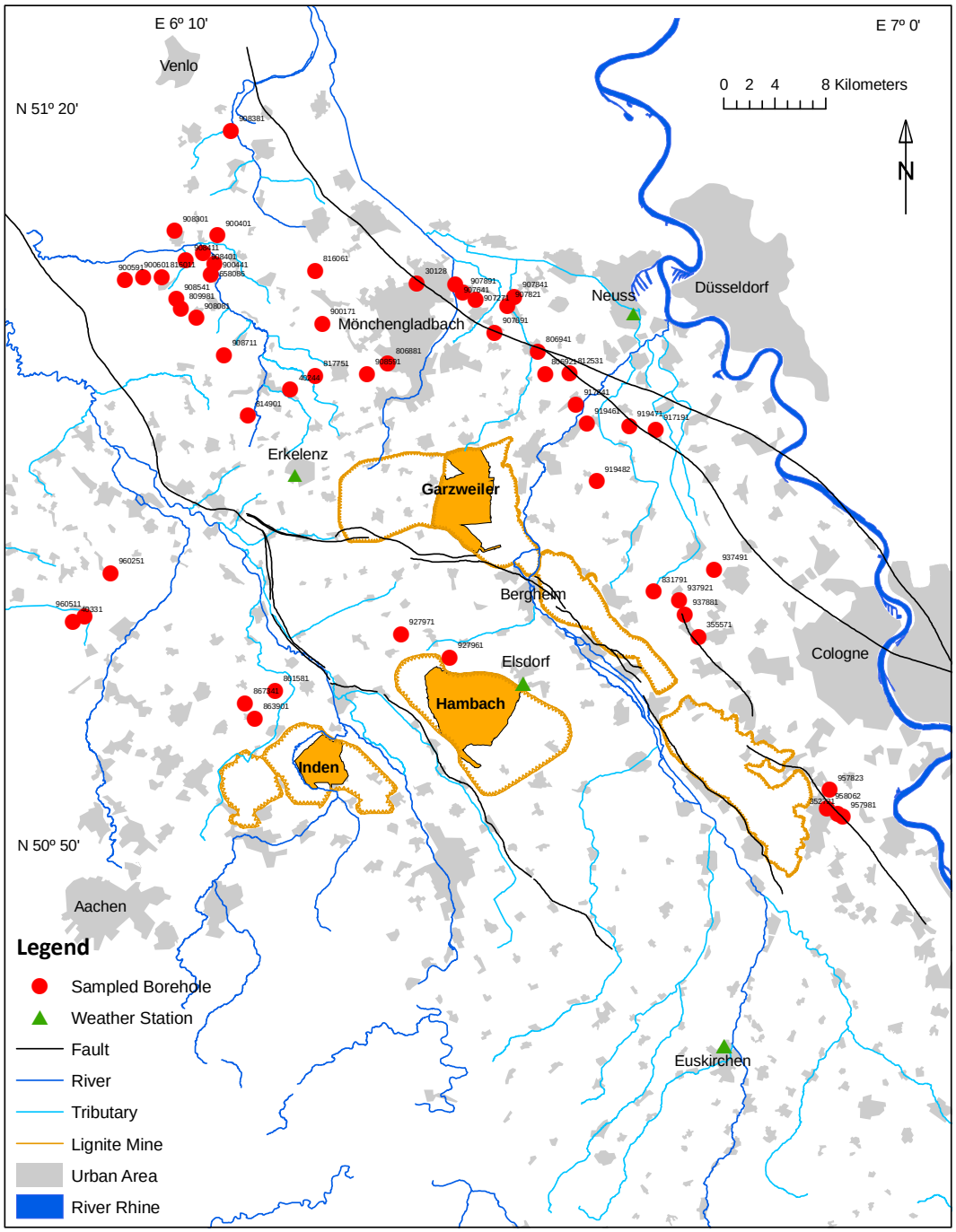

Figure 4.4. The spatial distribution of observation boreholes selected for sampling. The identification name of each observation borehole is provided in Appendix 1.

4.1.2. Sample collection techniques

4.1.2.1. $\delta^{2}H$ and $\delta^{18}O$

Collecting groundwater samples for $\delta^{2}H$ and $\delta^{18}O$ analysis follows a simple protocol. Samples were collected in the field using 150 mL HDPE bottles. Once the borehole had been pumped for a sufficient length of time based on the volume of groundwater within the borehole, raw unfiltered groundwater was used to rinse the bottles and caps three times after which the 150 mL HDPE bottles were completely filled using raw unfiltered groundwater so that no head space remained and the cap was tightened securely.

4.1.2.2. $\delta^{13}C_{DIC}$

Groundwater samples used for $\delta^{13}C_{DIC}$ analysis were collected in 150 mL glass bottles. Raw unfiltered groundwater was used to rinse the bottles and caps three times. The bottles were partially filled with raw groundwater before the addition of a $SrCl_2$–NH_4OH solution that had been prepared shortly before the sampling campaign and stored in an airtight 1 L vessel. The ratio of $SrCl_2$–NH_4OH to groundwater was 1:9 as described by Bishop (1990). The glass bottles were sealed using NESCOFILM tape and care was taken that no headspace remained.

4.1.2.3. Strontium isotopes

Groundwater samples collected for total strontium and strontium isotope ratio analyses were collected in 30 mL HDPE bottles. The bottles were rinsed with filtered groundwater three times before sample collection. Raw groundwater was filtered using Minisart® 0.45 μm syringe filters and then acidified using 70% HNO_3 to pH <2

as described by Bullen *et al*. (1996). These samples were stored in a refrigerator at 3-5 ^{o}C until analysis.

4.1.2.4. Dissolved noble gases

Groundwater samples for noble gas analyses were collected using the copper tube method as frequently described in the literature (eg. Weiss, 1968). The key points to note about this method are that air bubbles must be purged or prevented from forming inside the copper tube prior to clamping and that the stainless steel 'pinch-off' clamps must be fully tightened so that the contact areas of the clamps meet completely and no gaps remain. Clear Portex® tubing was used to facilitate visual inspection of bubble formation within the connecting tubes near each end of the copper sampling tube and near the ball valve fittings and jubilee clips. A simple ball valve was used to apply sufficient back pressure to maintain or exceed the original level of hydrostatic pressure during sampling. The stainless steel clamps were designed and manufactured so that when the hex bolts are fully tightened and the clamp contact areas meet, a precisely engineered aperture exists in the centre of the clamp to form an excellent seal. It is impossible to over tighten these clamps except for the possibility of shearing-off the bolt head. However, if insufficient torque is applied then there is the possibility of a poor seal and subsequent partial de-gassing of the sample. A long handled wrench was used to enable the bolts to be tightened with sufficient torque.

The copper tubes and stainless steel clamps were held in the desired position by a length of aluminium channel that had been custom designed and milled at the UEA mechanical workshop and included locating holes for two clamps at a fixed distance apart ensuring that the sample size was relatively constant.

Special care is required when transporting and storing the samples subsequent to collection because the ends of the copper tubes become very susceptible to damage once the clamps have been tightened. A purpose built storage rack was used to transport the samples in the field which provided adequate protection against tube damage.

4.2. Analytical techniques

4.2.1. Field parameter data and hydrochemistry

All field parameter data and hydrochemistry including ionic and trace element analysis were conducted by the Erftverband technicians in the field and at the Erftverband laboratories in Bergheim, Germany using a range of analytical instruments such as Ion Chromatography and Inductively Coupled Plasma - Mass Spectrometry (ICP-MS). The reader is referred to Skoog (2004) for a good overview of analytical chemistry and the relevant techniques and instruments.

4.2.2. Stable isotope analysis

4.2.2.1. Oxygen Isotopes

$\delta^{18}O$ analysis was conducted using a modification of the CO_2-H_2O technique based on the oxygen isotope equilibration of an aliquot of CO_2 with the groundwater sample under closed conditions as first described by Epstein and Mayeda (1953).

Glass reaction vessels were evacuated prior to an aliquot of CO_2 being admitted. 2.4 mL of raw groundwater was then injected into each reaction vessel. The

vessels were gently agitated for six hours in order for complete oxygen isotope equilibration to be achieved. The CO_2 is extracted and passed through a cold trap to remove water vapour before being analysed using a Europa SIRA II Isotope Ratio Mass Spectrometer (IRMS). The UEA laboratory reference standard is North Sea Water ($\delta^{18}O$ = -0.20‰ VSMOW). The standard is incorporated into the batch of groundwater samples with a total of 48 water samples being analysed per day. The analytical precision for $\delta^{18}O$ analysis is 0.04‰ VSMOW (± 2σ).

4.2.2.2. Hydrogen Isotopes

$\delta^{2}H$ analysis was conducted using the continuous flow technique where 0.1 μL of raw groundwater sample was manually injected using a 0.5 μL syringe into a stream of helium carrier gas. The 0.1 μL groundwater sample is carried though an oven where it is vaporised at 140 ºC and then reacted with activated carbon at 1422 ºC which evolves H_2 and CO_2 gas. Hydrogen is ionised in the source of a Europa GEO MS and the $(H^2H+H_3)/H_2$ ratio is measured using a special collector assembly designed for the widely separated H_2^+, H^2H^+ ion beams. Norwich Tap Water (NTW) was used as a standard for calibration ($\delta^{2}H$ = -44.9 ± 2‰ VSMOW). The analytical precision is considerably lower than $\delta^{18}O$ at ± 1.4‰ VSMOW (± 2σ).

4.2.2.3. $\delta^{13}C_{DIC}$ sample preparation and analysis

In the laboratory, the strontium carbonate precipitate ($SrCO_3$) that had formed in the groundwater sample from the addition and subsequent reaction of $SrCl_2$–NH_4OH in the field, was filtered using Whatman #1, Ø 55 mm filters under an atmosphere of nitrogen and using a vacuum pump. The $SrCO_3$ precipitate was then rinsed with polished deionised water for a further three minutes. The filter papers

containing the $SrCO_3$ precipitate were quickly transferred to individual clean Petri dishes and placed in a vacuum oven to dry at 70 ºC for approximately six hours. Once dried, the strontium carbonate precipitate was carefully scraped off the filter paper using a sharp blade and placed in small glass vials with airtight caps and stored in a vacuum desiccator until analysis. Approximately 150–200 μg of the strontium carbonate precipitate and 100–150 μg Carrera Marble (UEA-CMST, $\delta^{13}C$ = 2.01 ± 0.08 ‰ PDB) was used for analysis and calibration respectively.

The $\delta^{13}C_{DIC}$ analysis was conducted using a Europa SIRA II dual inlet mass spectrometer. The $SrCO_3$ is reacted with phosphoric acid (HP_3O_4) to produce carbon dioxide ($CO_{2(g)}$). The analytical precision for this method is ± 0.1‰ VPDB.

4.2.2.4. Strontium sample preparation and analysis

Strontium isotope analyses were conducted by Henriette Ueckermann and Jurian Hoogewerff within the School of Chemistry at the University of East Anglia (UEA). 12-14 mL of the prepared groundwater sample was decanted into 15 mL vessels to avoid contaminating the original sample and therefore preserving it for future use. 1 mL of the sample was then mixed with 9 mL of an internal standard to produce a tenfold dilution. The internal standard consisted of 2% HNO_3 with 10 ppb GeRhPt. The analysis was done using an Isoprobe Multiple Collector Inductively Coupled Plasma Mass Spectrometer (MC-ICP-MS) fitted with an array of faraday cups to measure an atomic mass range from 83 to 88. The analytical precision for this technique is 0.00007 (± 3σ).

4.2.3. Dissolved noble gases

4.2.3.1. Quadrupole mass spectrometry

Quadrupole mass spectrometry provides a cost effective analytical technique to determine noble gas abundances in groundwater (eg. Poole *et al.*, 1997; Kulongoski and Hilton, 2002), whereas magnetic sector mass spectrometry provides increased resolution and enables the quantification of noble gas isotopes with very low natural abundances such as ^{3}He, ^{21}Ne and ^{36}Ar (eg. Beyerle *et al.*, 2000). Quadrupole mass spectrometers consist of four parallel circular metal rods (see Figure 4.5), an ion source, ion optics for accelerating and focussing the ions through the aperture into the quadrupole filter, an exit aperture, a faraday cup and/or a secondary electron multiplier (SEM) detector, and a high vacuum (HV) system.

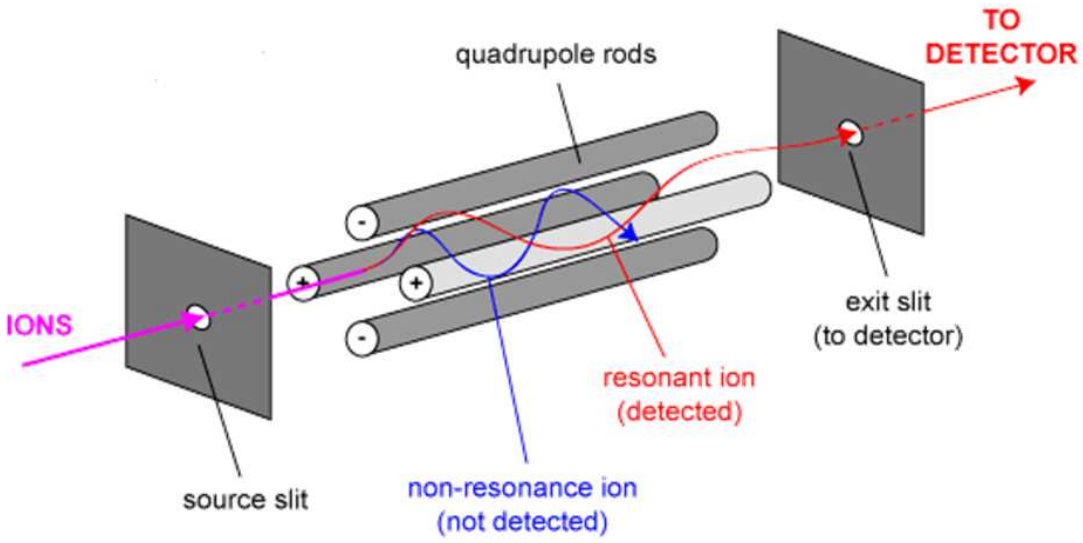

Figure 4.5. Schematic diagram of a typical quadrupole analyser (image produced by P. Gates, University of Bristol).

An opposing rod pair has an applied potential of +(U+Vcos(ωt)) and the remaining two rods have an applied potential of –(U+Vcos(ωt)). Where, U is a fixed DC voltage and Vcos(ωt) is an applied RF potential that has an amplitude V and frequency ω.

For mass separation, quadrupole mass spectrometers use a high radio frequency (RF) oscillating potential that affects the trajectory of ions along the flight path that is centred between the four parallel metal rods. For any given DC and AC voltage, only ions with a particular mass:charge ratio (m/z) will pass through the quadrupole filter to the detector. Quadrupole mass analysers including ion trajectories are discussed in detail by Batey (1987). Quadrupole mass spectrometers are widely used because of their robust performance, compact size and relatively low cost. Quadrupole mass spectrometers also offer rapid measurements and a high dynamic range in comparison to magnetic sector instruments.

Groundwater samples collected from the Lower Rhine Embayment during 2007/08 for this research were analysed for dissolved noble gases at the Stable Isotope Laboratory, UEA using a purpose built high vacuum preparation line and AN-5T quadrupole mass analyser operated in static mode. The instrument used and the principles of the analytical procedure have been described in depth by Poole *et al*. (1997) and Ingram (2005).

4.2.3.2. Isotope dilution mass spectrometry

Isotope dilution mass spectrometry (IDMS) is based on the principle that a known quantity of a spike isotope is added to the sample before analysis. The spike isotope is usually a stable isotope with low natural abundance, such as ^{3}He, ^{22}Ne, ^{36}Ar or ^{78}Kr in the case of noble gas analyses. The spike isotope(s) and sample are mixed

and the isotope ratio R of the spike isotope and the most naturally abundant isotope in the sample is measured using isotope ratio mass spectrometry (IRMS) typically for example, with a quadrupole mass analyser as described in Section 4.3.1. The isotope dilution equation is expressed as:

$$ {}_{i}N_{sample} = \frac{{}_{i}N_{spike}\left({}_{i}A^{h}{}_{spike} - {}_{i}R \cdot {}_{i}A^{l}{}_{spike}\right)}{{}_{i}R \cdot {}_{i}A^{l}{}_{sample} - {}_{i}A^{h}{}_{sample}} \qquad (4.1) $$

Where: N = number of atoms
A = isotope abundance (%)
R = isotope ratio

Uncertainty in IDMS measurements arise from errors in determining the spike concentration accurately and from isotope fractionation effects in the source of the mass spectrometer during analysis (Faure and Mensing, 2005).

4.2.3.3. Calibration

It is essential to calibrate instrument response to sample concentration. The calibration process for the noble gas analyses conducted during this research using the high vacuum (HV) preparation line and quadrupole mass spectrometer described by Poole *et al.* (1997) and Ingram (2005) involved calculating the tracer spike concentration by admitting an aliquot of the tracer spike with a known volume of analyte (atmospheric air). The tracer spike concentration will decrease with each subsequent analysis because it is not possible to maintain a constant pressure within

the tracer cylinder. Therefore, both the initial tracer spike concentration and the tracer depletion rate need to be calibrated.

The noble gas analysis system described by Poole *et al.* (1997) was designed to be calibrated using a simple atmospheric air spike of known volume (0.2176 cm^3) which is collected in a small inlet valve attached to the HV preparation line. The atmospheric abundance of each noble gas is well known and taken from the literature (eg. Ozima and Podosek, 2002) and the temperature, atmospheric pressure and relative humidity are recorded at the time the air spike was prepared. The tracer volume depletion rate is simply calculated from the tracer cylinder volume (309.5 cm^3) and the tracer aliquot volume (0.855 cm^3) respectively, and can be assumed to be constant at 0.002755.

This calibration procedure is quick and simple and only requires one initial determination and then re-calibration every 15-20 sample analyses. However, the calibration does not consider the linearity of the response of the mass spectrometer to noble gas concentrations that vary by several orders of magnitude, which is observed between the concentration of noble gases in the air spike and the noble gas concentrations present in a groundwater sample. This however, appears to have a negligible effect on the results obtained from previous use of the instrument by Poole *et al*. (1997). Ingram (2005) recognised that the design of the standard calibration technique made no attempt to check the linearity of the MS response and that previous use of the instrument had assumed that the response of the MS was linear over the range of concentrations measured. Ingram (2005) presents data that confirms the linearity of the mass spectrometer over a small range of 'typical' concentrations reasonably well but the calibration does not extend to the high helium concentrations that have been measured during this research. Unfortunately, the current design of the

instrument does not allow for the empirical calibration of linearity to be determined up to 3-4 orders of magnitude above atmospheric solubility equilibrium concentrations for helium. Therefore, for the purpose of this study it has been assumed that the response of the MS is linear over the range of concentrations measured. To support this assumption, groundwater samples containing high ^{4}He concentrations were analysed at both the Stable Isotope Laboratory at UEA and at the USGS Reston Laboratory, with the results comparing very well and thus providing additional confidence in the analytical procedure.

4.2.3.4. Experimental errors and propagation

Errors are incurred during sample analysis and propagated through the calculation process that is necessary to determine dissolved noble gas concentrations in a groundwater sample. Standard error propagation mathematics was applied to calculate the experimental uncertainty associated with noble gas concentrations.

Standard error propagation laws state that for summation or subtraction, the square of the error in the sum or difference of two numbers (A and B) is equal to the sum of the squares of individual absolute error estimated for values A and B. This can be expressed as:

$$(error\{A+B\})^2 = (error\{A-B\})^2 = (error\{A\})^2 + (error\{B\})^2$$

$$error(A+B) = \sqrt{(error\{A\})^2 + (error\{B\})^2} \qquad (4.2)$$

Where: A = *value A*
B = *value B*
$error\{A\}$ = *absolute error of A*
$error\{B\}$ = *absolute error of B*

For multiplication or division, the relative error in a product or quotient is equal to the square root of the sum of the squares of the relative errors in the individual factors. Absolute errors are calculated by multiplying both sides by the denominator. This can be expressed as:

For relative errors:

$$\left(\frac{error\{AB\}}{AB}\right)=\left(\frac{error\left\{\frac{A}{B}\right\}}{\left(\frac{A}{B}\right)}\right)=\sqrt{\left(\frac{error\{A\}}{A}\right)^2+\left(\frac{error\{B\}}{B}\right)^2} \qquad (4.3)$$

For absolute errors:

$$error\{AB\}=(AB)\sqrt{\left(\frac{error\{A\}}{A}\right)^2+\left(\frac{error\{B\}}{B}\right)^2} \qquad (4.4)$$

$$error\left\{\frac{A}{B}\right\}=\left(\frac{A}{B}\right)\sqrt{\left(\frac{error\{A\}}{A}\right)^2+\left(\frac{error\{B\}}{B}\right)^2} \qquad (4.5)$$

Where: A = *value A*
B = *value B*
$error\{A\}$ = *absolute error of A*
$error\{B\}$ = *absolute error of B*

4.2.3.5. Preparation of the tracer spike

The tracer spike was prepared in the Stable Isotope Laboratory at UEA using the rare noble gas isotopes of ^{3}He, ^{22}Ne, ^{36}Ar, ^{78}Kr and ^{129}Xe. These high purity gases were sourced from CHEMGAS of Boulogne, France and valve adaptors were manufactured by Chell Instruments in North Walsham, Norfolk, UK.

The tracer spike was prepared by taking the five rare isotopes (of approximately known concentrations) and expanding each gas into a glass vacuum line. By using multiple expansions and calibrated volumes along with a sensitive pressure gauge it was possible to calculate and isolate the desired concentration of each gas within the vacuum line. The rare noble gas isotopes were isolated in evacuated glass vessels attached to the vacuum line until the final stage of the process which involved mixing the five noble gas isotopes together and expanding them into a stainless still cylinder of known volume which would later be attached to the noble gas preparation line and used to admit the tracer spike into the noble gas preparation line with the sample gases before analysis. The quantity of each gas was calculated so that the abundance of the rare isotope would be approximately equal to the abundance of the most naturally occurring isotope in a 5-6 g groundwater sample size when analysed using IRMS.

4.2.3.6. Noble gas analysis

A detailed account of the analytical procedure is provided by Poole *et al.* (1997) and comprehensive step-by-step instructions are given by Ingram (2005). The following information provides additional content and includes recent operational

modifications and improvements that have been made to the analytical system during this research.

4.2.3.7. Sample preparation

The only preparation that the groundwater samples collected for noble gas analysis required was the splitting of copper tubes so that a suitable sample size was available for analysis. The sample size was calculated based on the capacity of the sample inlet cup and the estimated quantity of dissolved noble gases in a sample of a given size. A sample size of 5-6 g of groundwater was used and the copper tubes were split accordingly. This was done by tightening an additional swage clamp 10 cm inwards from one of the original clamps, and another additional swage clamp 14 cm inwards from the other recently attached clamp. Once the two additional clamps had been fully tightened the copper tube was cut using a copper pipe cutter at the mid-point between the two additional clamps. This produced both a 5-6 g sample with 7 cm of copper tube on each end necessary for attaching it to the preparation line, and a spare sample that could be divided into two more samples if duplicate or triplicate analysis was required. Note that due to the relative incompressibility of water only three samples could be made from one original cooper tube sample as the volume decreases slightly each time it is clamped.

4.2.3.8. Preparation Line and Quadrupole MS

Prior to attaching the sample inlet cup and copper tube containing the groundwater sample, and subsequent to each sample analysis, both cold traps were baked at 500 ºC for 60 minutes, and all component parts of the preparation line (see Figure 4.6) such as the argon trap, sample metering volumes, getter pumps, air spike

volume and tracer aliquot volume were pumped using the turbo molecular pump to a vacuum of $<10^{-3}$ mbar.

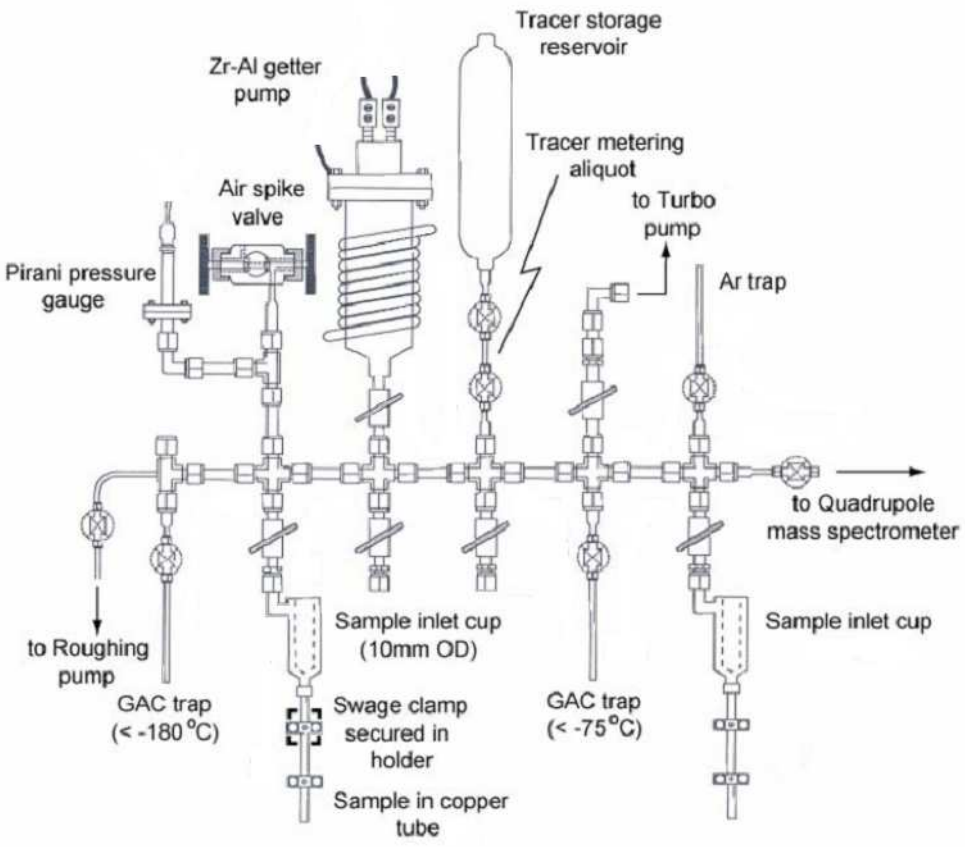

Figure 4.6. Schematic of the noble gas preparation line (after Ingram, 2005).

To achieve optimal operating conditions a current of approximately 1.5 A was applied continually to the preparation line and quadrupole heating tapes to warm the stainless steel and minimise out-gassing from the metal surfaces during analyses. If the preparation line or quadrupole MS were exposed to the atmosphere as a result of pump failure for example, it was necessary to increase the current applied to the quadrupole heating tape for several days, until the ^{40}Ar ion current intensity remained stable during analysis and a error of ≤1% is achieved for argon isotope ratio analysis.

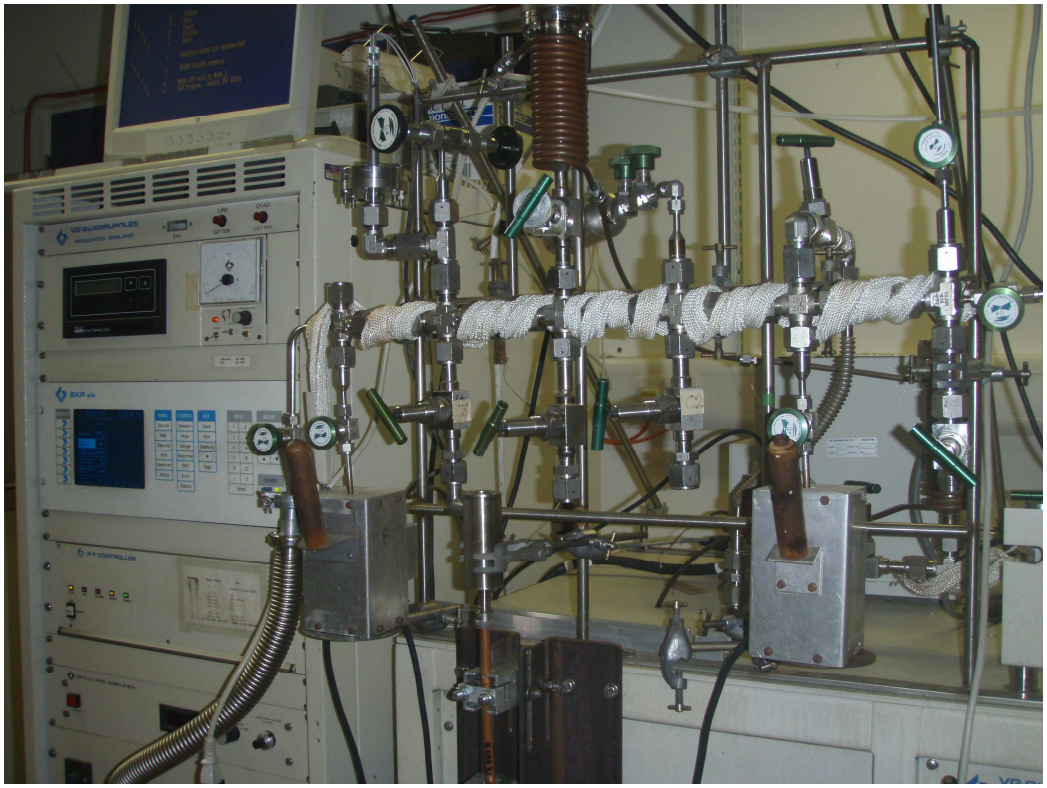

Figure 4.7. Photograph of the noble gas preparation line and the *SXP Elite* control system at the Stable Isotope Laboratory, UEA.

4.2.3.9. Getter pump activation

The noble gas preparation line and quadrupole MS has two SAES GP50 Zr-Al alloy getter pumps with St101 cartridges that need to be activated before the first sample analysis and again after two or three subsequent analyses. However, it was clear that getter pump activation was usually necessary after each analysis but this did depend on the volume of dissolved gas in the sample and the amount of water vapour that entered the preparation line during sample admission. The getter pumps are used to remove all reactive gas species from the sample. Hydrogen is adsorbed reversibly

and other active gases such as carbon monoxide, carbon dioxide, oxygen and nitrogen are adsorbed irreversibly onto the Zr-Al surface of the cartridge. Water vapour and hydrocarbons are adsorbed both reversibly and irreversibly (SAES Getter Pump Manual). Activation of the getter pumps occurs at ~600 ºC (3.5 A) for 45 minutes under a vacuum of 10^{-3} mbar achieved using the turbo pump. It was important to isolate the quadrupole getter pump from the quadrupole mass spectrometer before initiating the activation process. After 45 minutes, the temperature of the getter pumps is reduced to 400 ºC (2.25 A) and the quadrupole getter pump is isolated from the turbo pump. The preparation line getter pump must also be isolated from the preparation line at this stage. It is essential not to expose the getter pumps to water vapour or other reactive gas species once they have been activated; if that occurs, re-activation is necessary. Further technical information can be found at http://www.saesgetters.com.

4.2.3.10. Sample inlet cup attachment

Attaching the sample inlet cup correctly is essential to prevent the loss of sample gases or the addition of gas from the atmosphere as well as achieving a sufficient vacuum. All valves must be closed including the valve to the turbo pump before attaching the sample inlet cup. Each time the sample inlet cup is attached to the preparation line, a new VCR copper or nickel gasket is required. Special attention is needed to ensure that the sample inlet cup is thoroughly dry before attachment to the preparation line. Access to the internal surfaces of the inlet cup is particularly limited and therefore oven drying at 80 ºC for at least eight hours is recommended. Note that correct orientation of the inlet cup is essential for successfully attaching the sample

later. Once the inlet cup has been attached to the preparation line, the stainless steel blanking plug is inserted into the open end of the sample inlet cup. It is necessary to apply a small amount of vacuum grease to the rubber o-ring and finger-tighten the Cajon fitting. The turbo pump is isolated from the preparation line before opening the valve between the inlet cup and preparation line, and the roughing pump must be used to evacuate the inlet cup. If the pressure remains greater than 1 mbar for more than a few minutes, it is likely that the copper gasket has failed to produce an adequate seal or a small quantity of water is present in the sample inlet cup. Once a vacuum of <1 mbar has been achieved, the valve to the roughing pump can be closed and the valve to the turbo pump opened. It is necessary to continue pumping the sample inlet cup until a vacuum of 10^{-3} mbar has been reached.

4.2.3.11. Sample attachment

To correctly attach a copper tube containing a groundwater sample, the sample inlet cup must first be isolated from the preparation line. The stainless steel blanking plug is replaced with a pre-weighed copper tube containing approximately 5 mL of groundwater sample (see Section 4.3.6.1). The upper clamp of the sample should fit easily into the aluminium sample holder mounted below the inlet cup (Figure 4.6). If the inlet cup has not been aligned correctly it is difficult to locate the upper clamp in the aluminium sample holder and insert the copper tube into the sample inlet cup via the Cajon fitting. The aluminium sample holder must be adjusted to ensure that the correct height is achieved and it is secured using a 13 mm spanner to provide additional support for the copper tube. Once the sample is secure, and the turbo pump has been isolated from the preparation line, the sample inlet cup and upper end of the

copper tube are evacuated using the roughing pump until a vacuum of <1 mbar is achieved. The valve to the roughing pump can then be closed and the valve to the turbo pump is opened. It is very important to continue to pump the sample until a vacuum of 10^{-3} mbar has been reached and that this level of vacuum can be maintained if the turbo pump is isolated. An increase in pressure subsequent to the turbo pump being isolated indicates degassing of the sample across the cooper tube seal or an inadequate seal between sample and inlet cup.

4.2.3.12. Degassing the sample

Degassing the groundwater sample is a critical part of the analytical procedure and great care is required to ensure that it is done correctly. The valve to the sample inlet cup must be closed and the turbo pump should be isolated from the preparation line. The sample inlet cup is filled with ethanol and dry ice pellets. It is necessary to introduce the dry ice pellets individually until the ethanol has cooled sufficiently and sublimation has ceased. Ensuring that the sample is securely mounted in the aluminium holding device, the two 13 mm hex nuts of the clamp are slowly unscrewed using a ring spanner or long barrelled socket wrench. Note: the nuts are often very tight depending on storage time/conditions; however, they must not be loosened at any stage prior to this point as this will compromise the seal and could result in partial degassing of the sample. The clamp is completely removed and retained for weighing. A modified clamp is used to reform the copper tube. The modified clamp is placed over the cold weld perpendicular to the position of the original clamp and slowly tightened to open the seal. The sample degasses at this stage and the ethanol/dry ice mixture usually boils over. It is not necessary to fully

open the cold weld and doing so often results in the copper tube splitting and the sample being no longer useable. Any uncertainty regarding the copper tube is easily determined by monitoring the pressure as the sample gas is admitted to the preparation line. To ensure that the sample has been fully degassed, the copper tube is heated with a hot air gun to a temperature sufficient to vaporise the sample. It was noted that ice often formed where the cold weld had been opened and inside the lower section of the sample inlet cup. This prevented the remaining part of the groundwater sample from reaching the internal surface of the inlet cup where it is intended to freeze as a result of the dry ice pellets and ethanol mixture – these areas are given particular attention with the heat gun. The copper tube is heated for approximately 15 minutes in total until complete transfer of the groundwater sample from the copper tube to the inlet cup has occurred. The sample inlet cup requires refilling with dry ice pellets and ethanol during the heating process.

4.2.3.13. Expanding the sample gas into the Preparation Line

During the sample heating process, the valve to the turbo pump is closed and the valve to the tracer spike gas cylinder is opened and the tracer gases are expanded into the small tracer spike metering volume. It is very important that the second valve is closed to prevent the tracer gas mixture entering the preparation line. After two minutes the valve to the tracer cylinder must be closed and the valve to the preparation line is opened, expanding the aliquot of tracer gases into the preparation line. After a further two minutes the valve is closed and the tracer aliquot volume is isolated from the preparation line – this will reduce the possibility of contaminating the tracer gas mixture in the cylinder as the metering volume will only contain the

tracer spike gases. Using the current tracer gas mixture the pressure in the line will increase to approximately $4x10^{-2}$ mbar; but this will decrease with each subsequent analysis according to the tracer depletion factor. The valve to the sample inlet cup is then opened and the sample gas is expanded into the preparation line. The pressure in the line typically increases to approximately 1 mbar but this depends on the quantity of dissolved gas in the groundwater sample. However, a pressure of >2 mbar indicates that air has entered the system, usually during the cold weld opening and reforming procedure. If a pressure of >2 mbar is observed the analysis is abandoned.

The valve to the sample inlet cup must be open for five minutes and it is essential to ensure that the inlet cup remains full with dry ice pellets and ethanol – this removes any remaining water vapour that might have entered the preparation line. After 5 minutes the valve to the inlet cup is closed and the valve to the preparation line getter pump is opened. The getter pump removes all reactive gases from the sample. This is monitored by observing the Pirani gauge and pressure decrease with time. Depending on the operating condition of the getter pump the duration of this process ranges from thirty seconds to approximately ten minutes. If the getter pump fails to remove the reactive gases then re-activation is necessary and the run must be abandoned although increasing the current to the getter pump and therefore increasing the temperature has had positive results on some occasions (see Section 4.3.6.3).

4.2.3.14. Partitioning the noble gases for analysis

At this stage of the analytical procedure, the preparation line only contains the noble gases of helium, neon, argon, krypton and xenon. To facilitate accurate and precise isotope ratio measurements, the gases undergo cryogenic separation. Argon is

significantly more abundant than the other noble gases and it is therefore not necessary to isolate it from the other gases as they will not interfere with the measurements. The valve to the argon trap is opened for two minutes to collect an aliquot of gas for argon analysis later in the procedure. Ensuring that the valve to Cold Trap 1 is closed, a dewar of ethanol/dry ice slush is placed around the cold trap. Once Cold Trap 1 has reached the desired temperature (a thermocouple is used to check the temperature) the valve to Cold Trap 1 is opened for ten minutes – krypton and xenon are adsorbed onto the activated charcoal within the cold trap. A Pirani gauge is used to monitor the progress of this process. Initially, the pressure decreases steadily and then remains constant once all the krypton and xenon has been adsorbed onto the activated charcoal. After ten minutes the valve to Cold Trap 1 is closed but the dewar containing the ethanol/dry ice slush must remain as this is required later. Using a second dewar, liquid nitrogen is placed around Cold Trap 2 and then the valve is opened for ten minutes to remove argon from the remaining gas mixture in the preparation line. After ten minutes has elapsed the valve to Cold Trap 2 is closed – helium and neon are the only remaining gases in the preparation line at this stage and the pressure in the preparation line is usually just below the detection limit of the Pirani gauge.

4.2.3.15. Noble gas analysis using the SXP Elite system.

Ingram (2005) describes in detail the systematic procedure for admitting the noble gases from the preparation line to the quadrupole mass spectrometer for isotope ratio measurements. During this research it was determined by a number of investigative experiments that the system performed better if the quadrupole getter

pump remained isolated from the quadrupole mass spectrometer during the analysis of the noble gases. The SXP Elite settings are critical for accurate noble gas isotope ratio analysis and extensive testing was conducted during this research to determine the optimal settings. These control settings are presented in *Appendix 2*.

4.2.3.16. Air saturated water standards and solubility equations

To verify the overall analytical procedure, air saturated water (ASW) samples were analysed at a range of different temperatures. Open HDPE vessels (2.5 L) were used to equilibrate water with the atmosphere. The water containers were stored at known constant temperatures which were recorded at least twice daily and the ambient atmospheric pressure was also monitored and recorded over a 7-10 day period. The water was continually aerated gently during the equilibration period to facilitate gas exchange. Samples were collected in glass vessels and analysed in the same way as the groundwater samples in copper tubes.

Table 4.1. Air saturated water equilibration temperature and the corresponding equilibration temperature determined using NOBLE90.

ASW	**NOBLE90 NGT**	**Error (±)**
(ºC)		
3	2.5	8.4
3	0.2	5.3
13	9.1	8.8
13	9.9	9.1
15	**14.7**	**0.5**
15	**16.3**	**1.1**
21	20.1	2.1
21	9.5	5.0

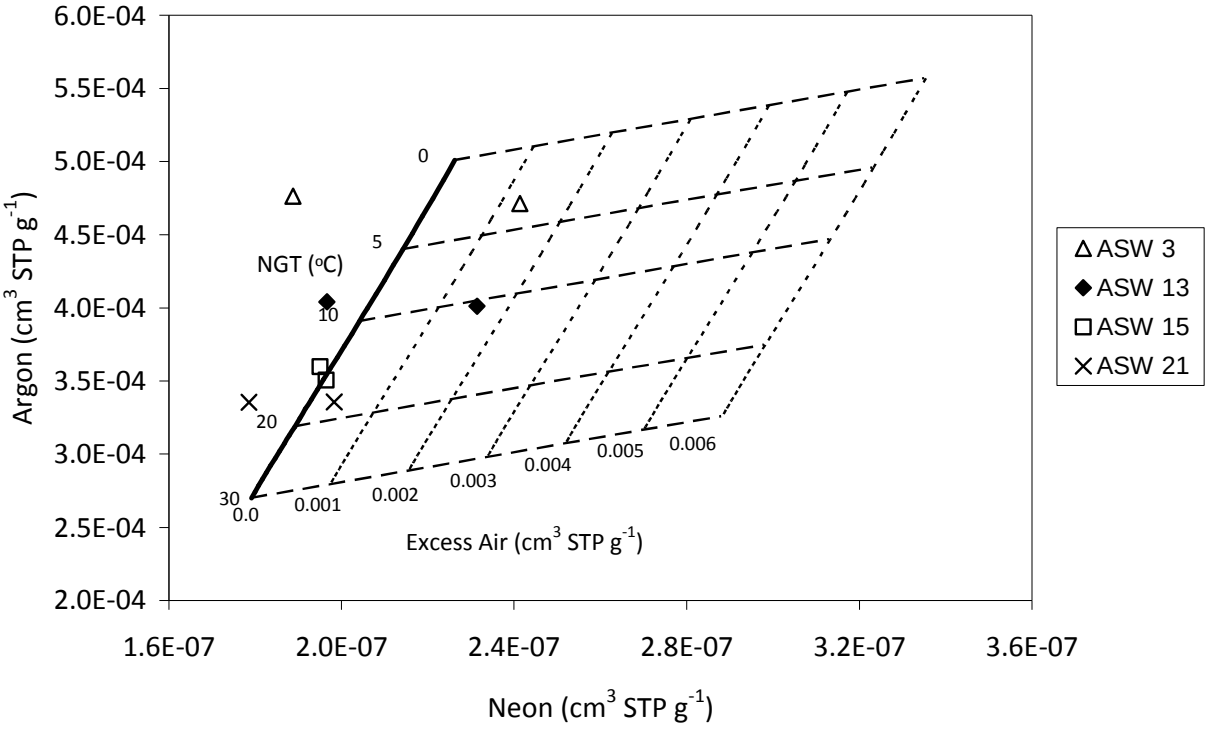

Figure 4.8. Cross plot of argon against neon for air saturated water (ASW) samples in relation to atmospheric solubility equilibrium concentrations and the presence of excess air.

The ASW water samples equilibrated at 3, 13 and 21 ºC (Table 4.1) were analysed before the quadrupole mass spectrometer was operating optimally which would explain the very poor accuracy and low precision of these results. It should be noted that all groundwater samples analysed during this period have not been presented in this thesis due to large analytical uncertainties. The quadrupole mass spectrometer and preparation line were vigorously tested and adjusted/tuned using air spikes to ensure that the final set of results were robust and as accurate as possible. All the data presented in this thesis were obtained subsequent to this point and that also includes the ASW 15 ºC samples which can be seen in Figure 4.8 and in Table 4.1. The analytical precision of determining noble gas isotope ratios using the

quadrupole mass spectrometer is between 0.2 and 1% but combined with the propagated error associated with the calculations required for determining noble gas concentrations in groundwater, the overall precision is 1.6% for helium, 1.4% for neon, 1.2% for argon, 2.5% for krypton and 6.0% for xenon. Replicate sample analysis (Table 4.2) shows that modelled NGTs using NOBLE90 have a larger uncertainty than suggested from the isotope ratio measurements and the additional error propagation due to the calculations required for determining noble gas concentrations from the raw isotope ratios but reproducibility is generally good.

Table 4.2. Replicate groundwater samples modelled for NGTs using NOBLE90.

Observation Borehole ID	1st		2nd	
	NGT	Error	NGT	Error
	(°C)			
Pulheim III (937491)	10.0	0.9	12.7	0.8
Myllendonk (907641)	13.6	0.8	10.7	0.8
SW Brühl 22 R1 (352721)	12.0	0.9	12.7	0.4

Noble gas solubility data and model equations were used for the initial graphical interpretation of the dissolved noble gas results including the ASW samples (Figure 4.8). The data in Table 4.3 and Table 4.4 were determined empirically by Weiss (1970; 1971) and Benson and Krause (1976) respectively, and has subsequently been presented concisely by Ozima and Podosek (2002). Equation 4.6 and Equation 4.7 were used to determine the equilibrium solubility relationships at $S = 0$.

Table 4.3. Solubility of gases in water and sea water for use in Equation 4.6.

Gas	A_1	A_2	A_3	B_1	B_2	B_3
He	-34.6261	43.0285	14.1391	-0.042340	0.022624	-0.0033120
Ne	-39.1971	51.8013	15.7699	-0.124695	0.078374	-0.0127972
Ar	-55.6578	82.0262	22.5929	-0.036267	0.016241	-0.0020114

(Weiss, 1970; 1971)

$$\ln \beta = A_1 + A_2\left(\frac{100}{T}\right) + A_3 \ln\left(\frac{T}{100}\right) + S\left[B_1 + B_2\left(\frac{T}{100}\right) + B_3\left(\frac{T}{100}\right)^2\right] \qquad (4.6)$$

(Weiss, 1970)

Table 4.4. Solubility of gases in pure water for use in *Equation 4.7*.

Gas	A_0	A_1	A_2
Kr	3.6326	5664.0	-1122400
Xe	2.0917	6693.5	-1341700

(Benson and Krause, 1976)

$$\ln k = A_0 + \frac{A_1}{T} + \frac{A_2}{T^2} \qquad (4.7)$$

(Benson and Krause, 1976)

$$\beta = k \times 1244.142 \qquad (4.8)$$

The Henry constant k (atm) is related to the Bunsen coefficient β (cm^3 STP g^{-1} H_2O atm^{-1}) by Equation 4.8 and both of these solubility parameters were used to calculate the solubility equilibrium concentrations that provided a simple graphical interpretation (see Figure 4.8, Figure 5.10, Figure 5.11 and Figure 5.12) of the measured noble gas concentrations in groundwater samples collected from the Lower Rhine Embayment.

5. Results

5.1. Hydrochemistry

The chemical interactions that occur between groundwater and the solid phases that make up the aquifer matrix create a large array of dissolved inorganic chemical constituents in groundwater and most of the solutes are present in ionic form (Freeze and Cherry, 1979). However, the distinctive chemical composition of groundwater is largely established in the unsaturated zone, and the hydrochemical evolution that occurs in the saturated zone follows a steady progressive path towards increasing aquifer confinement and/or discharge (Herczeg and Edmunds, 1999). The unconsolidated siliciclastic sedimentary deposits of the Lower Rhine Embayment consist of layered and mixed assemblages of minerals that are likely to cause large differences in hydrochemistry on both a local and regional scale. Silicate aquifers typically exhibit a wide range of hydrochemical facies because of variations in mineral content and the results of weathering reactions (Appelo and Postma, 2005).

The hydrochemical analyses of groundwater samples collected from the Lower Rhine Embayment during 2007/08 were kindly conducted by the Erftverband at their laboratories in Bergheim, Germany.

5.1.1. Hydrochemical facies

The concept of hydrochemical facies was first introduced by Chebotarev (1955). A hydrochemical facies is defined as a groundwater type that has a specific ionic composition set within well defined limits. Hydrochemical facies are particularly useful for identifying the hydrochemical evolution of groundwater as well as for investigating the spatial variability of groundwater chemistry in complex multi-

component systems such as the Lower Rhine Embayment. However, it must be noted that the use of hydrochemical facies does not yield definitive information regarding the geochemical processes that cause the observed changes in hydrochemistry and that groundwater residence times can only be inferred in a qualitative way. Table 5.1 shows a summary of major ion concentrations for groundwater samples collected from observation boreholes within the Lower Rhine Embayment during 2007/08. The complete data set for major ion concentrations for each groundwater sample is included in Appendix 3 and the interpretation and discussion of the results are given in Chapter 6.

The Durov diagram (Figure 5.1) was used to help define hydrochemical facies based on major ion composition. Figure 5.1 indicates that groundwater samples from the Lower Rhine Embayment can be divided into two groups based on the dominant cation which is either Ca^{2+} or Na^{+}. The dominant cation for the main cluster of groundwater samples is Ca^{2+}, and these sample points can be subdivided into five hydrochemical facies based on ionic composition and their relative concentrations. A small number of groundwater samples are dominated by Na^{+} ions and these can also be subdivided into two separate groups. It can be seen from Figure 5.1 that ionic composition varies more for anions than it does for cations but although HCO_3^{-} and SO_4^{2-} dominate in a large number of groundwater samples, there are a significant number a samples that have no clear dominant anion. Cl^{-} is the dominant anion in groundwater that originated from just one observation borehole in the Brühl region of the Lower Rhine Embayment.

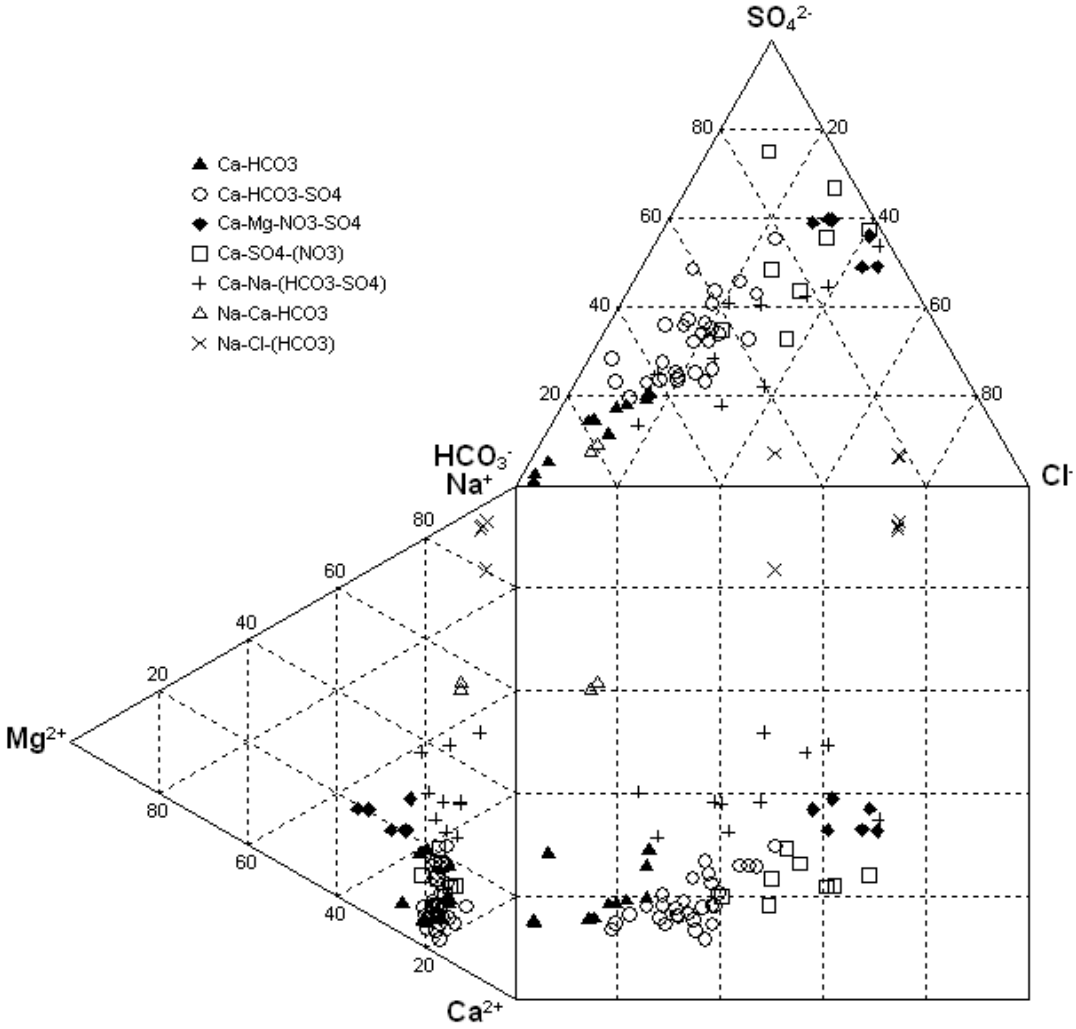

Figure 5.1. The Durov plot provides a graphical representation of the hydrochemical facies present in the Lower Rhine Embayment, Germany. The majority of groundwaters are of a Ca-HCO_3 or Ca-HCO_3-SO_4 hydrochemical type whilst a small number of samples are dominated by Na-Cl and are easily distinguishable from the main cluster of samples.

The most frequently occurring groundwater type is Ca-HCO_3-SO_4. It was possible to define seven different hydrochemical facies using the AquaChem® 3.7 software package and each hydrochemical facies has been assigned a specific symbol (see Figure 5.1). AquaChem® 3.7 determines groundwater type by converting measured ionic concentration data from mg L^{-1} to meq L^{-1} and then transforming the units to meq %. All parameters with values of less than 10% are removed and the remaining ions are used to define the groundwater type and create a string name. The ions are ordered by % with cations stated first followed by anions. Ca^{2+} is the dominant cation for Groups 1-5 which includes all of the points in the main cluster of samples. These groups are primarily composed of Ca-HCO_3 and Ca-HCO_3-SO_4 type groundwaters, with just a small number of samples displaying increased Mg^{2+}, NO_3^- or Na^+. It is evident from Figure 5.1 that a small number of groundwater samples show Na^+ as the dominant cation. These groundwaters include the most hydrochemically distinct groundwater type of Na-Cl-(HCO3) as well as Na-Ca-HCO_3 type groundwater.

Figure 5.2 illustrates the spatial distribution of hydrochemical facies within the Lower Rhine Embayment, whereas Figure 5.3 and Figure 5.4 display the spatial distribution of Na^+ and Cl^- respectively. Geographically, it is difficult to discern clear regional patterns perhaps with the exception of higher Na^+ concentrations near the Viersen fault. However, a full interpretation and discussion of the hydrochemical data summarised in Table 5.1 and presented in full in Appendix 3 is given in Chapter 6.

Table 5.1. Observed concentration range of major ions for each groundwater type from samples collected during 2007/08 in the Lower Rhine Embayment.

Group	Hydrochemical Facies	Ca^{2+}	Mg^{2+}	Na^{+}	K^{+}	HCO_3^{-}	SO_4^{2-}	Cl^{-}	NO_3^{-}
		Range of values observed (mg L^{-1})							
1	$Ca\text{-}HCO_3$	21.5-175.0	2.9-29.8	6.8-54.7	0.84-5.76	67-592	2.1-150.0	5.5-84.7	<0.2-194.8
2	$Ca\text{-}HCO_3\text{-}SO_4$	35.2-229.0	5.2-35.7	6.5-38.2	1.11-22.80	43-433	51.2-268.0	12.7-107.0	<0.2-133.2
3	$Ca\text{-}Mg\text{-}NO_3\text{-}SO_4$	38.3-65.2	15.1-20.6	19.3-39.3	3.18-9.35	6-31	67.1-176.0	23.9-69.3	60.2-152.3
4	$Ca\text{-}SO_4\text{-}(NO_3)$	59.7-182.0	8.0-25.5	14.1-28.6	1.62-14.3	6-110	67.3-474.0	32.4-68.1	1.5-190.8
5	$Ca\text{-}Na\text{-}(HCO_3\text{-}SO_4)$	7.5-212.0	1.2-37.9	5.2-128.0	0.93-18.00	6-549	5.7-335.0	5.3-205.0	<0.2-112.9
6	$Na\text{-}Ca\text{-}HCO_3$	50.8-50.9	11.2-11.4	93.5-99.4	13.2-15.0	409	28.9-36.4	32.5-34.5	<0.2
7	$Na\text{-}Cl\text{-}(HCO_3)$	53.0-83.3	8.5-85.7	372-1860	7.1-38.7	580-1312	71.8-306.0	347-2460	<0.2

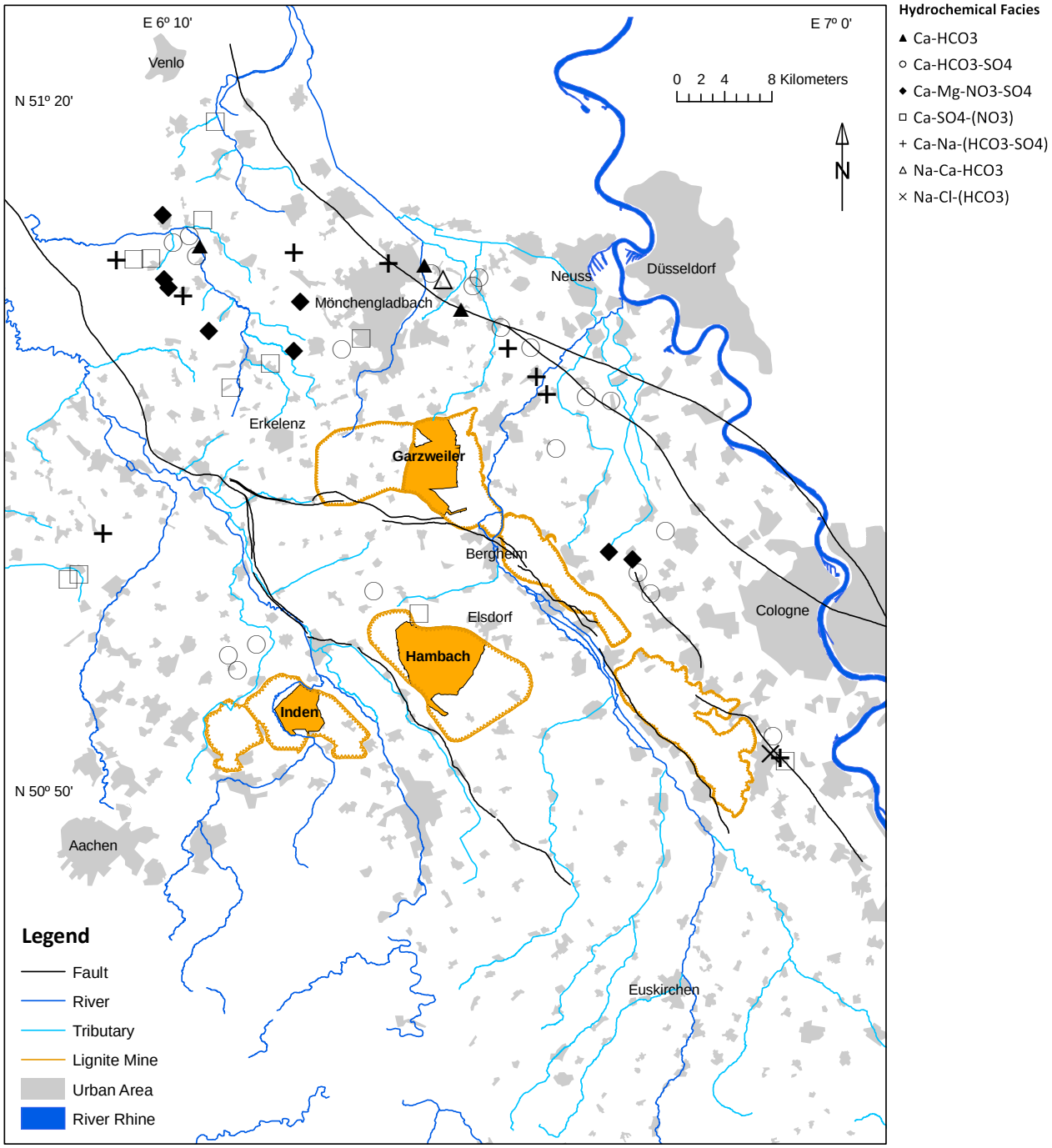

Figure 5.2. Spatial distribution of hydrochemical facies within the Lower Rhine Embayment.

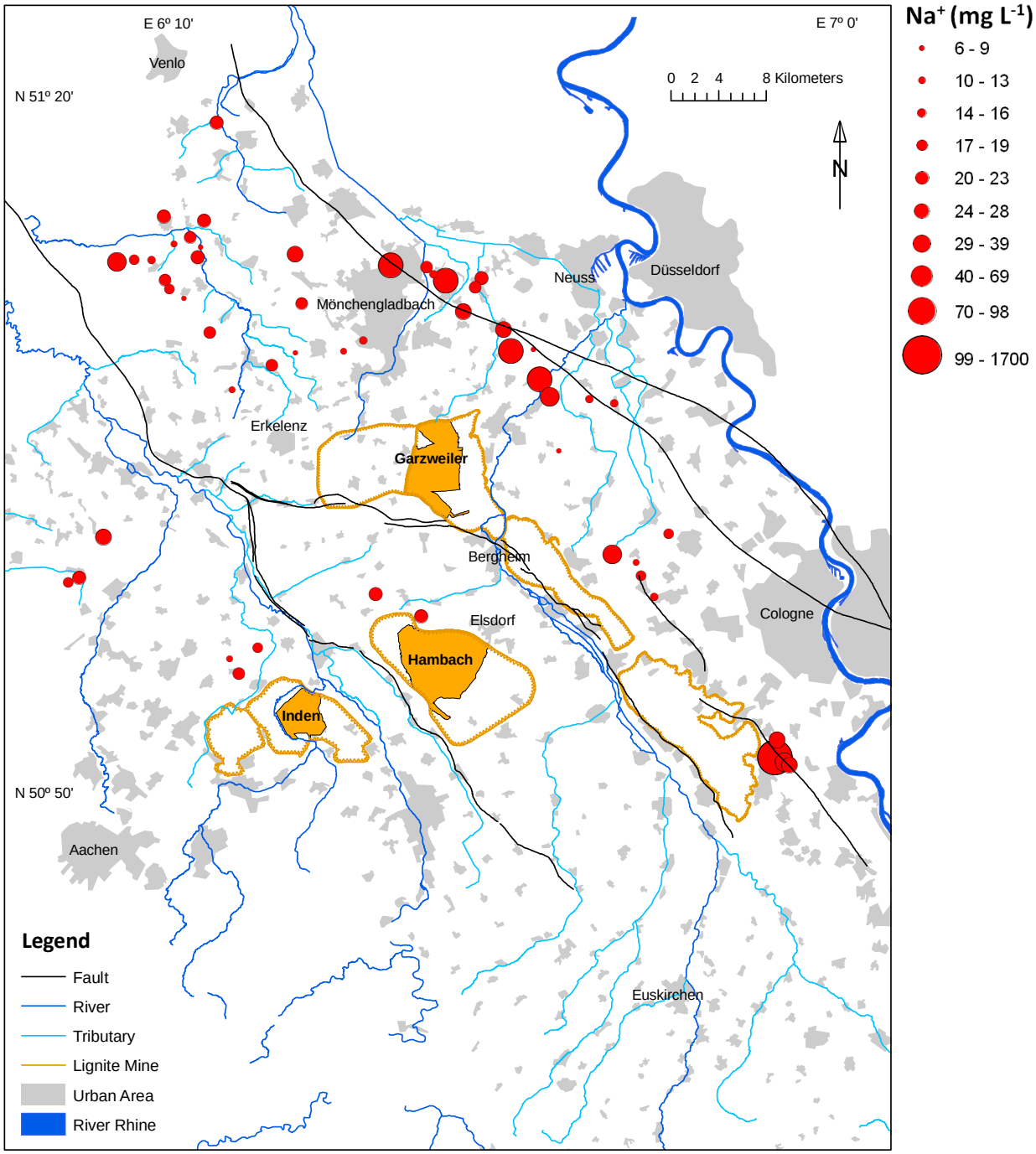

Figure 5.3. Spatial distribution of Na^+ concentration within the Lower Rhine Embayment.

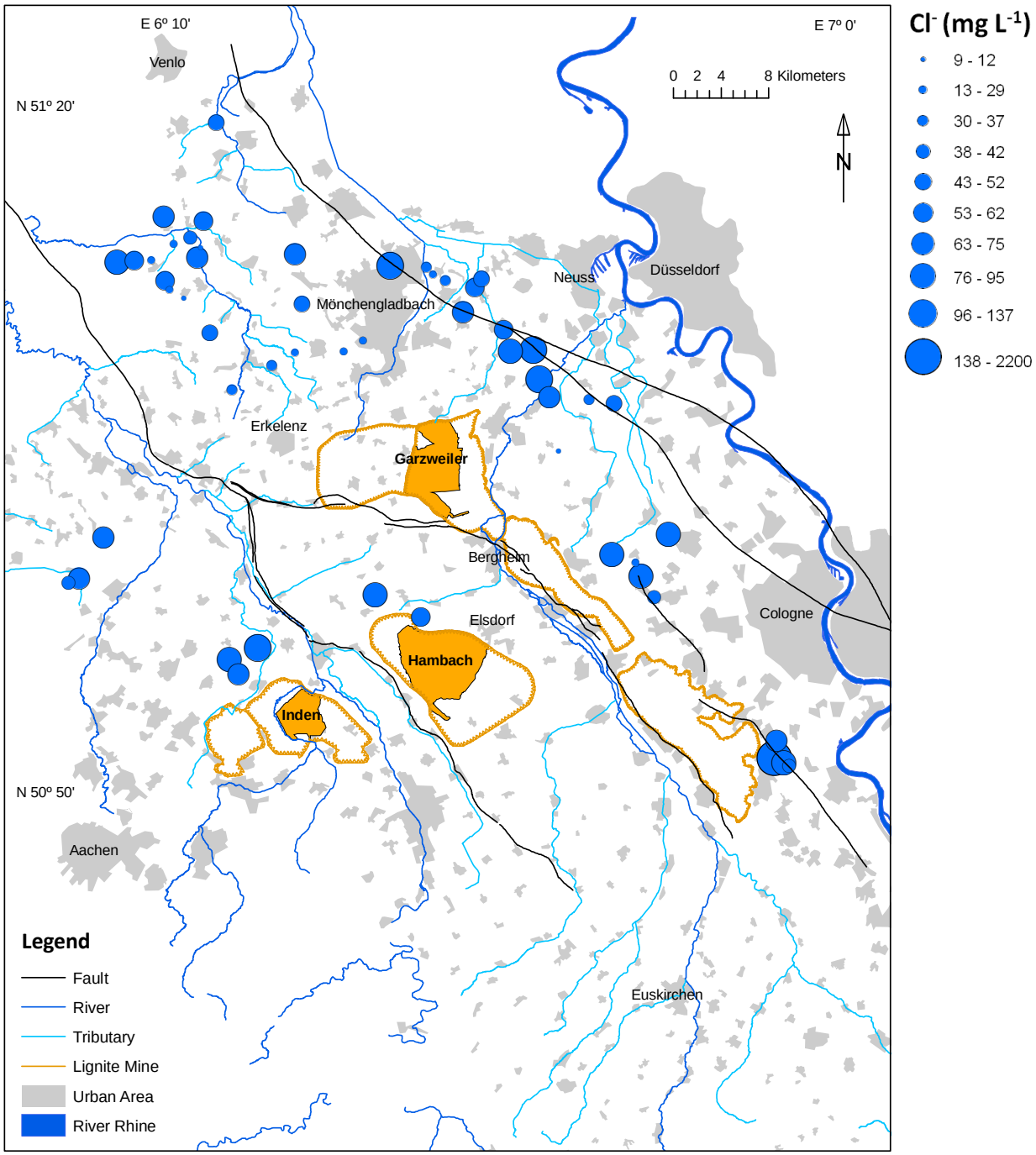

Figure 5.4. Spatial distribution of Cl^- concentration within the Lower Rhine Embayment.

5.2. Stable Isotopes

Naturally occurring stable isotopes are now frequently used in many hydrogeological investigations and they often form the foundation of a multi-tracer approach when it is necessary to determine the origin of groundwater, recharge processes, flow paths and to identify palaeo groundwater (see Chapter 3). Stable isotopes of hydrogen ($\delta^{2}H$), oxygen ($\delta^{18}O$), carbon ($\delta^{13}C_{DIC}$) and strontium ($^{87}Sr/^{86}Sr$) have been analysed for the purpose of this research to supplement the hydrochemical data described in Section 5.1 and to provide additional evidence to support dissolved noble gas data to form a multi-tracer approach. Table 5.2 contains all stable isotope data for groundwater samples that were analysed following the field sampling campaigns that occurred during 2007/08. The analytical precision quoted for each measurement is based on standard runs and it is assumed that due to groundwater samples having a very high degree of homogeneity, the precision of sample measurements is equal to that of the standard. Repeat analysis of groundwater samples to determine the precision of sample measurements was therefore not conducted.

5.2.1. Oxygen Isotopes

A large proportion of the observation boreholes that were sampled in the Lower Rhine Embayment during 2007/08 provided groundwater with a $\delta^{18}O$ value between -7.1 and -7.7‰. The long-term annual average $\delta^{18}O$ value for precipitation in the region of the Lower Rhine Embayment is -6 – -8‰ (IAEA, 2006) which is comparable to the $\delta^{18}O$ value of modern groundwater recharge. The vast majority of the groundwater samples that have $\delta^{18}O$ values in the range of -7.1 – -7.7‰ also plot on or very close to the Global Meteoric Water Line (GMWL) as defined by Craig (1961) confirming a modern meteoric origin (see Figure 5.5).

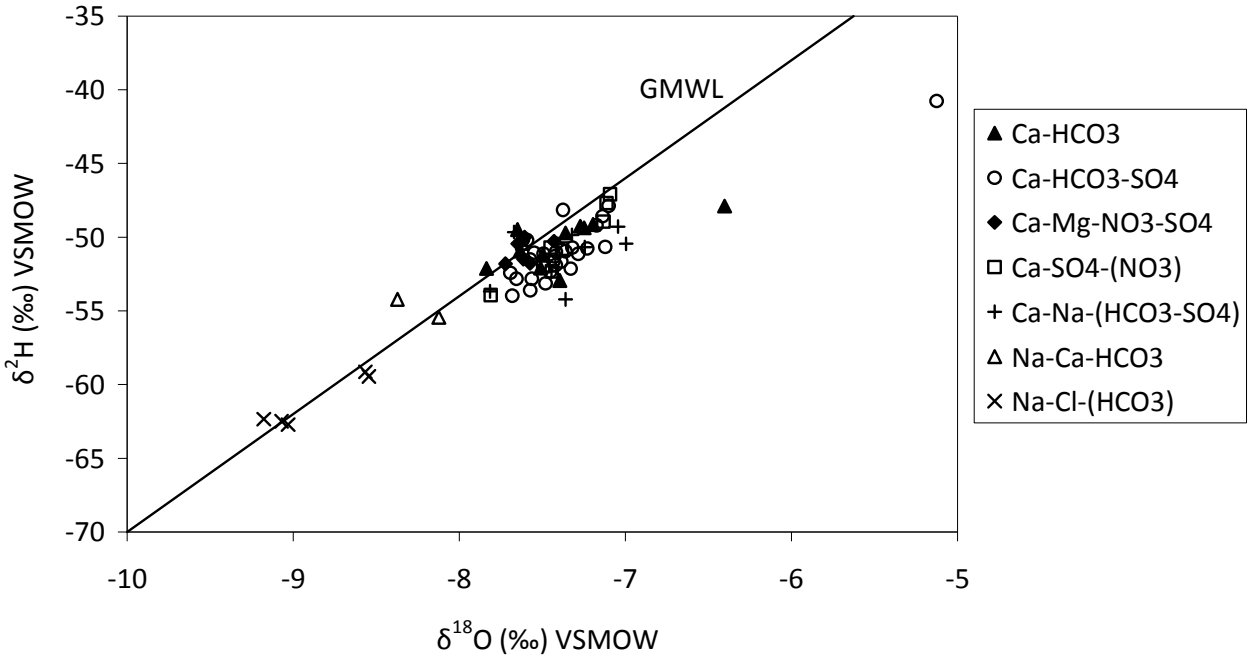

Figure 5.5. Isotopic composition of groundwater samples from the Lower Rhine Embayment in relation to the Global Meteoric Water Line (GMWL) defined by Craig (1961).

Interestingly, groundwater samples taken from observation boreholes in the Brühl region of the Lower Rhine Embayment yield both isotopically depleted and isotopically enriched $\delta^{18}O$ values relative to modern recharge of meteoric origin and current $\delta^{18}O$ values for local precipitation. The samples with relatively low $\delta^{18}O$ values range from -8.5 – -9.1‰ and plot on the GMWL which suggests a meteoric origin but perhaps under different climatic conditions to those that prevail today in this region. However, the samples that have high $\delta^{18}O$ values in the range of -5.1 – -6.4‰ plot to the right hand side of the GMWL. This suggests a typical evaporation trend from modern meteoric water to high $\delta^{18}O$ values and a change in the deuterium

excess value. This isotopic signature was only found in one shallow piezometer and the intermediate value of -6.4‰ from the same observation borehole but at slightly greater depth is likely to be a result of simple conservative mixing between the 'end-member' evaporite and modern meteoric water. The most plausible origin of the ^{18}O enriched groundwater is percolation from a local disused gravel/sand pit that is in very close proximity to the observation borehole. The spatial extent of this particular groundwater type is thought to be extremely localised and dispersion appears minimal suggesting recent recharge and/or a low hydraulic gradient; the latter being supported by potentiometric surface data.

Figure 5.6 shows the spatial distribution of $\delta^{18}O$ values across the Lower Rhine Embayment. It has been established from Table 5.2 and Figure 5.5 that the vast majority of the observation boreholes that were sampled contain modern recharge of meteoric origin. It therefore follows that one would expect to see a fairly uniform spatial distribution of $\delta^{18}O$ values between -7.1 and -7.7‰. From Figure 5.6 it is evident that this is indeed the case. The areas to note are in the southeast near the town of Brühl where both ^{18}O enriched (black circle) and ^{18}O depleted (pink circle) groundwaters are present and one additional area adjacent to the Viersen Fault and the village of Korschenbroich (Borehole 28/907271) where relatively low $\delta^{18}O$ values (-8.4‰) were also sampled and are given by the Na-Ca-HCO_3 groundwater type (see Figure 5.5). A full discussion of the oxygen isotope data is given in Chapter 6.

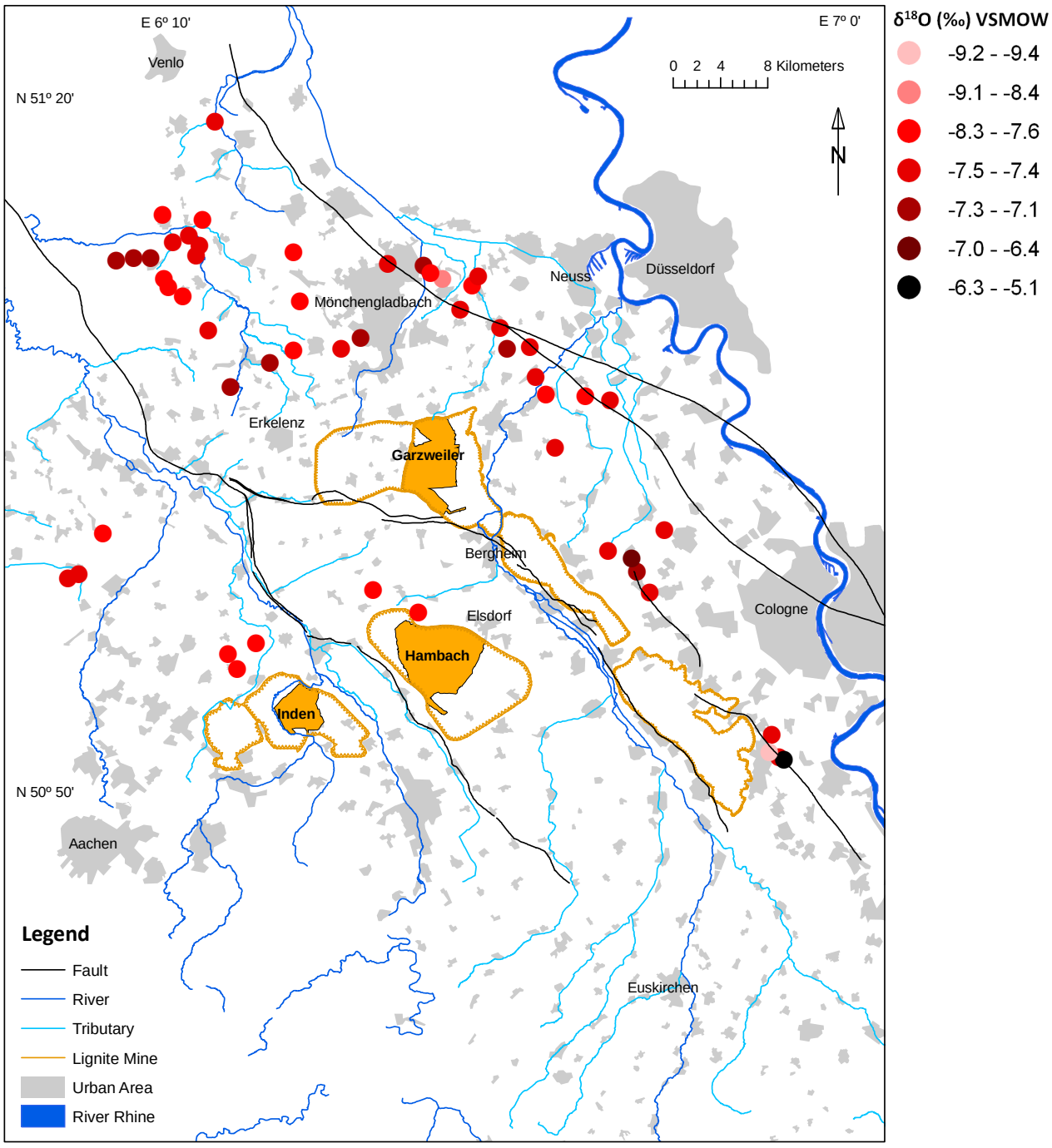

Figure 5.6. Spatial distribution of $\delta^{18}O$ values within the Lower Rhine Embayment.

Table 5.2. Stable isotope data and total strontium concentrations of samples collected during 2007/08 from the Lower Rhine Embayment, Germany.

ID Number	Location	δ^2H VSMOW (‰) (± **1.4**)	$\delta^{18}O$ VSMOW (‰) (± **0.04**)	$\delta^{13}C_{DIC}$ VPDB (‰) (± **0.1**)	$^{87}Sr/^{86}Sr$ (± **0.00007**)	Total Strontium (ppb)
21/927961	Steinstrass-H	-53.9	-7.81	-19.5	0.70967	293.4
21/927971	Guesten	-52.4	-7.69	-16.2	0.70939	335.7
21/960511	Gillrath 2	-52.3	-7.44	-20.9	0.71037	153.2
21/867341	Duerboslar	-50.1	-7.61	-16.9	0.70934	211.1
21/040331	WWk Gangelt Gp2	-51.9	-7.49	-28.2	0.70984	109.4
21/863901	Duerboslar	-53.6	-7.57	-17.9	0.70942	221.6
21/861581	Merzenhausen	-52.8	-7.65	-17.2	0.70927	257.2
28/900441	Mühlrather Mü	-51.2	-7.49	-18.6	0.70996	46.0
21/960251	Straeten	-50.8	-7.62	-26.9	0.71003	151.8
28/817751	Knoor	-50.9	-7.63	-17.4	0.71109	164.3
08/658086	WW Niederkr. P 5A	-48.1	-7.37	-23.7	0.71117	174.7
28/900401	Haverslohe 208	-52.8	-7.56	-19.6	0.70985	144.4
28/908381	Barlo	-50.8	-7.38	-25.3	0.71043	220.3

Table 5.2. Cont'd (2 of 6)

ID Number	Location	$\delta^{2}H$ VSMOW (‰) (± **1.4**)	$\delta^{18}O$ VSMOW (‰) (± **0.04**)	$\delta^{13}C_{DIC}$ VPDB (‰) (± **0.1**)	$^{87}Sr/^{86}Sr$ (± **0.00007**)	Total Strontium (ppb)
28/908301	Brüggen	-50.4	-7.65	-30.4	0.71177	198.2
28/908411	Heyen	-51.6	-7.43	-20.8	0.71051	94.9
28/908401	Born	-50.9	-7.36	-18.4	0.70956	168.6
28/900591	Vogelsberg 264	-49.3	-7.04	-17.1	0.71084	127.4
28/907271	Korschenbroich	-54.2	-8.37	-13.4	0.71310	1521.9
28/907841	Kl. Broi. 3	-51.6	-7.38	-16.5	0.71022	229.6
28/907821	Kl. Broi. 1	-51.5	-7.57	-13.5	0.70982	424.1
28/908541	Niederkr. Tab 13	-51.5	-7.61	-27.4	0.71204	167.8
28/908081	WW Niederkr. B6	-49.6	-7.67	-25.5	0.70956	18.1
28/809981	Oberkruechten	-50.0	-7.60	-23.8	0.71285	155.8
28/919461	Langwaden	-53.6	-7.81	-18.3	0.71036	176.4
28/919462	Langwaden	-53.9	-7.68	-16.5	0.70977	237.4
28/917841	Kapellen	-54.2	-7.36	-17.1	0.70981	253.0

Table 5.2. Cont'd (3 of 6)

ID Number	Location	$\delta^{2}H$ VSMOW (‰) (± **1.4**)	$\delta^{18}O$ VSMOW (‰) (± **0.04**)	$\delta^{13}C_{DIC}$ VPDB (‰) (± **0.1**)	$^{87}Sr/^{86}Sr$ (± **0.00007**)	Total Strontium (ppb)
28/919471	Neukirch.2	-51.0	-7.55	-18.2	0.70912	159.6
28/919472	Neukirch.2	-52.1	-7.51	-15.6	0.70919	133.0
27/957822	Fischenich	-50.6	-7.12	-	-	-
27/957823	Fischenich	-51.9	-7.42	-	-	-
27/957824	Fischenich	-59.1	-8.57	-	-	-
27/957981	Brühl 1	-40.8	-5.12	-	-	-
27/957982	Brühl 1	-50.4	-6.99	-	-	-
27/958061	Brühl 9	-62.5	-9.07	-	-	-
27/958062	Brühl 9	-62.3	-9.18	-	-	-
27/958063	Brühl 9	-62.7	-9.03	-	-	-
07/352721	SW Brühl 22 R1	-52.3	-7.44	-	-	-
07/352722	SW Brühl 22 R1	-59.4	-8.54	-	-	-
28/917191	Gohr	-51.3	-7.42	-17.9	-	133.9

Table 5.2. Cont'd (4 of 6)

ID Number	Location	$\delta^{2}H$ VSMOW (‰) (± **1.4**)	$\delta^{18}O$ VSMOW (‰) (± **0.04**)	$\delta^{13}C_{DIC}$ VPDB (‰) (± **0.1**)	$^{87}Sr/^{86}Sr$ (± **0.00007**)	Total Strontium (ppb)
28/816011	Lehmkuhl	-47.1	-7.09	-26.0	-	127.2
28/816012	Lehmkuhl	-50.7	-7.45	-21.9	-	131.4
28/900601	An Der Wae 265H	-48.9	-7.13	-23.1	-	178.0
80/030128	Eicken 276	-50.4	-7.40	-20.5	-	183.9
28/816061	Mackenstein	-51.8	-7.57	-26.2	-	183.4
28/907641	Myllendonk	-49.3	-7.25	-16.9	-	237.2
28/907271	Korschenbroich	-55.4	-8.12	-13.8	-	1352.8
01/040244	WWk Beeck Nr. 16	-49.2	-7.17	-20.5	-	155.4
21/908711	Merbecker Busch	-50.2	-7.43	-28.9	-	162.6
21/908712	Merbecker Busch	-49.8	-7.32	-20.9	-	17.5
21/814901	Tueschenbroich	-47.7	-7.11	-19.8	-	142.8
21/814902	Tueschenbroich	-48.6	-7.13	-19.9	-	134.6
28/806881	Rheydt	-47.8	-7.10	-22.5	-	1.9

Table 5.2. Cont'd (5 of 6)

ID Number	Location	$\delta^{2}H$ VSMOW (‰) (± **1.4**)	$\delta^{18}O$ VSMOW (‰) (± **0.04**)	$\delta^{13}C_{DIC}$ VPDB (‰) (± **0.1**)	$^{87}Sr/^{86}Sr$ (± **0.00007**)	Total Strontium (ppb)
28/806882	Rheydt	-52.1	-7.83	-16.8	-	660.6
28/908591	Gunhoven	-51.0	-7.41	-17.8	-	143.3
28/908592	Gunhoven	-51.1	-7.49	-15.0	-	129.1
28/900171	Herdterhof 0080a	-51.8	-7.72	-23.0	-	179.6
28/907891	Korschenbroich	-50.2	-7.59	-15.7	-	241.8
28/907892	Korschenbroich	-49.5	-7.65	-14.7	-	145.4
28/806941	Glehn	-52.1	-7.33	-16.2	-	315.6
28/907691	Pesch	-49.7	-7.36	-16.7	-	391.9
28/907692	Pesch	-49.3	-7.27	-15.8	-	329.5
28/812531	Dannerhof	-50.7	-7.32	-16.8	-	285.1
28/806921	Gut Bickhausen	-50.7	-7.24	-16.4	-	291.4
28/806922	Gut Bickhausen	-49.1	-7.19	-14.6	-	168.2
28/919482	Barrenstein 2	-	-7.39	-15.8	-	161.9

Table 5.2. Cont'd (6 of 6)

ID Number	Location	δ^2H VSMOW (‰) (± 1.4)	$\delta^{18}O$ VSMOW (‰) (± 0.04)	$\delta^{13}C_{DIC}$ VPDB (‰) (± 0.1)	$^{87}Sr/^{86}Sr$ (± 0.00007)	Total Strontium (ppb)
27/831791	Buesdorf	-52.9	-7.39	-17.0	-	253.0
27/937921	Fliested. 3	-47.9	-6.40	-	-	219.9
27/937922	Fliested. 3	-50.8	-7.23	-16.0	-	262.3
07/355571	Dansweiler 663	-53.1	-7.48	-18.9	-	248.6
27/937881	Glessen 4	-51.1	-7.28	-17.3	-	278.4
27/937491	Pulheim III	-52.3	-7.45	-17.4	-	276.8

5.2.2. Carbon Isotopes

Soil CO_2 has strong negative values typically in the range of -24 – -25‰ VPDB whereas marine carbonates have a $\delta^{13}C_{DIC}$ value of 0‰ VPDB. It therefore follows that the $\delta^{13}C_{DIC}$ value of dissolved carbonates will have an intermediate value in hydrochemically evolved groundwater whereas a relatively low $\delta^{13}C_{DIC}$ value indicates either very modern recharge or a limited carbonate source within the aquifer matrix. The concentration of CO_2 in the soil zone is significantly higher than the concentration of CO_2 in the atmosphere due to bacterial oxidation of organic matter and CO_2 respiration in the root zone (Clark and Fritz, 1997). During infiltration through the unsaturated zone, water equilibrates with soil CO_2 which leads to modern groundwater recharge having lower $\delta^{13}C_{DIC}$ values than atmospheric CO_2.

Table 5.2 contains the results of the $\delta^{13}C_{DIC}$ analyses. The results show that there is a wide range of $\delta^{13}C_{DIC}$ values within the sampled observation boreholes and piezometer nests. Low $\delta^{13}C_{DIC}$ values are typically observed to the west and northwest of the Garzweiler lignite mine with the lowest value of -30.44‰ at borehole 908301 (Brüggen). Figure 5.7 illustrates the $\delta^{13}C_{DIC}$ spatial variability from the observation boreholes sampled during 2007/08. From Figure 5.7 it can be seen that $\delta^{13}C_{DIC}$ values are higher (-13.5 – -20.8‰) along the eastern flank of the abandoned lignite mines of Fortuna, Bergheim, Frechen and Ville and this trend continues north towards Mönchengladbach and is also evident adjacent to the Viersen fault and to the west of the Kalk fault. Groundwater taken from shallow perched aquifers in close proximity to the Hambach and Inden mines also contain groundwater with a relatively high $\delta^{13}C_{DIC}$ signature in the range of -15 – -20‰.

Relatively low $\delta^{13}C_{DIC}$ values are typically found in the region northwest of the Garzweiler lignite mine where the natural groundwater regime is less impacted by mine de-watering than in other parts of the Lower Rhine Embayment. This indicates that the shallow boreholes that were sampled in this area contain very modern recharge and that the hydrochemical evolution of the groundwater with respect to the carbonate system is slow. Chapter 6 provides a detailed discussion of the carbon isotope data and carbonate evolution.

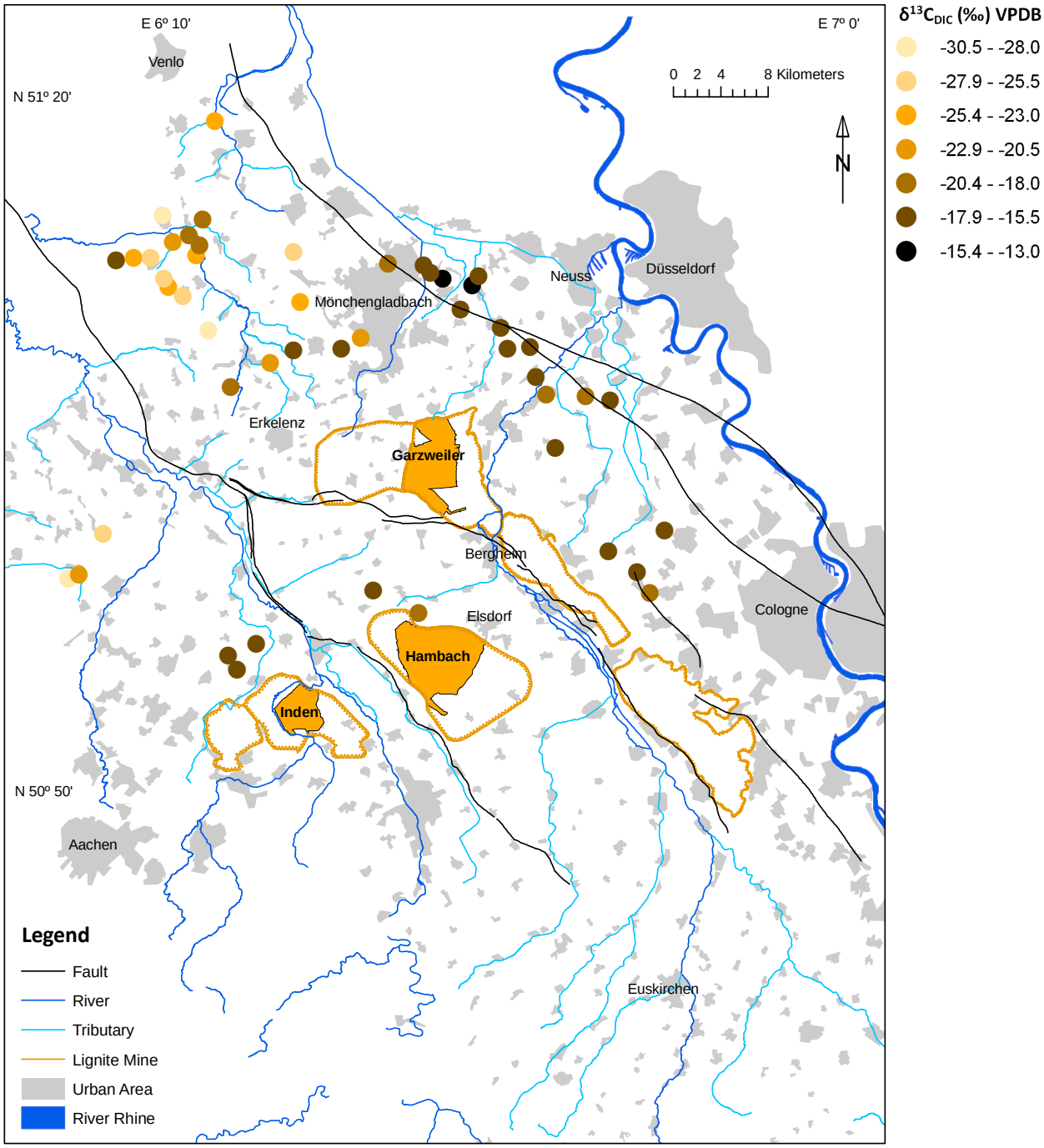

Figure 5.7. The spatial distribution of $\delta^{13}C_{DIC}$ values within the Lower Rhine Embayment.

5.2.3. Strontium

Strontium is a soluble trace element (alkali earth element) that is present in groundwater at concentrations that range from 0.01 – 10 mg L^{-1} (Freeze and Cheery, 1979). The naturally occurring isotopic composition of strontium in groundwater is unaffected by the removal of Sr^{2+} from groundwater through hydrochemical processes such a cation exchange or mineral precipitation making it an ideal geochemical tracer of solute provenance (eg. Neumann and Dreiss, 1995; Bullen *et al.*, 1996) and groundwater mixing (eg. Lyons *et al.*, 1995; Frost and Toner, 2004).

Figure 5.8 shows the $^{87}Sr/^{86}Sr$ ratio as a function of the reciprocal of the total Sr^{2+} concentration. Strontium isotope mixing lines between two end-member groundwater types theoretically have a linear relationship on Figure 5.8 and groundwater that results from such mixing would plot along a strontium isotope mixing line. It can be seen from Figure 5.8 that the main group of samples display a large range of $^{87}Sr/^{86}Sr$ values and the total strontium concentration range is between 95 – 424 ppb. It is therefore difficult to identify potential mixing lines. The maximum Sr^{2+} concentration measured during the research was 1522 ppb which is significantly higher than the other samples and occurred at just one location. This concentration was recorded from borehole 28/907271 Korschenbroich which is in close proximity to the Viersener fault and has depleted $\delta^{18}O$ values as described in Section 5.2.1. The two sample points that can be clearly distinguished from the main cluster of samples in Figure 5.8 have the lowest Sr^{2+} concentrations at 46 and 18 ppb and $^{87}Sr/^{86}Sr$ ratios of 0.7099 and 0.7095 respectively. These two groundwater samples were collected from observation boreholes close to the town of Mönchengladbach (observation boreholes; Mühlrather Mü and WW. Niederkr. B6 respectively) but from different aquifer horizons.

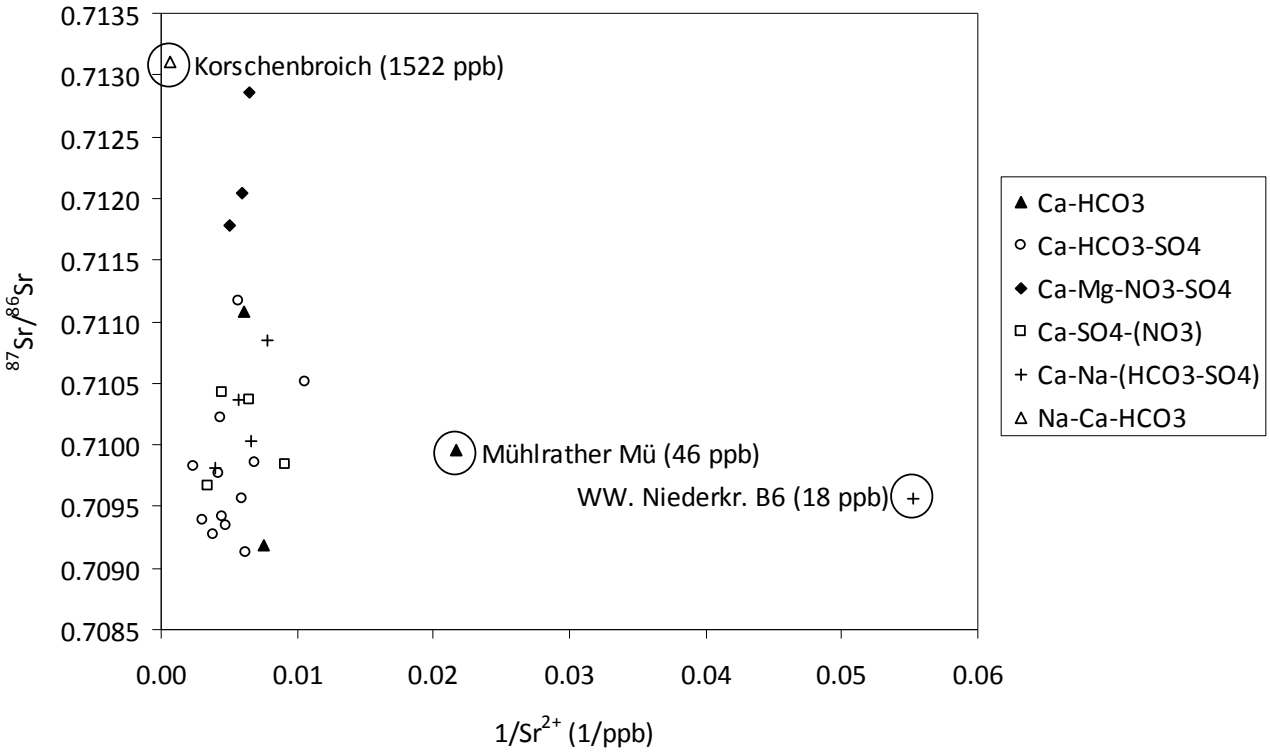

Figure 5.8. Cross plot of $^{87}Sr/^{86}Sr$ against $1/Sr^{2+}$.

Figure 5.9 displays the spatial distribution of $^{87}Sr/^{86}Sr$ using a colour ramp to illustrate the $^{87}Sr/^{86}Sr$ value. Although the data set is rather small, it is evident that the points show a large degree of scattering in the area west of Mönchengladbach in the relatively unperturbed multi-layered aquifer system. The small number of groundwater samples collected from the perched shallow aquifers slightly north of the Inden and Hambach open-cast lignite mines display a very consistent $^{87}Sr/^{86}Sr$ ratio suggesting similar recharge history and aquifer lithology at this location. Due to the data set being rather small and incomplete, and significantly, not including the Brühl area samples, the strontium results are not discussed further in Chapter 6.

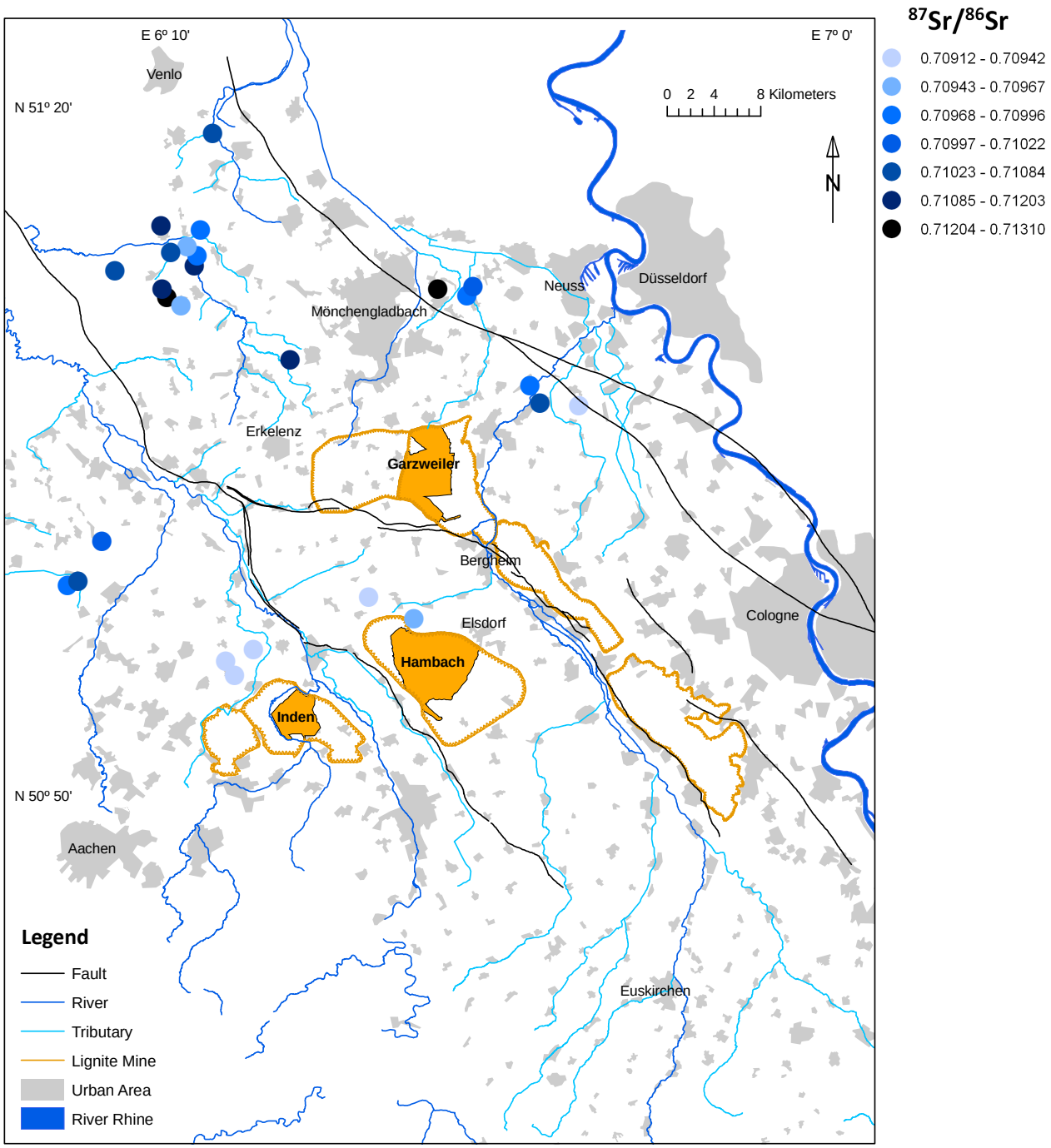

Figure 5.9. Spatial distribution of $^{87}Sr/^{86}Sr$ ratios within the Lower Rhine Embayment.

5.3. Noble Gases

All aspects of noble gas geochemistry relevant to this research including the hydrogeological applications of dissolved noble gases in groundwater have been discussed in Chapter 3 and an interpretation and discussion of the results presented here are given in Chapter 6.

5.3.1. Graphical interpretation of the data

The dissolved noble gas concentrations of groundwater samples collected from the Lower Rhine Embayment during 2007/08 are presented in Table 5.3. The data from Table 5.3 has been used to construct noble gas cross-plots of argon against neon (Figure 5.10), krypton against neon (Figure 5.11) and xenon against neon (Figure 5.12) which provide a simple but valuable graphical interpretation of the data. The solubility equilibrium relationships were determined using the solubility equations of Weiss (1970; 1971) and Benson and Krause (1976) as described in Chapter 5. Imposed graticules based on solubility equilibrium and excess air additions were used to facilitate the initial interpretation of NGTs and excess air concentrations assuming a constant pressure of 1 atm and a salinity of zero.

It can be seen from Figure 5.10, Figure 5.11 and Figure 5.12 that all groundwater samples plot within the theoretical range of expected values based on solubility equilibrium and that all of the samples contain at least a small amount of excess air. Figure 5.11 and Figure 5.12 both show slightly high mean NGTs based on the known mean annual surface temperature for the region (10.1 ^{o}C). Estimated recharge temperatures using this graphical method are usually based on a mean value taken for each noble gas perhaps with the exception of

helium to give an overall recharge temperature usually with no weighting of the more temperature sensitive heavier gases such as krypton and xenon (eg. Stute *et al*., 1995). Figure 5.13 enables one to infer a NGT in the range of 9–13 ºC for most groundwater samples which is in better agreement with the annual average surface temperature although precipitation records clearly show that rainfall in significantly higher during the warmer summer months which could explain the higher than expected NGTs. Xenon is the most temperature sensitive noble gas due to it having the largest atomic mass so it is usually favoured for determining NGTs. These noble gas cross-plots based on solubility equations provide a good first interpretation of the noble data but they do have limitations.

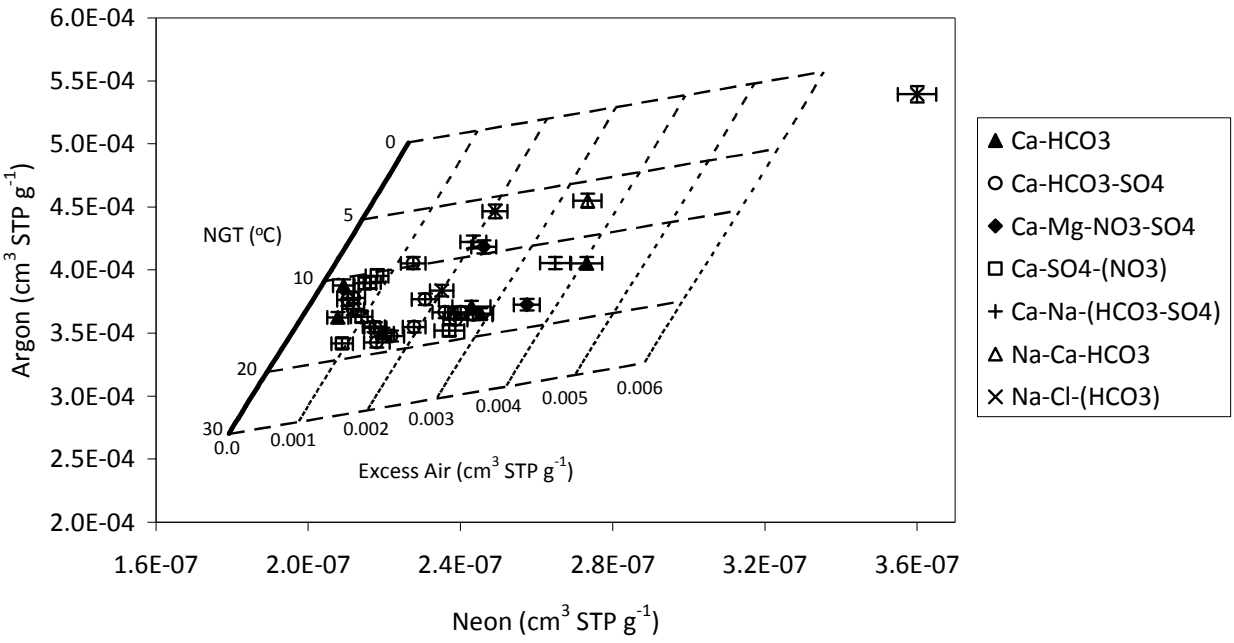

Figure 5.10. Noble gas cross-plot of argon against neon with imposed graticules that indicate excess air concentration and the NGT based on solubility equilibrium.

Typically a more sophisticated and accurate interpretation of noble gas concentrations is desirable. To facilitate this, a freely available non-linear, error weighted least squares inversion of five model parameters; temperature (T), salinity (S), pressure (P), excess air (A), and fractionation (F) is undertaken. The least squares fitting is conducted using the MATLAB routine NOBLE90 (Aeschbach-Hertig *et al.*, 1999; Peeters *et al.*, 2002). The results of the model fitting using NOBLE90 are illustrated in Figure 5.13 and calculate NGTs and excess air concentrations using all the measured noble gas concentrations simultaneously, although not always using helium due to additional subsurface sources. Chapter 6 provides a full discussion of the noble gas data and interpretation of NGTs and excess air concentrations.

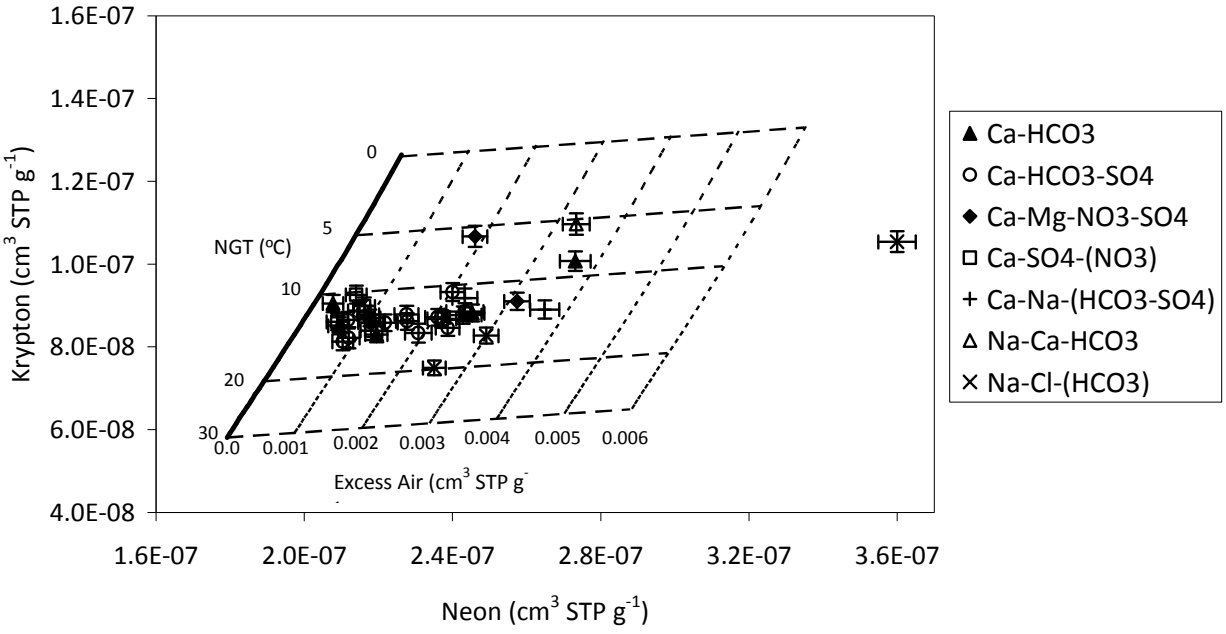

Figure 5.11. Noble gas cross-plot of krypton against neon with imposed graticules indicating the excess air concentration and the NGT based on solubility equilibrium.

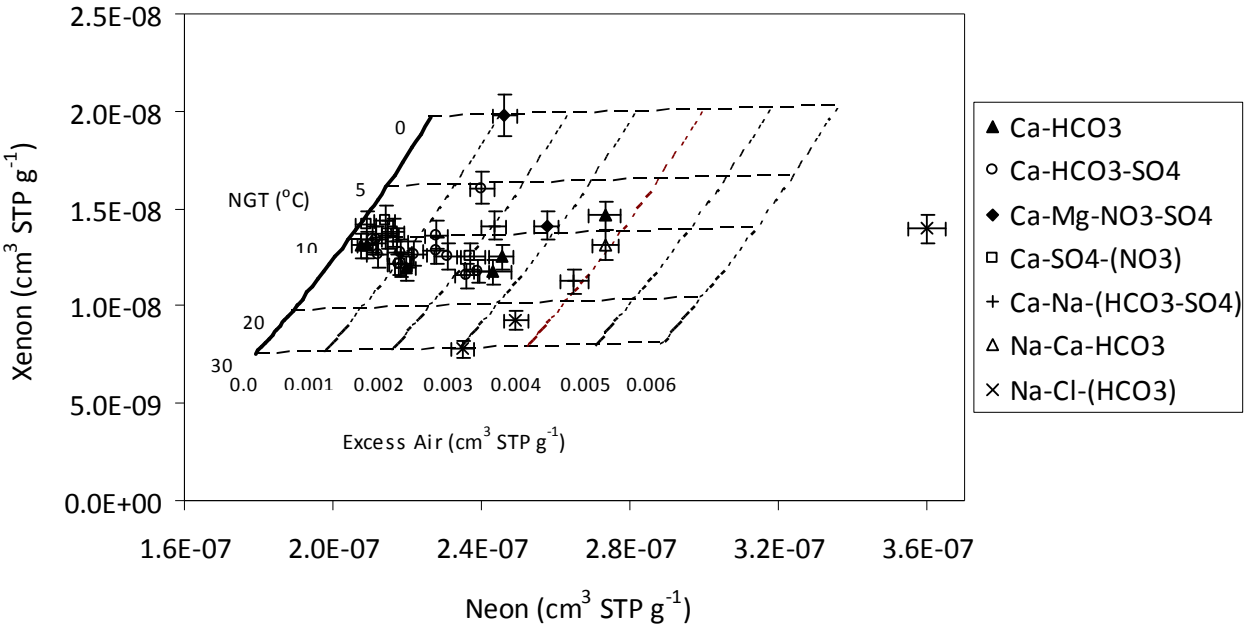

Figure 5.12. Noble gas cross-plot of xenon against neon with imposed graticules indicating the excess air concentration and the NGT based on solubility equilibrium.

Table 5.3. Measured noble gas concentrations.

ID Number	Location	He (10^{-8})	Ne (10^{-7})	Ar (10^{-4})	Kr (10^{-8})	Xe (10^{-8})
		(cm^3 STP g^{-1})				
28/917191	Gohr	4.582 ± 0.074	2.179 ± 0.033	3.427 ± 0.041	8.589 ± 0.201	1.278 ± 0.065
28/816011	Lehmkuhl	5.146 ± 0.081	2.371 ± 0.039	3.520 ± 0.042	8.680 ± 0.203	1.254 ± 0.063
28/816012	Lehmkuhl	4.405 ± 0.065	2.140 ± 0.028	3.629 ± 0.044	9.262 ± 0.215	1.438 ± 0.074
28/900601	An Der Wae 265H	4.506 ± 0.074	2.089 ± 0.028	3.417 ± 0.041	8.604 ± 0.201	1.416 ± 0.072
80/030128	Eicken 276	6.012 ± 0.090	2.172 ± 0.029	3.550 ± 0.042	8.781 ± 0.208	1.335 ± 0.069
28/816061	Mackenstein	5.717 ± 0.087	2.574 ± 0.034	3.724 ± 0.044	9.101 ± 0.212	1.410 ± 0.072
28/907641	Myllendonk	4.638 ± 0.072	2.093 ± 0.028	3.877 ± 0.047	8.512 ± 0.205	1.311 ± 0.068
28/907271	Korschenbroich	863.01 ± 11.25	2.734 ± 0.036	4.550 ± 0.054	10.969 ± 0.259	1.313 ± 0.074
01/040244	WWk Beeck Nr. 16	5.595 ± 0.081	2.387 ± 0.032	3.604 ± 0.043	8.462 ± 0.198	1.176 ± 0.060
28/806881	Rheydt	5.081 ± 0.101	2.400 ± 0.032	3.665 ± 0.042	9.325 ± 0.218	1.605 ± 0.081
28/806882	Rheydt	11.441 ± 0.158	2.731 ± 0.041	4.053 ± 0.049	10.070 ± 0.235	1.464 ± 0.074
28/900171	Herdterhof 0080a	5.387 ± 0.077	2.461 ± 0.033	4.183 ± 0.050	10.669 ± 0.256	1.982 ± 0.106
28/907892	Korschenbroich	5.386 ± 0.078	2.077 ± 0.027	3.624 ± 0.044	9.048 ± 0.211	1.308 ± 0.066

Table 5.3. Cont'd (2 of 3)

ID Number	Location	He (10^{-8})	Ne (10^{-7})	Ar (10^{-4})	Kr (10^{-8})	Xe (10^{-8})
		(cm^3 STP g^{-1})				
28/806941	Glehn	5.010 ± 0.073	2.218 ± 0.033	3.477 ± 0.042	8.583 ± 0.200	1.268 ± 0.065
28/812531	Dannerhof	4.858 ± 0.010	2.176 ± 0.029	3.542 ± 0.043	8.698 ± 0.203	1.215 ± 0.062
28/806922	Gut Bickhausen	5.092 ± 0.074	2.428 ± 0.050	3.709 ± 0.045	8.770 ± 0.204	1.176 ± 0.062
27/831791	Buesdorf	4.716 ± 0.084	2.195 ± 0.029	3.501 ± 0.042	8.302 ± 0.193	1.194 ± 0.061
27/937921	Fliested. 3	5.588 ± 0.092	2.453 ± 0.032	3.652 ± 0.044	8.817 ± 0.205	1.252 ± 0.063
07/355571	Dansweiler 663	5.584 ± 0.080	2.278 ± 0.030	3.549 ± 0.043	8.618 ± 0.201	1.364 ± 0.074
27/937881	Glessen 4	5.493 ± 0.078	2.433 ± 0.050	3.646 ± 0.044	8.851 ± 0.206	
27/937491	Pulheim III	5.399 ± 0.083	2.276 ± 0.032	4.054 ± 0.049	8.784 ± 0.206	1.280 ± 0.066
21/960511	Gillrath 2	4.764 ± 0.073	2.162 ± 0.029	3.900 ± 0.049	8.982 ± 0.211	1.378 ± 0.074
21/040331	WWk Gangelt Gp2	4.572 ± 0.070	2.149 ± 0.030	3.894 ± 0.047	8.873 ± 0.207	1.370 ± 0.073
21/863901	Duerboslar	4.653 ± 0.075	2.307 ± 0.035	3.766 ± 0.045	8.333 ± 0.229	1.252 ± 0.066
21/861581	Merzenhausen	3.910 ± 0.061	2.118 ± 0.028	3.692 ± 0.048	8.646 ± 0.201	1.339 ± 0.071
08/658086	WW Niederkr. P 5A	3.506 ± 0.054	2.120 ± 0.029	3.780 ± 0.050	8.221 ± 0.254	1.260 ± 0.066

Table 5.3. Cont'd (3 of 3)

ID Number	Location	He (10^{-8})	Ne (10^{-7})	Ar (10^{-4})	Kr (10^{-8})	Xe (10^{-8})
		(cm^3 STP g^{-1})				
28/900401	Haverslohe 208	3.665 ± 0.059	2.104 ± 0.028	3.763 ± 0.049	8.128 ± 0.210	1.343 ± 0.070
28/908381	Barlo	4.181 ± 0.067	2.181 ± 0.029	3.954 ± 0.052	8.387 ± 0.222	1.214 ± 0.064
27/957822	Fischenich	102.93 ± 1.33	7.807 ± 0.102	6.764 ± 0.081	11.76 ± 0.277	1.577 ± 0.083
27/957823	Fischenich	436.94 ± 5.81	2.360 ± 0.033	3.665 ± 0.044	8.716 ± 0.203	1.153 ± 0.059
27/957824	Fischenich	7269.37 ± 94.60	3.600 ± 0.050	5.393 ± 0.064	10.54 ± 0.249	1.398 ± 0.072
27/957982	Brühl 1	735.84 ± 9.40	2.433 ± 0.034	4.223 ± 0.051	9.182 ± 0.226	1.411 ± 0.074
27/958062	Brühl 9	12815.4 ± 289.0	2.491 ± 0.033	4.466 ± 0.053	8.273 ± 0.193	0.923 ± 0.048
27/958063	Brühl 9	16912.3 ± 385.1	2.351 ± 0.031	3.836 ± 0.046	7.491 ± 0.175	0.777 ± 0.040
07/352721	SW Brühl 22 R1	258.33 ± 3.37	2.649 ± 0.039	4.055 ± 0.049	8.902 ± 0.220	1.127 ± 0.064
01	ASW 14.5	5.823 ± 0.080	1.950 ± 0.027	3.597 ± 0.048	7.887 ± 0.183	1.185 ± 0.063
02	ASW 14.5	4.887 ± 0.071	1.965 ± 0.026	3.507 ± 0.045	7.283 ± 0.179	1.206 ± 0.063

5.3.2. NGTs and excess air modelled using NOBLE90

Figure 5.13 shows the modelled NGTs and excess air concentration that were interpreted using the MATLAB routine NOBLE90 (Aeschbach-Hertig *et al*., 1999; Peeters *et al*., 2002). The theory related to NOBLE90 is discussed in Chapter 3. The main cluster of samples contain between 5 and 37% excess air and have calculated recharge temperatures in the range of 10–16 ºC and a mean value of 12.5 ±1.3 ºC which is 1.7 ºC higher than the weighted mean annual surface temperature of 10.8 ºC. It is possible to identify three samples that appear to have a lower NGT but assuming that only the Na-Ca-HCO_3 and Na-Cl-(HCO_3) type groundwaters were recharged under cooler climatic conditions the mean NGT is 5.6 ±1.7 ºC and the Na-Cl- (HCO_3) groundwater has significantly higher excess air at 74% ΔNe.

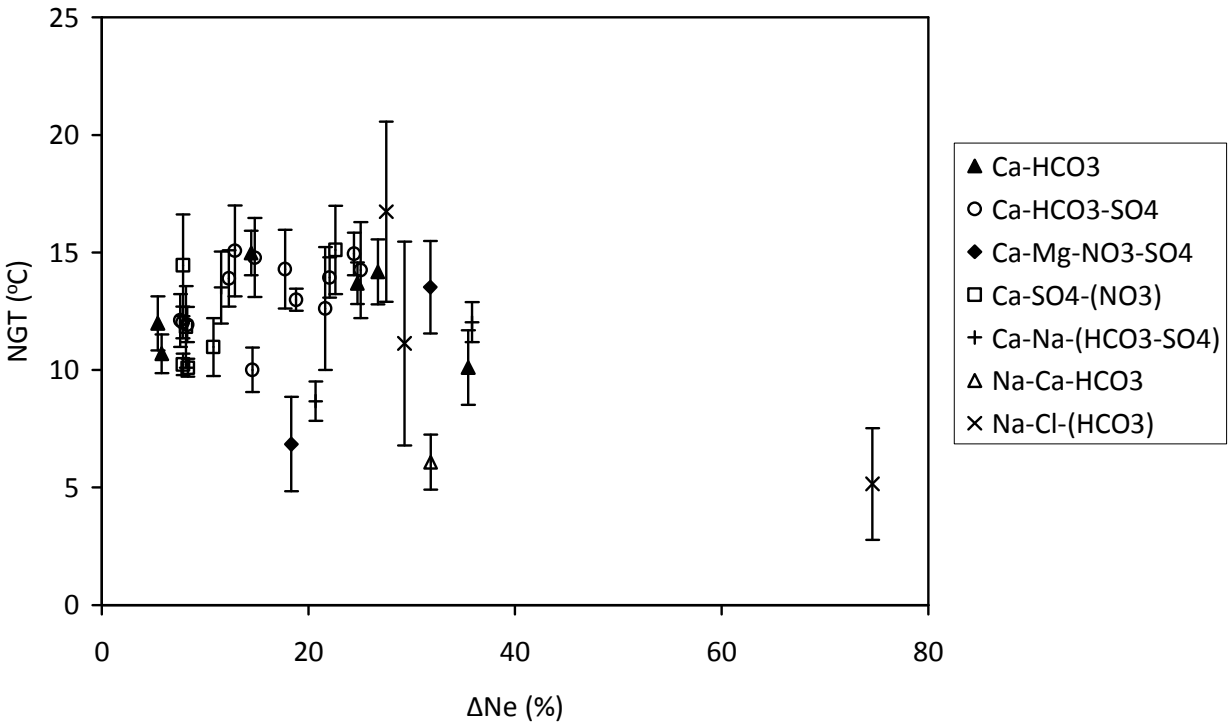

Figure 5.13. NOBLE90 modelled Noble Gas Temperatures plotted against excess air reported as ΔNe (%).

5.3.3. Radiogenic helium

Helium concentrations in most of the observation boreholes that were sampled during 2007/08 were in the range expected due to solubility equilibrium ($3.50x10^{-8}$ – $6.01x10^{-8}$ cm^3 STP g^{-1} H_2O). Helium was measured in groundwater samples from six observation boreholes at concentrations that were higher than solubility equilibrium. These concentrations ranged from slightly elevated ($1.14x10^{-7}$ cm^3 STP g^{-1}) to >3 orders of magnitude above atmospheric solubility equilibrium ($1.691x10^{-4}$ cm^3 STP g^{-1}). Four of the observation boreholes were situated in the Brühl region, with the Brühl 9 piezometer containing groundwater with the highest concentrations of helium at $1.691x10^{-4}$ and $1.281x10^{-4}$ cm^3 STP g^{-1} H_2O from the multi-depth piezometer nest. Chapter 6 provides an in-depth discussion and interpretation of these results.

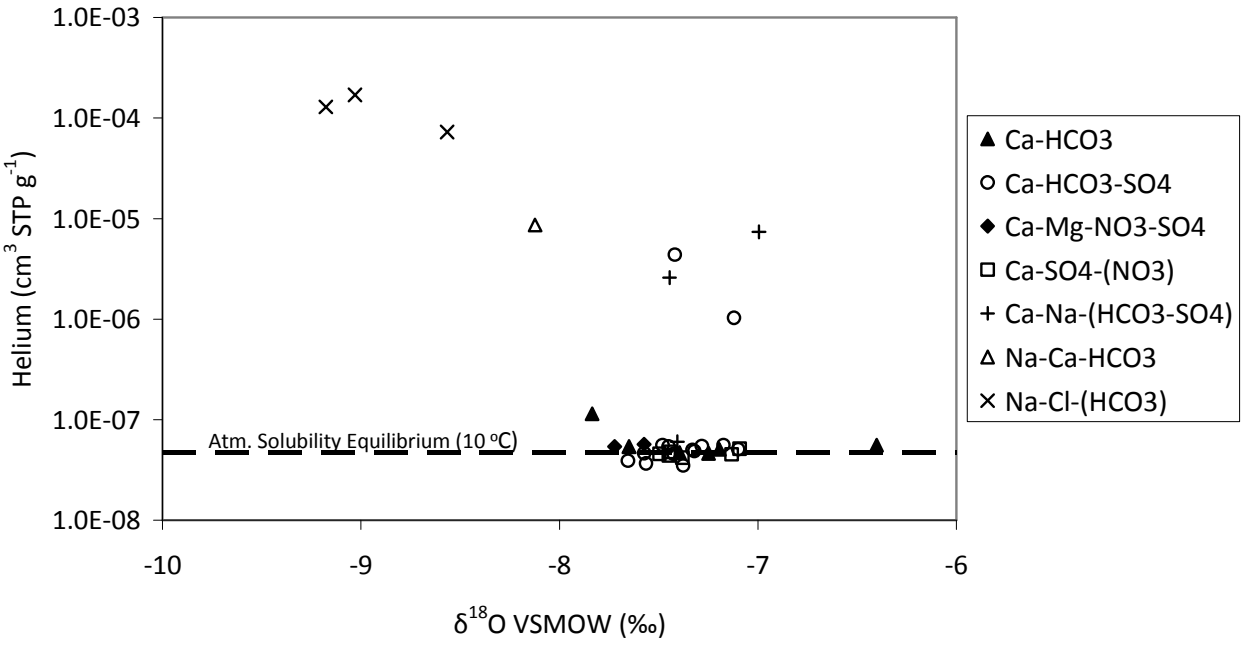

Figure 5.14. Cross-plot of helium concentration against $\delta^{18}O$. The dashed line indicates the theoretical concentration of helium based on solubility equilibrium at 10 ºC.

6. Discussion

6.1. Hydrochemistry

The unconsolidated siliciclastic sedimentary deposits of the Lower Rhine Embayment (LRE) consist of layered and mixed assemblages of minerals derived from a number of sources. Boenigk (2002) provides a detailed account of the sources and mineral compositions of the shallow Pleistocene sediments and determined that some of the assemblages have mineral compositions linking them to the Rhenish Massif and the East Eifel volcanic field. More commonly observed silicate based mineral deposits within the upper layers of the Lower Rhine Embayment include kyanite, staurolite, sillimanite, andalusite, green hornblende, epidote and garnet. These minerals are believed to have Tertiary marine and/or fluvial origins from the river Rhine (Boenigk, 2002). The work of Boenigk (2002) was developed further by Kemna (2008) to include a lithostratigraphical conceptual model for the Pliocene sediments that are overlain by the Pleistocene deposits. The mixed mineralogical assemblages are shown to vary significantly from bed to bed and this is likely to cause large differences in hydrochemistry on both a local and regional scale. Indeed, Appelo and Postma (2005) state that silicate aquifers often exhibit a wide range of hydrochemical facies because no single mineral dominates the weathering reactions. The mineralogy of the main aquifer system that occurs in the Miocene and Oligocene deposits is not well described in the literature. However, it is clear that the Lower Rhine Embayment presents a very complex hydrochemical system and that silicate weathering reactions are important processes that strongly influence groundwater hydrochemistry.

Silicate weathering reactions are controlled by carbon dioxide and organic acids present in the soil zone. The organic acids are produced from bacterial metabolism and root respiration within the unsaturated soil zone. These sources of soil

water acidity control the release of ions via the dissolution of silicate minerals (Herczeg and Edmunds, 2000). The following hydrolysis reactions in which carbonic acid is consumed resulting in a change of pH explain the release and uptake of solutes from silicate based minerals.

The weathering of silicate minerals to form clays and silicic acid in solution:

$$2CO_2 + 2NaAlSi_3O_8 + 11H_2O \rightleftharpoons Al_2Si_2O_5(OH)_4 + 2Na^+ + 2HCO_3^- + 4H_4SiO_4 \quad (6.1)$$

The weathering of cation enriched clays to form cation depleted clays:

$$3Na_{0.33}Al_{2.33}Si_{3.67}O_{10}(OH)_2 + H^+ + 11.5H_2O \rightleftharpoons 3.5Al_2Si_2O_5(OH)_4 + Na^+ + 4H_4SiO_4 \quad (6.2)$$

The chemical reactions that involve silicate minerals occur at a much slower rate than those that involve carbonate minerals and are sometimes irreversible as opposed to carbonates that can readily dissolve and re-precipitate (Herczeg and Edmunds, 2000). The primary source of silica in groundwater originates from chemical reactions including and similar to those described by Equation 6.1 and Equation 6.2, rather than originating from quartz material present in the aquifer system.

To develop an accurate and detailed interpretation of hydrochemical data taken from such a complex system that consists of layered and mixed assemblages such as the Lower Rhine Embayment, it would be necessary to consider the ‘order of encounter’ as described by Freeze and Cherry (1979). The ‘order of encounter’ involves establishing the order in which minerals are encountered as groundwater moves from recharge areas along defined flow paths. The order in which groundwater

encounters aquifer strata of different mineralogical composition significantly influences the hydrochemistry, and the chemical composition of groundwater continually evolves from the imposition of new, mineralogically controlled thermodynamic constraints (Freeze and Cherry, 1979). Although equilibrium with mineral phases can be reached on a local scale where the aquifer media is relatively homogeneous and flow rates are low, in most areas of the Lower Rhine Embayment discontinuous and layered heterogeneity are predominant and groundwater flow is significantly enhanced due to lignite mine de-watering. These features almost certainly cause disequilibrium to develop in most cases leading to complex spatial patterns in hydrochemistry. A typical hydrochemical study applying the 'order of encounter' approach essentially requires detailed knowledge of the mineralogy, lithology, stratigraphy and hydraulic head distribution. Considering the complex nature of the hydrogeological system in the Lower Rhine Embayment, such an approach would be both beyond the scope of this thesis and would deviate away from achieving the research aims and objectives set out in Chapter 1.

The hydrochemical data collected during this study has been used to establish hydrochemical trends on a regional scale and to indentify the key hydrochemical processes and reactions that provide an insight into regional flow mechanisms, as well as to provide additional evidence and strengthen the conceptual model that is based primarily on stable isotope data and dissolved noble gas concentrations. The discussion of Lower Rhine Embayment hydrochemistry that follows describes the important processes and reactions that are essential for understanding groundwater dynamics on both a local and regional scale.

6.1.1. Sodium and chloride

Sodium (Na^+) and chloride (Cl^-) ions are ubiquitous in groundwater. The chloride anion is highly soluble, highly mobile and is generally not involved in geochemical reactions within the aquifer. The chloride ion does not participate in any important subsurface redox reactions and does not easily adsorb onto clay minerals (Clark and Fritz, 1997). It is therefore an accurate assumption that chloride acts as a conservative tracer and follows the flow path of water molecules. Sodium cations tend to be more reactive and move less readily through the hydrological cycle, and the flow rate of sodium in groundwater largely depends on the cation exchange capacity (CEC) of the aquifer. A simple cross plot of sodium against chloride (Figure 6.1) with a 1:1 molar ratio halite dissolution line is useful to establish whether Na^+ enrichment or depletion is dominant.

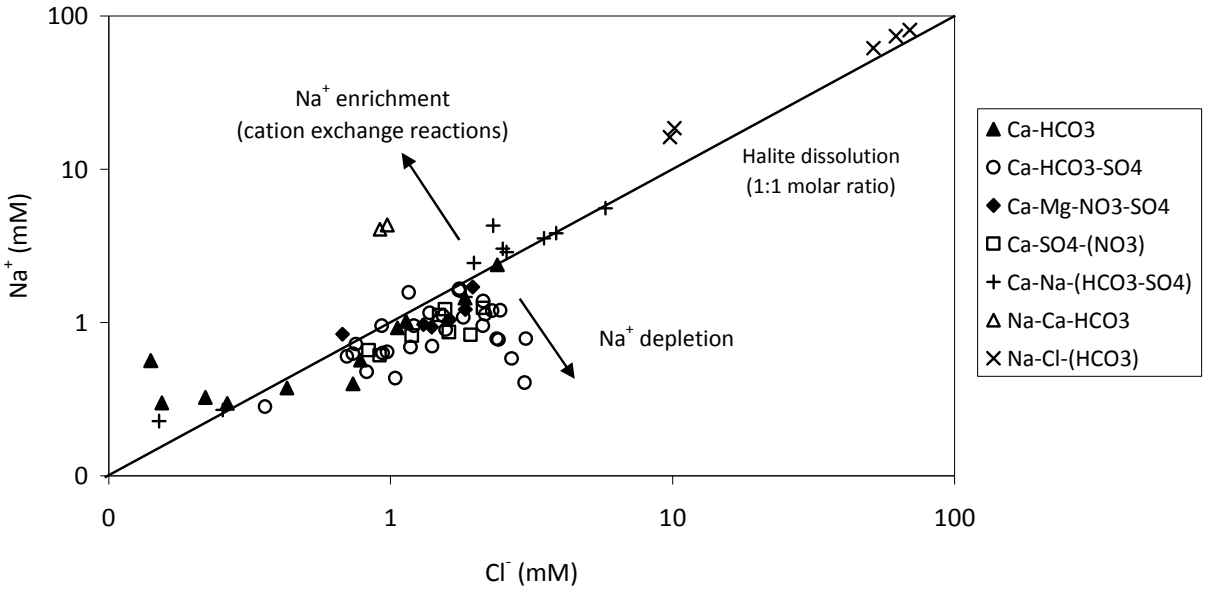

Figure 6.1. A simple cross plot of sodium against chloride ion data for groundwater samples collected during 2007/08 from the Lower Rhine Embayment. The 1:1 molar ratio halite dissolution line describes mixing between groundwater samples that plot close to the line and illustrates processes such as cation exchange for groundwater samples that plot above the line.

Sodium enrichment can indicate the occurrence of cation exchange reactions that often become significant during the hydrochemical evolution of groundwater. Chloride enrichment in sedimentary basins usually originates from trapped seawater, connate fluids and/or evaporite formations (Lavastre *et al.*, 2005; Clark and Fritz, 1997) although these sources would not typically lead to an enrichment of chloride relative to sodium. Anthropogenic sources of chloride such as the wet deposition of the acid gas HCl from lignite fuelled power station emissions can have a small enrichment effect in this region but reverse ion exchange reactions leading to sodium depletion are the most likely cause. However, it is possible that sodium depleted groundwater such as the Ca-HCO_3-SO_4 hydrochemical facies, is simply the result of low Na^+ concentrations within the aquifer matrix rather than reverse ion exchange reactions.

Figure 6.1 shows that only a small number of samples have enriched sodium concentrations relative to chloride, suggesting that cation exchange reactions are not a common feature of the shallow aquifer systems which follows the standard model that cation exchange is typically a feature of groundwater at depth and with a well developed level of hydrochemical evolution (Chebotarev, 1955). Cation exchange reactions mainly involve colloidal (10^{-3}–10^{-6} mm) particles because they have a high electrical charge to surface area ratio. Colloidal-sized clay particles such as alumino-silicate minerals (Al_2SiO_5) are common in the shallow Pleistocene deposits (Boenigk, 2002) and could form important ion exchange sites. However, the modern shallow groundwater samples show little evidence to suggest that such reactions are of significance in the upper aquifer layers of the Lower Rhine Embayment.

From Figure 6.1 the Na-Ca-HCO_3 hydrochemical facies displays a definite trend of Na^+ enrichment. These groundwater samples were collected from observation

borehole 907271 in the Korschenbroich area of the Lower Rhine Embayment, and the mean Cl^- concentration of the two samples is 0.95 mM. The Na-Ca-HCO_3 groundwater type sampled from observation borehole 907271 is believed to originate from greater depth within the aquifer system which would explain the Na^+ enrichment as a result of cation exchange reactions under increasing confinement and long residence time. The transport mechanisms responsible for the upward flow of groundwater from depth in this area are related to the Viersen Fault. The stable isotope and noble gas data associated with the Na-Ca-HCO_3 type groundwater are discussed in Section 6.2 and Section 6.3 respectively.

Figure 6.1 also shows a Na-Cl-(HCO_3) dominated hydrochemical facies. The concentrations of helium in the Na-Cl-(HCO_3) type groundwater samples are very high suggesting a long residence times. Deep circulating groundwaters with long residence times are often reported to have high salinity. Such increases in salinity over time can result from an addition of NaCl from evaporite formations, weathering reactions or from seawater intrusion (in coastal areas), formation brines or connate waters. The precise mechanism of salinisation is often difficult to identify with any degree of certainty and this is certainly the case with the Na-Cl-(HCO_3) groundwater sampled from observation boreholes in the Brühl region of the Lower Rhine Embayment. However, NaCl salinity is characteristic of a marine influence or a deep aquifer system that contains remnant seawater (Clark and Fritz, 1997).

6.1.2. Hydrochemical facies

Durov diagrams are very useful for establishing and defining hydrochemical facies and determining the hydrochemical evolution of groundwater and indentifying processes such as cation exchange. The hydrochemical facies illustrated in Figure 6.2 were defined using AquaChem® and are described in Chapter 5. The key feature of

the data plotted in Figure 6.2 is the ionic composition of the Na-Ca-HCO_3 and Na-Cl-(HCO_3) groundwater types relative to the main cluster of samples. The Na-Ca-HCO_3 groundwater type occupies a region of the ternary plot that is often associated with cation exchange reactions whereas the Na-Cl-(HCO_3) groundwater type is characteristic of a palaeo groundwater. Stable isotope data and dissolved helium concentrations discussed in Section 6.2 and Section 6.3 respectively suggest that the Na-Cl-(HCO_3) groundwater type represents a distinct end member groundwater.

The main cluster of groundwater samples in Figure 6.2 display a wide range of hydrochemical facies, characteristic of silicate aquifers in which no single mineral dominates the weathering reactions (Appelo and Postma, 2005). It is difficult to identify an evolutionary trend in hydrochemistry because of the large spatial distribution of the sampled observation boreholes and the complex nature of the layered aquifer system. Groundwater samples were typically collected from several different aquifers units in any given area and from adjacent aquifers that are effectively isolated by low permeability fault zones and/or the juxtaposition of contrasting lithology. However, it is suggested that the Ca-Mg-NO_3-SO_4 and Ca-SO_4-(NO_3) hydrochemical facies represent the most recent and hydrochemically immature groundwater recharge because of the dominant ions associated with anthropogenic inputs and soil zone processes.

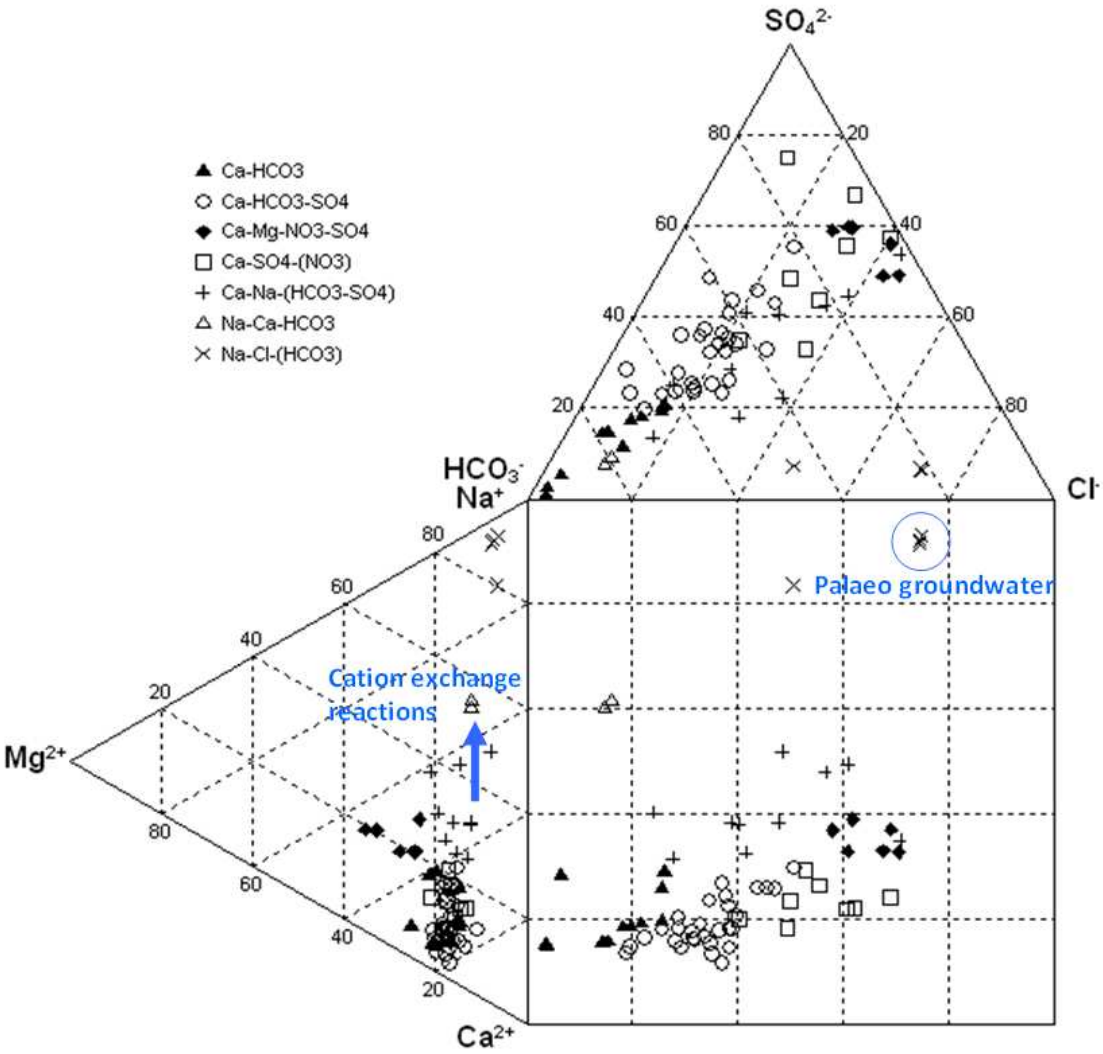

Figure 6.2. Durov diagram displaying the major ion composition of groundwater samples collected during 2007/08 from the Lower Rhine Embayment, Germany. The Durov plot clearly identifies dominant ions and processes such as cation exchange as well as graphically illustrates small differences in hydrochemistry.

6.1.3. Redox reactions

The redox potential expressed as Eh tends to follow a natural evolution towards lower values with increased residence time. Initially, precipitation has a high redox potential due to the influence of atmospheric oxygen and specifically the

relatively high concentration of dissolved oxygen present. Typically, precipitation at pH 7 will have an Eh of 750 mV (Freeze and Cherry, 1979). However, the redox potential quickly decreases within the soil zone due to the oxidation of organic matter which can potentially remove a large proportion of the dissolved oxygen, but this is largely dependent on the quantity of organic matter present in the soil zone.

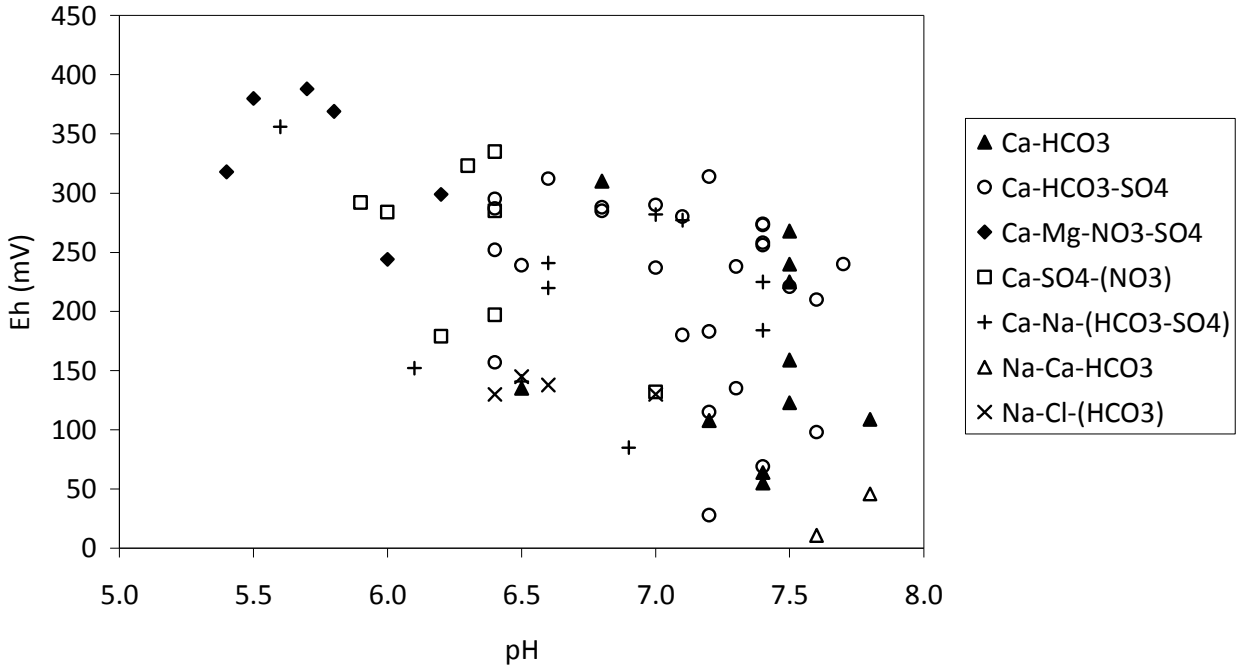

Figure 6.3. Electrochemical evolution of groundwater describes a decline in redox potential with increasing aquifer confinement. The most recent groundwater recharge is identified by a hydrochemical facies that contain Mg^{2+} and NO_3^- as dominant ions. These groundwater types generally show the lowest pH values and highest redox potentials, as expected.

The hydrochemical data in Table 5.4 suggests that redox reactions are only of significance in one area of the Lower Rhine Embayment that has been sampled during this research. Nitrate and ammonium concentrations in the Brühl region suggest that the Na-Cl-(HCO_3) type groundwater found in observation borehole Brühl 9 (958061, 957062 and 958063), Fischenich (957824) and Brühl SW 22 R1 (352722) creates a

reducing environment. The Na-Cl-(HCO_3) groundwater present in the deepest Brühl 9 piezometer (958063) contains nitrate and ammonium both at concentrations that are below the analytical detection limit of 0.05 and 0.2 mg L^{-1} respectively. The two other piezometers at the Brühl 9 location (958062 and 958061) are at shallower depths and show elevated ammonium concentrations of 2.95 and 2.77 mg L^{-1} but nitrate levels remain below the limit of detection. This suggests that the Na-Cl-(HCO_3) type groundwater is mixing with modern recharge of meteoric origin (which is characterised as having nitrate concentrations in the range of ~90 mg L^{-1}) in the upper layers of this aquifer and the process of dissimilatory nitrate reduction to ammonium (DNRA) can be inferred to account for the high ammonium concentrations. Smith and Duff (1988) suggest that nitrate reduction in carbon limited aquifers favours the process of denitrification over DNRA implying that there must be a source of organic carbon in the shallow aquifer.

The piezometer nest at Fischenich (957822, 957823 and 957824) displays an interesting vertical nitrate gradient with the highest concentration (92.1 mg L^{-1}) at shallow depth (957822) suggesting modern recharge and decreasing with depth until the nitrate concentration falls below the limit of detection at the greatest depth sampled at this location (76 m; 957824). The remaining two observation boreholes in this locality also provide insight into the source and subsequent mixing of the Na-Cl-(HCO_3) groundwater as these boreholes have been identified as containing both Na-Cl-(HCO_3) and Ca-HCO_3-SO_4 groundwater types. The borehole at Brühl SW 22 R1 (352722) contains the Na-Cl-(HCO_3) groundwater type and shows an elevated NH_4^+ concentration but a very low NO_3^- concentration, whereas the shallow piezometer within the same nest contains Ca-Na-(HCO_3-SO_4) type groundwater that has a relatively high nitrate concentration of 55.3 mg L^{-1} and low NH_4^+ concentration. This suggests that a degree of mixing is occurring and that dissimilatory nitrate reduction

to ammonium is evident as the nitrate concentration is less than expected from the surrounding areas that are known to contain modern groundwater (Schenk, 1982). The Brühl 1 observation borehole also contains two hydrochemical facies and a range of ammonium and nitrate concentrations.

6.1.4. Carbonate system evolution

Carbonate minerals such as calcite dissolve in groundwater due to the dissolution of CO_2 in water to form H_2CO_3 and the subsequent two-step dissociation of H_2CO_3 described by Equation 6.3, Equation 6.4 and Equation 6.5, as well as from the production of organic acids from root respiration and bacterial metabolism in the soil zone (Herczeg and Edmunds, 2000). The reader is referred to Appelo and Postma (2005) for a detailed account of the processes involved in carbonate mineral dissolution.

$$CO_{2(g)} + H_2O \rightleftharpoons H_2CO_3 \quad (6.3)$$

$$H_2CO_3 \rightleftharpoons H^+ + HCO_3^- \quad (6.4)$$

$$HCO_3^- \rightleftharpoons H^+ + CO_3^{2-} \quad (6.5)$$

Deines *et al*. (1974) described carbonate evolution in groundwater in terms of open and closed system models. According to Deines *et al*. (1974) open system evolution involves the reaction of carbonate minerals with water that is in contact with a gas phase of fixed P_{CO2} and continuous isotopic exchange exists between the CO_2 reservoir and the solution, whereas in closed system evolution water is isolated from the CO_2 reservoir before carbonate dissolution occurs. However, in reality most carbonate system evolution falls somewhere in between these two models. It is also

possible that during the course of groundwater evolution along a flow path from recharge area to discharge zone, carbonate dissolution will occur under both sets of conditions typically moving from open system to closed system evolution with increasing aquifer confinement (Deines *et al.*, 1974).

The first observation to note from Figure 6.4 is that the P_{CO2} values calculated using PHREEQC for groundwater samples collected from all observation boreholes are above the P_{CO2} value of atmospheric air ($10^{-3.4}$ atm). This suggests that the groundwater present in the sampled aquifers attained excess CO_2 relative to atmospheric equilibrium solubility during infiltration through the soil zones where P_{CO2} values are typically higher than atmospheric levels. It can also be seen from Figure 6.4 that a large number of samples have not reached calcite saturation. The most recent recharge indicated by higher concentrations of Mg^{2+} and NO_3^- such as the Ca-Mg-NO_3-SO_4 and Ca-SO_4-NO_3 groundwater types are immature with respect to carbonate evolution suggesting either very recent recharge or more likely that the aquifer is carbonate limited and carbonate evolution is a slow process. Considering that the upper aquifer system primarily consists of silicate based material it is not particularly unusual that calcite saturation has not been reached in aquifers that contain the most recent recharge.

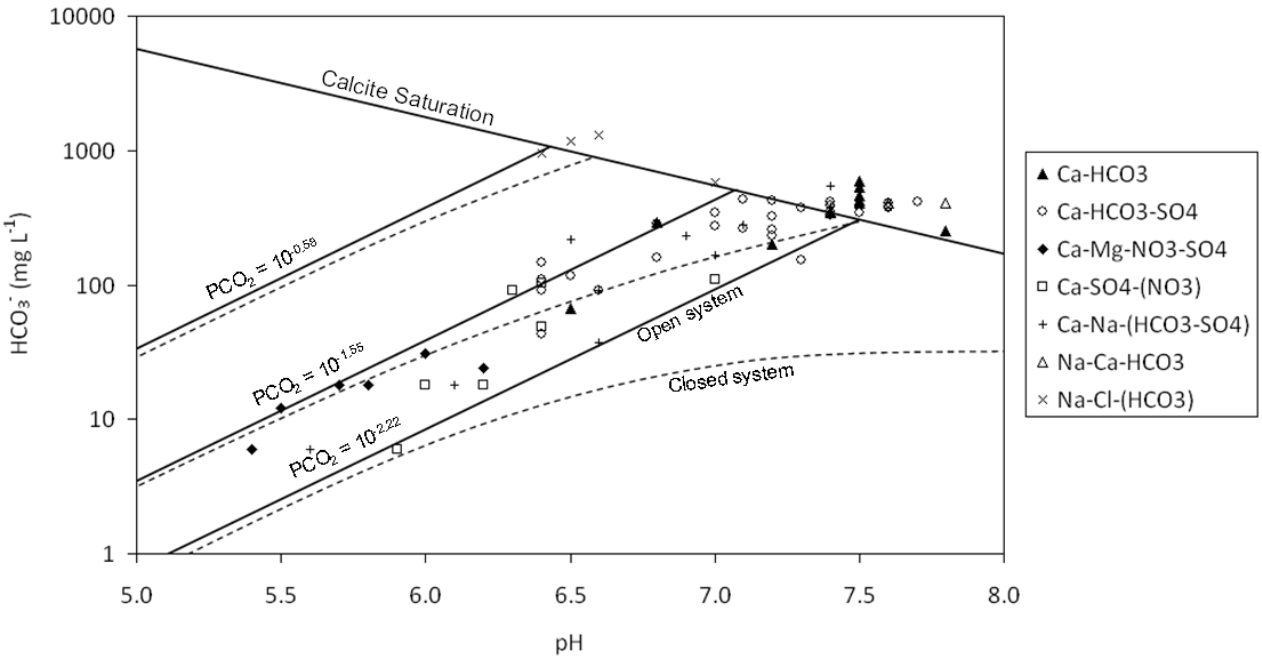

Figure 6.4. Open and closed system models of carbonate system evolution (after Deines *et al*., 1974).

The pH values of the groundwater samples are between 5.4 and 7.8 suggesting that dissolved inorganic carbon exists primarily as HCO_3^-. The groundwater samples defined as having a Na-Cl-(HCO_3) hydrochemical facies appear to have evolved under the highest P_{CO2} conditions and therefore also have the highest HCO_3^- concentrations of up to 1312 mg L^{-1}. The Na-Cl-(HCO_3) groundwater type clearly evolved under different conditions to the other groundwater samples. From Figure 6.4 it is difficult to determine whether carbonate evolution occurred under open or closed conditions however, it is likely that excess CO_2 in these samples did not originate from the soil zone during recharge but was generated within the subsurface or deeper in the crust. According to Vrolijk *et al*. (2005) the most likely processes that generate CO_2 in the crust are mantle or magmatic emanations, degradation of organic matter, diagenetic reactions involving clay and carbonate rocks and/or thermal de-carbonation

of carbonate rocks by metamorphic processes. The exact origin of the Na-Cl-(HCO_3) groundwater is unknown but stable isotope data and dissolved noble gas concentrations suggest a deep basinal origin which would explain the high concentrations of dissolved CO_2.

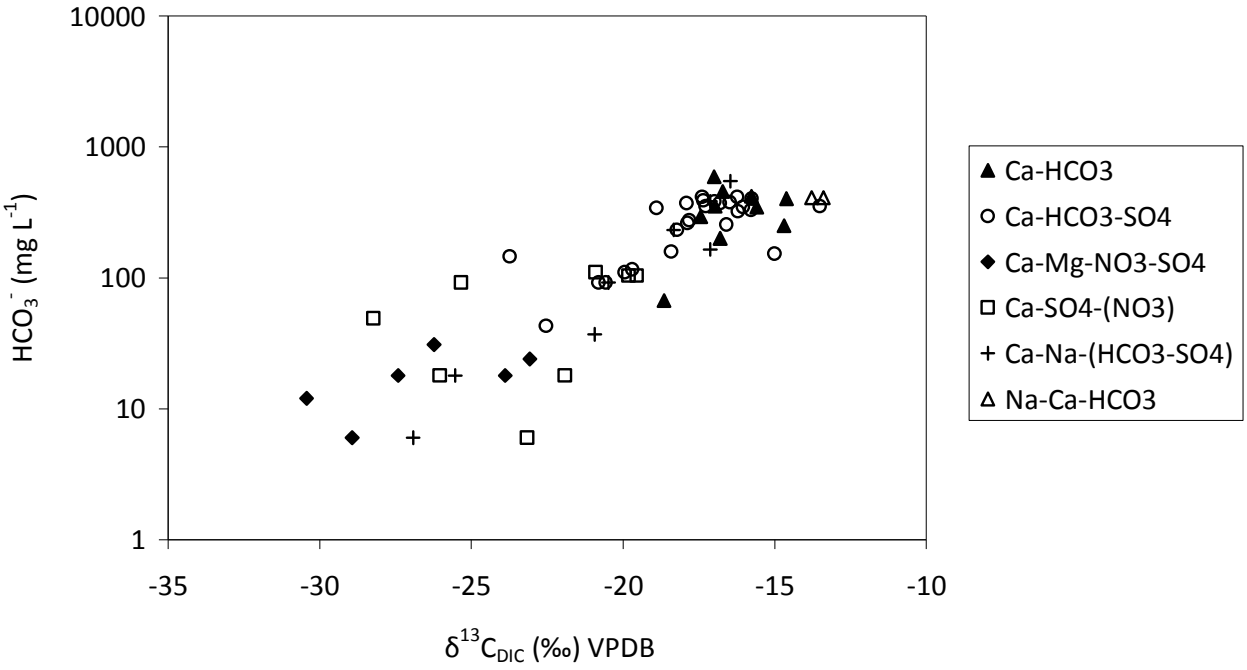

Figure 6.5. Carbonate evolution indicated by HCO_3^- and $\delta^{13}C$.

The $\delta^{13}C_{DIC}$ of groundwater evolves to less negative values during weathering reactions within the aquifer. The evolution is controlled by aquifer composition (eg. silicate or carbonate) and whether evolution occurs under open or closed system conditions as described by Deines *et al.* (1974). In silicate dominated systems such as the shallow sand aquifers of the Lower Rhine Embayment, dissolved inorganic carbon typically does not evolve much further than the initial conditions established in the soil zone. However, in areas with carbonate material present, the dissolution of calcite

and dolomite provide an additional source of ^{13}C enriched carbon that can have a large effect on $\delta^{13}C_{DIC}$ values (Clark and Fritz, 1997). Figure 6.5 shows the distribution of $\delta^{13}C_{DIC}$ values for a number of groundwater samples collected from the Lower Rhine Embayment. It is important to note that unfortunately groundwater samples collected from the Brühl region were not analysed for $\delta^{13}C_{DIC}$ because the field sampling technique for $\delta^{13}C_{DIC}$ analysis described by Bishop (1990) and stated in Chapter 4 was not available during the sampling campaign that included the Brühl region. The hydrochemistry and stable isotope data ($\delta^{2}H$ and $\delta^{18}O$ values) indicates that all the groundwater samples presented in Figure 6.5 represent modern groundwater of meteoric origin with just one exception – the Na-Ca-HCO_3 groundwater type. The Ca-Mg-NO_3-SO_4 and Ca-SO_4-(NO_3) dominated groundwater types display the lowest $\delta^{13}C_{DIC}$ values suggesting a short residence time. Relatively low $\delta^{13}C_{DIC}$ values are characteristic of soil zone conditions and groundwater tends to evolve towards more positive $\delta^{13}C_{DIC}$ values with the dissolution of calcite, dolomite and silicate minerals. The Ca-HCO_3 and Na-Ca-HCO_3 dominated groundwater types shown in Figure 6.5 have more positive $\delta^{13}C_{DIC}$ values and therefore are likely to represent the most hydrochemically evolved groundwater. Groundwater in equilibrium with calcite and evolved under closed conditions generally maintains a stable isotopic composition within the aquifer medium although $\delta^{13}C$ values often become slightly more positive with increased residence time even when equilibrium with calcite has been reached – perhaps due to a loss of Ca^{2+} from solution (Clark and Fritz, 1997). This could explain why the Na-Ca-HCO_3 groundwater samples have the highest $\delta^{13}C_{DIC}$ values of -13.4 and -13.8‰ (see Figure 6.5). Figure 6.4 shows that the Na-Ca-HCO_3 groundwater has reached calcite saturation and ^{4}He data (presented in Section 6.3.1) suggests a significantly longer residence time than modern recharge. The Ca-HCO_3 dominated groundwater samples are all in equilibrium with calcite and

originate to the east and southeast of Mönchengladbach possibly suggesting that this region is not carbonate limited or that the residence time of groundwater in this region is longer than it is in areas to the west and northwest of Mönchengladbach. The aquifer systems of the Lower Rhine Embayment consist primarily of silicate based sands and gravels. The weathering of silicate minerals is a slow process in comparison to carbonate systems but forms an important sink for CO_2.

Figure 6.6 shows that the Na-Cl-(HCO_3) groundwater has evolved hydrochemically in a hydrogeological setting that is significantly different to the shallow layered aquifer system of the LRE that consists primarily of modern groundwater of meteoric origin. An interesting observation illustrated by Figure 6.6 is that the Na-Cl-(HCO_3) type groundwater and the Na-Ca-HCO_3 type groundwater appear to plot on a mixing line even though the Na-Ca-HCO_3 groundwater is not present in the same location as the Na-Cl-(HCO_3) groundwater. However, stable isotope data and dissolved noble gas concentrations suggest that the Na-Ca-HCO_3 - dominated groundwater could be linked to the Na-Cl-(HCO_3) dominated groundwater because of similar depleted $\delta^{18}O$ values and ^4He concentrations that exceed those expected due to atmospheric solubility equilibrium. Hydrochemical data support this hypothesis and provides evidence that the Na-Cl-(HCO_3) type groundwater could be widely distributed at depth within the deep basement system but is only observed at shallow depth in areas of deep faulting and intense lignite mine de-watering. It is perhaps possible that small point-source-like emanations of ^4He enriched, Na-Cl-(HCO_3) dominated palaeo groundwater occur in such areas throughout the Lower Rhine Embayment.

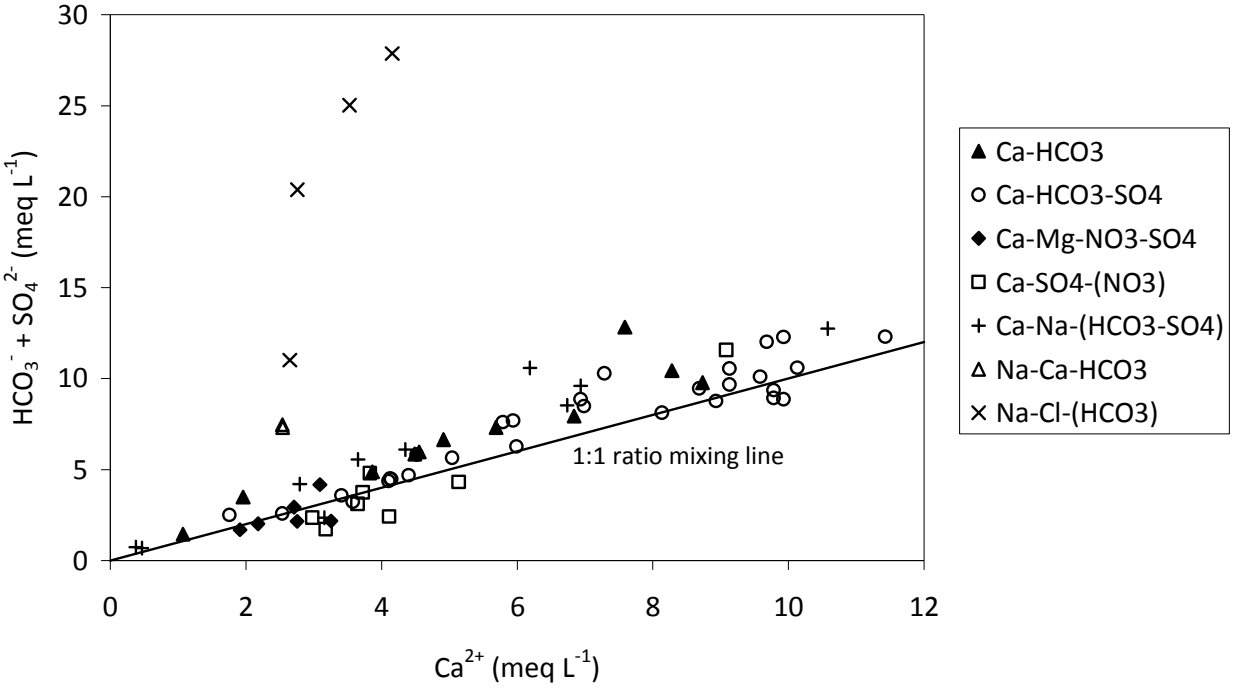

Figure 6.6. A simple cross plot of HCO_3^- + SO_4^{2-} against Ca^{2+} illustrates mixing between samples that plot close to the 1:1 ratio line. Processes such as sulphate reduction would cause deviations from the 1:1 ratio mixing line.

Figure 6.6 shows that the Na-Cl-(HCO_3) dominated groundwater has evolved under conditions that have led to low Ca^{2+} but relatively high HCO_3^- concentrations. For groundwater to follow this evolutionary path it would be necessary for a high production rate of H^+ ions in the subsurface. It is possible that a mechanism such as the oxidation of pyrite (FeS_2) could provide the source of the H^+ ions but it is perhaps more likely that the source of H^+ ions originates from the production of CO_2 in the subsurface. In the Lower Rhine Embayment the coalification (diagenesis) of lignite is a possible source of CO_2 which would in turn generate the necessary concentration of H^+ ions to account for the observed trend of low Ca^{2+} and high HCO_3^- displayed by the Na-Cl-(HCO_3) groundwater. The chemical reaction involving the diagenesis of lignite that produces CO_2 is given by the following equation:

$$C_nH_2O \rightarrow \frac{n}{2}CO_{2(g)} + \frac{1}{2}C_nH_{2n+2} \qquad (6.6)$$

Under anaerobic groundwater conditions, the oxidation of organic matter is achieved via SO_4^{2-} reduction. Groundwater in which dissolved CO_2 has been generated by sulphate reduction usually exhibits a low sulphate concentration.

The Na-Cl-(HCO_3) dominated groundwater is clearly an old, mineralized and highly evolved groundwater that has a high concentration of dissolved CO_2 that originates from one or more of the processes discussed previously, and this would account for the hydrochemical trends that the Na-Cl-(HCO_3) type groundwater displays.

6.2. Stable Isotopes

6.2.1. Hydrogen and Oxygen

The principal stable isotopes of hydrogen and oxygen (δ^2H and $\delta^{18}O$) have been used extensively in hydrogeological studies (eg. Rozanski, 1985; Zuber *et al.*, 2004; Von Rohden *et al.*, 2010). These isotopes of the water molecule provide evidence for determining the origin of groundwater due to a variation in isotopic composition that occurs as a result of isotopic fractionation processes. The reader is referred to Chapter 3 and Gat (1996; 2010) for a comprehensive overview.

Stable isotopes (δ^2H and $\delta^{18}O$) have been successfully applied to infer the presence of palaeo groundwater in many aquifer systems (eg. Rozanski, 1985; Fontes *et al.*, 1991; Deák and Coplen, 1996; Vaikmäe *et al.*, 2001) due to the lower evaporation rates and increased recharge rates that occur under cooler climatic

conditions (Gat, 2010). However, when considering groundwater recharge during the last glacial maximum (LGM) it is important to note that changes in vegetation cover probably had a large influence on recharge rates, and that precipitation is typically lower during glacial periods (Coplen *et al*., 2000).

The term 'palaeo groundwater' is used in the literature to generally refer to groundwater that displays a depleted isotopic signature suggesting groundwater recharge occurred under cooler climatic conditions, usually during the late Pleistocene epoch. However, many deep aquifer systems contain much older groundwater that probably originated as connate waters of marine origin or as formation brines and these are also referred to as palaeo groundwaters in the literature (Coplen *et al*., 2000). Modern groundwater recharge of Holocene age is usually categorised as either pre- or post industrial, but they often display a similar isotopic signature. Distinguishing between pre- and post industrial recharge is useful when interpreting groundwater hydrochemistry due to the occurrence of industrial and agricultural pollution over the last ~200 years and the resultant changes in hydrochemical composition.

The stable isotope data presented in Figure 6.7 shows that the majority of the observation boreholes sampled within the Lower Rhine Embayment during 2007/08 contain modern groundwater recharge of meteoric origin. The main cluster of sample points in Figure 6.7 exhibit a wide range of hydrochemical compositions (see Figure 6.2) but display a limited range of $\delta^{2}H$ and $\delta^{18}O$ values suggesting modern recharge of Holocene age. The isotopic signatures of the groundwater samples collected from the shallow aquifers of the Lower Rhine Embayment are characteristic of present day precipitation in this region of Germany (IAEA, 2006) with $\delta^{18}O$ values in the range of -7 – -8‰ and falling on or very close to the Global Meteoric Water Line (GMWL). This evidence is consistent with a modern meteoric origin and explains the limited range of observed isotopic compositions.

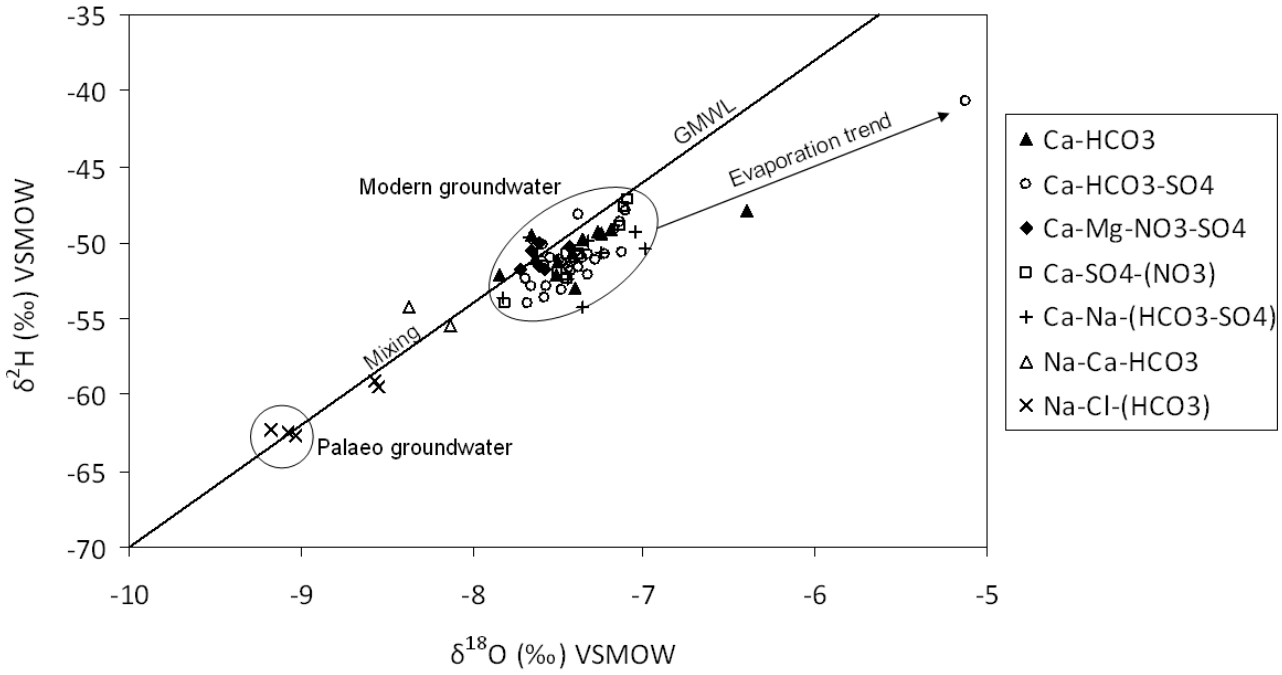

Figure 6.7. Isotopic composition of groundwater in the Lower Rhine Embayment, Germany with reference to the Global Meteoric Water Line (GMWL) after Craig (1961).

Although it has been established that the majority of the observation boreholes sampled in the Lower Rhine Embayment contain modern groundwater of meteoric origin there are however, two exceptions to note from Figure 6.7. The first exception is the seven groundwater samples that have relatively low $\delta^{18}O$ values, and the second exception being the two groundwater samples with high $\delta^{18}O$ values that plot to the right hand side of the GMWL. The groundwater samples that have low $\delta^{18}O$ values all plot on the GMWL suggesting a meteoric origin as opposed to a geothermal source or evaporation trend. The small cluster of three sample points between -9.0 and -9.2‰ originate from a single observation borehole but from piezometers reaching different depths. Based on the stable isotope data presented in Figure 6.7 as well as hydrochemical and dissolved noble gas concentrations that are discussed in Section 6.1 and Section 6.3 respectively, it can be inferred that the Na-Cl dominated

groundwater has a significantly different recharge history, evolutionary path and residence time in comparison to the main cluster of groundwater samples that represent modern recharge of meteoric origin. The Na-Cl-(HCO_3) hydrochemical facies appears to be of meteoric origin as it plots on the GMWL suggesting that recharge probably occurred under cooler climatic conditions than those that predominate today and therefore leading to the conclusion that this is indeed a palaeo groundwater.

The groundwater samples that plot between the Na-Cl palaeo groundwater and the main cluster of samples that represent modern recharge are thought to be a result of mixing between the two groundwater types. The presence of the Na-Cl-(HCO_3) groundwater and the subsequent mixing with modern recharge has only been observed in a localised area within the town of Brühl in the south western region of the Lower Rhine Embayment. However, groundwater collected from a single observation borehole in the village of Korschenbroich (ID number 907271) north of the Brühl area and in close proximity to the Viersen Fault has an isotopic composition that plots very close to the GMWL and has a mean $\delta^{18}O$ value of -8.2‰. The groundwater sample taken from borehole 907271 appears to have an isotopic and noble gas signature that is consistent with mixing between the Na-Cl palaeo groundwater and modern recharge in the shallow aquifers. However, this groundwater type (Na-Ca-HCO_3) was only observed at one location in the Korschenbroich area despite additional targeted sampling of neighbouring boreholes, suggesting that the origin of this groundwater could be deep within the aquifer system and linked to the Viersen Fault.

Although it is possible to infer the presence of palaeo groundwater using the stable isotopes of oxygen and hydrogen, it is not possible to determine precise temperature changes. A number of studies successfully combined the use of stable isotopes with ^{14}C age-dating to provide an estimate of residence time and therefore

determining the climatic conditions at the time of recharge based on other palaeo climate proxies (eg. Fontes *et al*., 1991; Deák and Coplen, 1996; Vaikmäe *et al*., 2001).

Deák and Coplen (1996) successfully applied $\delta^{18}O$ measurements and ^{14}C dating techniques to distinguish between Holocene and Pleistocene recharge in the Great Hungarian Plain in central Europe. Based on the results of the ^{14}C groundwater dating, modern recharge was simply defined as having a $\delta^{18}O$ value more positive than -10‰ whereas palaeo groundwater (groundwater recharged during the Pleistocene) was defined as having a $\delta^{18}O$ value more negative than -10‰ (Deák and Coplen, 1996). Rozanski (1985) presented a large range of stable isotope data from a number of authors for European palaeo groundwaters. Rudolph *et al*. (1984) presented stable isotope data from southern Germany (Nürnberg region) with $\delta^{18}O$ values in the region of -10 to -11‰ for palaeo groundwater. These values are slightly more negative than the $\delta^{18}O$ value of -9‰ that was determined for palaeo groundwater from the Lower Rhine Embayment.

More recently it has become common to combine stable isotope measurements not only with groundwater age-dating techniques such as ^{14}C, but also with dissolved noble gas measurements to form a multi-tracer approach which allows groundwater residence times to be accurately determined as well as enabling the precise mean annual surface temperature at the time of recharge to be calculated (eg. Andrews and Lee, 1979; Stute and Deák, 1989; Stute *et al*., 1995; Beyerle *et al*., 1998; Aeschbach-Hertig *et al*., 2002; Lehmann *et al*., 2003; Zuber *et al*., 2004). The calculated noble gas temperatures (NGTs) for modern and palaeo groundwater from the Lower Rhine Embayment are discussed in Section 6.3.

6.3. Dissolved noble gases

6.3.1. Helium in groundwater

Helium isotopes are typically used in groundwater studies as a semi-quantitative measure of groundwater residence time (Andrews and Lee, 1979; Zhou and Ballentine, 2006), to identify deep crustal or mantle fluxes (Marty *et al*., 1993) or to investigate the sealing properties of aquitards (Marty *et al*., 2003). A full review of dissolved noble gases in groundwater including helium isotopes is given in *Chapter 3*. Groundwater samples collected during 2007/08 from the Lower Rhine Embayment were analysed for dissolved helium and the results are presented in Figure 6.8.

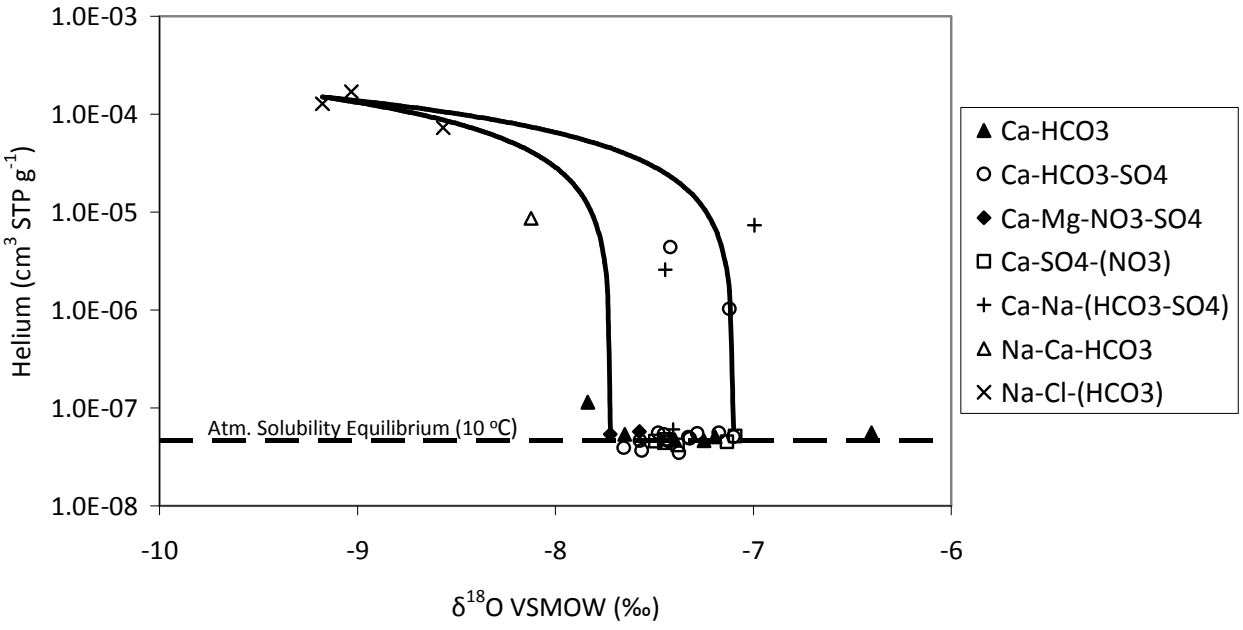

Figure 6.8. Cross plot of helium concentration against $\delta^{18}O$ value for groundwater samples collected during 2007/08 from the Lower Rhine Embayment, Germany. The solid lines represent a simple binary mixing model envelope between end member groundwater types and the dashed line indicated the expected helium concentration due to atmospheric solubility equilibrium at 10 ºC.

The first observation to note from Figure 6.8 is that the main cluster of sample points represents modern groundwater recharge of meteoric origin due to their isotopic composition and proximity to the GMWL as discussed in Section 6.2. These groundwater samples have helium concentrations in the range expected from atmospheric solubility equilibrium and the addition of excess air. The dashed line in Figure 6.8 represents atmospheric solubility equilibrium at 10 ºC which approximates the mean annual surface temperature of the region.

The Na-Cl dominated groundwater has helium concentrations of 1.28×10^{-4} and 1.69×10^{-4} cm^3 STP g^{-1} H_2O in groundwater samples collected from the Brühl 9 observation borehole (piezometers of 958062 and 958063 respectively). These helium concentrations exceed that expected for groundwater in solubility equilibrium with the atmosphere by more than three orders of magnitude and are the highest helium concentrations measured in groundwater samples collected from the Lower Rhine Embayment during this research. Excess helium of this magnitude probably results from the *in situ* production of radiogenic ^4He within the subsurface due to the decay of U and Th series elements, and subsequent accumulation in groundwater over time, in addition to a large helium flux to the aquifer system from an external and perhaps previously trapped reservoir. Much smaller helium excesses could be explained by an excess air component of ^3He and ^4He from the dissolution of entrained air of atmospheric origin during water table fluctuations (Ingram *et al.*, 2007), the β-decay of bomb tritium to tritiogenic ^3He, $^6Li(n,\alpha)^3H$ reactions that produce nucleogenic ^3He, as well as mantle contributions of both ^3He and ^4He (Castro, 2004).

In deep circulating groundwater from sedimentary basins it is typically assumed that a crustal component is primarily responsible for large excesses of helium that originate from *in situ* production or a crystalline basement (Castro, 2004).

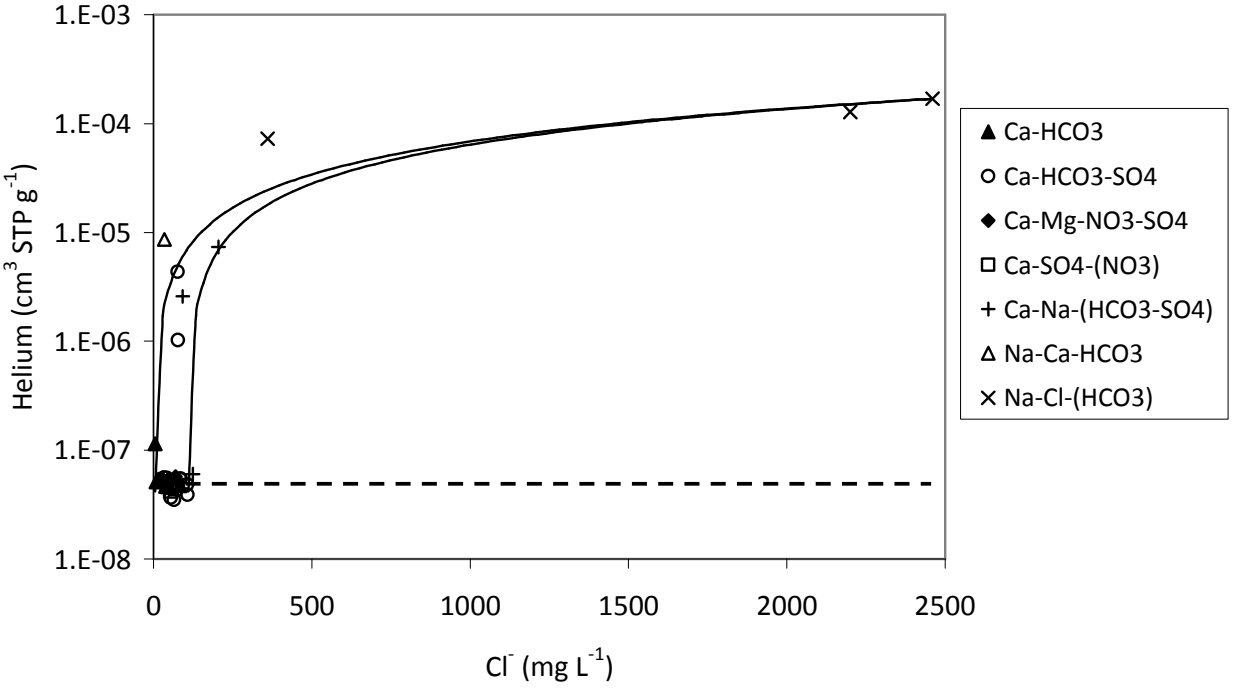

Figure 6.9. Cross plot of helium against chloride for groundwater samples collected during 2007/08 from the Lower Rhine Embayment. The solid lines represent a simple binary mixing model envelope between end member groundwater types.

Accurate ^{3}He measurements provide a quantitative way to distinguish between the various sources of excess ^{3}He and ^{4}He in groundwater due to well known $^{3}He/^{4}He$ ratios (Clark *et al.*, 1976). Unfortunately, it was not possible to include ^{3}He measurements as a component of this research even though such measurements would have provided great insight into the origin of excess helium present in a number of observation boreholes in the Brühl region of the Lower Rhine Embayment.

Helium-4 has been used in a number of studies as a semi-quantitative tool for determining groundwater age (Zhou and Ballentine, 2006). Calculations based on *in situ* accumulation of radiogenic ^{4}He using estimates of U and Th concentrations in Lower Rhine Embayment sediments and ^{4}He groundwater age equations given by Mahara and Igarashi (2003) and Zhou and Ballentine (2006) appear to yield

unrealistically long aquifer residence times in the range of 10^8 years. A number of studies have reported ^{4}He concentrations to be higher than those that can be explained by *in situ* radiogenic production (eg. Torgersen and Clark, 1985; Takahata and Sano, 2000). Marty *et al.* (2003) reported that the *in situ* production of ^{4}He in the Trias aquifer of the Paris Basin accounted for <1% of the observed ^{4}He present in groundwater based on ^{14}C dating to determine groundwater residence times. An explanation of the high helium content in the shallow aquifer layers of the Lower Rhine Embayment requires a significant contribution from an external source outside the aquifer system. A number of studies have suggested that generally, it is likely that excess helium in sedimentary aquifers originates from deep in the continental crust (Torgersen and Clark, 1985; Castro *et al.*, 1998) or that it originates from deep circulating basinal fluids (Pinti and Marty, 1998). Solomon *et al.* (1996) suggested that a high external flux of helium to shallow groundwater could originate from a previously trapped reservoir of helium. Unfortunately, the precise origin of the dissolved helium present in groundwater samples collected from the shallow aquifers in the Brühl region of the Lower Rhine Embayment remains uncertain, and without accurate ^{3}He measurements the potential sources are difficult to resolve. However, potential sources of helium can be identified by considering the mechanisms by which helium has migrated to the shallow aquifer system. The primary mechanisms responsible for the transport of helium from deep in the continental crust to shallow groundwater systems include fluid advection and/or bulk diffusion. Zhou and Ballentine (2006) state that these processes are unlikely to account for the necessary rate of helium mass transport from the crust to shallow groundwater. Therefore, external helium fluxes to near-surface groundwater aquifers of the magnitude necessary to produce observed helium concentrations several orders of magnitude in excess of those expected from atmospheric solubility equilibrium must be the result of

large scale tectonics such as crustal extension (Ballentine and Burnard, 2002). Indeed, the high helium concentrations measured from groundwater samples taken from the Brühl region have led to the inference that deep crustal fluids have migrated from depth to the shallow aquifers via conduit flow within the Bornheim fault zone that connects deep and shallow aquifer layers that are otherwise isolated by confining clay layers and lignite seams of very low permeability. These findings provide geochemical evidence to validate the conduit-barrier model proposed by Bense and Person (2006) that describes faults as barriers to lateral groundwater flow but as conduits or preferential flow paths for vertical displacement of groundwater in the Lower Rhine Embayment.

To improve the groundwater residence time estimate based on ^{4}He concentration it is necessary to consider all sources of ^{4}He which include an atmospheric component, *in situ* radiogenic production as well as an external flux of ^{4}He given by the following equations:

$$\left[{}^4He\right] = \left[{}^4He\right]_{ASW} + \left[{}^4He\right]_{insituproduction} + \left[{}^4He\right]_{externalflux} \qquad (6.7)$$

$$\left[{}^4He\right]_{insituproduction} = \frac{\rho \eta S \left(1-\varphi\right)}{\varphi} t \qquad (6.8)$$

$$\left[{}^4He\right]_{externalflux} = \frac{F}{\varphi h} t \qquad (6.9)$$

(Zhou and Ballentine, 2006)

φ = aquifer porosity
η = transfer rate from stratum to groundwater (usually 1)
ρ = stratum density (g cm^{-3})
t = residence time (year)
h = aquifer thickness (cm)
F = average crustal flux (cm^3 STP [^{4}He] cm^{-2} year^{-1})
S = source function given by: 0.2355×10^{-12}[U]{1+0.123([Th]/[U]-4)}
[U] and [Th] in ppm

The residence time (^{4}He age) in years is therefore given by the equation:

$$t = \frac{\left[{}^4He\right] - \left[{}^4He\right]_{ASW}}{\left(\frac{F}{\varphi h} + \frac{\rho \eta S (1-\varphi)}{\varphi}\right)} \qquad (6.10)$$

The values used to estimate residence time using Equation 6.10 were very under constrained. However, an external average crustal flux value $F = 4x10^9$ atoms ^{4}He m^{-2} s^{-1} (Torgersen, 2010) and U and Th concentrations of 3 and 8 ppm respectively were used to calculate *t*. The estimated ^{4}He age of the palaeo groundwater end member using this method is in the range of $2x10^7$ years.

6.3.2. Groundwater end member characterisation

The Na-Cl-(HCO_3) dominated groundwater has been characterised by numerous hydrochemical, isotopic and noble gas tracers and labelled as a pre-Holocene palaeo groundwater. This groundwater body can be considered to be an end member groundwater with a true geochemical composition similar to that of the groundwater sampled from the deepest piezometer within the Brühl 9 observation borehole. Ionic constituents are dominated by Na and Cl, and the hydrochemical composition creates a reducing environment. The relatively low $\delta^{18}O$ value of -9.1‰ suggests that recharge occurred under cooler climatic conditions than those that predominate today because of the -1.3 – -2.0‰ shift, but stable isotope data also suggests a meteoric origin. Significantly, ^{4}He concentrations are over three orders of magnitude higher than those expected due to atmospheric solubility equilibrium.

Modern groundwater of meteoric origin is considered to be a second end member groundwater. In terms of stable isotope and noble gas data the modern groundwater displays little variation (Figure 6.7 and Figure 6.8) but hydrochemical compositions display a wide range of values due to variations in mineralogy and aquifer composition (see Figure 6.2). The $\delta^{18}O$ values of modern groundwater generally fall in the region of -7.1 to -7.8‰ and are in good agreement with the isotopic composition of precipitation for the region (IAEA, 2006). Noble gas concentrations are close to solubility equilibrium with small additions of excess air but no identified crustal or mantle sources.

Noble gases, oxygen isotopes ($\delta^{18}O$) and chloride ions are all considered as conservative tracers so it is therefore appropriate to formulate a simple binary mixing model to describe the conservative mixing of the two end member groundwaters (Figure 6.8 and Figure 6.9).

6.3.3. Groundwater mixing

Mixing between two distinct groundwater end members can be quantified using simple linear algebra:

$$\delta_{sample} = \chi \cdot \delta_{modern} + (1 - \chi) \cdot \delta_{palaeo} \qquad (6.11)$$

This simple binary mixing relationship can be applied to noble gases, oxygen isotopes ($\delta^{18}O$) and chloride ions because they are all considered as conservative geochemical or hydrochemical tracers. Such a simple mixing model appears to fit the helium and $\delta^{18}O$ data rather well (Figure 6.8 and Figure 6.9). The small number of data points that fall outside of the mixing model envelope can be explained by perhaps a different end member composition in terms of slightly lower $\delta^{18}O$ values for modern groundwater

of meteoric origin that simply have not been sampled yet, or for samples that fall to the right hand side of the model, mixing with a third groundwater type. Ternary mixing is clearly a feature of the Brühl region where the two regional end member groundwaters are also mixing with localised evaporated water that is believed to have percolated into the shallow aquifer from a disused sand/gravel pit. This local signature is characterised by a hydrochemical composition dominated by $Ca\text{-}SO_4\text{-}NO_3$ and a high $\delta^{18}O$ value of -5.2‰. The two sample points that exhibit enriched $\delta^{18}O$ values and plot on an evaporation trend line (see Figure 6.7) originate from a single observation borehole in the Brühl area and are believed to have a very limited spatial occurrence.

It remains uncertain whether the helium and $\delta^{18}O$ values of the palaeo groundwater end member represent the true end member composition or if the groundwater sampled from observation borehole 958063 has already been exposed to mixing with modern groundwater in the shallow aquifer prior to the point of sampling. However, it is certain that the palaeo groundwater originates from a well constrained location associated with the Bornheim fault and mixes with modern recharge in the upper layers of the shallow aquifer system. This suggests that the fault acts as a preferential flow path for deep circulating palaeo groundwater with a very long residence time to bypass the intermediate depths of the aquifer system and therefore directly connecting the deep basement system with the shallow aquifer layers that contain the most modern recharge.

6.3.4. Noble gas palaeothermometer

Dissolved noble gases in groundwater have been used in numerous studies to provide palaeoclimate information (eg. Mazor, 1972; Andrews and Lee, 1979; Rudolph *et al.*, 1984; Stute and Deák, 1989; Andrews, 1992; Stute *et al.*, 1992;

Blavoux *et al*., 1993; Osenbrück *et al*., 1993; Stute *et al*., 1995a; Stute *et al*., 1995b; Dennis *et al*., 1997; Beyerle *et al*., 1998; Aeschbach Hertig *et al*., 2002; Beyerle *et al*., 2002; Zuber *et al*., 2004) as discussed in Chapter 3.

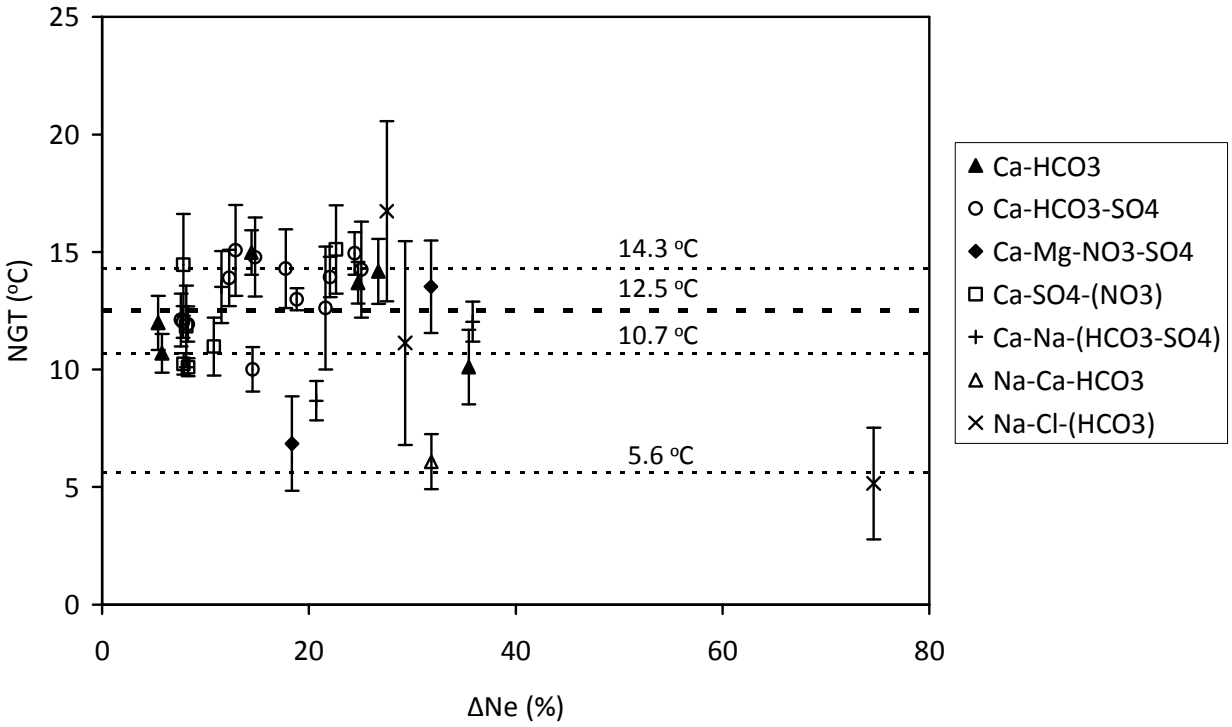

Figure 6.10. Noble gas temperatures (NGTs) modelled using NOBLE90 plotted against excess air given as ΔNe (%).

The measured concentrations of the noble gases Ne, Ar, Kr and Xe were interpreted using NOBLE90 (Aeschbach-Hertig *et al*., 2000; Peeters *et al*., 2002) in terms of temperature (*T*) and excess air (*A*). As discussed in Chapter 3, there are five model parameters (temperature (*T*), salinity (*S*), pressure (*P*) excess air (*A*) and fractionation (*F*)) but it was assumed that S ~ 0 for recharge of meteoric origin and *P* was determined from the mean altitude of the study area within the Lower Rhine Embayment. If fractionation (*F*) is set to zero the closed system equilibration (CE)

model reduces to the unfractionated excess air (UA) model and produces the same results for temperature (*T*) and excess air (*A*). The noble gas concentrations for all the groundwater samples that were successfully analysed for dissolved noble gases were interpreted using the three model equations used in NOBLE90. However, the assessment of χ^2 and probability (%) values indicated that the unfractionated excess air (UA) model produced the best fit for all the samples and no samples were rejected due to a poor model fit. Figure 6.10 shows the calculated NGTs plotted against excess air using the UA model. The uncertainty of T was scaled to account for the goodness-of-fit by NOBLE90 and the UA model consistently yielded the smallest degree of uncertainly for calculated NGTs.

Figure 6.10 shows that there are potentially three trends in recharge temperature but it was assumed from hydrochemical and stable isotope data that the main cluster of samples all represent modern groundwater recharge (with the exception of the Na-Cl-(HCO_3) groundwater) and that the mean temperature of 12.5 ±1.3 ºC calculated using these points would therefore represent the average recharge temperature of modern groundwater accurately. However, the weighted mean annual surface temperature is 10.8 ºC which is 1.7 ºC lower than the calculated NGT. Although the uncertainty limits of the calculated NGT (1.3 ºC) could explain most of this offset, it is possible that the UA model does not adequately describe all the mechanisms that control noble gas concentrations at the water table.

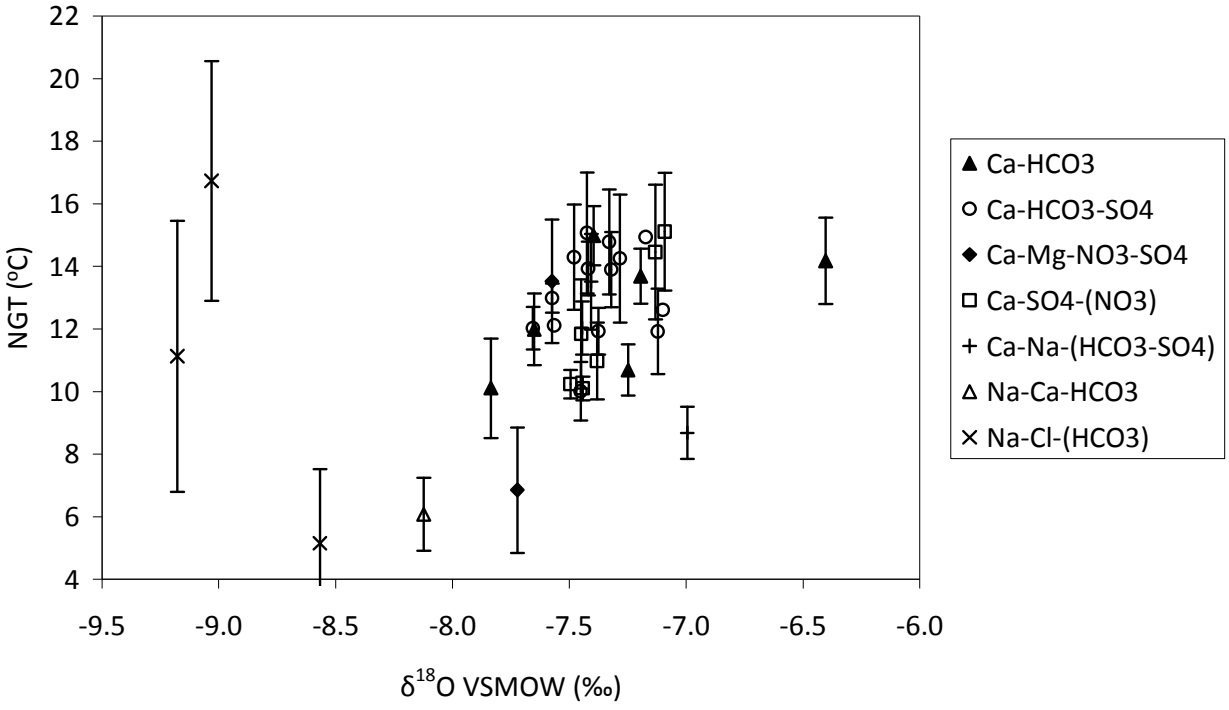

Figure 6.11. Cross plot of Noble Gas Temperature (NGT) against $\delta^{18}O$.

Noble gas temperatures have been used as a climate proxy for determining the surface temperature during the last glacial maximum (LGM) (eg. Stute *et al.*, 1995). A number of palaeo groundwaters that have been identified by groundwater age-dating techniques such as ^{14}C, display a temperature decrease of 5–7 ºC (eg. Andrews and Lee, 1979; Blavoux *et al.*, 1993; Stute *et al.*, 1995) whilst some studies report a smaller temperature decrease in the range of 2–3 ºC for LGM groundwaters (eg. Osenbrück *et al.*, 1993).

The data presented in Figure 6.10 is not inconsistent with these findings although the evidence is limited. The palaeo groundwater identified in the Brühl region displays relatively low $\delta^{18}O$ values and a shift of -1.3 – -2.0‰ from modern recharge. The mean NGT calculated for the Na-Cl-(HCO_3) and Na-Ca-HCO_3 is 5.6 ±1.7 ºC which is 6.9 ºC cooler than the mean NGT determined for modern groundwater (12.5 ±1.3 ºC) within the Lower Rhine Embayment aquifer system. The

remaining Na-Cl-(HCO_3) type groundwater sample points do not agree with this trend but this could be because of the difficulties experienced during sampling due to the high dissolved gas content of the groundwater in the Brühl 9 observation borehole and could also explain the large error bars that are associated with several of the Na-Cl-(HCO_3) dominated groundwater samples.

It is not possible to state precisely with any degree of certainty the exact climatic conditions under which the Na-Cl-(HCO_3) type groundwater was recharged, or even the origin of the Na-Cl-(HCO_3) type groundwater. Carbon-14 age-dating of groundwater samples collected from the Brühl 9 observation borehole during 2007 was conducted by the USGS but the results suggested that the samples were ^{14}C free. This was interpreted as groundwater with a residence time that exceeded 30,000 years. However, Maloszewski and Zuber (1991) initially came to the same conclusion when using ^{14}C to date groundwater samples from a carbonate aquifer in Poland as the samples were found to be ^{14}C free. It was later determined using tritium that the groundwaters were in fact of Holocene age and the loss of ^{14}C was explained by matrix diffusion and matrix exchange factors (Maloszewski and Zuber, 1991). Obtaining a reliable groundwater age estimate for the palaeo groundwaters from the Brühl region would certainly form an important component of any further work and could possibly be achieved by applying either ^{36}Cl or ^{81}Kr dating techniques.

6.3.5. Noble gas determined excess air

The relationship between ΔNe and seasonal water table fluctuations has been considered by a number of authors (eg. Stute and Schlosser, 1993; Wilson and McNeill, 1997; Ingram *et al*., 2007). Ingram *et al*. (2007) state that a good correlation between excess air (ΔNe) and mean annual water table fluctuation (Δh_{av}) suggests that air entrainment is directly linked to water table fluctuations and not aquifer lithology

as suggested by Wilson and McNeill (1997). However, the laboratory column experiments designed by Holocher *et al*. (2002) specifically to investigate the link between excess air and water table fluctuations did not provide conclusive evidence. Ingram *et al*. (2007) used the closed system equilibration model (CE Model) described by Aeschbach-Hertig *et al*. (1999) to determine excess air values. However, the 'best fit' of the data occurred when the fractionation factor *F*, was set to zero in which case the CE Model reduces to the basic unfractionated excess air (UA) Model described by Andrews and Lee, (1979) and Stute and Schlosser (1993). The CE Model has the ability to describe the theoretical relationship between excess air and water table fluctuations. The derivation of this relationship is described by Aeschbach-Hertig *et al*. (2002) and is also reported by Ingram *et al*. (2007).

Noble gas determined excess air values for groundwater samples collected from the Lower Rhine Embayment were plotted against mean annual water table fluctuation data for all observation boreholes that displayed a regular annual water table fluctuation. The Δh_{av} values were calculated using water table elevation data records dating back to the 1970s and provided by the Erftverband. Up to six readings were taken each year so it was possible to determine the maximum annual amplitude which was then used to calculate a mean value for the time period of the records if the magnitude of the amplitude remained fairly consistent over time. Figure 6.12A shows that there is a good correlation between ΔNe and Δh_{av} and that the results are consistent with both the data published by Ingram *et al*. (2007) and with the theoretical relationship predicted by the CE model described by Aeschbach-Hertig *et al*. (2002). It is evident that the samples from the Lower Rhine Embayment have relatively low ΔNe values and a corresponding low mean annual water table fluctuation (see Figure 6.12B).

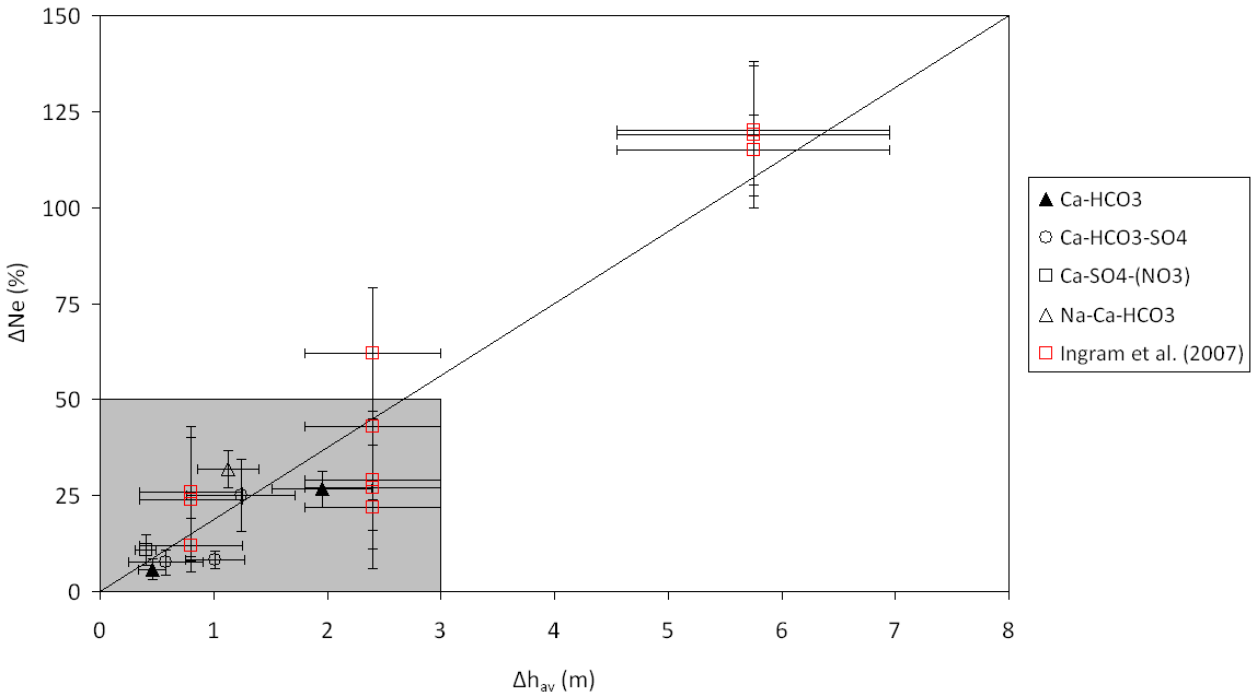

Figure 6.12A. Excess air expressed as ΔNe (%) plotted against mean annual water table fluctuation. The data can be seen to be consistent with the results presented by Ingram *et al*. (2007) for values at the lower range of the scale. Figure 6.12B shows an expanded view of the grey area.

An important point to note is that the vast majority of the aquifers in the Lower Rhine Embayment do not display a consistent seasonal water table fluctuation, primarily due to groundwater abstraction for lignite mine dewatering purposes. All of the sampled boreholes that are in close proximity to active or abandoned lignite mines are, or have in the recent past, been significantly affected by mine dewatering (as discussed in Chapter 2). Time series data provided by the Erftverband was used to assess the behaviour of the water table from the 1970s to the present day. These data were available for each of the sampled boreholes as this was one of the criteria used during the initial borehole selection process. The records show that most aquifers in the Lower Rhine Embayment are affected by lignite mining to some extent. Typically,

the water table in many areas displays a trend of either constant drawdown, or drawdown followed by subsequent rebound in areas where mining has now ceased or moved further away. However, recovery of the water table subsequent to significant drawdown appears to be a slow process. An analysis of excess air concentration was not conducted on samples that were collected from boreholes that had corresponding water table records that displayed trends other than regular annual water table fluctuations because without applying accurate groundwater age-dating techniques such as ^{3}H-^{3}He or ^{85}Kr it would be impossible to state with any degree of certainty, at which point along a time series of hydraulic head values groundwater recharge had occurred and therefore making it difficult to correlate a particular trend in water table behaviour with excess air concentration.

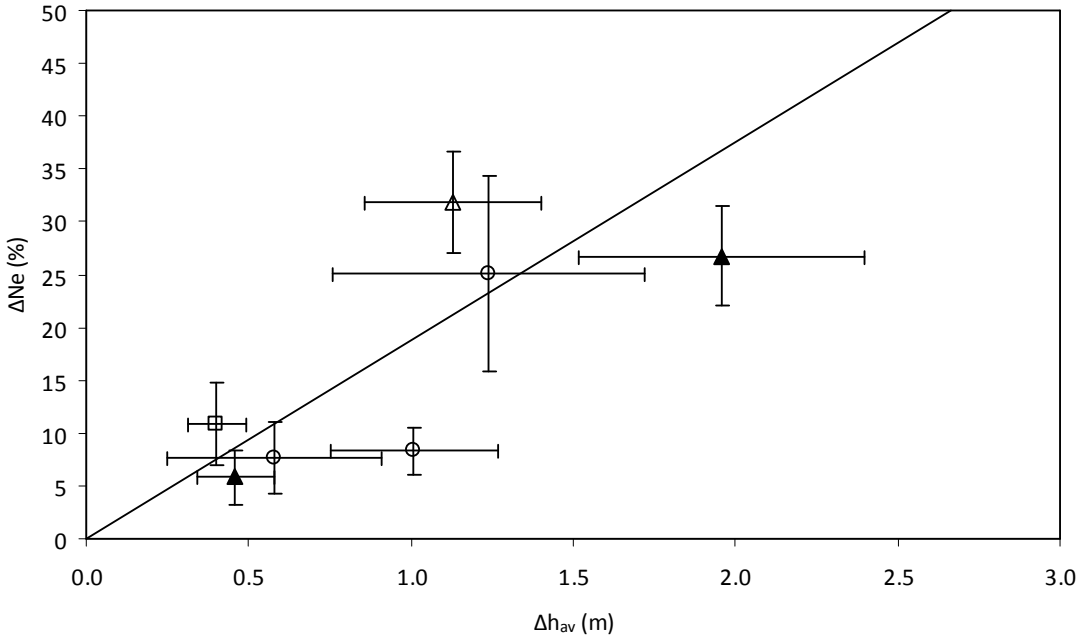

Figure 6.12B. An expanded view of the grey shaded region of Figure 6.12A and without the data from Ingram *et al*. (2007).

6.3.6. The conceptual hydrochemical model

The analysis of dissolved noble gases, stable isotopes of hydrogen, oxygen, carbon and strontium, and hydrochemical composition has provided strong evidence to suggest that groundwater flow dynamics in the Brühl region of the Lower Rhine Embayment, and particularly in close proximity to the Bornheim fault, are of great interest in terms of European palaeo groundwaters and fluid flow processes associated with fault zones in sedimentary basins. The multiple tracer approach has allowed a conceptual model to be developed that elucidates the mechanisms involved, and helps explain the observed occurrence of palaeo groundwater at very shallow depth in the Brühl region. The conceptual model describes a deep circulating groundwater that has a residence time sufficient for the accumulation of significant concentrations of helium (more than three orders of magnitude higher than atmospheric solubility equilibrium) from *in situ* production derived from the decay of U and Th series elements in the subsurface. It is also very likely that an external flux of helium also contributes significantly to the total helium concentration of the palaeo groundwater. Hydrochemical analysis of the palaeo groundwater indicates that Na^+ and Cl^- are the dominate ions and that the hydrochemical evolutionary history of the groundwater involved very high P_{CO2} conditions and a significant subsurface source of H^+.

The occurrence of palaeo groundwater in shallow aquifers is strongly linked to the Bornheim fault. Geochemical and temporal hydraulic head data suggest that the groundwater originates from depth and flows almost upwards within the Bornheim fault core material and/or the adjacent footwall material and is driven by de-watering of nearby open cast lignite mines. Due to the complex nature of the layered sand and gravel aquifer system and the intercalated clay and lignite layers of low permeability it is possible that the precise flow path is more complex than simple conduit flow.

However, the conduit-like flow associated with the Bornheim fault is probably directly linked to nearby lignite mining activities and specifically to large scale mine de-watering that has a large impact on hydraulic head distribution throughout most of the region. The lignite mines that are within a few kilometres of the Bornheim fault have been abandoned and subsequently restored to recreational and agricultural land.

The palaeo groundwater emanates from the Bornheim fault like a ‘point source’ injection and forms a plume of groundwater that is easily distinguishable from the modern meteoric recharge that is typically found in the shallow aquifers of this region due to its hydrochemical composition (see Figure 6.13).

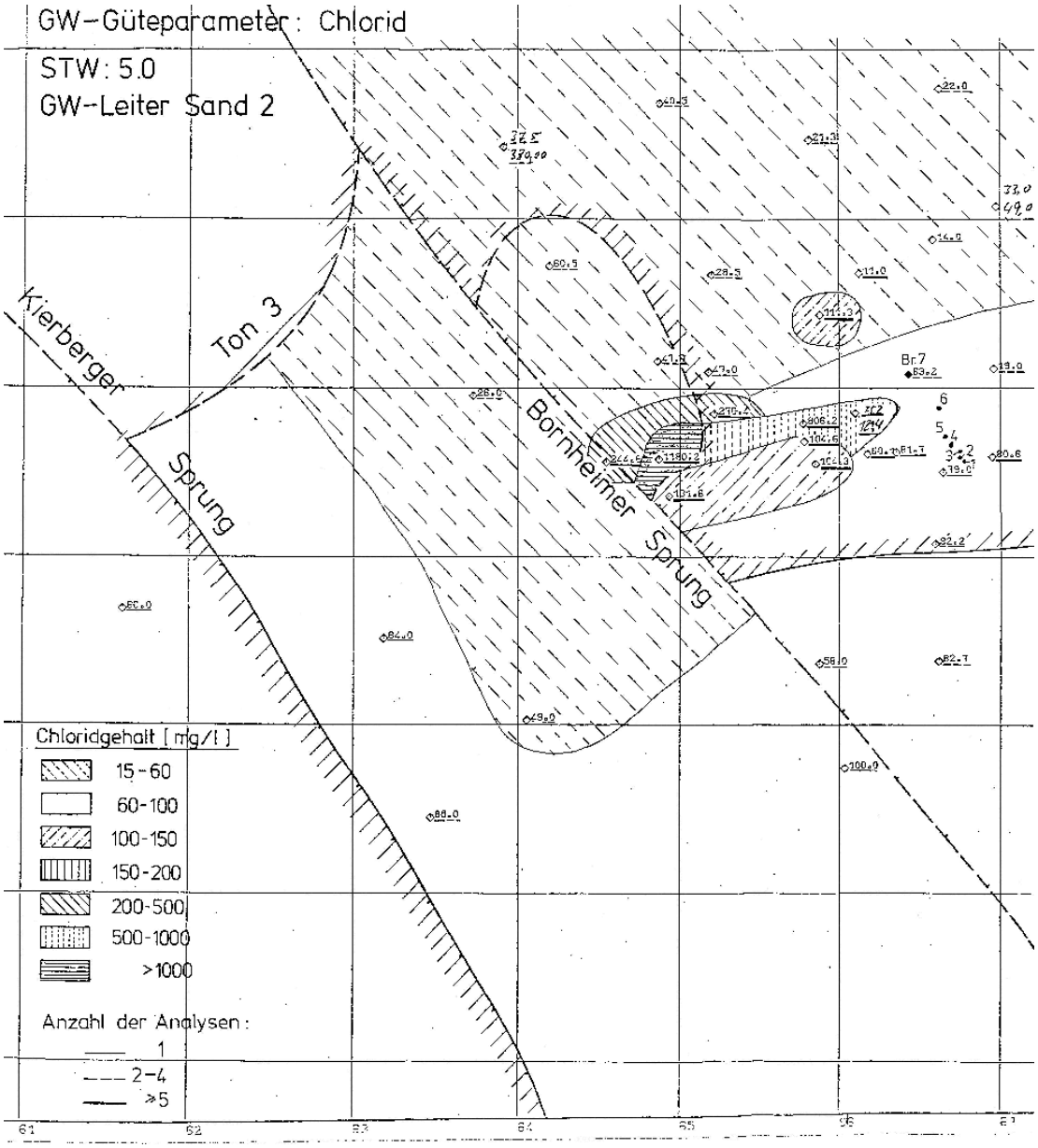

Figure 6.13. Spatial distribution of the palaeo groundwater plume that emanates from the Bornheim fault based on Cl^- concentration measurements taken from 1979 to 1981 (reproduced from Schenk, 1982).

It is hypothesised that the emplacement of the palaeo groundwater at shallow depth occurred during the active de-watering of the nearby lignite mines and that conduit flow from depth is not occurring at the present time. The plume-like emanation also appears to be slow to disperse perhaps due to the shallow hydraulic head gradients that currently exist in this region. Schenk (1982) first identified the plume of palaeo groundwater near the Bornheim fault in the early 1980s and accurately mapped its distribution based on Cl^- measurements (Figure 6.13). Schenk (1982) recognised that the groundwater was linked to the Bornheim fault but without the application of geochemical and isotopic tracers was unable to establish the flow path or origin of the groundwater.

The locations of the four observation boreholes situated in the Brühl region are mapped in Figure 6.14. It can be seen that observation boreholes 352722 and 957982 are within just a few metres of the Bornheim fault. Figure 6.14 also shows that the Brühl 9 observation borehole (958063) is located to the west of the Bornheim fault and that groundwater flow is from west to east as indicated by the hydraulic head gradient. The 3-dimensional diagram in Figure 6.14 illustrates the relative positions of the observation boreholes and their depths in relation to the Bornheim fault and the sediment deposits of varying geological age. The Brühl 9 observation borehole yields the highest concentration of dissolved helium, Cl^- and the most depleted $\delta^{18}O$ values.

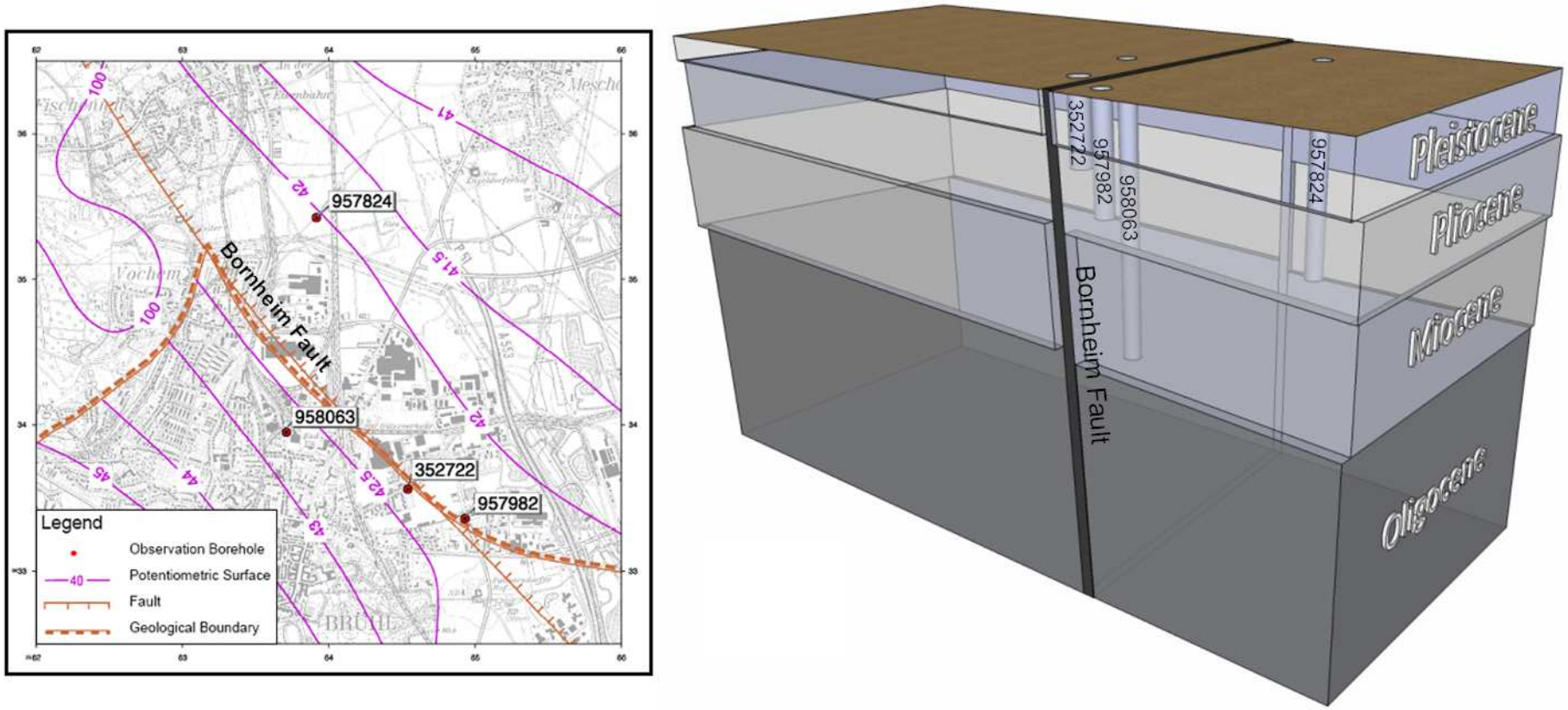

Figure 6.14. Plan view of the Brühl region and 3-dimensional cross section show the locations and relative depths of the observation boreholes as well as the proximity to the Bornheim fault.

As discussed in Section 6.3.2 the groundwater at the Brühl 9 location is thought to accurately represent the end member composition. It is unclear why the end member composition is found slightly up-gradient from the Bornheim fault if the fault plane represents the point source origin of the palaeo groundwater. The most likely explanation is that during periods of intense lignite mine de-watering that acted as the driving force of fluid flow along the fault the direction of groundwater flow would have been reversed as a cone of depression developed below the lignite mine. As mining began to decline in the area and finally ceased entirely, the natural direction of groundwater flow slowly restored itself and the plume of palaeo groundwater could be identified to the east of the Bornheim fault.

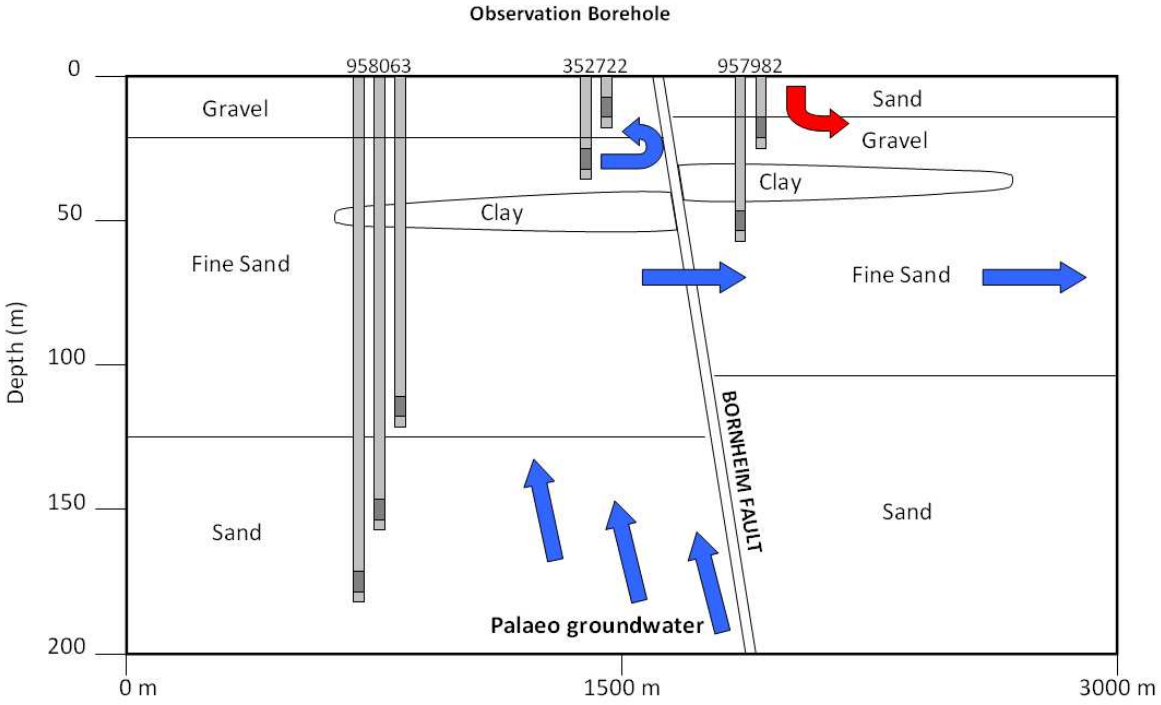

Figure 6.15. Cross section of the Bornheim fault indicating the upward flow of palaeo groundwater from depth (blue arrows), the general 'west to east' flow direction in the shallow aquifers and the percolation of evaporated water from a surface gravel/sand pit (red arrow).

An alternative and perhaps more simple hypothesis is that the palaeo groundwater flows through the fault core and within the adjacent footwall material creating a more complex flow path and the plume emanates from the shallow aquifers to the west of the Bornheim fault in a more diffuse way. The stable isotopes of hydrogen and oxygen and dissolved helium data indicate that the Bornheim fault is acting as a barrier to horizontal groundwater flow at shallow depth near observation borehole 352722 (see Figure 6.15) which could explain the slow rate of advective dispersion and dilution.

7. Conclusions and Further Work

7.1. Conclusions

Hydrochemical, stable isotope and noble gas tracer techniques have provided valuable insight into basin scale groundwater flow dynamics in the Lower Rhine Embayment aquifer system. The large variation in hydrochemical composition of groundwater samples collected during 2007/08 is a result of the mixed mineralogical assemblages that exist in the shallow Pleistocene and Pliocene deposits. Stable isotopes of hydrogen and oxygen were used to identify palaeo groundwater in the shallow aquifers of the Brühl region. The hydrochemical composition of the palaeo groundwater indicates that it is dominated by Na^+ and Cl^- ions and suggests that hydrochemical evolution occurred under higher P_{CO2} conditions than more recent groundwater recharge and is easily distinguishable from the modern groundwater component that is dominant throughout the Lower Rhine Embayment.

Groundwater samples were analysed for dissolved noble gas concentrations and numerical modelling using the NOBLE90 geochemical model was employed to interpret dissolved gas concentrations in terms of excess air, water table fluctuations and noble gas temperatures (NGTs). Noble gas determined excess air concentrations correlated well with groundwater level fluctuations and the results were consistent with the values predicted by the closed system equilibration (CE) model proposed by Aeschbach-Hertig *et al.* (2002) and agreed well with the data reported by Ingram *et al.* (2007). The mean NGT of modern groundwater recharge was 12.5 ±1.3 ºC which is consistent with the regional weighted mean annual surface temperature of 10.8 ºC. Determining accurate noble gas temperatures for palaeo groundwater samples was problematic due to the high dissolved gas concentrations of the groundwater and gas

exsolution during the sampling procedure. However, the results obtained do provide some evidence to suggest that the mean recharge temperature of the palaeo groundwater is 5.6 ºC which is not inconsistent with the 5–7 ºC decrease in recharge temperatures from the Pleistocene to the Holocene that has been reported by other authors (eg. Andrews and Lee, 1979; Blavoux *et al*., 1993; Stute *et al*., 1995), although with only a small number of palaeo groundwater samples being successfully analysed there is a degree of uncertainty surrounding this conclusion.

Dissolved helium concentrations in groundwater samples collected from the Brühl region have provided additional evidence to confirm the presence of palaeo groundwater in shallow aquifers. Helium concentrations were observed at a maximum of $1.7x10^{-4}$ cm^3 STP g^{-1} H_2O which is 3-4 orders of magnitude higher than the concentration expected due to solubility equilibrium with the atmosphere and suggests a very long residence time. The source of helium is uncertain but *in situ* radiogenic production and a terrigenic flux probably account for a large proportion of the observed helium. The precise origin of the palaeo groundwater is unknown but due to the close proximity of the Bornheim fault, it is hypothesised that the fault creates a preferential flow path. Groundwater exchange between the deep basinal aquifers and the upper aquifer layers is frequently impeded by confining clay layers and very low permeability lignite. This suggests that palaeo groundwater from depth is mixing with modern water of meteoric origin in the upper aquifers as a result of advective flow from depth towards the upper aquifer layer within the Bornheim fault, or that flow is occurring in the adjacent footwall of the fault and follows a more complex flow path towards the surface. There is no evidence of thermal anomalies from observation boreholes in close proximity to the Bornheim fault implying that the flow rates along the fault are either too low to generate a temperature anomaly, or that conduit flow

within the fault zone is not occurring at present. It is therefore hypothesised that the plume of deep basinal palaeo groundwater, characterised by its high helium content and relatively low $\delta^{18}O$ value, was emplaced during a period of enhanced flow caused by large scale groundwater abstraction from a nearby lignite mine. The mine has now been abandoned and natural flow conditions have been restored reversing the direction of groundwater flow. Hydraulic head gradients are low in this area so advective dispersion and dilution appear to occur at a slow rate. Today, exploitation of lignite occurs at the Inden, Garzweiler and Hambach mines. Upward fluid flow associated with fault zones could be widespread in areas adjacent to the large open cast lignite mines due to the large hydraulic head gradients that have been created across some faults and the enhanced transient flow rates that are the result of large scale mine de-watering. Unfortunately, the observation boreholes in these regions are particularly deep and so sampling for dissolved gases is problematic. However, this research has provided strong geochemical evidence to support the conduit-barrier fault zone model proposed by Bense and Person (2006).

More broadly, this research has contributed to the understanding and ability to predict fluid flow patterns in unconsolidated sedimentary basins and has relevance for some of the largest groundwater aquifer systems and hydrocarbon reservoirs in the world, such as those in the Gulf of Mexico and the North Sea Basin that are largely analogous to the Lower Rhine Embayment. Understanding the flow dynamics of deep basinal groundwater and the complex hydraulic behaviour of fault zones in unconsolidated sedimentary basins is critical for successfully and safely implementing schemes such as carbon capture and storage (CCS) and nuclear waste disposal as well as for more general water resources management purposes.

7.2. Further work

It is clear that the Lower Rhine Embayment is a complex hydrogeological system, and that the application of additional environmental tracers and groundwater age-dating techniques would significantly improve our understanding of the origin, residence time and flow paths of the palaeo groundwater identified in the shallow aquifers of the Brühl region. Further work would primarily seek to elucidate the origin of deep circulating groundwater found in shallow aquifers. There are a number of new research questions that need to be addressed to enhance our understanding of groundwater dynamics in the Lower Rhine Embayment and provide further insight into the role of fault zones such as: What is the origin and age of the deep basinal fluids found within shallow aquifers of the LRE? Is there an exchange between deep basinal fluids and modern groundwater at shallow depth along fault zones that behave as conduit-barrier systems and what is the spatial and temporal variability of this process? Are these basinal fluids emplaced in shallow aquifers during periods of intense mining activity and subsequent lowering of the water table or is it a natural phenomenon that is enhanced by groundwater abstraction? In regions where current groundwater abstraction is significant, is the flux of groundwater along faults large enough to result in transient thermal anomalies within aquifers flanking those faults? Do geochemical and thermal anomalies occur simultaneously? Does the absence of thermal anomalies but the presence of geochemical anomalies indicate historical fluid migration along fault zones or low flow velocities? What are the implications of deep basinal fluid flow along faults for nuclear waste storage, CCS programmes and water resource management? A full range of helium, neon and argon isotope ratios could be used to identify and quantify the various sources of ^{3}He and ^{4}He and their contribution to the total helium content of groundwater samples. Chlorine-36 would be the most

appropriate groundwater age-dating tool for determining the age of LRE palaeo groundwater and the application of ^{36}Cl has been successful in age-dating very old groundwater in numerous deep circulating systems (eg. Love *et al*., 2000; Lehmann *et al*., 2003; Sturchio *et al*., 2004). Although the interpretation of ^{36}Cl ages is not routine due to a number of parameters that are difficult to constrain, such as atmospheric residence time (Balderer *et al.*, 2004) and additional sources of ^{36}Cl in groundwater; for example, anthropogenic inputs from nuclear weapons testing in the South Pacific Ocean between 1952 and 1959, and radiogenic production of ^{36}Cl deep in the subsurface; it could be argued that in the Lower Rhine Embayment the difficulties with ^{36}Cl age-dating are minimised because of the absence of groundwater with very high salinity such as deep basement brines or other sources of Cl such as evaporite deposits that are found further north in the North Sea Basin. Krypton-81 has the potential to provide an alternative to ^{36}Cl age-dating, but currently no laboratories worldwide are offering ^{81}Kr measurements for dating very old groundwater, and it would also be significantly more expensive than ^{36}Cl dating.

It has been established that geochemical anomalies indicate the presence of deep circulating groundwater in shallow aquifers, but it is uncertain whether these basinal fluids are emplaced in shallow aquifers during periods of intense mining activity and subsequent lowering of the water table or whether it is a natural phenomenon that is enhanced by groundwater abstraction. Tritium/helium-3 (^{3}H-^{3}He) groundwater age-dating could be used to determine whether the plume of palaeo groundwater is a relic of historical mining practices or whether fluid movement along the plane of the Bornheim fault is still an active process today. By dating the modern component of groundwater it would be possible to build a comprehensive conceptual model of flow dynamics in a given area which in turn could lead to the development

of more generic models with relevance to similar sedimentary basins worldwide. ^{3}H-^{3}He dating would form a key part of any further research and would allow the determination of recharge rates, flow velocities and residence times for the modern groundwater component that is believed to dominate in many shallow aquifer systems.

In regions where current groundwater abstraction is significant, it would be insightful to determine whether the flux of groundwater along faults is large enough to result in transient thermal anomalies within aquifers flanking such faults. This could also indicate whether thermal anomalies and geochemical anomalies occur simultaneously and whether the absence of thermal anomalies but the presence of geochemical anomalies indicates historical fluid migration along fault zones or if it is the result of low flow velocities.

The Lower Rhine Embayment is a well instrumented study area (~15,000 observation boreholes in an area of 4,220 km^2) that provides a unique opportunity to constrain fluid flow mechanisms and processes associated with fault zones in unconsolidated sedimentary basins, and therefore provides an unrivalled opportunity to improve our understanding of fault hydraulics and so further the development of generic models for fault zone hydrogeology in similar settings worldwide. A comprehensive understanding of deep basinal fluid flow along fault zones in sedimentary basins is an essential prerequisite for safe nuclear waste storage, CCS programmes and more general water resources management.

Appendices

Appendix 1.

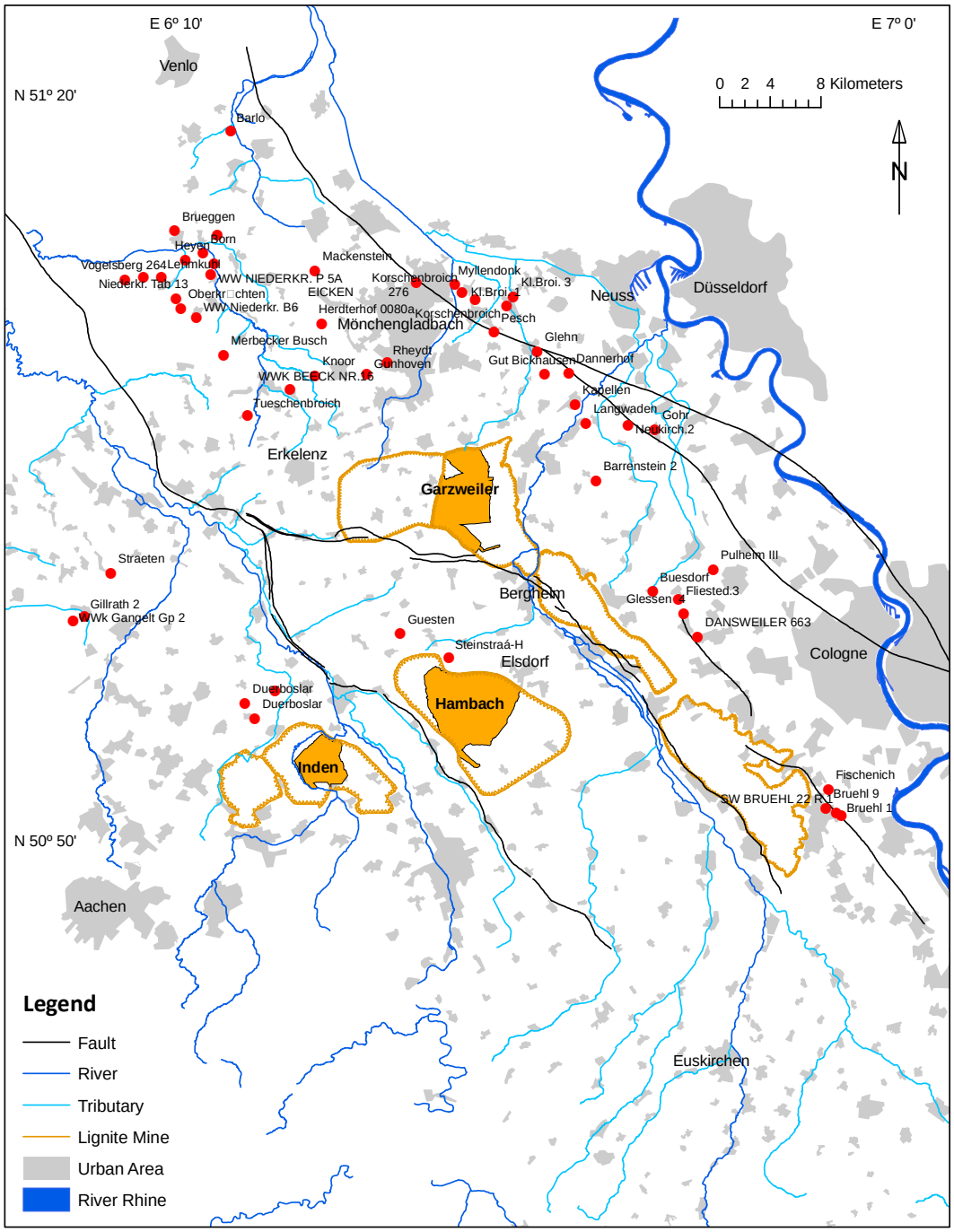

Figure 1. Sampled observation borehole identification names.

Appendix 2.

Table 1. SXP Elite operational settings for helium isotopes.

Helium		
Source	Emission	ON
	Filament	1(Th)
	Emission Current	0.50 mA
	Electron Current	70 eV
	Source Volts	4.0 V
	Focus	-110 V
	Lens 4	-110 V
Filter	Pole Bias	0.0 V
	High Mass Resolution	32%
	Low Mass Resolution	50%
	Ion Energy Ramp	0.0 eV
	Total Ion	OFF
	Zero Ion	OFF
Detector	Faraday/SEM	SEM
	SEM Bias	2000 V
	Gain Range 1	9 – 10
	Range 2 Extra Gain	X 1E0
	Amplifier Response	30 ms
	Amplifier Zero	0.0
	Pulse Counting	OFF
Ions	Polarity	+
	Internal/External	INT
	Lens 1	0 V
	Lens 2	0 V
	External Mass	OFF
Spectrum	First Mass	2.0 amu
	Mass Span	3 amu
	Scan Rate	1.000 amu/s
	Single/Rep Composition	R
	Scale	1
	Scan Two Regions	N
	First Mass Region 2	20.0 amu

Table 2. SXP Elite operational settings for neon isotopes.

Neon		
Source	Emission	ON
	Filament	1(Th)
	Emission Current	0.50 mA
	Electron Current	**40 eV**
	Source Volts	4.0 V
	Focus	-110 V
	Lens 4	-110 V
Filter	Pole Bias	0.0 V
	High Mass Resolution	32 %
	Low Mass Resolution	50 %
	Ion Energy Ramp	0.0 eV
	Total Ion	OFF
	Zero Ion	OFF
Detector	Faraday/SEM	SEM
	SEM Bias	2000 V
	Gain Range 1	9-10
	Range 2 Extra Gain	X 1E0
	Amplifier Response	30 ms
	Amplifier Zero	0.0
	Pulse Counting	OFF
Ions	Polarity	+
	Internal/External	INT
	Lens 1	0 V
	Lens 2	0 V
	External Mass	OFF
Spectrum	First Mass	18.0 amu
	Mass Span	5 amu
	Scan Rate	1.000 amu/s
	Single/Rep Composition	R
	Scale	1
	Scan Two Regions	N
	First Mass Region 2	20.0 amu

Table 3. SXP Elite operational settings for argon isotopes.

Argon		
Source	Emission	ON
	Filament	1(Th)
	Emission Current	0.50 mA
	Electron Current	70 eV
	Source Volts	4.0 V
	Focus	-110 V
	Lens 4	-110 V
Filter	Pole Bias	0.0 V
	High Mass Resolution	32 %
	Low Mass Resolution	50 %
	Ion Energy Ramp	0.0 eV
	Total Ion	OFF
	Zero Ion	OFF
Detector	Faraday/SEM	SEM
	SEM Bias	1650 V
	Gain Range 1	9 – 10
	Range 2 Extra Gain	X 1E0
	Amplifier Response	30 ms
	Amplifier Zero	0.0
	Pulse Counting	OFF
Ions	Polarity	+
	Internal/External	INT
	Lens 1	0 V
	Lens 2	0 V
	External Mass	OFF
Spectrum	First Mass	35.0 amu
	Mass Span	6 amu
	Scan Rate	1.000 amu/s
	Single/Rep Composition	R
	Scale	1
	Scan Two Regions	N
	First Mass Region 2	20.0 amu

Table 4. SXP Elite operational settings for krypton isotopes.

Krypton		
Source	Emission	ON
	Filament	1(Th)
	Emission Current	0.50 mA
	Electron Current	70 eV
	Source Volts	4.0 V
	Focus	-110 V
	Lens 4	-110 V
Filter	Pole Bias	0.0 V
	High Mass Resolution	32 %
	Low Mass Resolution	50 %
	Ion Energy Ramp	0.0 eV
	Total Ion	OFF
	Zero Ion	OFF
Detector	Faraday/SEM	SEM
	SEM Bias	2000 V
	Gain Range 1	10 – 11
	Range 2 Extra Gain	X 1E0
	Amplifier Response	100 ms
	Amplifier Zero	0.0
	Pulse Counting	OFF
Ions	Polarity	+
	Internal/External	INT
	Lens 1	0 V
	Lens 2	0 V
	External Mass	OFF
Spectrum	First Mass	76.0 amu
	Mass Span	12 amu
	Scan Rate	2.000 amu/s
	Single/Rep Composition	R
	Scale	1
	Scan Two Regions	N
	First Mass Region 2	20.0 amu

Table 5. SXP Elite operational settings for xenon isotopes.

Xenon		
Source	Emission	ON
	Filament	1(Th)
	Emission Current	0.50 mA
	Electron Current	70 eV
	Source Volts	4.0 V
	Focus	-110 V
	Lens 4	-110 V
Filter	Pole Bias	0.0 V
	High Mass Resolution	32 %
	Low Mass Resolution	50 %
	Ion Energy Ramp	0.0 eV
	Total Ion	OFF
	Zero Ion	OFF
Detector	Faraday/SEM	SEM
	SEM Bias	2000 V
	Gain Range 1	10-11
	Range 2 Extra Gain	X 1E0
	Amplifier Response	100 ms
	Amplifier Zero	0.0
	Pulse Counting	OFF
Ions	Polarity	+
	Internal/External	INT
	Lens 1	0 V
	Lens 2	0 V
	External Mass	OFF
Spectrum	First Mass	128.0 amu
	Mass Span	9 amu
	Scan Rate	2.000 amu/s
	Single/Rep Composition	R
	Scale	1
	Scan Two Regions	N
	First Mass Region 2	20.0 amu

Appendix 3.

Table 1. Major and minor ion concentrations (analyses were conducted at the Erftverband laboratories in Bergheim, Germany)

ID Number	Location	Ca^{2+}	Mg^{2+}	Na^{+}	K^{+}	NH_4^{+}	Fe^{2+}	Mn^{2+}	HCO_3^{-}	SO_4^{2-}	Cl^{-}	NO_3^{-}
		($mg\ L^{-1}$)										
21/927961	Steinstrass-H	182.0	25.5	28.1	2.50	<0.05	4	0.126	104	474.0	55.3	6.5
21/927971	Guesten	183.0	26.6	27.5	2.24	<0.05	3.19	0.133	323	252.0	81.4	<0.2
21/960511	Gillrath 2	74.6	12.5	28.6	11.90	1.04	4.06	0.238	110	92.7	75.6	54
21/867341	Duerboslar	196.0	27.4	13.4	9.29	<0.05	0.01	<0.005	384	147.0	95.4	58
21/040331	WWk Gangelt Gp2	59.7	9.3	18.9	2.88	<0.05	0.03	<0.005	49	74.1	42.2	76.6
21/863901	Duerboslar	179.0	23.9	21.9	1.26	<0.05	0.04	0.006	372	128.0	75.3	73.9
21/861581	Merzenhausen	196.0	26.3	18.0	3.03	<0.05	0.08	<0.005	354	150.0	107	57.1
28/900441	Muehlrather Mue	21.5	2.9	6.8	1.39	<0.05	3.26	0.06	67	16.6	9.33	<0.2
21/960251	Straeten	63.2	12.2	33.8	3.78	<0.05	0.02	0.015	6	108.0	65.4	112.9
28/817751	Knoor	91.3	20.5	9.2	2.95	<0.05	0.02	<0.005	293	56.2	26.1	0.9
08/658086	WW Niederkr. P 5A	83.0	14.4	24.9	16.90	<0.05	0.09	0.065	146	99.8	64.3	44.7
28/900401	Haverslohe 208	82.7	12.8	25.4	4.85	<0.05	0.18	0.049	116	125.0	54.4	33.2
28/908381	Barlo	103.0	16.1	25.8	1.62	<0.05	<0.01	<0.005	92	135.0	52.7	125.7

Table 1. Cont'd (2 of 6)

ID Number	Location	Ca^{2+}	Mg^{2+}	Na^{+}	K^{+}	NH_4^{+}	Fe^{2+}	Mn^{2+}	HCO_3^{-}	SO_4^{2-}	Cl^{-}	NO_3^{-}
		($mg\ L^{-1}$)										
28/908301	Brüggen	65.2	17.8	27.9	5.32	<0.05	<0.01	0.624	12	94.6	65.2	152.3
28/908411	Heyen	50.8	8.2	13.8	2.20	<0.05	<0.01	0.033	92	51.2	24.8	39.1
28/908401	Born	88.2	11.7	21.9	3.90	<0.05	0.03	0.918	159	99.8	42.9	36.6
28/900591	Vogelsberg 264	56.0	6.0	69.8	16.30	<0.05	0.09	<0.005	165	71.6	88.7	4.4
28/907271	Korschenbroich	50.9	11.2	93.5	13.20	0.91	0.71	0.024	409	28.9	32.5	<0.2
28/907841	Kl. Broi. 3	140.0	12.4	26.6	22.80	<0.05	0.02	1.836	378	110.0	48.8	5.4
28/907821	Kl. Broi. 1	163.0	19.0	20.7	3.28	0.06	0.01	<0.005	354	111.0	55.6	59.3
28/908541	Niederkr. Tab 13	55.2	15.1	24.0	3.48	<0.05	0.02	0.024	18	88.7	57.4	102.3
28/908081	WW Niederkr. B6	9.3	1.2	6.2	1.59	<0.05	1.19	0.01	18	18.0	9	<0.2
28/809981	Oberkruechten	38.3	16.4	19.3	3.18	<0.05	0.02	0.227	18	67.1	23.9	108.5
28/919461	Langwaden	87.2	15.8	56.4	5.88	<0.05	0.03	<0.005	232	110.0	70	26.5
28/919462	Langwaden	116.0	19.8	37.4	2.81	0.06	1.08	0.152	256	164.0	61.9	<0.2
28/917841	Kapellen	135.0	18.0	88.2	18.00	<0.05	0.04	<0.005	384	107.0	137	20.4

Table 1. Cont'd (3 of 6)

ID Number	Location	Ca^{2+}	Mg^{2+}	Na^{+}	K^{+}	NH_4^{+}	Fe^{2+}	Mn^{2+}	HCO_3^{-}	SO_4^{2-}	Cl^{-}	NO_3^{-}
		($mg\ L^{-1}$)										
28/919471	Neukirch.2	101.0	15.0	14.8	1.69	<0.05	0.02	<0.005	232	88.2	34.5	23.5
28/919472	Neukirch.2	89.9	14.4	6.9	0.84	<0.05	0.54	0.007	348	7.2	5.47	<0.2
27/957822	Fischenich	229.0	35.7	26.0	1.52	<0.05	0.06	<0.005	421	259.0	76.9	92.1
27/957823	Fischenich	199.0	31.4	31.7	1.81	<0.05	0.61	0.203	433	249.0	75.6	3.7
27/957824	Fischenich		8.5	426.0	9.72			0.129		77.5	360	<0.2
27/957981	Brühl 1	146.0	24.2	36.2	10.90	<0.05	0.02	<0.005	287	268.0	41.1	21
27/957982	Brühl 1	124.0	37.9	128.0	14.70	1.02	8.08	0.501	220	335.0	205	<0.2
27/958061	Brühl 9	55.3	51.9	1420.0	30.20	2.77	2.91	0.175	964	220.0	1830	<0.2
27/958062	Brühl 9	70.7	73.3	1700.0	33.50	2.95	2.33	0.114	1171	280.0	2200	<0.2
27/958063	Brühl 9	83.3	85.7	1860.0	38.70	<0.05	2.64	0.126	1312	306.0	2460	<0.2
07/352721	SW Brühl 22 R1	139.0	21.9	66.4	10.90	0.33	0.02	<0.005	281	240.0	91.5	55.3
07/352722	SW Brühl 22 R1	53.0	15.9	372.0	7.10	3.23	0.91	0.697	580	71.8	347	<0.2
28/917191	Gohr	120.0	18.3	16.1	2.52	<0.05	0.14	0.018	262	94.3	49.8	52.7

Table 1. Cont'd (4 of 6)

ID Number	Location	Ca^{2+}	Mg^{2+}	Na^{+}	K^{+}	NH_4^{+}	Fe^{2+}	Mn^{2+}	HCO_3^{-}	SO_4^{2-}	Cl^{-}	NO_3^{-}
		($mg\ L^{-1}$)										
28/816011	Lehmkuhl	63.7	8.0	15.2	4.97	1.04	0.25	0.183	18	68.2	29.6	156.3
28/816012	Lehmkuhl	76.7	8.8	19.1	5.17	0.41	17.7	0.707	18	216.0	68.1	1.5
28/900601	An Der Wae 265H	82.4	16.1	19.9	4.09	<0.05	0.16	0.084	6	111.0	57.1	190.8
80/030128	Eicken 276	73.2	14.9	81.7	6.01	<0.05	0.01	0.009	92	194.0	124	18.7
28/816061	Mackenstein	61.9	18.0	39.3	7.23	<0.05	0.14	0.073	31	176.0	69.3	60.2
28/907641	Myllendonk	114.0	13.7	21.2	5.51	1.51	4.29	0.381	354	72.6	37.5	<0.2
28/907271	Korschenbroich	50.8	11.4	99.4	15.00	1.04	0.66	0.029	409	36.4	34.5	<0.2
01/040244	WWk Beeck Nr. 16	68.3	9.5	21.9	3.25	<0.05	<0.01	0.01	92	99.4	33	63.7
21/908711	Merbecker Busch	43.6	20.6	21.5	5.16	<0.05	<0.01	0.148	6	91.8	49.5	121.3
21/908712	Merbecker Busch	7.5	1.8	5.2	0.93	<0.05	2.55	0.065	37	5.7	5.35	<0.2
21/814901	Tueschenbroich	73.1	9.8	14.1	14.30	<0.05	0.02	0.012	104	67.3	32.4	114.7
21/814902	Tueschenbroich	71.7	10.1	14.5	11.20	<0.05	<0.01	0.01	110	68.2	33.2	96.5
28/806881	Rheydt	35.2	5.2	14.4	2.17	0.12	12.04	0.183	43	86.1	26.1	2.9

Table 1. Cont'd (5 of 6)

ID Number	Location	Ca^{2+}	Mg^{2+}	Na^{+}	K^{+}	NH_4^{+}	Fe^{2+}	Mn^{2+}	HCO_3^{-}	SO_4^{2-}	Cl^{-}	NO_3^{-}
		($mg\ L^{-1}$)										
28/806882	Rheydt	39.2	8.3	13.0	5.76	0.42	1.63	0.108	201	9.1	5	<0.2
28/908591	Gunhoven	90.6	12.9	11.0	2.22	<0.05	0.01	0.014	275	63.2	29.2	2.3
28/908592	Gunhoven	82.2	14.4	10.0	1.53	<0.05	3.03	0.278	153	89.0	36.8	<0.2
28/900171	Herdterhof 0080a	54.3	17.3	22.3	9.35	<0.05	0.16	0.016	24	122.0	46.4	89.4
28/907891	Korschenbroich	139.0	14.6	16.6	8.16	0.59	3.35	0.585	403	108.0	26.7	<0.2
28/907892	Korschenbroich	77.4	10.4	8.6	2.31	0.24	1.67	0.162	250	37.1	15.2	<0.2
28/806941	Glehn	192.0	25.9	38.2	3.61	<0.05	0.01	0.008	415	158.0	62.3	133.2
28/907691	Pesch	175.0	22.6	33.2	3.16	<0.05	<0.01	0.274	458	109.0	65.1	76.6
28/907692	Pesch	137.0	16.7	23.4	2.72	<0.05	<0.01	0.253	421	50.0	40.2	36.2
28/812531	Dannerhof	199.0	25.7	9.3	2.01	<0.05	0.06	0.026	372	133.0	106	69.9
28/806921	Gut Bickhausen	212.0	26.7	98.8	1.47	0.14	<0.01	0.009	549	180.0	82	189
28/806922	Gut Bickhausen	98.5	16.5	7.5	1.46	<0.05	3.48	0.128	403	2.1	7.81	0.9
28/919482	Barrenstein 2	119.0	18.9	6.5	1.41	<0.05	3.02	0.265	329	110.0	12.7	<0.2

Table 1. Cont'd (6 of 6)

ID Number	Location	Ca^{2+}	Mg^{2+}	Na^{+}	K^{+}	NH_4^{+}	Fe^{2+}	Mn^{2+}	HCO_3^{-}	SO_4^{2-}	Cl^{-}	NO_3^{-}
		(mg L^{-1})										
27/831791	Buesdorf	152.0	29.8	54.7	1.84	<0.05	0.1	0.008	592	150.0	84.7	194.8
27/937921	Fliested. 3	166.0	28.1	13.1	1.46	<0.05	<0.01	<0.005	537	78.0	27.7	20.8
27/937922	Fliested. 3	194.0	30.3	27.6	4.52	<0.05	0.13	0.023	348	303.0	86.8	<0.2
07/355571	Dansweiler 663	174.0	23.5	15.9	1.11	<0.05	<0.01	<0.005	342	185.0	41.7	54.4
27/937881	Glessen 4	203.0	33.0	17.8	1.59	<0.05	<0.01	0.005	390	202.0	85.6	59.3
27/937491	Pulheim III	183.0	30.5	18.0	1.69	<0.05	<0.01	0.006	415	138.0	84.4	52.2

References

Aeschbach-Hertig, W., H. El-Gamal, M. Wieser and L. Palcsu (2008) Modeling excess air and degassing in groundwater by equilibrium partitioning with a gas phase. *Water Resour. Res.*, **44**(8)**,** W08449.

Aeschbach-Hertig, W., F. Peeters, U. Beyerle and R. Kipfer (1999) Interpretation of dissolved atmospheric noble gases in natural waters. *Water Resources Research,* **35(**9)**,** 2779-2792.

Aeschbach-Hertig, W., F. Peeters, U. Beyerle and R. Kipfer (2000) Palaeotemperature reconstruction from noble gases in ground water taking into account equilibration with entrapped air. *Nature* **405**, 1040-1044.

Aeschbach-Hertig, W., M. Stute, J. F. Clark, R. F. Reuter & P. Schlosser (2002) A paleotemperature record derived from dissolved noble gases in groundwater of the Aquia Aquifer (Maryland, USA). *Geochimica et Cosmochimica Acta*, **66**(5)**,** 797-817.

Andrews, J. N. (1992) Mechanisms for noble gas dissolution by groundwaters. In: *Isotopes of Noble Gases as Tracers in Environmental Studies*. IAEA, Vienna, 87-110.

Andrews, J. N. (1985) The isotopic composition of radiogenic helium and its use to study groundwater movement in confined aquifers. *Chemical Geology,* **49,** 339-351.

Andrews, J. N. and D. J. Lee (1979) Inert gases in groundwater from the Bunter Sandstone of England as indicators of age and palaeoclimatic trends. *Journal of Hydrology*, **41**(3-4)**,** 233-252.

Appelo, C. A. J. and D. Postma (2005) *Geochemistry, Groundwater and Pollution; 2nd Edition*. CRC Press, Amsterdam.

Balderer, W., H. A. Synal and J. Deak (2004) Application of the chlorine-36 method for the delineation of groundwater infiltration of large river systems: example of the Danube River in western Hungary. *Environmental Geology*, **46**(6)**,** 755-762.

Ballentine, C. J. and P. G. Burnard (2002) Production, Release and Transport of Noble Gases in the Continental Crust. *Reviews in Mineralogy and Geochemistry,* **47**(1)**,** 481-538.

Ballentine, C. J. and C. M. Hall (1999) Determining paleotemperature and other variables by using an error-weighted, nonlinear inversion of noble gas concentrations in water. *Geochimica et Cosmochimica Acta,* **63**(16)**,** 2315-2336.

Batey, J. H. (1987) Quadrupole Gas Analysers. *Vacuum*, **37**, 659-668.

Bense, V. & R. van Balen (2003) Hydrogeological aspects of fault zones on various scales in theRoer Valley Rift System. *Journal of Geochemical Exploration*, **78-79,** 317-320.

Bense, V.F. and R.T. Van Balen (2004) The impact of clay-smearing and fault relay on groundwater flow patterns in the Lower Rhine Embayment, *Basin Research,* **16**, 397-411.

Bense, V. F. (2004) The hydraulic properties of faults in unconsolidated sediments and their impact on groundwater flow – a study in the Roer Valley Rift System and adjacent areas in the Lower Rhine Embayment. PhD Thesis.

Bense, V.F., E.H. van den Berg, and R.T. van Balen (2003) Deformation mechanisms and hydraulic properties of fault zones in unconsolidated sediments; the Roer Valley Rift System, the Netherlands. *Hydrogeology Journal*, **11**, 319-332.

Bense, V. F. and M. A. Person (2006) Faults as conduit-barrier systems to fluid flow in siliciclastic sedimentary aquifers. *Water Resour. Res.,* **42**(5)**,** W05421.

Bense, V. F., M. A. Person, K. Chaudhary, Y. You, N. Cremer & S. Simon (2008) Thermal anomalies indicate preferential flow along faults in unconsolidated sedimentary aquifers. *Geophys. Res. Lett.,* **35**(24)**,** L24406.

Benson, B. B. and Krause, D. J. (1976) Empirical laws for dilute aqueous solutions of non-polar gases. *Journal of Chemical Physics*, **64**, 689-709.

Bertleff, B., Ellwanger, D., Szenkler, C., Eichinger, L., Trimborn, P. and Wolfendale, N. (1993) Interpretation of hydrochemical and hydroisotopical measurements on paleaogroundwaters in Oberschwaben, south German alpine foreland, with focus on Quaternary geology. In: *Proceedings of an International Symposium on Applications of Isotope Techniques in Studying Past and Current Environmental Changes in the Hydrosphere and the Atmosphere*, **329/63**, IAEA, Vienna, 337-357.

Bethke, C. M., X. Zhao and T. Torgersen (1999) Groundwater flow and the ^{4}He distribution in the Great Artesian Basin of Australia. *Journal of Geophysical Research,* **104**(B6)**,** 12999-13011.

Beyerle, U., Purtschert, R., Aeschbach-Hertig, W., Imboden, D.M., Loosli, H.H., Wieler, R. and Kipfer, R. (1998) Climate and groundwater recharge during the last glaciation in an ice-covered region. *Science*, **282**, 731-734.

Beyerle, U. (1999) *Groundwater Dynamics, Paleoclimate and Noble Gases*. PhD Thesis, Swiss Federal Institute of Technology, Zürich, Switzerland.

Beyerle, U., W. Aeschbach-Hertig, D. M. Imboden, H. Baur, T. Graf and R. Kipfer (2000) A Mass Spectrometric System for the Analysis of Noble Gases and Tritium from Water Samples. *Environ. Sci. Technol.,* **34**(10)**,** 2042-2050.

Bickle, M., A. Chadwick, H. E. Huppert, M. Hallworth and S. Lyle (2007) Modelling carbon dioxide accumulation at Sleipner: Implications for underground carbon storage. *Earth and Planetary Science Letters,* **255**(1-2)**,** 164-176.

Bishop, P. K. (1990) Precipitation of dissolved carbonate species from natural waters for $\delta^{13}C$ analysis -- A critical appraisal. *Chemical Geology: Isotope Geoscience section,* **80**(3)**,** 251-259.

Blavoux, B., Dray, M., Fehri, A., Olive, P., Gröning, M., Sonntag, C., Hauquin, J. P., Pelissier, G. and Pouchan, P. (1993) Palaeoclimatic and hydrodynamic approach to the Aquitaine basin deep aquifer (France) by means of environmental isotopes and noble gases. In: *Isotope techniques in the study of past and current environmental changes in the hydrosphere and the atmosphere*, **293/305**, IAEA, Vienna, 293–305.

Boenigk, W. (2002) The Pleistocene drainage pattern in the Lower Rhine Basin. *Netherlands Journal of Geosciences/Geologie en Mijnbouw* **81**(2), 201–209.

Bowen, G. J. and J. Revenaugh (2003) Interpolating the isotopic composition of modern meteoric precipitation. *Water Resour. Res.,* **39**(10)**,** 1299.

Brennwald, M. S., F. Peeters, D. M. Imboden, S. Giralt, M. Hofer, D. M. Livingstone, S. Klump, K. Strassmann and R. Kipfer (2004) Atmospheric noble gases in lake sediment pore water as proxies for environmental change. *Geophys. Res. Lett.,* **31**(4)**,** L04202.

Bullen, T. D., D. P. Krabbenhoft and C. Kendall (1996) Kinetic and mineralogic controls on the evolution of groundwater chemistry and $^{87}Sr/^{86}Sr$ in a sandy silicate aquifer, northern Wisconsin, USA. *Geochimica et Cosmochimica Acta,* **60**(10)**,** 1807-1821.

Castro, M. C. (2004) Helium sources in passive margin aquifers--new evidence for a significant mantle ^{3}He source in aquifers with unexpectedly low in situ $^{3}He/^{4}He$ production. *Earth and Planetary Science Letters,* **222**(3-4)**,** 897-913.

Castro, M. C., A. Jambon, G. de Marsily and P. Schlosser (1998) Noble gases as natural tracers of water circulation in the Paris Basin 1. Measurements and discussion of their origin and mechanisms of vertical transport in the basin. *Water Resources Research,* **34,** 2443-2466.

Castro, M. C., L. Ma and C. M. Hall (2009) A primordial, solar He-Ne signature in crustal fluids of a stable continental region. *Earth and Planetary Science Letters,* **279**(3-4)**,** 174-184.

Cey, B. D., G. B. Hudson, J. E. Moran and B. R. Scanlon (2008) Impact of Artificial Recharge on Dissolved Noble Gases in Groundwater in California. *Environmental Science Technology,* **42,** 1017-1023.

Chan, M. A., W. T. Parry and J. R. Bowman (2000) Diagenetic Hematite and Manganese Oxides and Fault-Related Fluid Flow in Jurassic Sandstones, Southeastern Utah. *AAPG Bulletin,* **84**(9)**,** 1281-1310.

Chebotarev, I. J. (1955) Metamorphism of natural water in the crust of weathering. *Geochimica et Cosmochimica Acta,* **8**, 22–212.

Childs, C., A. Nicol, J. J. Walsh and J. Watterson (2003) The growth and propagation of synsedimentary faults. *Journal of Structural Geology,* **25**(4)**,** 633-648.

Clark, I. and Fritz, P. (1997) *Environmental Isotopes in Hydrogeology*. CRC Press LLC, Boca Raton, Florida.

Clarke, W. B., W. J. Jenkins and Z. Top (1976) Determination of tritium by mass spectrometric measurement of ^{3}He. *Int. J appl. Radiat. Isotopes*, **27**, 515-522.

Clever, H.L. (1979a) Helium and neon. In: *IUPAC solubility data series* (Ed H.L. Clever), **1**, Pergamon press, Oxford.

Clever, H.L. (1979b) Krypton, xenon and radon. In: *IUPAC Solubility Data Series* (Ed H.L. Clever), **2**, Pergamon press, Oxford.

Clever, H.L. (1980) Argon. In: *IUPAC Solubility Data Series* (Ed H.L. Clever), **4**, Pergamon press, Oxford.

Collon, P., W. Kutschera, H. H. Loosli, B. E. Lehmann, R. Purtschert, A. Love, L. Sampson, D. Anthony, D. Cole, B. Davids, D. J. Morrissey, B. M. Sherrill, M. Steiner, R. C. Pardo and M. Paul (2000) ^{81}Kr in the Great Artesian Basin, Australia: a new method for dating very old groundwater. *Earth and Planetary Science Letters,* **182**(1)**,** 103-113.

Coplen, T.B., Herczeg, A., and Barnes, C.J. (2000) *Isotope engineering - using stable isotopes of the water molecule to solve practical problems*. In: Environmental Tracers in Subsurface Hydrology (Eds. P. G. Cook and A. Herczeg), Kluwer Academic Publishers, Boston, 79-110.

Craig, H. (1961) Isotopic variations in meteoric waters. *Science*, **133**, 1702-1703.

Criss, R. E. (1999) *Principles of stable isotope distribution*. Oxford University Press, New York.

Cuisiat, F. and E. Skurtveit (2010) An experimental investigation of the development and permeability of clay smears along faults in uncemented sediments. *Journal of Structural Geology,* **In Press, Corrected Proof**.

Dansgard, W. (1964) Stable isotopes in precipitation. *Tellus*, **16**, 436-468.

Deák, J., and Coplen, T.B. (1996) Identification of Holocene and Pleistocene groundwaters in Hungary using oxygen and hydrogen isotopic ratios. In *Isotopes in Water Resources Management*, **1**, IAEA Vienna, 438.

Deines, P., D. Langmuir and R. S. Harmon (1974) Stable carbon isotope ratios and the existence of a gas phase in the evolution of carbonate ground waters. *Geochimica et Cosmochimica Acta,* **38**(7)**,** 1147-1164.

Dennis, F., J. N. Andrews, A. Parker, J. Poole and M. Wolf (1997) Isotopic and noble gas study of Chalk groundwater in the London Basin, England. *Applied Geochemistry,* **12**(6)**,** 763-773.

Dewhurst, D. N. and R. M. Jones (2003) Influence of physical and diagenetic processes on fault geomechanics and reactivation. *Journal of Geochemical Exploration,* **78-79**, 153-157.

Du, X., R. Purtschert, K. Bailey, B. E. Lehmann, R. Lorenzo, Z. T. Lu, P. Mueller, T. P. O'Connor, N. C. Sturchio and L. Young (2003) A new method of measuring ^{81}Kr and ^{85}Kr abundances in environmental samples. *Geophys. Res. Lett.*, **30**.

Edmunds, W. M. (2001) Palaeowaters in European costal aquifers – the goals and main conclusions of the PALAEAUX project. *Geological Society of London Special Publications, **189***, 1-16.

Egholm, D. L., O.R. Clausen, M. Sandiford, M.B. Kristensen and J.A. Korstgård (2008) The mechanics of clay smearing along faults. *Geology*, **36**, 787-790.

Ekwurzel, B., P. Schlosser, W. M. Smethie Jr, L. N. Plummer, E. Busenberg, R. L. Michel, R. Weppernig and M. Stute (1994) Dating of shallow groundwater: Comparison of the transient tracers ^{3}H/^{3}He, chlorofluorocarbons, and ^{85}Kr. *Water Resources Research,* **30**(6)**,** 1693-1708.

Epstein, S. and T.K. Mayeda (1953) Variations of the ^{18}O/^{16}O ratio in natural waters, *Geochim. Cosmochim. Acta* **4**, 213–224.

Erftverband (2006) *Jahresbericht.* Bergheim, Germany.

Ernst, L. F. and De Ridder, N. A. (1960) High resistance to horizontal ground-water flow in coarse sediments due to faulting, *Geologic en Mijnbouw* **39**, 66–85.

Faure, G. and Mensing, T. M. (2005) Isotopes: Principles and Applications. 3rd Ed. Wiley, New Jersey.

Faybishenko, B. A. (1995) Hydraulic Behavior of Quasi-Saturated Soils in the Presence of Entrapped Air: Laboratory Experiments. *Water Resour. Res.*, **31**(10)**,** 2421-2435.

Fontes, J. C., Andrews, J. N., Edmunds, W. M., Guerre, A. and Travi, Y. (1991) Paleorecharge by the Niger River (Mali) deduced from groundwater geochemistry. *Water Resources Research,* **27**(2), 199-214.

Fontes, J. C. and J. M. Matray (1993) Geochemistry and origin of formation brines from the Paris Basin, France: 1. Brines associated with Triassic salts. *Chemical Geology,* **109**(1-4)**,** 149-175.

Freeze, R. A. and Cherry, J. A. (1979) *Groundwater*. Prentice-Hall, Inc., Englewood Cliffs, New Jersey.

Fricke, H. C. and O'Neil, J. R. (1999) The correlation between 18O/16O ratios of meteoric water and surface temperature; its use in investigating terrestrial climate change over geologic time. *Earth and Planetary Science Letters*, **170**, 181-196.

Friedli, H., Lotscher, H., Oeschger, H., Siegenthaler, U. and Stauffer, B. (1986) Ice core record of the $^{12}C/^{13}C$ ratio of atmospheric CO_2 in the past two centuries. *Nature*, **324**, 237-238.

Frost, C. D. and Toner, R. N. (2004) Strontium Isotopic Identification of Water-Rock Interaction and Ground Water Mixing. *Groundwater*, **42**(3), 418-432.

Fulljames, J. R., Zijerveld, L. J. J. and Franssen, R. C. M. W. (1997) Fault seal processes: systematic analysis of fault seals over geological and production time scales. *NPF Special Publication*, **7**, 51-59.

Gat, J. R. (1996) Oxygen and hydrogen isotopes in the hydrologic cycle. *Annual Review of Earth and Planetary Sciences,* **24**(1)**,** 225-262.

Gat, J. (2010) *Isotope Hydrology – A Study of the Water Cycle*. Imperial College Press, London.

Geluk, M. C., E. J. Th. Duin, M. Dusar, R. H. B. Rijkers, M. W. van den Berg, and P. van Rooijen (1994) Stratigraphy and tectonics of the Roer Valley Graben, *Geologie en Mijnbouw*, **73**, 129–141.

Gilfillan, S. M. V., C. J. Ballentine, G. Holland, D. Blagburn, B. S. Lollar, S. Stevens, M. Schoell and M. Cassidy (2008) The noble gas geochemistry of natural CO_2 gas reservoirs from the Colorado Plateau and Rocky Mountain provinces, USA. *Geochimica et Cosmochimica Acta,* **72**(4)**,** 1174-1198.

Gilfillan, S. M. V., B. S. Lollar, G. Holland, D. Blagburn, S. Stevens, M. Schoell, M. Cassidy, Z. Ding, Z. Zhou, G. Lacrampe-Couloume & C. J. Ballentine (2009) Solubility trapping in formation water as dominant CO2 sink in natural gas fields. *Nature,* **458**(7238)**,** 614-618.

Griesshaber, E., R. K. O'Nions and E. R. Oxburgh (1992) Helium and carbon isotope systematics in crustal fluids from the Eifel, the Rhine Graben and Black Forest, F.R.G. *Chemical Geology,* **99**(4)**,** 213-235.

Hager, H. (1993) The origin of the Tertiary lignite deposits in the Lower Rhine region, Germany. *International Journal of Coal Geology,* **23**(1-4)**,** 251-262.

Hall, C. M., M. C. Castro, K. C. Lohmann and L. Ma (2005) Noble gases and stable isotopes in a shallow aquifer in southern Michigan: Implications for noble gas paleotemperature reconstructions for cool climates. *Geophys. Res. Lett.*, **32**(18)**,** L18404.

Heaton, T. H. E., A. S. Talma and J. C. Vogel (1986) Dissolved gas paleotemperatures and ^{18}O variations derived from groundwater near Uitenhage, South Africa. *Quaternary Research*, **25**(1)**,** 79-88.

Heaton, T. H. E. & J. C. Vogel (1981) "Excess air" in groundwater. *Journal of Hydrology*, **50,** 201-216.

Herch, A. (2000) The thermal springs of Aachen/Germany – what Charlemagne didn't know. *Environmental Geology*, **39**(5), 437-447.

Herczeg, A. L. and Edmunds, W. M. (2000) Inorganic ions as tracers. In Cook, P.G. and Herczeg, A., eds., *Environmental Tracers in Subsurface Hydrology*, Boston, Kluwer Academic Publishers, 31-77.

Herrmann, F., C. Jahnke, F. Jenn, R. Kunkel, H.-J. Voigt, J. Voigt and F. Wendland (2009) Groundwater recharge rates for regional groundwater modelling: a case study using GROWA in the Lower Rhine lignite mining area, Germany. *Hydrogeology Journal*, **17**(8)**,** 2049-2060.

Hoehn, E., H. R. Von Gunten, F. Stauffer and T. Dracos (1992) Radon-222 as a groundwater tracer. A laboratory study. *Environmental Science & Technology*, **26**(4)**,** 734-738.

Holocher, J., Peeters, F., Aeschbach-Hertig, W., Hofer, M., Brennwald, M., Kinzelbach, W. and Kipfer, R. (2002) Experimental investigations on the formation of excess air in quasi-saturated porous media. *Geochimica et Cosmochimica Acta*, **66**, 4103-4117.

Holocher, J., F. Peeters, W. Aeschbach-Hertig, W. Kinzelbach & R. Kipfer (2003) Kinetic Model of Gas Bubble Dissolution in Groundwater and Its Implications for the Dissolved Gas Composition. *Environ. Sci. Technol.*, **37**(7)**,** 1337-1343.

Houtgast, R. F., R. T. Van Balen, L. M. Bouwer, G. B. M. Brand and J. M. Brijker (2002) Late Quaternary activity of the Feldbiss Fault Zone, Roer Valley Rift System, the Netherlands, based on displaced fluvial terrace fragments. *Tectonophysics*, **352**(3-4)**,** 295-315.

IAEA/WMO (2006) Global Network of Isotopes in Precipitation. The GNIP Database. Accessible at: http://www.iaea.org/water

Ingram, R. G. S. (2005) *An integrated hydrochemical study of the Sandringham Sands, west Norfolk (UK).* PhD Thesis, University of East Anglia, Norwich, United Kingdom.

Ingram, R. G. S., K. M. Hiscock and P. F. Dennis (2007) Noble Gas Excess Air Applied to Distinguish Groundwater Recharge Conditions. *Environmental Science & Technology*, **41**(6)**,** 1949-1955.

Kemna, H. A. (2008) A Revised Stratigraphy for the Pliocene and Lower Pleistocene Deposits of the Lower Rhine Embayment. *Netherlands Journal of Geosciences*, **87**(1), 91-105.

Kipfer, R., W. Aeschbach-Hertig, F. Peeters & M. Stute (2002) Noble Gases in Lakes and Ground Waters. *Reviews in Mineralogy and Geochemistry*, **47**(1)**,** 615-700.

Klump, S., Y. Tomonaga, P. Kienzler, W. Kinzelbach, T. Baumann, D. M. Imboden and R. Kipfer (2007) Field experiments yield new insights into gas exchange and excess air formation in natural porous media. *Geochimica et Cosmochimica Acta*, **71**(6)**,** 1385-1397.

Kulongoski, J. T. and D. R. Hilton (2002) A quadrupole-based mass spectrometric system for the determination of noble gas abundances in fluids. *Geochem. Geophys. Geosyst.,* **3**(6)**,** 1032.

Lavastre, V., N. Jendrzejewski, P. Agrinier, M. Javoy and M. Evrard (2005) Chlorine transfer out of a very low permeability clay sequence (Paris Basin, France): ^{35}Cl and ^{37}Cl evidence. *Geochimica et Cosmochimica Acta,* **69**(21)**,** 4949-4961.

Lavastre, V., C. L. G. L. Salle, J.-L. Michelot, S. Giannesini, L. Benedetti, J. Lancelot, B. Lavielle, M. Massault, B. Thomas, E. Gilabert, D. Bourlès, N. Clauer and P. Agrinier (2010) Establishing constraints on groundwater ages with ^{36}Cl, ^{14}C, ^{3}H, and noble gases: A case study in the eastern Paris basin, France. *Applied Geochemistry,* **25**(1)**,** 123-142.

Lehmann, B. E., H. H. Loosli, D. Rauber, N. Thonnard and R. D. Willis (1991) ^{81}Kr and ^{85}Kr in groundwater, Milk River aquifer, Alberta, Canada. *Applied Geochemistry,* **6**(4)**,** 419-423.

Lehmann, B. E., A. Love, R. Purtschert, P. Collon, H. H. Loosli, W. Kutschera, U. Beyerle, W. Aeschbach-Hertig, R. Kipfer, S. K. Frape, A. Herczeg, J. Moran, I. N. Tolstikhin and M. Gröning (2003) A comparison of groundwater dating with 81Kr, 36Cl and 4He in four wells of the Great Artesian Basin, Australia. *Earth and Planetary Science Letters,* **211**(3-4)**,** 237-250.

Lehner, F.K. and Pilaar, W.F. (1997) On a mechanism of clay smear emplacement in synsedimentary normal faults. In: Hydrocarbon Seals: Importance for Exploration and Production (Ed. by P.Møller-Pedersen & A.G.Koestler), NPF Spec. Pub., **7**, 39–50.

Loosli, H. H. (1992) Applications of ^{37}Ar, ^{39}Ar and ^{85}Kr in hydrology, oceanography and atmospheric studies: Current state of art. In: *Isotopes of Noble Gases as Tracers in Environmental Studies*. IAEA, Vienna, 75-84.

Love, A. J., A. L. Herczeg, L. Sampson, R. G. Cresswell and L. K. Fifield (2000) Sources of chloride and implications for ^{36}Cl dating of old groundwater, Southwestern Great Artesian Basin, Australia. *Water Resour. Res.,* **36**(6)**,** 1561-1574.

Lyons, W. B., S. W. Tyler, H. E. Gaudette and D. T. Long (1995) The use of strontium isotopes in determining groundwater mixing and brine fingering in a playa spring zone, Lake Tyrrell, Australia. *Journal of Hydrology,* **167**(1)**,** 225-225.

Mahara, Y. and T. Igarashi (2003) Changes in isotope ratio and content of dissolved helium through groundwater evolution. *Applied Geochemistry,* **18**(5)**,** 719-738.

Maloszewski, P. and Zuber, A. (1991) Influence of matrix diffusion and exchange reactions on radiocarbon ages in fissured carbonate aquifers. *Water Resources Research*, **27**(8), 1937-1945.

Marty, B., S. Dewonck and C. France-Lanord (2003) Geochemical evidence for efficient aquifer isolation over geological timeframes. *Nature,* **425**(6953)**,** 55-58.

Marty, B., T. Torgersen, V. Meynier, R. K. O'Nions and G. de Marsily (1993) Helium Isotope Fluxes and Groundwater Ages in the Dogger Aquifer, Paris Basin. *Water Resour. Res.,* **29,** 1025-1035.

Matray, J. M., Lambert, M. and Fontes, J. C. (1994) Stable isotope conservation and origin of saline waters from the Middle Jurassic aquifer of the Paris Basin, France. *Applied Geochemistry*, **9**, 297-309.

Mazor, E. (1972) Paleotemperatures and other hydrological parameters deduced from noble gases dissolved in groundwaters; Jordan Rift Valley, Israel. *Geochimica et Cosmochimica Acta,* **36**(12)**,** 1321-1336.

Mazor, E. (1977) Geothermal tracing with atmospheric and radiogenic noble gases. *Geothermics,* **5**(1-4)**,** 21-36.

Mercury, L., D. L. Pinti and H. Zeyen (2004) The effect of the negative pressure of capillary water on atmospheric noble gas solubility in ground water and palaeotemperature reconstruction. *Earth and Planetary Science Letters,* **223**(1-2)**,** 147-161.

Metz, B., Davidson, O., de Coninck, H., Loos, M. and Meyer, L. (2005) *Carbon Dioxide Capture and Storage – IPCC Special Report*. Cambridge University Press, UK, 431.

Morrison, P. and Pine, J. (1955) Radiogenic origin of the helium isotopes in rocks. *Ann. N.Y. Acad. Sci.* **62**, 69-92.

Mosbrugger, V., C. T. Gee, G. Belz and A. R. Ashraf (1994) Three-dimensional reconstruction of an *in situ* Miocene peat forest from the Lower Rhine Embayment, northwestern Germany - new methods in palaeovegetation analysis. *Palaeogeography, Palaeoclimatology, Palaeoecology,* **110**(3-4)**,** 295-317.

Neumann, K. and Dreiss, S. (1995) Strontium 87/strontium 86 ratios as tracers in groundwater and surface waters in Mono Basin, California. *Water Resources Research,* **31**(12), 3183-3193.

Osenbrück, K., Weise, S. M., Zuber, A., Grabczak, J. and Ciezkowski, W. (1993) Noble gas temperatures and ages of some glacial and buried brine waters in Poland. In: *Isotope techniques in the study of past and current environmental changes in the hydrosphere and the atmosphere*. IAEA, Vienna, 319-336.

Osenbrück, K., S. Stadler, J. Sültenfuß, A. O. Suckow and S. M. Weise (2009) Impact of recharge variations on water quality as indicated by excess air in groundwater of the Kalahari, Botswana. *Geochimica et Cosmochimica Acta,* **73**(4)**,** 911-922.

Ozima, M. and Podosek, F.A. (2002) *Noble Gas Geochemistry*. Cambridge Universtiy Press.

Peeters, F., U. Beyerle, W. Aeschbach-Hertig, J. Holocher, M. S. Brennwald and R. Kipfer (2003) Improving noble gas based paleoclimate reconstruction and groundwater dating using 20Ne/22Ne ratios. *Geochimica et Cosmochimica Acta,* **67**(4)**,** 587-600.

Pinti, D. L. and B. Marty (1995) Noble gases in crude oils from the Paris Basin, France: Implications for the origin of fluids and constraints on oil-water-gas interactions. *Geochimica et Cosmochimica Acta*, **59**(16)**,** 3389-3404.

Pinti, D. L. and Marty, B. (1998) The origin of helium in deep sedimentary aquifers and the problem of dating very old groundwaters. In : Parnell J (Ed.), Dating and duration of fluid flow and fluid-rock interaction, Special Publication **144**, Geological Society, London, 53-68.

Pinti, D. L., B. Marty and J. N. Andrews (1997) Atmosphere-derived noble gas evidence for the preservation of ancient waters in sedimentary basins. *Geology*, **25**, 111-114.

Poole, J. C., G. W. McNeill, S. R. Langman and F. Dennis (1997) Analysis of noble gases in water using a quadrupole mass spectrometer in static mode. *Applied Geochemistry,* **12**(6)**,** 707-714.

Rawling, G. C., L. B. Goodwin and J. L. Wilson (2001) Internal architecture, permeability structure, and hydrologic significance of contrasting fault-zone types. *Geology,* **29**(1)**,** 43-46.

Rijkers, R., E. J. Th. Duin, M. Dusar and V. Langenaeker (1993) Crustal structure of the London-Brabant Massif, southern North Sea. *Geol. Mag.*, **130**, 569-574.

Rozanski, K. (1985) Deuterium and oxygen-18 in European groundwaters -- Links to atmospheric circulation in the past. *Chemical Geology: Isotope Geoscience section,* **52**(3-4)**,** 349-363.

Rudolph, J., H.K. Rath and C. Sonntag (1984) Noble gases and stable isotopes in ^{14}C-dated palaeowaters from central Europe and the Sahara. *Isotope Hydrology 1983,* IAEA Vienna, 467–477.

Saar, M. O., M. C. Castro, C. M. Hall, M. Manga and T. P. Rose (2005) Quantifying magmatic, crustal, and atmospheric helium contributions to volcanic aquifers using all stable noble gases: Implications for magnatism and groundwater flow. *Geochemistry Geophysics Geosystems,* **6**(3).

Savchenko, V. P. (1935) The problems of geochemistry of helium. *Natural Gases,* **9**, 53-197. (In Russian)

Schäfer, A., D. Hilger, G. Gross and F. von der Hocht (1996) Cyclic sedimentation in Tertiary Lower-Rhine Basin (Germany) -- the `Liegendrucken' of the brown-coal open-cast Fortuna mine. *Sedimentary Geology,* **103**(3-4)**,** 229-247.

Schäfer, A., T. Utescher, M. Klett and M. Valdivia-Manchego (2005) The Cenozoic Lower Rhine Basin – rifting, sedimentation, and cyclic stratigraphy. *International Journal of Earth Sciences,* **94**(4)**,** 621-639.

Schlosser, P., M. Stute, H. Dorr, C. Sonntag and K. O. Munnich (1988) Tritium/^{3}He dating of shallow groundwater. *Earth and Planetary Science Letters,* **89**(3-4)**,** 353-362.

Schmatz, J., P. J. Vrolijk and J. L. Urai (In Press) Clay smear in normal fault zones - The effect of multilayers and clay cementation in water-saturated model experiments. *Journal of Structural Geology,* **In Press, Corrected Proof**.

Sharp, Z. (2007) *Principles of Stable Isotope Geochemistry*. Pearson Prentice Hall, Upper Saddle River, NJ.

Shipton Z. K., Evans J. P., Kirschner D., Kolesar P. T., Williams A. P. and Heath J. (2004) Analysis of leakage through 'low-peameability' faults from natural reservoirs in the Colorado Plateau, east-central Utah. In: Geological Storage of Carbon Dioxide (eds. S. J. Baines and R. H. Worden). *Geological Society*, **233**, 43–58.

Skoog, D. A. (2004) *Fundamentals of Analytical Chemistry* (8th Ed.). Thomson, London.

Smith, R. L. and J. H. Duff (1988) Denitrification in a Sand and Gravel Aquifer. *Appl. Environ. Microbiol.,* **54**(5)**,** 1071-1078.

Solomon, D. K., A. Hunt and R. J. Poreda (1996) Source of radiogenic helium-4 in shallow aquifers: Implications for dating young groundwater. *Water Resources Research,* **32**(6)**,** 1805-1813.

Solomon, D. K., R. J. Poreda, S. L. Schiff and J. A. Cherry (1992) Tritium and Helium 3 as Groundwater Age Tracers in the Borden Aquifer. *Water Resources Research,* **28**(3)**,** 741-755.

Sperrevik, S., Færseth, R. B. and Gabrielsen, R. H. (2000) Experiments on clay smear formation along faults. *Petroleum Geoscience*, ***6***(2), 113-123.

Sperrevik, S., P. A. Gillespie, Q. J. Fisher, T. Halvorsen, and R. J. Knipe (2002) Empirical estimation of fault rock properties, in Hydrocarbon Seal Quantification, NPF Spec. Publ., **11**, edited by A. G. Koestler and R. Hunsdale, 109–125, Elsevier, New York.

Strassmann, K. M., M. S. Brennwald, F. Peeters and R. Kipfer (2005) Dissolved noble gases in the porewater of lacustrine sediments as palaeolimnological proxies. *Geochimica et Cosmochimica Acta,* **69**(7)**,** 1665-1674.

Stoessell, R. K. and L. Prochaska (2005) Chemical Evidence for Migration of Deep Formation Fluids into Shallow Aquifers in South Louisiana. *Gulf Coast Association of Geological Societies Transactions,* **55,** 794-808.

Sturchio, N. C., X. Du, R. Purtschert, B. E. Lehmann, M. Sultan, L. J. Patterson, Z.-T. Lu, P. Mueller, K. Bailey, T. P. O'Connor, L. Young, R. Lorenzo, B. M. Kennedy, M. van Soest, Z. El Alfy, B. El Kaliouby, Y. Dawood, and A. M. A. Abdallah (2004) One million year old groundwater in the Sahara revealed by krypton-81 and chlorine-36. *Geophysical Research Letters*, **31**, L05503.

Stute, M., M. Forster, H. Frischkorn, A. Serejo, J. F. Clark, P. Schlosser, W. S. Broecker, and G. Bonani (1995a) Cooling of Tropical Brazil (5°C) During the Last Glacial Maximum. *Science*, **269** (5222), 379-383.

Stute, M., Clark, J.F., Schlosser, P., Broecker, W.S. and Bonani, G. (1995b) A 30,000- yr continental paleotemperature record derived from noble gases dissolved in groundwater from the San-Juan Basin, New-Mexico. *Quaternary Research,* **43**, 209-220.

Stute, M. and J. Deak (1989) Environmental isotope study (^{14}C, ^{13}C, ^{18}O, D, noble gases) on deep groundwater circulation systems in Hungary with reference to paleoclimate. *Radiocarbon,* **31**(3)**,** 902-918.

Stute, M., and P. Schlosser (1993), Principles and applications of the noble gas paleothermometer, in Climate Change in Continental Isotopic Records, *Geophys. Monogr. Ser.*, **78**, edited by P. K. Swart et al., 89–100, AGU, Washington D. C.

Stute, M., C. Sonntag, J. Deak and P. Schlosser (1992) Helium in deep circulating groundwater in the Great Hungarian Plain: Flow dynamics and crustal and mantle helium fluxes. *Geochimica et Cosmochimica Acta,* **56**(5)**,** 2051-2067.

Sun, T., C. M. Hall, M. C. Castro, K. C. Lohmann and P. Goblet (2008) Excess air in the noble gas groundwater paleothermometer: A new model based on diffusion in the gas phase. *Geophys. Res. Lett.*, **35**.

Takahata, N. and Sano, Y. (2000) Helium flux from a sedimentary basin, *Appl. Radiat. Isotopes*, **52**, 985–992.

Takaoka, N. and Y. Mizutani (1987) Tritiogenic ^{3}He in groundwater in Takaoka. *Earth and Planetary Science Letters*, **85**(1-3)**,** 74-78.

Tans, P. and Keeling, R. (2010) NOAA/ESRL (www.esrl.noaa.gov/gmd/ccgg/trends/) and Scripps Institution of Oceanography (scrippsco2.ucsd.edu/).

Thonnard, N., R. D. Willis, M. C. Wright, W. A. Davis and B. E. Lehmann (1987) Resonance ionization spectroscopy and the detection of ^{81}Kr. *Nuclear Instruments and Methods in Physics Research Section B: Beam Interactions with Materials and Atoms*, **29**(1-2)**,** 398-406.

Tolstikhin, I., B. E. Lehmann, H. H. Loosli and A. Gautschi (1996) Helium and argon isotopes in rocks, minerals, and related ground waters: A case study in northern Switzerland. *Geochimica et Cosmochimica Acta*, **60**(9)**,** 1497-1514.

Torgersen, T. (2010) Continental degassing flux of ^{4}He and its variability. *Geochemistry Geophysics Geosystems*, **11**(6), Q06002.

Torgersen, T. and W. B. Clarke (1985) Helium accumulation in groundwater, I: An evaluation of sources and the continental flux of crustal 4He in the Great Artesian Basin, Australia. *Geochimica et Cosmochimica Acta*, **49**(5)**,** 1211-1218.

Torgersen, T., M. A. Habermehl and W. B. Clarke (1992) Crustal helium fluxes and heat flow in the Great Artesian Basin, Australia. *Chemical Geology*, **102**(1-4)**,** 139-152.

Tucker, M. E. (2003) *Sedimentary rocks in the field – The geological field guide series*. John Wiley and Sons Ltd, Chichester, England.

Unterweger, M. P. and L. L. Lucas (2000) Calibration of the National Institute of Standards and Technology tritiated-water standards. *Applied Radiation and Isotopes,* **52**(3)**,** 527-531.

Vaikmäe, R., L. Vallner, H. H. Loosli, P. C. Blaser and M. Juillard-Tardent (2001) Palaeogroundwater of glacial origin in the Cambrian-Vendian aquifer of northern Estonia. *Geological Society, London, Special Publications,* **189**(1)**,** 17-27.

Van Der Zee, W. and J. L. Urai (2005) Processes of normal fault evolution in a siliciclastic sequence: a case study from Miri, Sarawak, Malaysia. *Journal of Structural Geology,* **27**(12)**,** 2281-2300.

Von Rohden, C., A. Kreuzer, Z. Chen, R. Kipfer and W. Aeschbach-Hertig (2010) Characterizing the recharge regime of the strongly exploited aquifers of the North China Plain by environmental tracers. *Water Resour. Res.,* **46**(5)**,** W05511.

Vrolijk, P., Myers, R., Sweet, M., Shipton, Z., Dockrill, B., Evans, J., Heath, J. and Williams, A. (2005) Anatomy of reservoir-scale normal faults in central Utah: Stratigraphic controls and implications for fault zone evolution and fluid flow. *Geological Society of America*, Field Guide 6.

Wang, Y., Huntington, T. G., Osher, L. J., Wassenaar, L. I., Trumbore, S. E., Amundson, R. G., Harden, J. W., McKnight, D. M., Schiff, S. L., Aiken, G. R., Lyons, W. B., Aravena, R. O. and Baron, J. S. (2008) *Carbon Cycling in Terrestrial Environments*. In: Isotope Tracers in Catchment Hydrology (Eds. C. Kendall and J. J. McDonnell), Elsevier, Kidlington, Oxford, 577-610.

Weiss, R. F. (1968) Piggyback sampler for dissolved gas studies on sealed water samples. *Deep Sea Research and Oceanographic Abstracts,* **15**(6)**,** 695-699.

Weiss, R. F. (1970) The solubility of nitrogen, oxygen and argon in water and seawater. *Deep-sea Research*, **17,** 721-735.

Weiss, R. F. (1971) Solubility of Helium and Neon in Water and Seawater. *Journal of Chemical Engineering Data*, **16**, 235-241.

Weiss, R. F. and Kyser, T. K. (1978) Solubility of Krypton in Water and Seawater. *Journal of Chemical and Engineering Data*, **23**, 69-72.

Yokochi, R., L. J. Heraty and N. C. Sturchio (2008) Method for Purification of Krypton from Environmental Samples for Analysis of Radiokrypton Isotopes. *Analytical Chemistry*, **80**(22)**,** 8688-8693.

Yuce, G. (2007) A Geochemical study of the groundwater in the Misli basin and environmental implications. *Environmental Geology*, **V51**(5)**,** 857-868.

Zhou, Z. and C. J. Ballentine (2006) ^{4}He dating of groundwater associated with hydrocarbon reservoirs. *Chemical Geology*, **226**(3-4)**,** 309-327.

Ziegler, P.A. (1994) Cenozoic rift system of western and central Europe: an overview. *Geologie en Mijnbouw* **73**, 99-127.

Zuber, A., S. M. Weise, J. Motyka, K. Osenbruck and K. Rozanski (2004) Age and flow pattern of groundwater in a Jurassic limestone aquifer and related Tertiary sands derived from combined isotope, noble gas and chemical data. *Journal of Hydrology*, **286**(1-4)**,** 87-112.